Analysis of heat transport dynamics in fractured and porous media for the development of low enthalpy geothermal systems

Abstract
The tests conducted in these three years therefore aim to characterize the dynamics of heat transport in porous and fractured aquifers to optimize the efficiency of circuited low enthalpy geothermal systems. Therefore have been built two prototypes at the bench-scale at environmental geo engineering laboratory of the Polytechnic of Bari, that have been performed to analyse the dynamics of heat transport in fractured and porous media. From this study it was found that the specific surface of the medium plays an extremely important role. By varying the specific surface area, the subsurface reservoir formationsis able to retain more or less heat due to variation of thermal dispersion. From the present studies, have been found, in fact, that an subsurface reservoir formations characterized by a low specific surface, at the same flow rate, at the same hydraulic and thermal properties, presents high capability to store heat respect to the subsurface reservoir formations characterized by a high specific surface system that has better properties to dissipate heat. In fact, if the fractures in the reservoir have a high density and are well connected, such that the matrix blocks are small, the optimal conditions for thermal exchange are not reached as the matrix blocks have a limited capability to store heat. Therefore, subsurface reservoir formations with large porous matrix blocks will be the optimal geological formations to be exploited for geothermal power development. The estimation of the average effective thermal conductivity coefficient shows that it is not efficient to store thermal energy in rocks with high fracture density because the fractures are surrounded by a matrix with more limited capacity for diffusion giving rise to an increase in solid thermal resistance.

DICATECh

2017

Nicoletta Maria Allegretti

Analysis of heat transport dynamics in fractured and porous media for the development of low enthalphy geothermal systems

02

D.R.R.S

Doctor of Philosophy in Environmental and Building Risk and Development

Coordinator: Prof. Michele Mossa

XXIX CYCLE Curriculum: Environmental Geoengineering

DICATECh
Department of Civil, Environmental, Building Engineering and Chemistry

POLITECNICO DI BARI

02
2017

Nicoletta Maria Allegretti

# Analysis of heat transport dynamics in fractured and porous media for the development of low enthalpy geothermal systems

Prof.ssa Ing. Concetta I. Giasi
DICATECh, Politecnico di Bari
Prof. Ing. Pastore Nicola
DICATECh, Politecnico di Bari
Prof.ssa Ing. Cherubini Claudia
Department of Mechanical, Aerospace & Civil Engineering
Brunel University of London (United Kindom)
School of civil engineering, The university of Queensland (Australia)

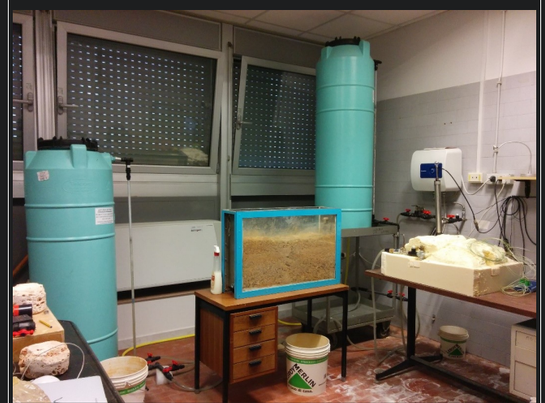

D.R.R.S

POLITECNICO DI BARI

02
2017

Doctor of Philosophy in Environmental and Building Risk and Development

Coordinator: Prof. Michele Mossa

XXIX CYCLE Curriculum: Environmental Geoengineering

DICATECh
Department of Civil, Environmental, Building Engineering and Chemistry

# Analysis of heat transport dynamics in fractured and porous media for the development of low enthalpy geothermal systems


Prof.ssa Ing. Concetta I. Giasi
DICATECh, Politecnico di Bari

Prof. Ing. Pastore Nicola
DICATECh, Politecnico di Bari

Prof.ssa Ing. Cherubini Claudia
Department of Mechanical, Aerospace & Civil Engineering Brunel University of London (United Kindom)
School of civil engineering
University of Queensland (Australia)

Nicoletta Maria Allegretti

| | | |
|---|---|---|
| D.R.R.S | **POLITECNICO DI BARI** | 02 |
| Dottorato di Ricerca in Rischio e Sviluppo ambientale, territoriale ed edilizio | | 2017 |
| Coordinatore: Prof. Michele Mossa | | |
| XXIX CICLO Curriculum: Geoingegneria Ambientale | | |
| DICATECh<br>Dipartimento di Ingegneria Civile, Ambientale, del Territorio, Edile e di Chimica | | |
| | **Analisi delle dinamiche del trasporto di calore in mezzi fratturati e porosi per lo sviluppo di sistemi geotermici a bassa entalpia** | |
| | Prof.ssa Ing. Concetta I. Giasi<br>DICATECh, Politecnico di Bari | |
| | Prof. Ing. Pastore Nicola<br>DICATECh, Politecnico di Bari<br><br>Prof.ssa Ing. Cherubini Claudia<br>Department of Mechanical, Aerospace & Civil<br>Engineering Brunel University of London (United Kindom)<br>School of civil engineering<br>University of Queensland (Australia) | |
| | Nicoletta Maria Allegretti | |

*Alla mia famiglia*

EXTENDED ABSTRACT

Low enthalpy geothermal energy is a renewable resource that is still underexploited nowadays, in relation to its potential for development in the society worldwide. Most of its applicability have already been investigated, such as: heating and cooling of private and public buildings, roads defrost, cooling of industrial processes, food drying systems, desalination.

Some of the main limitations related to the development of low-enthalpy geothermal system are represented by the initial costs, the lack of knowledge that the public has in this topic and the negative effect that a geothermal system could cause during time on environmental factors.

The lack of knowledge regarding the heat transfer dynamics of fractured aquifers and porous, leads to oversizing the systems by further increasing the initial costs.

In order to optimize the efficiency of the systems that use groundwater as geothermal resource, the flow and heat transfer in dynamic aquifers need to be well characterized. The low enthalpy geothermal resource, however, is always usable and easily available. Experiments carried out in this research have been developed mainly in order to be able to analyze the potential and to optimize short-circuited low-enthalpy geothermal systems. This type of system has been designed especially to decrease the environmental impact caused by the injection of water at a temperature higher than the ground water temperature. In this way, in fact, it is possible to reduce thermal variations within a same area of interest.

The tests conducted in these three years therefore aim to characterize the dynamics of heat transport in porous and fractured aquifers to optimize the efficiency of circuited low enthalpy geothermal systems.
Therefore has been built a prototype at the bench-scale at environmental geo engineering laboratory of the Polytechnic of Bari. On this prototype several test have been performed to analyse the dynamics of heat transport in a single fracture and in a fracture networks. The heat transport has been compared with the mass transport.
During these three years of PhD study, some experiments have been conducted which have enabled the production of some papers, published in international scientific journals. The dynamics of heat transfer have been studied in fractured media and in porous media at different grain sizes. First of all the heat transport in fractured media was studied, and compared this with the mass. In order to model the obtained thermal breakthrough curves, the Explicit Network Model (ENM) has been used, which is based on an adaptation of a Tang's solution for the transport of the solutes in a semi-infinite single fracture embedded in a porous matrix.
Parameter estimation, time moment analysis, tailing character and other dimensionless parameters have permitted to better understand the dynamics of heat transport and the efficiency of heat exchange between the fractures and matrix. The results have been compared with the previous experimental studies on solute transport.
Subsequently, some tests in situ have been performed on fractured chalky, at the experimental platform of Polytechnic of La Salle Beauvais. A natural gradient test has been carried out using hot water as a tracer. Subsequently, have been analyzed in the laboratory the dynamics of the heat transport in porous media, so has been created another prototype at bench-scale. Several tests are conducted in laboratory on prototype, at bench-scale, filled with different grain size materials. The experiments consisted in injecting hot water flow at known temperatures in a porous medium column. The thermal response curves (BTCs) have been obtained. This study has permitted to investigate the critical issues regarding the heat transport in porous media to vary the grain size, and obtain the results regarding the relationship between the flow rate and the heat loss

and the heat balance and validity of the non-thermal equilibrium, to describe the behaviour of fluid and solid phase varying the particle size, which allowed, by comparing the data obtained in previous tests with fractured, to obtain important results. From these studies it was found that the specific surface of the medium plays an extremely important role. By varying the specific surface, the geothermal system (aquifer) seems to retain more or less heat. It would seem that aquifer characterized by an high specific surface, at the same flow rate, is better suited to retain heat, therefore a low specific surface system lends itself better to accumulate heat, to store it and to be therefore exploited as a heat accumulator. On the contrary, a system characterized by low specific surface area is more suited to enter heat from a geothermal system, as it tends to dissipate earlier heat respect to a high specific surface system. From this emerges another important factor affecting a fractured system. Furthermore, the theoretical thermal dispersion is much lower than the dispersion observed by laboratory tests. In fact, the thermal dispersion for a fractured system plays a very important role, is very significant as regards the behaviour of the between-extruded heat and is not negligible. The channelling effect plays an important role as well as the fracture matrix interaction. In the case of a fractured system, in fact, the channeling effect in the thermal BTCS and in the different parameters analyzed is very clear. The long tail and the anticipated peak depend channelling effect and matrix-fracture interaction.

This study show that the specific surface of the medium plays an extremely important role. By varying the specific surface area, the subsurface reservoir formations is able to retain more or less heat due to variation of thermal dispersion.

From the present studies, have been found, in fact, that an subsurface reservoir formations characterized by a low specific surface, at the same flow rate, at the same hydraulic and thermal properties, presents high capability to store heat respect to the subsurface reservoir formations characterized by a high specific surface system that has better properties to dissipate heat In fact, if the fractures in the reservoir have a high density and are well connected, such that the matrix blocks are small, the optimal conditions for thermal exchange are not reached as the matrix blocks have a limited capability to store heat. Therefore, subsurface reservoir formations with large porous

matrix blocks will be the optimal geological formations to be exploited for geothermal power development.
In fact, if the fractures in the reservoir have a high density and are well connected, such that the matrix blocks are small, the optimal conditions for thermal exchange are not reached as the matrix blocks have a limited capability to store heat.
The estimation of the average effective thermal conductivity coefficient shows that it is not efficient to store thermal energy in rocks with high fracture density because the fractures are surrounded by a matrix with more limited capacity for diffusion giving rise to an increase in solid thermal resistance.
On the other hand, isolated permeable fractures will tend to lead to the more distribution of heat throughout the matrix.
The study could help to improve the efficiency and optimization of industrial and environmental systems, and may provide a better understanding of geological processes involving transient heat transfer in the subsurface.
Future developments of the current study will be carrying out investigations and experiments aimed at further deepening the quantitative understanding of how fracture arrangement and matrix interactions affect the efficiency of storing and dissipation thermal energy in aquifers. This result could be achieved by means of using different formations with different fracture density and matrix porosity.
Results from this study are very interesting for further development of existing geothermal technologies. It would be interesting to proceed with the study of heat transport to vary the thickness, roughness and other key parameters of fractures and continue to study new geothermal systems that allow, starting from the experimental knowledge, to contain greater the environmental impact on water and soil of low enthalpy geothermal systems, and at the same time allow to reduce the costs while achieving an optimization of the system.

key words: heat transport, fractured media, porous media, physical model, geothermal, low enthalpy

EXTENDED ABSTRACT

L’energia geotermica a bassa entalpia è una risorsa rinnovabile che è ancora poco sviluppata al giorno d'oggi rispetto al suo potenziale sviluppo in Italia e in tutto il Mondo. La maggior parte delle sue possibilità di impiego sono già state studiate, come ad esempio: riscaldamento e il raffreddamento degli edifici privati e pubblici, sbrinamento di strade, raffreddamento di processi industriali, sistemi di essiccamento delle di produzioni agroalimentari, desalinizzazione.
Due dei principali limiti legati allo sviluppo del sistema geotermico a bassa entalpia riguardano i costi iniziali, la poca conoscenza che l’opinione pubblica ha su questo argomento e cosa potrebbe provocare nel tempo la variazione termica su acqua e suolo dovuta allo sfruttamento di questi sistemi geotermici.
Al fine di ottimizzare l'efficienza degli impianti che usano le acque sotterranee come risorsa geotermica, il flusso e la dinamica di trasporto di calore in falde acquifere hanno bisogno di essere ben caratterizzati. La mancata conoscenza riguardo le dinamiche di trasporto di calore di acquiferi fratturati ma anche porosi porta a sovradimensionare gli impianti aumentando ulteriormente i costi iniziali.
La risorsa geotermica a bassa entalpia, tuttavia, è sempre utilizzabile e facilmente disponibile.
Le sperimentazioni effettuate in questo percorso di ricerca sono state sviluppate principalmente nell’ottica di poter analizzare le potenzialità e per ottimizzare sistemi geotermici aperti a bassa entalpia che operano all'interno dello stesso pozzo geotermico, quindi sistemi cortocircuitati. Questo tipo di sistema è stato pensato soprattutto per diminuire l'impatto ambientale dovuto dall'iniezione di acqua a temperatura maggiore

rispetto alla temperatura di presa. In questo modo, infatti, è possibile contenere le variazioni termiche all'interno di una stessa area di interesse.
Nel corso di questi tre anni di dottorato sono stati condotti diversi esperimenti a scala di banco con i quali sono stati prodotti dei lavori pubblicati su riviste scientifiche internazionali. Gli esperimenti si sono divisi in due macro categorie accumunate dall'unico obiettivo di comprendere le dinamiche di trasporto di calore: studio di calore in mezzi fratturati e studio di calore in mezzi porosi a diversa granulometria. Il primo test ha riguardato in particolare lo studio del trasporto di calore in mezzi fratturati. Pertanto si è costruito un prototipo a scala di banco presso il laboratorio di geo-ingegneria ambientale del Politecnico di Bari. Su questo prototipo sono stati eseguiti diversi test in particolare è stato analizzato il comportamento del trasporto di calore prima in singola frattura e successivamente in un network di fratture. Il trasporto di calore è stato così confrontato con il trasporto di massa.
Sono state ottenute delle curve di risposta termica (BTCs) che sono state modellate con l' *Esplicit Network Model* (ENM), che si basa su un adattamento della soluzione di un Tang per il trasporto dei soluti in una singola frattura semi-infinita incorporata in una matrice porosa.
La stima del *time moment analisys*, *tailing* e altri parametri adimensionali hanno permesso di comprendere meglio le dinamiche di trasporto di calore e l'efficienza di scambio termico tra le fratture e matrice. I risultati sono stati confrontati con i precedenti studi sperimentali in materia di trasporto di soluti.
Successivamente, sono state eseguite delle prove in sito presso la piattaforma sperimentale dell'università di *LaSalle di Beauvais* (Francia) con la quale per due anni c'è stato un rapporto di collaborazione con l'obiettivo di studiare il trasporto di calore in mezzi gessosi fratturati. Sono state eseguite delle prove a gradiente naturale utilizzando il calore come tracciante. Successivamente ci si è concentrati sullo studio delle dinamiche del trasporto di calore in mezzi porosi. E' stato creato un altro prototipo per studiare il trasporto di calore in mezzi porosi. Sono tati condotti diversi test sul prototipo a scala di banco riempito con materiale avente diversa granulometria. Gli esperimenti consistevano nell'iniettare portate d'acqua calda a temperatura nota in corrispondenza

di termocoppie posizionate lungo una colonna mezzo poroso. Sono state così ottenute delle curve di risposta termica (BTCs). Questo studio ha permesso di studiare le criticità riguardanti il trasporto del calore in mezzi porosi al variare della granulometria, ed ottenere dei risultati in merito al rapporto tra la velocità di flusso e la dispersione termica e la validità dell'equilibrio termico e del non equilibrio termico per descrivere il comportamento tra fase fluida e solida al variare della granulometria, che hanno permesso, confrontando i dati ottenuti nei test precedenti con il fratturato di ottenere dei risultati importanti. Dal confronto di questi studi, è emerso che la superficie specifica del mezzo gioca un ruolo estremamente importante nelle dinamiche di trasporto di calore. Al variare della superficie specifica, il sistema geotermico (acquifero) riesce a trattenere più o meno calore. In particolare, gli studi effettuati, dimostrano che un acquifero caratterizzato da un mezzo con alta superficie specifica, a parità di portata, si presta meglio a trattenere calore, pertanto un sistema a bassa superficie specifica si presta meglio ad accumulare calore, ad immagazzinarlo e ad essere quindi sfruttato come accumulatore di calore. Al contrario, un sistema caratterizzato da bassa superficie specifica è maggiormente indicato per immettere calore proveniente da un sistema geotermico, in quanto tende a cedere molto prima il calore rispetto ad un sistema ad elevata superficie specifica. Da questo emerge un altro fattore importante che riguarda un sistema fratturato. Il valore della dispersione termica teorica risulta molto inferiore rispetto al valore della dispersione osservata dai test di laboratorio. Infatti la dispersione termica per un sistema fratturato gioca un ruolo molto importante, è molto significativa per l'analisi delle dinamiche del trasporto di calore e non è trascurabile. E' emerso inoltre che anche l'effetto channeling gioca un ruolo importante così come l'interazione frattura matrice. Nel caso di un sistema fratturato, infatti, l'effetto channeling nelle curve di risposta termica (BTCs) e nei diversi parametri analizzati è molto evidente. La lunga coda e il picco anticipato dipendono dell'effetto channeling e dall' interazione matrice-frattura.

Dall'analisi di questi studi emerge che la superficie specifica del mezzo gioca un ruolo estremamente importante. Infatti variando la superficie specifica, le formazioni caratteristiche di un acquifero tenderebbero ad immagazzinare più o meno calore. Mezzi con bassa superficie specifica del mezzo, a parità di portata, proprietà idrauliche e termiche,

presentano elevata capacità di immagazzinare calore rispetto a formazioni caratterizzate da un'alta superficie specifica che presentano migliori proprietà di dissipare calore. Se le fratture hanno un'alta densità e sono ben collegate, tale che i blocchi matriciali sono piccoli, la condizione ottimali per lo scambio termico non è raggiunta in quanto i blocchi della matrice hanno una limitata capacità di accumulare calore. Pertanto, sembrerebbe che le formazioni con matrice porosa a grandi blocchi siano le formazioni geologiche ottimali da sfruttare per lo sviluppo di energia geotermica.
La stima della effettiva coefficiente di conducibilità termica media dimostra che le rocce con alta densità di fratturazione non si prestano ad immagazzinare l'energia termica, poiché le fratture sono circondate da una matrice con più limitate capacità di diffusione dando luogo ad un aumento della resistenza termica. Lo studio potrebbe contribuire a migliorare l'efficienza e l'ottimizzazione dei sistemi industriali e ambientali, e può permettere una migliore comprensione dei processi geologici che comportano un trasferimento di calore nel sottosuolo. Gli sviluppi futuri di questo studio si baseranno su ulteriori indagini ed esperimenti volti ad comprendere quantitativamente come l'interazione frattura-matrice può influenzare l'efficienza di uno stoccaggio e i fenomeni di dissipazione di energia termica nelle falde acquifere. Questo risultato potrebbe essere ottenuto attraverso esperimenti di laboratorio che utilizzino formazioni differenti con diversa densità di frattura e porosità della matrice. Sarebbe interessante procedere con lo studio del trasporto di calore al variare dello spessore, rugosità e altri parametri chiave delle fratture e proseguire con studiare nuovi sistemi geotermici che permettano di contenere l'impatto ambientale sull'acqua e sul suolo di sistemi geotermici a bassa entalpia, e allo stesso tempo di diminuire i costi ottenendo un'ottimizzazione del sistema.

Parole chiave: trasporto di calore, mezzo fratturato, mezzo poroso, modello fisico, geotermia, bassa entalpia

INDEX

# *INTRODUCTION*

The present research work has the objective to investigate the heat transfer mechanisms in fractured aquifers and porous aquifers, for the development of low-enthalpy geothermal systems for heating and cooling of buildings, for cooling of waters from industrial process, and drying of food products.

The low enthalpy geothermal energy, especially in Italy, is still underdeveloped compared to the potential.

The reasons for this non-development of the resource is due primarily to the economical investments that a low enthalpy geothermal system involves. Especially, the costs are related to the excavations that should be carried by the installation of geothermal probes. Other reasons are due to miss information and disclosures on the low enthalpy geothermal resource and the preconceptions that revolve around the use of this resource. This study aims to determine which of aquifer fractured and porous is suitable better towards a low enthalpy geothermal system for cooling and heating. The low enthalpy geothermal resource, however, is always usable and easily available. Soil can naturally store energy from atmosphere and heat flow coming up from rock basement. The energy stored in the ground can be extracted with a Borehole Heat Exchanger (BHE) that uses the heat stored in soil to supply power to a heat pump that supplements the power needed for heating a space. Ground source heat exchanger coupled with heat pump is the most popular direct use of low-enthalpy geothermal energy. This is a widespread type of acclimatization system, because it can be used for heating or cooling, and can be developed anywhere, and anytime with a very low environmental impact.

# *I PART*
# *LOW ENTHALPY GEOTHERMAL RESOURCES*

In this first part shows more information in the literature regarding geothermal energy, its limitations and its potential, highlighting possible future developments. Ample space has been given to the technologies of low-enthalpy geothermal systems and the laws that govern the transport of heat.

# *CHAPTER 1*
# *GEOTHERMAL SYSTEM AND RESOURCES*

## 2.1.0 Basic concept of geothermal energy: thermal structure of the Earth

The feasibility of producing geothermal heat is strongly dependent on the thermal and geological conditions of the subsurface.
The Earth's structure can be approximated by a series of concentric spherical shells. The large-scale features of the Earth's internal structure are shown in Fig.1.

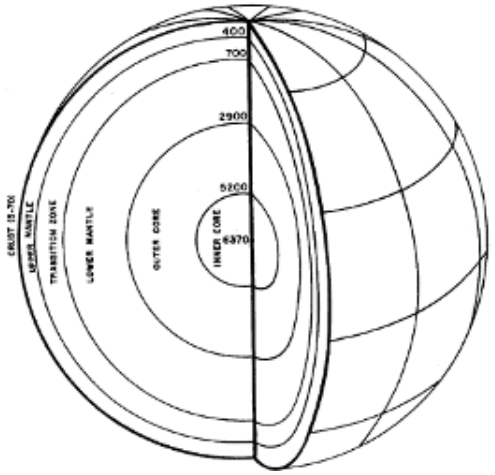


Figure 1 Internal structure of the Earth. Thickness of the crust and depths to various discontinuities from the Earth's surface are given in kilometres [Geothermal Energy: An Alternative Resource for the 21st Century Di Harsh K. Gupta, Sukanta Roy].

The core, constituted by the two innermost regions, has the greatest average density, exceeding 104 $kgm^{-3}$. In spite of differing views on the details of the composition of the core, it is now fairly well accepted that iron–nickel alloy is the most probable constituent. However, the observed characteristics of the core do not match with its being purely iron-nickel-too dense-and the presence of some lighter material is postulated. Silicon has been proposed to be an alloying element in the core. For this to be true, it is necessary to assume the presence of suitable conditions, in the early history of the Earth, making it possible for large quantities of silicon to reduce-stripping away oxygen atoms and adding electrons. Sulphur is another light element that has been suggested as being present in the core. This would require a different set of conditions to exist in the early history of the Earth. Irrespective of its origin, certain aspects of the present structure of the core are well established from seismological evidence. The outer part is molten since it does not transmit shear waves. The study of compressional waves, which travel through the inner part of the core, shows higher velocities, leading to the suggestion that the inner core is solid.

Results of the study of free oscillation of the Earth, as well as the detection of seismic waves that have travelled through the inner core as shear waves, confirm the above suggestion (Geothermal Energy: An Alternative Resource for the 21st Century Di Harsh K. Gupta, Sukanta Roy).

The mantle overlies the core. It has an average density of 4.5 $^{-103}$ kgm $^{-3}$, indicating that its constituents are rocky rather than metallic. The composition of the mantle is not completely determined. However, based on its density, seismic wave velocities, and study of rocks that are believed to have come from the mantle, oxygen and silicon are believed to predominate, with magnesium and iron being the most abundant metallic ions. On the basis of seismic wave properties, the mantle could also be divided into a number of concentric shells. The lower mantle extends from a depth of about 700km within the Earth to the top of the core at 2,900 km. As a result of the increase in pressure, the seismic velocity and density increase with depth in the lower mantle. The amount of iron in the silicate minerals also increases with depth, a factor that also contributes to the increase in density and velocity. The sudden changes in seismic

velocity in the transition zone extending from about 400 km depth to the top of the lower mantle are more likely related to alterations in the crystal structure than to changes in the composition (Geothermal Energy: An Alternative Resource for the 21st Century Di Harsh K. Gupta, Sukanta Roy)

Along with the Earth's structure and composition, know the temperature distribution within the Earth has been one of the fundamental research problems that impact our understanding of the evolution of the Earth. The present day temperature distribution inside the Earth depends on:

1 The original temperature distribution shortly after formation,
2 The distribution and intensity of heat sources, both of which are time-dependent,
3 The mechanism of internal heat transfer- conduction, convection or both (Veroogen, J., 1980)

Even after several decades of theoretical and experimental research, the thermal structure of the Earth continues to be poorly understood. The uncertainty is mostly because the temperature distribution is inseparable from the hypothesis of the Earth's origin. A probable model of temperature distribution with depth within the Earth is shown in Fig. 2.

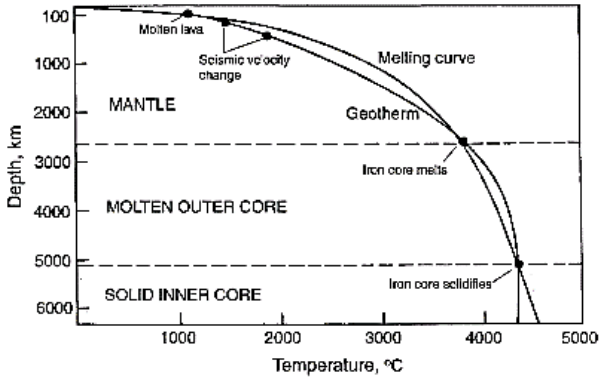


Figure 2 Variation of temperature with depth within the Earth (modified from Press and Seiver, 1998). In deeper portions, overall uncertainties in temperatures could be as much as 1,000 –1,500 °C.

### 2.1.2 A short history of geothermal energy in Italy

Italy was a pioneering country in exploiting the potentials of geothermal resources for energy power production. Already in 1904, when Piero Ginori Conti successfully experimented with the generation of electricity from geothermal steam, the first geothermal power plant was built in Larderello in Tuscany (Luzzini, 2012). Italy is presently ranked in the top five countries worldwide for geothermal power production and, according to the European Geothermal Energy Council, it is expected to produce by 2020 an electricity installed capacity of 1965 MW and 15.600 GWh, which is the 4,2% of the national energy demand (Zervos et al., 2011).
Data collected in 2010 show that the geothermal production in Italy is now only 1,8% of the total national electricity production, but it is about 25% for Tuscany, where the two major geothermal areas of the country are located: Larderello-Travale/Radicondoli and Mount Amiata (Bertani, 2012).
The use of geothermal baths is strongly rooted in the Italian culture, at least since oman times. The direct use of geothermal heat has important applications, e.g., the district heating systems of town of Ferrara in Emilia Romagna, and the last decade saw a revived and growing interest in the use of geothermal heat pump technologies for exploiting low temperature resources. However, actual levels of knowledge and understanding of the potentials of geothermal resources as a renewable energy source and the implications of their use are generally low in the Italian society. One of the most importante project Italy has been the VIGOR dedicated to the assessment of the feasibility of developing geothermal energy in four regions of southern Italy (Albanese et al., 2014) and to the diffusion of knowledge of the numerous geothermal energy technologies (Botteghi et al., 2012; Abate et al., 2014).

### 2.1.3 Geothermal energy utilization: high and low enthalpy geothermal systems

Geothermal energy consists traditionally in the exploitation of the earth heat. In the underground, temperature increases on average between 18°C and 20°C per kilometre of depth, and a larger geothermal gradient can be found in many places (Lubimova, E.A.,

1969). Table 1 reports the classifications proposed by a number of authors. A standard method of classification, as with terminology, would avoid confusion and ambiguity, but until such a method exists, we must indicate the temperature values or ranges involved case by case, since terms such as low, intermediate and high are meaningless at best, and frequently misleading. Frequently a distinction is made between water or liquid dominated geothermal systems and vapour-dominated (or dry steam) geothermal systems (White, D. E., 1973).

Table 1 Classification of geothermal resources based on temperature (°C)

| | **Muffer and Catadi (1978)** | **Hochstein (1990)** | **Benderitter and Cormy (1990)** | **Nicholson (1993)** | **Axelsson and Gunnlaugsson (2000)** |
|---|---|---|---|---|---|
| **Low enthalphy resources** | <90 | <125 | <100 | ≤150 | >190 |
| **Intermediate enthalpy resources** | 90-150 | 125-225 | 100-200 | – | – |
| **High enthalpy resources** | >150 | >225 | >200 | >150 | >190 |

Geothermal systems can be classified into:

1) Low energy (associated with low depth)
2) High-energy systems (in many cases associated with high depth).

High-energy systems can be developed by pumping directly the hot geo-fluid in one well and injecting the cooled geo-fluid in another well, using a heat exchanger at the surface that vaporises a working fluid used to turn an electricity-generating turbine (Lubimova, E.A., 1969). Electricity generation is the most important form of utilization of high-temperature geothermal resources (150 °C). The medium-to-low temperature resources (<150 °C) are suited to many different types of application.

Low enthalpy geothermal energy systems, for which the ground temperature is too low to produce electricity are generally developed using heat pumps to produce directly heat.

Two kinds of systems are currently investigated for low (or very low) energy systems:

a) In low permeability or unsaturated media, groundwater can not be exploited in sufficient amount, geothermal probes (or Boreholes Heat Exchangers) can be installed (Gehlin, S., 2002);
b) In highly permeable geological formations, groundwater can be pumped to the surface (Castello, M., 2004).

In the former case, a coolant fluid is circulated in the probes to extract the underground heat. A closed loop of pipe, placed either horizontally (1 to 2 m deep) or vertically (50 to 100 m deep, Borehole Thermal Energy Storage - BTES), is placed in the ground. A coolant fluid is circulated through the plastic pipes to either collect heat from the ground in the winter or reject heat to the ground in the summer.

In the last case, an open loop system uses groundwater directly in the heat exchanger and then discharges it into another faraway well, into a stream or lake, depending upon environment conditions and local regulation.

All these systems must be optimised in relation with the most adequate ground source heat pump system to be designed in accordance with the local geological and hydro-geological conditions. The development of such systems requires estimating the heat fluxes that can be injected or extracted from the underground. It is thus important to develop computation and modelling tools for assessing the hydrogeological feasibility of such systems.

The classical Lindal diagram (Fig. 3), which shows the possible uses of geothermal fluids at different temperatures, still holds valid, but the generation of electric energy in binary cycle plants can now be added above 85 °C.

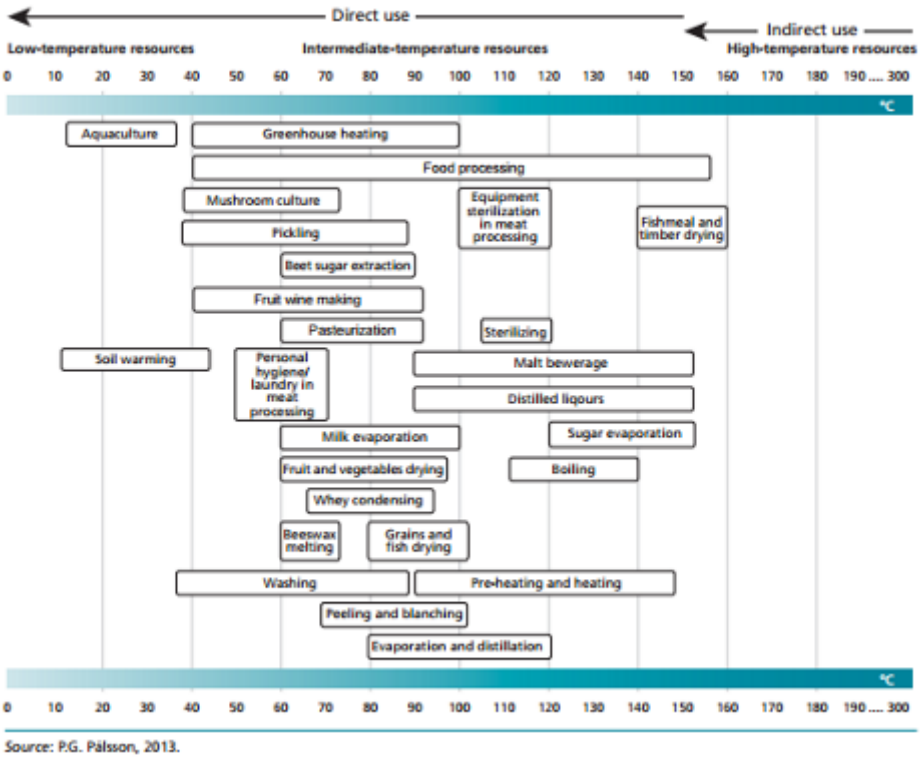


Source: P.G. Pálsson, 2013.

Figure 3 Lindal diagram of potential uses of geothermal energy in the agriculture, and agro-industry sectors.(Source: P.G. Pálsson, 2013).

In direct applications, geothermal reservoirs of low to intermediate temperature (20-150 °C) are exploited, mainly in heat pumps for heating and cooling, greenhouses, pools and spas, space heating, aquaculture and industrial processes.

High-temperature geothermal reservoirs (150-300 °C) are exploited for indirect use applications, including steam and electricity production (Islandsbanki, 2011). Electricity is also generated using intermediate-temperature (70-149 °C) geothermal resources. The electricity from conventional or binary power plants is used in industrial processes, and hot water from binary power plants can be used for direct applications (Ogola, Davidsdottir and Fridleifsson, 2012). Steam and superheated water are normally used

in certain agro industrial processes that require high temperatures, although lower temperatures can sometimes be used, especially for drying agricultural products (Lund, 1996).

Sources of geothermal energy for agricultural and agro-industrial uses Agricultural and agro-industrial uses form a very important part of geothermal energy applications. In general, four types of direct application of geothermal energy in agriculture can be identified (Popovski, 2009):

- greenhouse heating;
- aquaculture (fish farming and algae production);
- agro-industrial processes;
- soil heating (of open-field plant root systems).

The sources of geothermal energy for agricultural and agro-industrial uses include low- and intermediate-temperature geothermal resources, as well as the waste heat and cascading water from geothermal power plants (Fig.4).

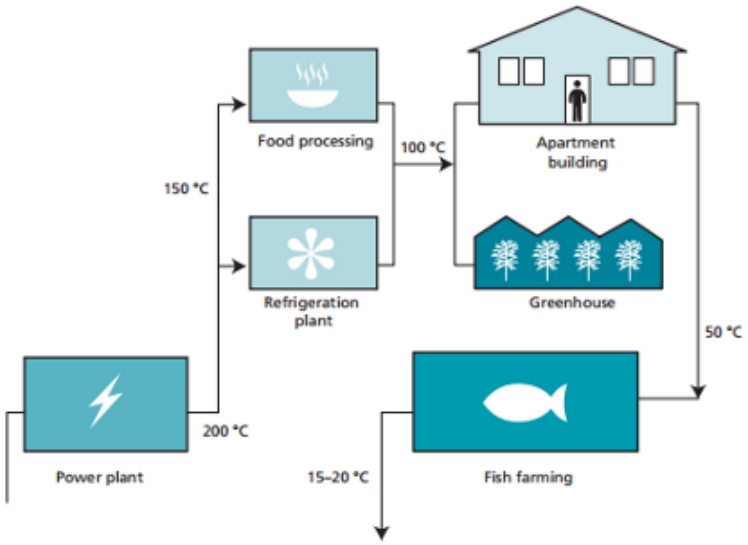


Figure 4 Cascading from a geothermal power plant, Source: Geo-Heat Center, Klamath Falls, Oregon (USA). Adapted with permission.

The lower limit of 20 °C is exceeded only in very particular conditions, or by the use of heat pumps.

The Lindal diagram (Fig.3) emphasizes two important aspects of the utilization of geothermal resources (Gudmundsson, 1988):

1) First, with cascading and combined uses, it is possible to enhance the feasibility of geothermal projects,
2) Second, the resource temperature may limit the possible uses.

Existing designs for thermal processes can, however, be modified for geothermal fluid utilization in certain cases, thus widening its field of application. The Lindal diagram, as it has been widely referred to in literature, is more or less valid even to this day and serves as a rough illustration of the temperature requirements. It must be noted that many of the applications are practiced over a range of temperatures rather than a single temperature as suggested in the diagram. It can be seen from the Lindal diagram that, in general, the agricultural and aqua cultural applications require the lowest temperatures, followed by space heating and industrial applications. Few additional industrial applications with specific temperature requirements have been described by Lienau (1995).

One very common and extensive application in recent times has been in geothermal (ground source) heat pumps. A geothermal heat pump makes use of the relatively stable temperature at a depth of a few meters in the ground (low enthalpy geothermal resources). This kind of resources associated with heat pumps is always utilizable. Indeed during winter, the subsurface temperature is warmer than the room temperature inside a house, whereas during summer the subsurface temperature may be cooler. Geothermal exchange technology takes advantage of the thermal energy stored in the surface area of the Earth (first 100 m). Up to 10–15 m deep approximately, ground heat is supplied by the sun and rain. From there the underground temperature increases about 3 °C per 100 m depth, due to the internal thermal energy of the Earth. On average, the underground temperature at 10 m depth remains constant throughout the year and substantially equal to the average temperature of the place (Buzăianu, A.; et al 2015, Carmo, C.; et al 2015, Droulia, F et al 2009, Graf, S.; et al 2016).

Initially geothermal exchange systems were developed for heating in cold climates, hence its development in northern European countries, USA and Canada, but they are also suitable for cooling, increasing their profitability and interest in countries of southern latitudes. In cooling mode, heat is extracted from the building and this is transferred to the ground. In heating mode, heat is extracted from the Earth and it is transferred to the building (Fig. 5).

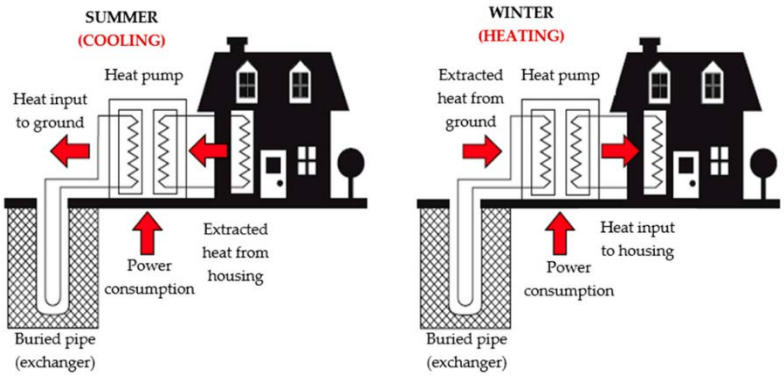


Figure 5 Typical operation of a geothermal exchange system with heat pump.

Of course the underground temperature remains unchanged (or it does so very slightly depending on depth), but the room temperature is what changes. (Márquez, J., et al 2016).

There are four basic types of ground loop systems:

1. horizontal,
2. vertical,
3. and pond/lake are closed-loop systems
4. the open-loop option

Which one of these is best depends on the climate, soil conditions, available land, and local installation costs at the site. All of these approaches can be used for residential and commercial building applications.

Closed-loop systems

Closed-loop ground-coupled heat pumps and open-loop indirect groundwater heat pumps are considered to be one of the most energy efficient and environmental friendly air-conditioning systems for temperate zones (Hikari et al., 2007). The extensive use of these technologies is still limited in Italy, mainly because of a lack of information on the advantages and uncertainties on possible long term environmental effects. This has led to excessive administrative restrictions by local agencies and has discouraged new investments by private and public enterprises. Nevertheless the recent increase in primary non-renewable energy costs and the new public policies aimed at reducing greenhouse gas emissions, especially in the European Union (EC, 2006), have stimulated efforts by public agencies and private stakeholders to develop these new technologies by means of research activities and industrial applications (Lo Russo, S. & Civita, M.V., 2009).

Most closed-loop geothermal heat pumps circulate an antifreeze solution through a closed loop - usually made of plastic tubing - that is buried in the ground or submerged in water. A heat exchanger transfers heat between the refrigerant in the heat pump and the antifreeze solution in the closed loop. The loop can be in a horizontal, vertical, or pond/lake configuration.

One variant of this approach, called direct exchange, does not use a heat exchanger and instead pumps the refrigerant through copper tubing that is buried in the ground in a horizontal or vertical configuration. Direct exchange systems require a larger compressor and work best in moist soils (sometimes requiring additional irrigation to keep the soil moist), but you should avoid installing in soils corrosive to the copper tubing. Because these systems circulate refrigerant through the ground, local environmental regulations may prohibit their use in some locations.

Closed-loop systems require a heat exchanging circulating fluid, often referred to as antifreeze. A good antifreeze solution will have the following favourable qualities:

1. low cost
2. low toxicity

3. low viscosity
4. low volatility
5. low corrosivity
6. low flammability
7. low freezing temperature
8. high thermal conductivity
9. long service life

The amount of fluid contained within the pipe is dependent on the length and diameter of the pipe. For example, a ¾-inch inner diameter pipe that stretches for 1000 feet will contain 25-30 gallons of fluid underground. The antifreeze solution types vary as to their risk to the environment. The common types of solutions include the following:

1. water
2. potassium acetate
3. sodium chloride water
4. calcium chloride water
5. ethanol and water
6. methanol and water
7. ethylene glycol and water
8. propylene glycol and water

Polyethylene is the only type of pipe that is recommended. This material is flexible, very resistant to weathering and good heat transfer medium. Some manufacturers guarantee the life of the pipe to be at least 50 years. Also, the joints can be fused together by heat, which creates a strong connection. Pipe diameters of 3/4-inch or one inch are most commonly used. Larger sized pipe tends to be more difficult to handle and more expensive. The amount of subsurface pipe needed depends on several factors including energy demand, structure and size of the building, climate, and location of the loop and thermal conductivity of the subsurface. Many contractors offer computer analysis that

determines the necessary length of pipe to meet the energy requirements of the building.

Closed-loop systems: Horizontal

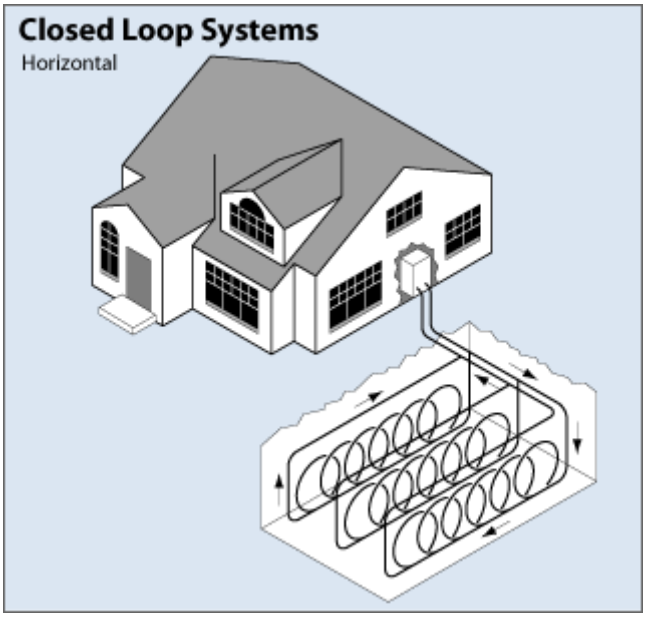


Figure 6 Closed-loop systems: Horizontal

This type of installation is generally most cost-effective for residential installations, particularly for new construction where sufficient land is available. It requires trenches at least four feet deep. The most common layouts either use two pipes, one buried at six feet, and the other at four feet, or two pipes placed side-by-side at five feet in the ground in a two-foot wide trench. The Slinky method of looping pipe allows more pipe in a shorter trench, which cuts down on installation costs and makes horizontal installation possible in areas it would not be with conventional horizontal applications.

A horizontal loop can be placed in narrow, 5-10 feet deep trenches that are hundreds of feet long. The ground loop can be installed in parallel trenches that do not require such lengths. Loops of overlapping coils require even shorter trenches. An installer can place 500 feet of overlapped coils in an 80 foot trench, or two loops totalling 1000 feet of pipe in the same trench. Coils can be laid flat at the bottom of a trench or placed

vertically in a narrow trench. The depth of the trench must be below the frost line to avoid any problems in the winter. A depth of five feet is usually sufficient in Pennsylvania. For domestic systems that use a pond, the minimum pond size should be 6-8 feet deep and 1/2 acre in area (approximately 150 feet by 150 feet).

Closed-loop systems: Vertical

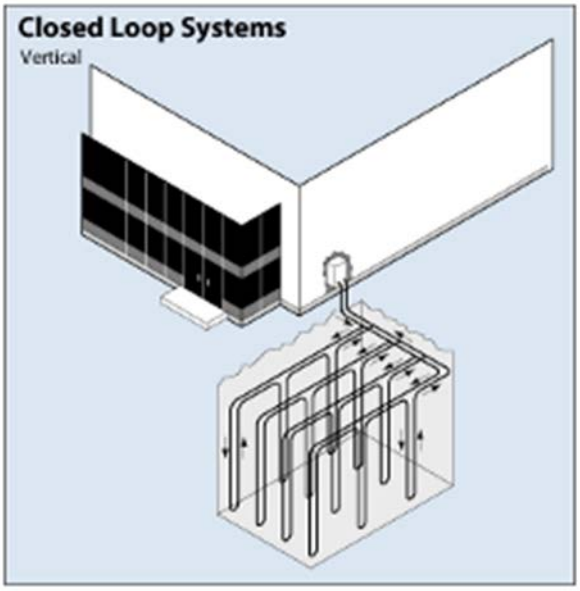


Figure 7 Closed-loop systems: Vertical

Large commercial buildings and schools often use vertical systems because the land area required for horizontal loops would be prohibitive. Vertical loops are also used where the soil is too shallow for trenching, and they minimize the disturbance to existing landscaping. For a vertical system, holes (approximately four inches in diameter) are drilled about 20 feet apart and 100 to 400 feet deep. Into these holes go two pipes that are connected at the bottom with a U-bend to form a loop. The vertical loops are connected with horizontal pipe (i.e., manifold), placed in trenches, and connected to the heat pump in the building.

Closed-loop systems: Pond/Lake

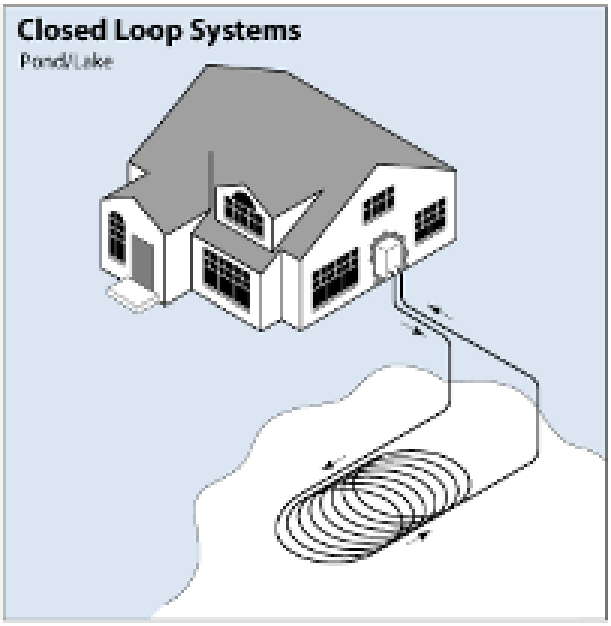


Figure 8 Closed-loop systems: Pond/Lake

If the site has an adequate water body, this may be the lowest cost option. A supply line pipe is run underground from the building to the water and coiled into circles at least eight feet under the surface to prevent freezing. The coils should only be placed in a water source that meets minimum volume, depth, and quality criteria.

Open-loop system

This type of system uses well or surface body water as the heat exchange fluid that circulates directly through the GHP system. Once it has circulated through the system, the water returns to the ground through the well, a recharge well, or surface discharge. This option is obviously practical only where there is an adequate supply of relatively clean water, and all local codes and regulations regarding groundwater discharge are met.

Open GSHP systems, also known as groundwater heat pump (GWHP) systems, typically depend upon groundwater to supply or accept heat. Open systems do not confine

fluid to a loop of pipes; they use a pumping well to move water through the heat pump. Although surface water could possibly be used, most open systems rely on groundwater. The water is disposed of by a surface or subsurface method. The water supply well must yield enough water to transport the required amount of heat.

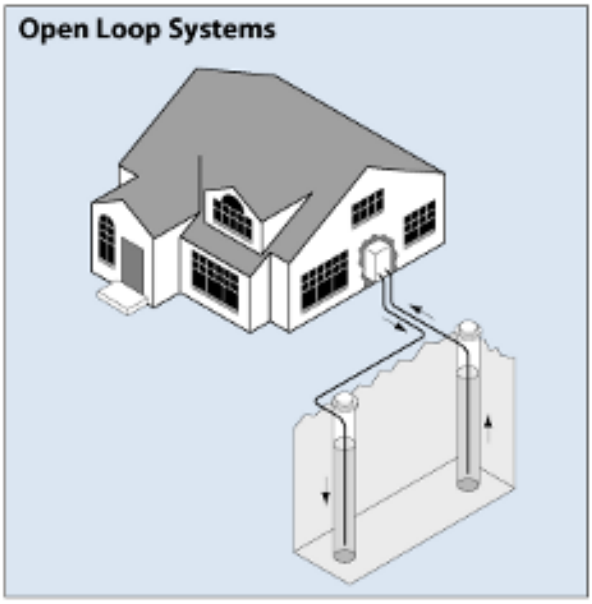


Figure 9 Open-loop system

Hybrid systems

Hybrid systems using several different geothermal resources, or a combination of a geothermal resource with outdoor air (i.e., a cooling tower), are another technology option. Hybrid approaches are particularly effective where cooling needs are significantly larger than heating needs. Where local geology permits, the "standing column well" is another option. In this variation of an open-loop system, one or more deep vertical wells is drilled. Water is drawn from the bottom of a standing column and returned to the top. During periods of peak heating and cooling, the system can bleed a portion of the return water rather than reinjecting it all, causing water inflow to the column from the surrounding aquifer. The bleed cycle cools the column during heat rejection, heats it during heat extraction, and reduces the required bore depth.

Therefore, heat pumps can be used both for heating as well as cooling. The advantage of ground source heat pumps relative to air source heat pumps is that the difference of room temperature from the ground temperature is always smaller than the difference of the room temperature from the outside air temperature. Therefore, ground source heat pumps need to do less work than air source heat pumps. Heat pump systems use groundwater aquifers and soil temperatures in the range 5–30 °C. A comprehensive review of the working of ground source heat pumps, efficiency and cost considerations is given by Clauser (2006). Direct heat use is one of the oldest, most versatile and also the most common form of utilization of geothermal energy. Bathing, space and district heating, agricultural applications, aquaculture and some industrial uses are the best-known forms of utilization, but heat pumps are the most widespread. There are many other types of utilization, on a much smaller scale, some of which are unusual. Space and district heating has made great progress in Iceland, where the total capacity of the operating geothermal district heating system had risen to about 1,200 MWt by the end of 1999, but systems are also widely distributed in the East European countries, as well as in the United States, China, Japan, France and so on. Geothermal district heating systems are capital-intensive.

The main costs are initial investment costs, for production and injection wells, down-hole and transmission pumps, pipelines and distribution networks, monitoring and control equipment, peaking stations and storage tanks. Operating expenses, however, are comparatively lower than in conventional systems, and consist of pumping power, system maintenance, control and management. A crucial factor in estimating the initial cost of the system is the thermal load density, or the heat demand divided by the ground area of the district. A high heat density determines the economic feasibility of a district heating project, since the distribution network is expensive. Some economic benefit can be achieved by combining heating and cooling in areas where the climate permits. The load factor in a system with combined heating and cooling would be higher than the factor for heating alone, and the unit energy price would consequently improve (Lund, J.W et al, 2000).

Space cooling is a feasible option where absorption machines can be adapted to geothermal use. The technology of these machines is well known, and they are readily available on the market. The absorption cycle is a process that utilizes heat instead of electricity as the energy source. The refrigeration effect is obtained by utilizing two fluids: a refrigerant, which circulates, evaporates and condenses, and a secondary fluid or absorbent. For applications above 0 °C (primarily in space and process conditioning), the cycle uses lithium bromide as the absorbent and water as the refrigerant. For applications below 0 °C an ammonia/water cycle is adopted, with ammonia as the refrigerant and water as the absorbent. Geothermal fluids provide the thermal energy to drive these machines, although their efficiency decreases with temperatures lower than 105 °C.

Geothermal 'space conditioning' (heating and cooling) has expanded considerably since the 1980s, following on the introduction and widespread use of heat pumps. The various systems of heat pumps available permit us to economically extract and utilize the heat content of low-temperature bodies, such as the ground and shallow aquifers, ponds and so on (Mands, E. et al 2001).

As our engineering readers will already know, heat pumps are machines that move heat in a direction opposite to that in which it would tend to go naturally, that is, from a cold space or body to a warmer one. A heat pump is effectively nothing more than a refrigeration unit (Rafferty, 1997). Any refrigeration device (window air conditioner, refrigerator, freezer and so on) moves heat from a space (to keep it cool) and discharges that heat at higher temperatures. The only difference between a heat pump and a refrigeration unit is the desired effect, cooling for the refrigeration unit and heating for the heat pump. A second distinguishing factor of many heat pumps is that they are reversible and can provide either heating or cooling in the space. The heat pumps, of course, need energy to operate, but in suitable climatic conditions and with a good design, the energy balance will be a positive one.

Ground-coupled and groundwater heat pump systems have now been installed in great numbers in twenty-seven countries, for a total thermal capacity of 6,875 MWt (in 2000).

The majority of these installations are in:

- the United States (4,800 MWt)
- Switzerland (500 MWt)
- Sweden (377 MWt)
- Canada (360 MWt)
- Germany (344 MWt)
- Austria (228 MWt) (Howard, J.H. (Ed.), 1975).

Aquifers and soils with temperatures in the 5 to 30 °C range are being used in these systems. World estimates, the equivalent savings in fuel oil add up to about 25 million tonnes per year and about 24 million tonnes in carbon emissions to the atmosphere per year (Ryan, G.P., 1981). Therefore, although the use of high-enthalpy geothermal resources for generation of electric power continues to be more popular, the economic as well as environmental benefits of using moderate-to-low enthalpy fluids to meet domestic heating, agricultural and several industrial energy needs should not be ignored today.

There is a large potential for development of direct use of geothermal energy in many parts of the World. Rising prices of oil over the past few years, the rapid increase in atmospheric $CO_2$ concentration resulting from burning of fossil fuels, and the extensive fallout of both the factors on the world economy has generated renewed interest in efficient utilization of low-enthalpy geothermal resources as an energy alternative for several nonelectrical applications such as space heating, greenhouse and aquaculture facilities, heat pumps and many industrial applications. The long-term economics of using geothermal resources for nonelectrical uses work out to be more attractive when compared with the requirements of conventional fuel resources in well-endowed geothermal regions, especially in the cold-climatic regimes of middle- and high-latitude belts. According to recent world estimates, the equivalent savings in fuel oil add up to about 25 million tonnes per year and about 24 million tonnes in carbon emissions to the atmosphere per year (Lund, J. W., et al, 2005). Direct use of geothermal waters turns out to be a more efficient process relative to generation of electric power from

geothermal resources because the losses incurred in the former are not imposed by the laws of thermodynamics. However, one difficulty with direct use is the fact that low-temperature geothermal waters cannot be transported to large distances without substantial heat loss. In these usages, heat is lost primarily due to inadequate insulation, low flow rates, and terminal temperature differences in heat exchangers and drains. The basic components of a low-enthalpy thermal distribution system are:

- assembly of transmission and distribution piping with pipelines of varying diameters depending upon flow rates,
- downhole and circulation pumps, along with regulators, valves, expansion joints, etc.,
- suitable heat exchangers for extracting heat from the warm geothermal waters. An up-to-date review of engineering and design practices is given in Lund et al. (1998).

A critical requirement in the system is adequate thermal insulation to prevent excessive heat loss and temperature drop in the fluid. There is a continuous decline in fluid pressure along the pipelines due to viscous friction losses. Changes in elevation along the pipeline affect the hydrostatic head. Therefore, to prevent pressure from dropping below a value that would result in local boiling, and to maintain sufficient flow throughout the entire network, pumps are essential. Surge tanks are required to prevent sudden and potentially damaging changes in the pressure due to sudden changes or surges in the flow. Impurities, such as hydrogen sulphides, carbon dioxide, chlorides, silica, bicarbonates and entrained sand particles cause corrosion, erosion and scaling in the distribution pipelines. Chemical corrosion and/or mechanical erosion can cause pipeline failure, whereas scaling increases pumping requirements as well as disrupting the operation of heat exchangers. Depending upon the severity of impurities, it may be necessary to provide special lining material for the pipeline.

Necessary allowance also needs to be made to accommodate axial expansion of metallic pipes due to high temperatures of the fluid. Excessive stresses caused by axial expansion could cause failure in pipeline, supports, joints or anchors. Conventional expansion devices; such as slip joints, bellows, U- or Z-shaped expansion joints; placed

at regular intervals along the pipeline provide adequate protection. At the present time, the most commonly used piping materials are carbon steel (which can withstand fluid temperatures exceeding 100 °C), fiberglass-reinforced plastic, polyvinyl chloride and asbestos cement.

Various methods are in use to provide insulation for the pipeline system. These range from placing the prefabricated pipe within another pipe with insulation in between, to burying the pipe in trenches under the Earth. The insulation material must be waterproof and watertight. Carbon steel pipes are insulated with polyurethane foam, rock wool or fiberglass. Conventional steel pipes are usually wrapped with polyvinyl chloride before burying in the ground. The nature and thickness of insulation depends on many factors such as the temperature of the fluids, flow rates, transmission length, type of soil and local water table. Many direct-use applications require geothermal fluids to be transmitted several kilometres from the site of its production. In such cases, it is necessary to estimate the temperature drop as a function of distance of transmission, flow rate, fluid temperature, etc. Temperature losses are lower for larger diameter pipes or higher flow rates.

### 2.1.4 Low enthalpy geothermal resources

In Italy, in recent years, the use of low-enthalpy geothermal energy for heating and cooling purposes of residential and commercial units increased mainly in the northern regions (Lo Russo et al 2011; Gemelli et al 2011). In the southern ones, the development of these solutions involves primarily the cooling phase during summer season (Magraner et al 2010, Galgaro et al 2012, Mendrinos et al 2012). To assess the ground ability to exchange heat with buildings, a better knowledge of the thermal properties of the subsoil is necessary (Yasar et al 2008, Sharqawy et al 2009, Pouloupatis et al 2011, Liebel et al 2012). In detail, conduction is the principal mode of heat transmission in the earth. Therefore, a correct evaluation of the thermal conductivity of rocks is fundamental to properly size borehole heat exchangers and related pumps (Robertson 1988, Clauser and Huenges 1995, Banks 2012). This feature is one of the main input

parameters in geothermal modeling since it directly controls the steady state temperature field and is a reference value to validate data obtained by indirect control methods applied in situ (hydrogeological and geothermal exploration). A general review of the thermal conductivity values described in literature for rocks and loose materials has been performed (Majorowicz et al 1987; Lee and Deming, 1998; Vosteen et al 2003; Waples and Waples 2004a; Waples and Waples 2004b; Davis et al 2007; Gruescu et al 2007; Alishaev et al 2012). However, at local scale, the different climate and environmental condition, together with the structural and geological features of the territory can modify porosity (i.e. water content), texture and homogeneity of the material, leading to thermal conductivity values significantly different from those defined from literature.

### 2.1.5 Low enthalpy geothermal resources in South of Italy

An overview of the geological and hydrogeological features of the four regions involved in the VIGOR Project (Calabria, Campania, Apulia and Sicily) has been performed. Relying on the Geological Map of Italy, scale 1:250.000 edited by ISPRA, the igneous, metamorphic and sedimentary outcrops can be easily recognized (Fig.10). The figure clearly shows that sedimentary rocks and deposits are dominant everywhere, magmatic rocks are located in the volcanic areas of Sicily (Mt. Etna) and Campania (Campi Flegrei-Ischia Island) whereas almost all metamorphic rocks can be found in northern Sicily and in Calabria.

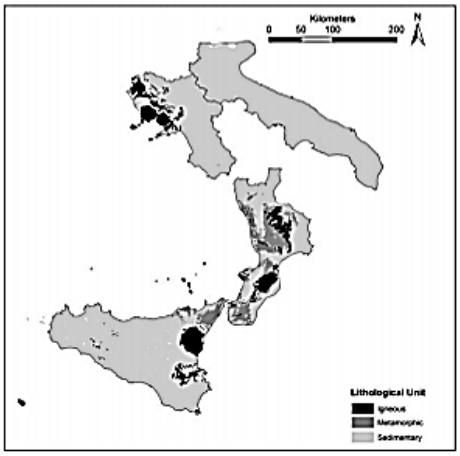


Figure 10 Areal distribution of the igneous, metamorphic and sedimentary rocks outcrops in the southern Italian regions involved in the VIGOR project (scale 1:250.000).

To validate at local scale the ($Wm^{-1}K^{-1}$) values of rocks and loose materials obtained from the screening of international literature, an extensive sampling campaign was carried out in the summer of 2012. Selected samples, representative of the main geological units (i.e. having the largest areal extent and present in the most urbanized areas) were

collected all over the territory and tested for thermal conductivity in laboratory (Fig.11).


Figure 11 Location of samples (Galgaro et al 2012, Di Sipio et al 2012)

The material taken in situ (about 294 samples) tries to respect, as far as possible, the lithological heterogeneity of the considered geological units, as known from literature. Aim of that work is to create a regional database of thermal conductivity for geological materials, comparable with the one created from literature data. It must be taken into consideration that the presence or absence of water is able to significantly improve the ability to conduct heat, so that particular attention must be paid in the measurement of wet and dry material. The consequence related to the influence of the entire stratigraphic sequence and to the thickness of the subsoil generally affected by geothermal heat exchangers (about 150 m) is treated in other works.

In every region the geological unit with the greatest areal extent has been selected according to the Geological Map of Italy 1:250.000 (Table 2, Fig.12).

| Region | Geological unit | Area ($km^2$) |
|---|---|---|
| Calabria | Granites and granodiorites-Paleozoic cycle | 2004 |
| Campania | Clays, limestones and clay unit (turbiditic) - Paleogene | 1864 |
| Apulia | Skeletal limestones of neritic and carbonate platform facies - Upper Cretaceous | 4955 |
| Sicily | Clays and marls – middle-lower Miocene | 2924 |

Table 2 The geological unit selected (VIGOR Project).

Each unit consists of several lithologies, formed in different geological period and characterized by different values of conductivity, as granite and granodiorites (Granites and granodiorites); clay, marl, calcarenites, limestone (Clays, limestones and clay unit); limestone, dolomite, dolomitic limestone, skeletal limestone (Skeletal limestones of neritic and carbonate platform facies); clay, marl, calcarenites, limestone (Clays and marls). Moreover, these units can be found in every other region but with a smaller extent. However, the outcrops may be subjected to weathering and fracturing phenomena that locally, in the same formation, determine variation of open porosity and, in this way, of the thermal properties of the rocks. Therefore, direct thermal measurements performed in situ or in laboratory on natural materials, duly selected according to the geological configuration, are necessary and strict recommended in order to create a regional database representative of the actual condition of the territories, useful for planners, public administrations and operators involved in the geothermal sector. In detail, for every geological unit identified in Table 3, several samples have been collected and analyzed in dry condition.

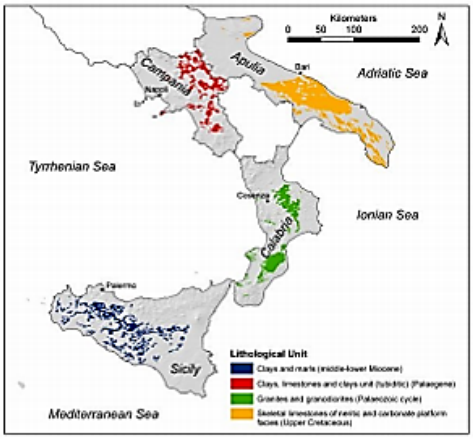


Figure 12 Distribution of the geological unit in South Italy.

All of them have been subjected to at least two series of measurements, each constituted by continuous detection of 8 values. The first two recordings were generally discarded due to possible contact problem between the probe and the analyzed surface, and the remaining six were averaged. The weighted average of the 12 values obtained from the two series of measurements was considered representative of the analyzed sample. The median of the thermal conductivity values defined for the samples belonging to the same geological unit was then attributed to the whole geological formation. In Calabria, 8 granites and 3 granodiorites have been analyzed resulting in a total of 110 values to be treated statistically. In dry condition the thermal conductivity ranges from 0.4 $Wm^{-1}K^{-1}$ for the most weathered granite (CAL30.1, granitic saprolite, Fig.13a) till 3.5 $Wm^{-1}K^{-1}$ for the hardest samples (CAL22.1, metamorphosed, Fig.13b), while the Granites and granodiorites unit has a value of 2.4 $Wm^{-1}K^{-1}$. The Clays, limestones and clay unit of Campania, the Skeletal limestones of neritic and carbonate platform facies of Puglia and the Clays and marls of Sicily show a dry of 2.0, 2.5 and 1.6 Wm-$1K^{-1}$ , respectively (Fig.13 c-h, Table 3).

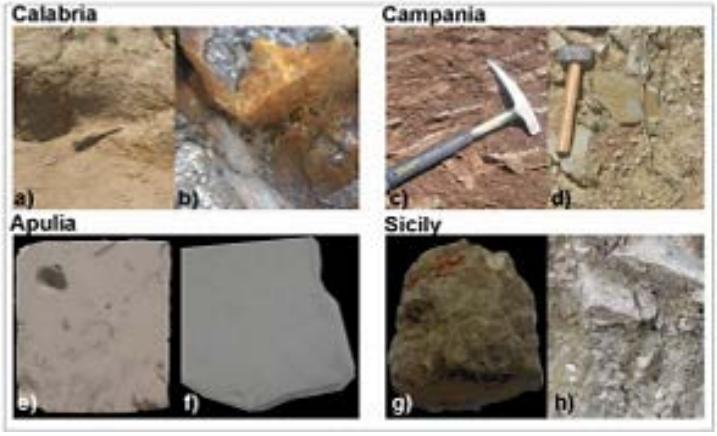


Figure 13 Overview of the rock materials collected and sandstone from Campania; skeleton limestone and limestone of Bari (e-f) from Apulia; clay and marl (g-h) from Sicily.

Table 3 Thermal conductivity values ($Wm^{-1}K^{-1}$ ) of the main geological units derived by direct measurements on samples (dry condition).

| **Geological unit** | **Nr. of sample** | $\lambda_{dry}$ | $\lambda_{wet}$ | $\lambda_{bib}$ |
|---|---|---|---|---|
| Granites and granodiorites | 8 granite<br>3 granodiorites | 1.3 | 3.5 | 2.4 |
| Clays, limestones and clay unit (turbiditic) | 3 marls<br>1 clay<br>1 calcarenite<br>1 sandstone | 0.4 | 3.2 | 2.0 |
| Skeletal limestones of neritic and carbonate platform facies | 7 limestone of Altamura<br>20 limestone of Bari<br>3 dolomite of Galatina<br>1 limestone of Melissano | 1.7 | 3.7 | 2.5 |
| Clays and marls | 2 clay<br>3 marl | 1.6 | 2.8 | 2.2 |

In Table 4 the dry assigned are always lower than those derived from the literature screening. In fact, in the subsoil the water saturates the porosity of rocks by increasing their ability to transfer heat. In this project, some tests on saturated materials were

carried out for Calabria and Sicily rocks. In the first case the final wet derived from the processing of data belonging to granite and granodiorites increases up to 2,8 $Wm^{-1}K^{-1}$ , comparable with the bibliographic one. The samples characterized by the minimum and maximum value of wet are always the granitic saprolite (CAL 30.1, 1.3 $Wm^{-1}K^{-1}$ ) and the fresh metamorphosed granite (CAL 22.1, 3.9 $Wm^{-1}K^{-1}$ ). In the second one, the Clays and marls unit reaches a wet value of 2.8 $Wm^{-1}K^{-1}$ , greater than that obtained from literature screening (2.2 $Wm^{-1}K^{-1}$ ), and in the range 1.30 to 4.2 $Wm^{-1}K^{-1}$ . Instead, the data registered in dry condition are significantly lower, ranging from 0.9 till 2.0 $Wm^{-1}K^{-1}$ .

Table 4 Comparison between thermal conductivity values ($Wm^{-1}K^{-1}$ ) measured in dry and wet conditions and derived by literature

| **Geological unit** | $\lambda_{dry}$ | $\lambda_{wet}$ | $\lambda_{bib}$ |
|---|---|---|---|
| Granites and granodiorites | 2.4 | 2.8 | 2.8 |
| Clays, limestones and clay unit (turbiditic) | 2.0 | - | 2.3 |
| Skeletal limestones of neritic and carbonate platform facies | 2.5 | - | 2.9 |
| Clays and marls | 1.6 | 2.8 | 2.2 |

The correct determination of thermal conductivity referred to the main geological units of a region, based not just on the data reported in literature but on direct measurements on properly taken samples, requires the knowledge of the geological, structural and hydrogeological features of territories at local scale, due to the presence of several lithology in a single formation and the existence of the same lithology in different geological units. For example, water saturation considerably improves the heat transfer conduction in the subsoil. Therefore, determining the thermal conductivity values in dry condition is a precautionary measure that allows the design of geothermal plants suited to the actual conditions of the subsoil. Moreover, the creation of a database dedicated

to the measured thermal properties collection is accessible also for the exploitation of geothermal energy resources in medium and high enthalpy, where the knowledge of thermal conductivity is a key parameters for modelling the potential of deep subsurface structure. Further development of this work has to take into consideration the influence on thermal conductivity values both of the entire stratigraphic sequence and of groundwater up to a depth of about 150 m, useful for shallow geothermal application. Data directly measured in laboratory on small samples must be validated by outputs derived by Thermal Response Test (TRT) to point out the possibility to extend the information collected at local scale to a wider area, allowing a regional mapping of the thermal properties. In Fig. 14, 15, 16, 17, 18 are been reported the Apulia maps with some important date about thermal conductivity, air temperature average annual, open loop: isofreatiche shares , suitability for use of open-loop systems, closed loop: energy exchanged with the ground.

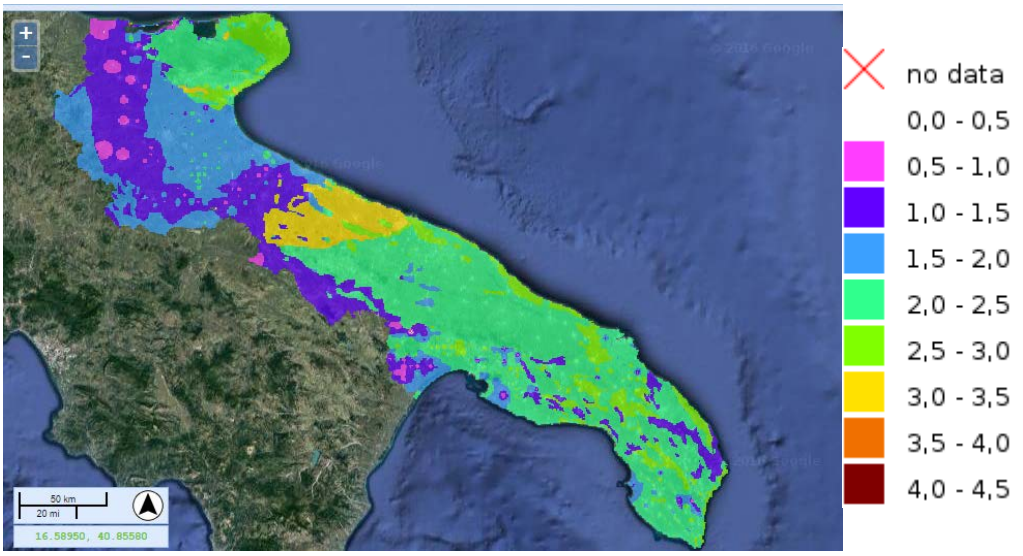


Figure 14 Geothermal potential surface [up to 100 m] _Calculated thermal conductivity (W/m°K) (http://www.vigor-geotermia.it/geo-portal/)

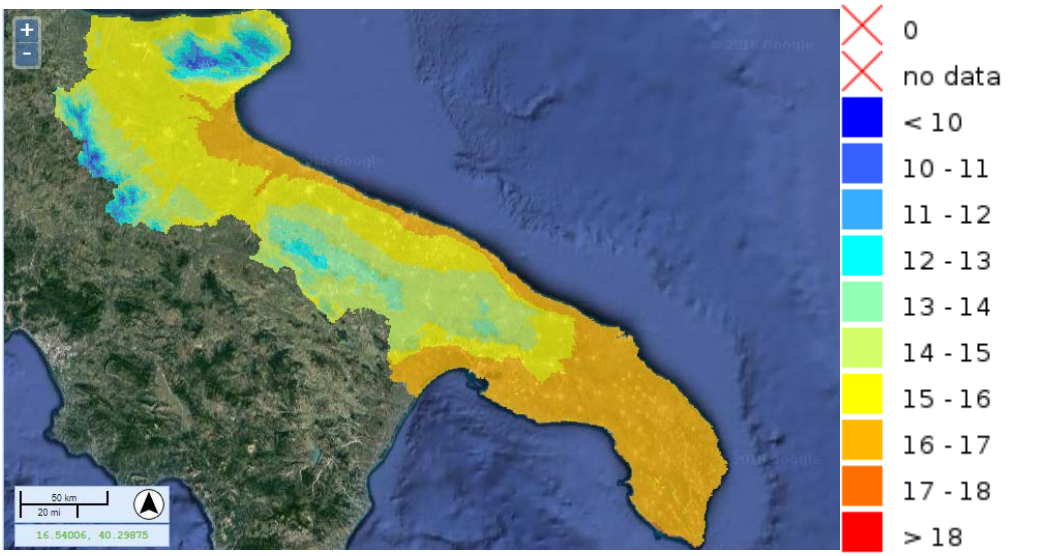


Figure 15 Geothermal potential surface [up to 100 m] _Air temperature average annual °C (http://www.vigor-geotermia.it/geo-portal/)


Figure 16 Geothermal potential surface [up to 100 m]_Open loop: Isofreatiche shares [m s.l.m.] (http://www.vigor-geotermia.it/geo-portal/)

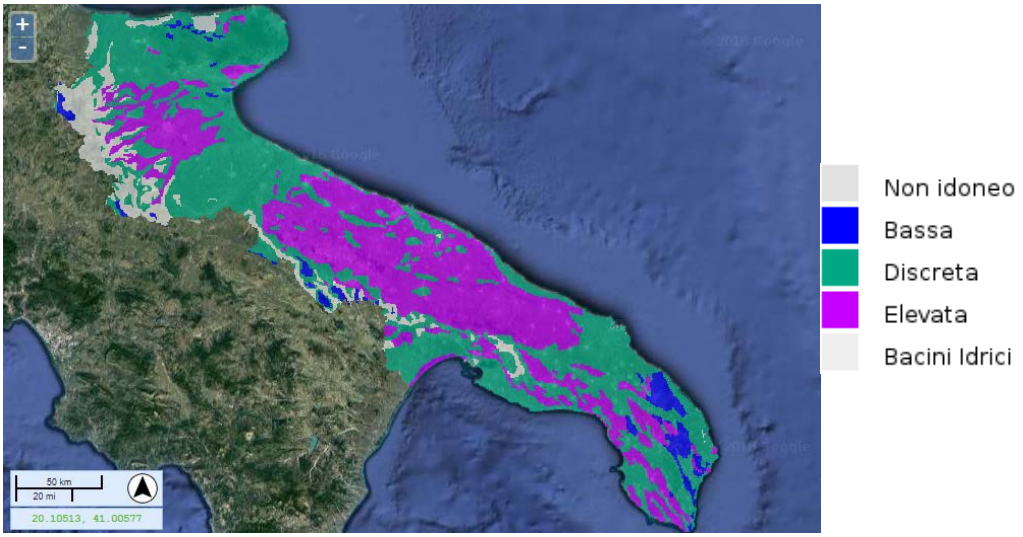


Figure 17 Geothermal potential surface [up to 100 m] _Suitability for use of open-loop systems (http://www.vigor-geotermia.it/geo-portal/)

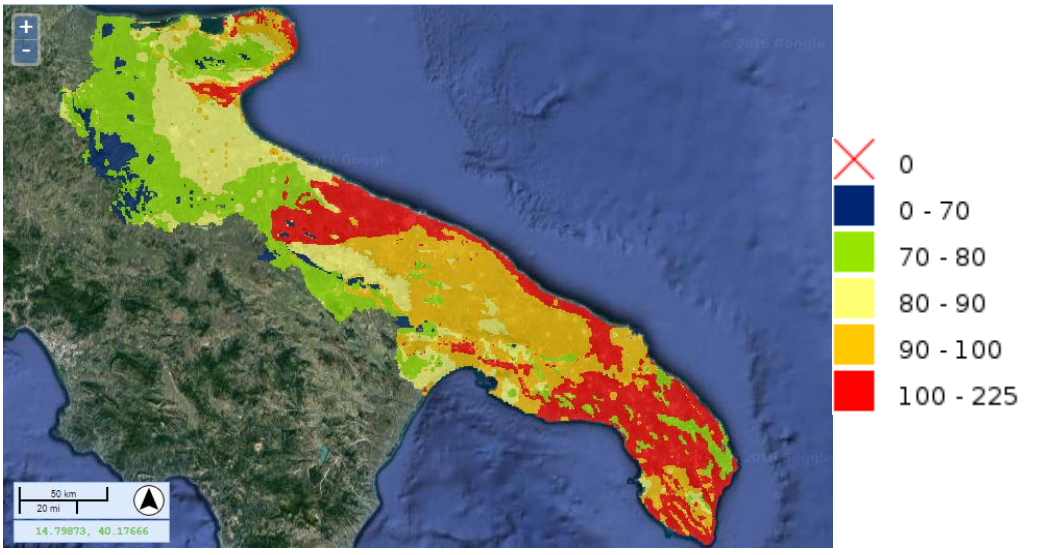


Figure 18 Geothermal potential surface [up to 100 m]_Closed loop: energy exchanged with the ground (http://www.vigor-geotermia.it/geo-portal/)

### 2.1.6 ATES (aquifer thermal energy storage)

The technology ATES (Aquifer Thermal Energy Storage) is a particular type of thermal storage which uses the water of the subsoil as a reservoir, taking it from two different wells with sufficient space out between them. During the summer season, the ground water is extracted from the "cold well", and is used for cooling the condenser of the refrigerator (or heat exchanger), and then placed in the subsoil in the "hot well" and, after being used in the evaporator of the heat pump (or heat exchanger), it is injected in the cold well, providing the following summer season. This technology, calls for the slowest possible speed of groundwater, since it has to ensure that the water of the wells will be mixed with each other, and in any case the motion of groundwater should not take away with them, the storage of cold water from a drain and hot water on the other.

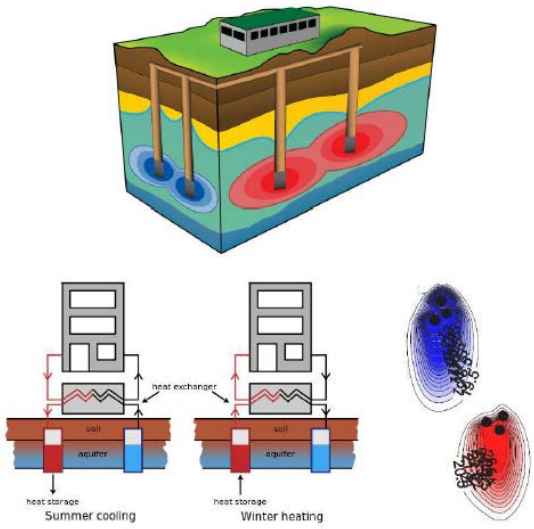


Figure 19 ATES Aquifer Thermal Energy Storage

### 2.1.7 Benefits and costs of exploiting low temperature geothermal energy

Low Temperature Geothermal Energy (LTGE), the energy accumulated in the ground from heat exchange with the atmosphere at low temperature, is an alternative energy source capable of satisfying the energy demand for domestic heating and cooling. In Italy, where over 20% of total energy consumption is due to domestic heating, the use of this renewable energy is being considered to improve the energy performance of buildings. The importance of LTGE is due to the advantages it has over other renewable energies: it allows for the highest savings relative to costs in comparison to conventional energy sources; it is available everywhere at any time; and its exploitation has the lowest environment impact. The advantages of LTGE are due to the manner in which this energy accumulates and regenerates naturally in the ground. The soil has a high thermal inertia, and, at moderate depths, the temperature is not subjected to daily and seasonal temperature fluctuations in the atmosphere and remains constant throughout the year to approximately a few tenths of degree. The basic idea of the exploitation of LTGE is that the heat of soil can be extracted by using heat pumps, taking advantage of temperature differences with the domestic environment. Although the accumulation of heat in the soil occurs naturally, the crucial consideration is how much of this potential can be practically and economically exploited for heating. Lund J, et al, 2004, provided a survey of the principal types of installation. A widely used configuration for a geothermal installation consists of one or more vertical wells. In each well, a Borehole Heat Exchanger (BHE) is installed, which is a U or coaxial heat exchanger circuit that collects energy from the ground. A BHE generally reaches a depth between 80 and 130 m. The main cost driver is the excavation of the vertical borehole, which is proportional to its depth and depends on the thermal efficiency of rocks and the energy demand. The thermal quality of the ground may cause variation of costs up to 50%. The initial investment ($t_0$) represents the highest part of the costs of an installation, and it is the prime factor influencing project feasibility. The installation of a BHE tends to be a capital-intensive investment, typified by large upfront costs with revenues distributed over a period up to 30 years, which is the average lifetime of an installation, and requires a careful analysis of convenience.

### 2.1.8 The need for regional assessments of resources

In Europe, economic analysis of Low Temperature Geothermal Energy (LTGE) has been conducted mainly at the national scale and produced statistics that refer indistinctly to entire nations. These include national counting of new installations, nationwide market projections, measurement of geothermal energy produced yearly and its weight in the national energy balance. The statistics reveal that the exploitation of LTGE has reached different levels of progress on the European continent. Currently, Germany is the leading country in developing geothermal heat pumps. In this country, the number of pumps increased 100% in 2006, and since then the number of installations has increased at an average rate of 20% per year, corresponding to approximately 30,000 new units, as reported by (Schellschmidt R, et al, 2010). In the same study, it was estimated that LTGE could meet 40% of the energy needs of Germany. Switzerland, with an annual increase of 10% in installations, is in a phase of rapid expansion. In Sweden, LTGE exploitation started to spread decades ago: today, 95% of new houses are built with geothermal installations. In Italy, there is a high market potential (EURISPES. Rapporto Italia 2010. Eurispes, 2010). In 2006, the production of LTGE for heating was 640 MW (thermal), and it is expected to grow to 6000 MW by 2020, which is an increase of 17% in the number of pumps. This increase in production roughly corresponds to the needs of about 200,000 houses of 100 $m^2$ of Climate-House Class “E” (Lantschner N., 2005), with a yearly average consumption of 120 $kWh/m^2$. A decisive impulse for the exploitation of LTGE was the European Directives aimed at reducing greenhouse effects, encouraging sustainable development and providing new impulse to the economy. The EU Emission Trading System (ETS), which began in 2000, established an EU-wide cap-and-trade scheme for emissions of greenhouse gases. The scheme imposes mandatory maximum allowances for $CO_2$ emissions from industries. Participants to ETS are encouraged to trade allowances in the form of Renewable Energy Certificates (RECs) to match their actual level of emissions. Within the same frame of directives, local administrations are in charge of making local energy plans and promoting the investment into renewable energies. A regional community can profit from this financial

system because a region with no conventional energy resources in its territory could balance its energetic budget with the sale of RECs (Schellschmidt R et al., 2010). The financial benefit is demonstrated by the flourishing of Energy Service Companies (ESCO). These companies assume the risk of the initiative to improve energy efficiency in the buildings of clients, and they share the economic benefits. Although the statistics and the ongoing initiatives for LTGE show a convenient investment scenario, a confident investment and incentives decision activity requires the support of LTGE models at the regional scale, because that is where local administration and investors operate. Typical decision parameters at the regional scale are as follows: the total upfront capital to be invested in the BHE installation to satisfy the energy demand for domestic heat of the whole region; the overall savings over conventional energy purchases; the entire income represented by the RECs; the value represented by improvement of energy performance of buildings throughout the region. Additional decisional parameters for investors are the following: the differences in attractiveness of the investment from one site to another; the changing in cost over time due to the foreseeable improvements of technology efficiency. Considering these issues, it has been built an energy-economic model of the LTGE that includes indicators useful for energy planning and decision making at the regional scale. In the next section, it is summarized the state of the art tools and modelling methods for the low-enthalpy geothermal potential.

### 2.1.9 Estimation of geothermal potential

The theoretical basis for every physical model of heat flow is represented by Fourier's law, which expresses the relationship between the heat flow through a solid body, its thermal conductivity and the temperature gradient. In the ground, the heat transfer takes place by conduction in the solid rock and, at a different rate, through the groundwater that saturates the rock pores. For engineering applications, the specific Heat Extraction (sHE) is used (Verein Deutscher Ingenieure, 2001).

For a U-type heat exchanger circuit, the sHE usually ranges between 40 and 70 W per borehole meter. In designing the installation, the depth of the BHE is calculated by dividing the energy demand by the average specific heat extraction of the site. The sHE

can be measured with precision from thermo-physical tests conducted on site and through knowledge of the ground exchanger system (Menichetti M et al, 2009), or a coarse estimate can be done on a rough recognition of the rock type. Typical values of sHE are established for the main types of rocks (Table 6). In (Ondreka J, et al., 2007), using a GIS platform, they calculated the potential of LTGE over a limited region of Germany spanning several square kilometres. For each point of the territory, the geothermal power was calculated by multiplying the depth for the average sHE of the rock. At each site, the average specific Heat Extraction, $sHE_{agg}$, of layered ground was calculated with the following formula:

$$sHE_{agg} = \frac{1}{Th_{agg}} \sum_{k-1}^{n} ([sHE_k] x [Th_k]) \tag{1}$$

where $sHE_k$ is the specific heat extraction of each layer k, and $Th_k$ is the thickness of the k-th layer, $Th_{agg}$ is the overall depth. The calculation is repeated for each cell of a geographic grid virtually lying on the region. This procedure was also applied by [33] in a limited portion of Marche region. This model is based only on the lithology, which has a predominant effect over any other natural factor on the LTGE. Although this choice introduces approximations, it provides a reliable assessment of LTGE in the territory. In addition to lithology, there is agreement on a set of variables that can be used to further refine the model, such as mean surface temperature of the soil, vegetation coverage, insolation, and the natural geothermal gradient. Among the secondary variables, the Ground Surface Temperature (GST) is particularly important and is an expression of local climatic conditions. As stated in (Signorelli S et al, 2004), the efficiency of the BHE increases linearly with the GST, whose average is equal to the average Surface Air Temperature (SAT) increased by an additive constant of 1,6 °C. The SAT in turn is calculated by interpolating the temperature measured at meteorological stations and averaged over a period of 10 yrs. Once the GST is determined for a site, it is converted in a metric correction, $\Delta Z_{GST}$, to be applied to the BHE depth calculated based on BHE

and energy demand. The $\Delta Z_{GST}$ is calculated at every site in the region using a third order polynomial function that relates it to the GST, and it is positive or negative depending on whether GST is below or above the regional average, and it is zero at the sites where the GST is equal to its regional average.

Table 5 Typical specific heat extraction of different rocks for 2400 operating hours

| **Ground** | **Specific heat extraction, sHE (W/m)** |
|---|---|
| General guideline values Poor ground (dry sediment) | 20 |
| Normal rocky ground saturated sediment | 50 |
| Consolidated rock with high thermal conductivity | 70 |
| **Individual rocks** | |
| Gravel, sand, dry | <20 |
| Gravel, sand, water saturated | 55-65 |
| Gravel, sand, with strong groundwater flow | 80-100 |
| Clay, loam, dump | 30-40 |
| Limestone (massive) | 45-60 |
| Sandstone | 55-65 |
| Siliceous magmatite | 55-70 |
| Basic magmatite | 35-55 |
| Gneiss | 60-70 |

### 2.1.10 Geothermal heat pumps

Heat pumps function in the same way as a standard household fridge. The following basic principles are used:

- A liquid absorbs heat as it vaporises (e.g. boiling water turning into steam);
- Compressing a gas increases its temperature;
- Expanding a gas reduces its temperature;
- As a gas loses heat, it will turn back into a liquid (e.g. steam condensing back to water).

The main heat pump components are the refrigerant, evaporator, compressor, condenser and expansion valve. To heat or cool a building, a heat pump uses a liquid refrigerant such as R-22, which has a very low evaporation point: -40° F. When heating a home, for example, the cold liquid refrigerant absorbs heat and evaporates as it passes next to warmer antifreeze solution or groundwater in the evaporator (heat exchanger). The refrigerant gas travels through a compressor where it is squeezed and heated further to about 180° F. The refrigerant then moves to the condenser where heat is released to surrounding cooler air (forced air system) or to circulating water (hydronic system). In forced air systems, a blower transports the warmed air around the building through a duct network. The venting is usually composed of insulated metal pipes, diffusers and grilles. The ducts carry the heated air, which usually has a temperature between 85-110 °F. This is much lower than temperatures produced by fossil fuel furnaces, but higher than that of conventional air source heat pumps. Therefore, the volume of air that must be moved to supply the same amount of heat is much greater – the duct system and blower must be larger than those for conventional heating and cooling. A hydronic system uses a pump to circulate the heated or cooled water through a series of radiators in the building. As the refrigerant loses heat to the air or water, it condenses back to a liquid under high pressure. It then passes through an expansion device where the pressure is lowered and the refrigerant cools further. Finally, the refrigerant returns to the evaporator to repeat the cycle. To provide cooling to a home in the summer, the

process would be reversed by changing the direction of the reversing valve on the refrigerant loop. The roles of the condenser and the evaporator are reversed during the cooling cycle. Heat from the home would be absorbed by the refrigerant (at the air distribution loop) and then transferred to the water or antifreeze at the ground loop, which in turn carries the heat to the subsurface. An additional device known as a desuperheater can be used in either the heating or cooling mode to apply existing compressor heat to heat water. The desuperheater is attached directly after the compressor.
In a geothermal heat pump, the first heat exchanger is placed in the circuit with the ground loop, the second in the circuit with the building. The refrigerant can gain heat from the ground loop and lose it to the building, or can operate in reverse; heating or cooling the building respectively (Fig. 20).

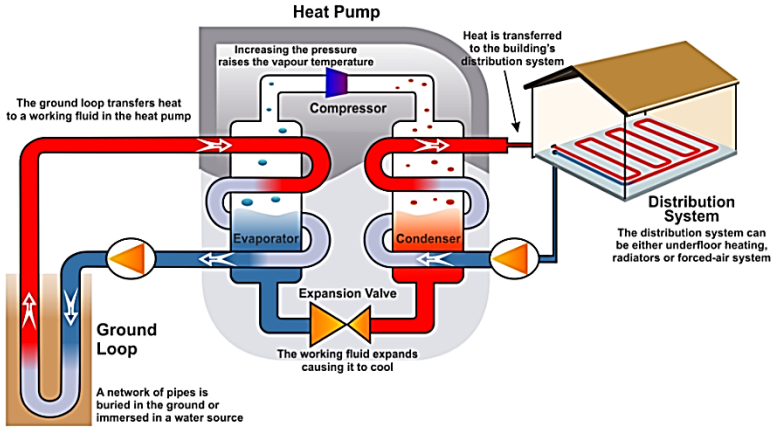


Figure 20 Operating cycle of a geothermal heat pump

According to the EPA, GSHP systems can reduce energy usage by over 40 percent in comparison to air source heat pumps. Compared to electric resistance heating with standard air-conditioning equipment, GSHP systems can reduce energy usage by over 70 percent. Additional savings can be obtained with the use of other energy-efficient procedures and materials including insulation and thermally improved windows. A domestic heat pump is typically a 3 or 4 ton capacity unit. One ton of cooling equals

12,000 BTUs per hour. A small business office or a church might require a 15 to 25 ton unit, whereas a high school might require a system greater than 200 tons.

Geothermal (ground-source) heat pumps have the largest energy use and installed capacity worldwide, accounting for 70, 90%of the installed capacity and 55,15% of the annual energy use.

The installed capacity is 50,258 MWt and the annual energy use is 326,848 TJ/year, with a capacity factor of 0.206 (in the heating mode). Although, most of the installations occur in North American, Europe and China, the number of countries with installations increased from 26 in 2000, to 33 in 2005, to 43 in 2010, and to 48in 2015. The equivalent number of installed 12 kW units (typical of USA and Western Europe homes) is approximately 4,19 million. This is a 52% increase over the number of installed units reported in 2010, and over three times the number of units reported in 2005. In Europe, most units are sized for the heating load and are often designed to provide the base load with peaking by fossil fuel. As a result, these units may be in operation up to 6000 equivalent full-load heating hours per year (capacity factor of 0.68), such as in the Nordic countries(especially in Finland). Unless the actual number of equivalent full-load heating hours was reported, a value of 2200 h/year (and higher for some of the northern countries) was used for energy output (TJ/year) calculations, based on a report by Curtis et al.(2005). The energy use reported for the heat pumps was deduced from the installed capacity (if it was not reported), based on an average coefficient of performance (COP) of 3.5, which allows for one unit of energy input (usually electricity) to 2.5 units of energy output, for a geothermal component of 71% of the rated capacity [i.e., (COP- 1)/COP = 0.71]. The cooling load was not considered as geothermal as in this case, heat is discharged into the ground or groundwater. Cooling; however, has a role in the substitution of fossil fuel sand reduction in greenhouse gas emission and is included in later discussions. The leaders in installed units are: United States, China, Sweden, Germany and France.

### 2.1.11 Greenhouse gas emission savings of ground source heat pump systems in Europe

Nowadays, it is widely accepted that greenhouse gases (GHGs) influence global climate. To impede this development, in March 2007, the European Council made a commitment to reduce GHGs until 2020 by at least 20% compared to 1990 [36]. This means a net GHG reduction of 368 million tons of $CO_2$ per year. The new Europe 2020 Strategy (European Commission. Europe 2020, European Commission. Conclusions of the Lisbon European Council. SN 100/00, 23–24 March, 2000 )represents the current roadmap of the European Union for economic renewal, which was adopted in June 2010 and replaced the Lisbon Strategy (European Commission, 2011).

The program's main goals are to evenly decrease GHG emissions by 30%, if the conditions are right, to reach a 20% share of total energy consumption from renewable energy, and to raise the energy efficiency. In March 2011, the EU launched a new Energy Efficiency Action Plan with more details on specific actions to be taken. Particular focus is set on minimizing energy consumption of buildings, given that this sector accounts for 40% of total energy consumption in Europe (European Commission, 2010). GHG savings by use of renewable energy sources are considered an elementary component to achieve the ambitious targets. Among others, heat pump systems for the heating (and cooling) of buildings are recommended as high-efficiency alternative systems (Fridleifsson IB, 2008).

They are not only common as small scale applications for residential heating, cooling and hot water provision, but of increasing importance also for larger buildings such as schools, industrial and office buildings, and in district heating systems (e.g. Thorsteinsson HH, 2010, Yu Xing C, 2011). Meanwhile, these systems already contribute to strategic low carbon emission plans of cities (e.g. Schimschar S, et al ,2011, Hughes L et al, 2011) and even entire countries (e.g. Schimschar S, et al, 2011, US DoE. Energy efficiency and renewable energy, Geothermal Technologies Program. U.S. Department of Energy; 2004, Blum P et al, 2011). Accordingly, their spread is fuelled by grant programs and government incentives (e.g. Boait PJ, et al 2011, Caird S et al 2010), special electricity heat pump tariffs, and even without extra subsidy funds they show economic

and environmental advantages (Blumsack S, 2009., Esen H, 2006). Bristow and Kennedy (2010) recently presented a comprehensive analysis of the competitiveness of alternative heating technologies in Canada, and included the risk of future energy price development. GSHPs turned out to be exceptionally good and sustainable investments, not just with respect to energy efficiency and GHG emission savings, but especially in terms of life cycle costs. This was demonstrated for both small residential homes with substantial grants of 61% for the capital costs and for larger buildings even without any financial support. In other countries, the economic virtues will depend on the specific conditions encountered there. Obviously, a major role is played by the competitive heating technologies as well as by the practical experience with GSHP installation and maintenance. The European Heat Pump Association (EHPA) defined a traditional heat mix for Europe (50% gas, 30% oil, 10% solid fuel, 10% electricity) to approximate standard heating practice and related emissions. This served as a basis to roughly evaluate GHG savings potential by (all) heat pump applications in Europe. These are dominated by air source heat pump (ASHP) systems but also include GSHP systems. Extrapolating currently observed growth rates of 5.4 million heat pump units per year, a number of 70 million installed units in Europe is expected for 2020. Given these assumptions, all heat pumps would yield an avoidance of 230 million tons of GHGs in comparison to standard heating practices. Accordingly, heat pumps would contribute over 20%ofthe EU energy saving goal, 20% of the renewable energy input and 20% of the $CO_2$ emission target. This forecast is only based on the most frequent application of heat pumps in single family houses. EHPA hypothesizes that this number could be even higher when including multi-family houses, commercial buildings, as well as accounting for improvements in power production efficiency, and including efficiency of heat pumps and improved insulation standards. Rybach (2008) presents a discussion on the prominent role of GSHPs among the heat pumps based on the EHPA study. However, this role is not quantified, and no details on the relative contribution of GSHPs for achieving Europe's $CO_2$ emission targets are given. In this study, he emphasizes the difference between $CO_2$ emission reduction and saving. New GSHP installations alone do not reduce, they only avoid additional emission. Real emission reduction is achieved

only when at the same time a fossil-fired burner - with the same capacity - is taken out of service. This is for example the case in renovation/refurbishment.

### 2.1.12 GSHP installed numbers and capacity

The worldwide number of GSHPs is rapidly growing, and GSHPs are gaining more importance, especially in Europe (e.g. Boait PJ,et al 2011, Caird S, etg al 2010). This is stimulated by the search for environmental alternatives to traditional heating technologies, both for new and retrofitted buildings. Today, GSHPs are established in most European countries. EHPA provides detailed statistical data for heat pumps of eight European Countries (Austria, Finland, France, Germany, Italy, Norway, Sweden and Switzerland). A share of 20% of GSHPs was calculated in 2008, with the majority of heat pumps using air as the energy source. The annual GSHP sales in these countries from 2005 to 2008 ranged between 75,000 and 110,000. The EHPA calculates 6.74 Mt GHG annual emission savings by all heat pumps installed during this period, with about 40% (2.7 Mt) originating from GSHPs. The sales report by the EHPA as well as the worldwide reviews on direct geothermal energy by Lund and co-workers from 2000, 2005 and 2010 (Curtis R,2005, Seyboth K, 2008), reports by the EurObserv'er and by Rybach and Sanner (2000) are consulted to obtain estimates on the stock of GSHPs in Europe. We identified nineteen European countries, for which significant numbers of GSHPs were reported. The results are listed in Table 6 and show a continuous, overall exponential increase in installed GSHPs throughout Europe (annually 23% in numbers, 28% in produced TJ). The numbers represent averages from available statistics and thus may slightly differ from exact values due to the heterogeneous origin of the country-specific numbers, the difficulty of separating residential applications from others, and differences in the respective reporting periods.

Table 6 Average reported number of ground source heat pumps in European countries in the years 2000, 2005, and 2008 ; average size is 12 kW (n.a., no reliable data available).

| Country | | Year | | |
|---|---|---|---|---|
| | | 2000 | 2005 | 2008 |
| Austria | AUT | 19,000 | 35,810 | 48,641 |
| Belgium | BEL | n.a. | 6000 | 9500 |
| Czech Republic | CZE | 390 | 3727 | 9168 |
| Denmark | DNK | 250 | 6000 | 11,250 |
| Estonia | EST | n.a. | 3500 | 4874 |
| Finland | FIN | 10,000 | 29,106 | 46,412 |
| France | FRA | 4000 | 63,830 | 121,900 |
| Germany | DEU | 18,000 | 61,912 | 148,000 |
| Hungary | HUN | 20 | 230 | 4000 |
| Ireland | IRL | n.a. | 1500 | 9500 |
| Italy | ITA | 100 | 6000 | 12,000 |
| Netherlands | NLD | 900 | 1600 | 14,600 |
| Norway | NOR | 500 | 14,000 | 26,000 |
| Poland | POL | 4000 | 8100 | 11,000 |
| Slovenia | SVN | 66 | 300 | 3440 |
| Spain | ESP | n.a. | n.a. | 7000 |
| Sweden | SWE | 55,000 | 230,094 | 320,687 |
| Switzerland | CHE | 21,000 | 38,128 | 61,000 |
| United Kingdom | GBR | 40 | 550 | 10,350 |
| Total | | 133,266 | 510,387 | 879,322 |

In 2008, about 880,000 GSHPs were in operation in these nineteen European countries. Using the significant growth rates as illustrated in Fig. 21, the current number of GSHPs can be expected to be well above one million (about 1.2-1.3 million). Rough extrapolation indicates that within one decade from 2000 to 2010 this number increased by about one order of magnitude. Nevertheless, even if exponential growth rates were predicted in 2007, recent European heat pump sales show a minor decrease in 2009 and 2010 (Boait PJ, 2011). The 2008 sales data shows that with regard to direct geothermal energy use, Sweden is the most advanced country, and it hosts about one third of all GSHPs in Europe. Heat pump manufacturers report that 97% of newer Swedish houses are built with heat pumps (Blumsack S, 2009). About 75% of European GSHPs are installed in Sweden, Germany, France and Switzerland.

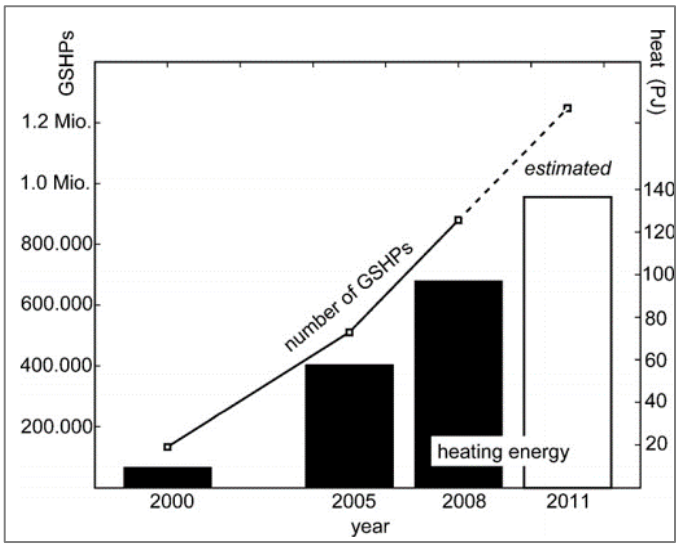


Figure 21 Development of total number of GSHPs and provided energy for space heating ("heat", 1 PJ = 1000 TJ) in European countries (2000–2011).

An apparent concentration can be observed in Scandinavia and central Europe, i.e. in the countries with colder climate in contrast to, for instance, the Mediterranean countries with warmer climate. Comparing the total final consumption in the residential sector for space heating to that fraction supplied by GSHPs, geothermal heating plays an important role only in Scandinavia (Table 7). In 2008, Sweden provided 20.3%, Norway 9.4% and Finland 7.1% of space heating by GSHPs. Switzerland reaches a remarkable, although lower value of 5.4%. In all other countries, the fraction is about 1%, and thus we calculate a mean proportion of GSHP heating of only 1.4%for the studied European countries.

Table 7 Final demand of (total) space heating energy (rounded to thousands) and supply by GSHPs in residential sector in European countries in the years 2000, 2005, and 2008

| | Heating demand (TJ) | | | GSHP (TJ) | | | Relative contribution | | |
|---|---|---|---|---|---|---|---|---|---|
| | 2000 | 2005 | 2008 | 2000 | 2005 | 2008 | 2000 | 2005 | 2008 |
| Climate corrected | | | | | | | | | |
| AUT | 224,000 | 207,000 | 209,000 | 1275 | 2050 | 3229 | 0.6% | 1.0% | 1.5% |
| BEL | 310,000 | 333,000 | 295,000 | | 312 | 495 | 0.0% | 0.1% | 0.2% |
| CZE | 166,000 | 181,000 | 186,000 | 44 | 301 | 927 | 0.0% | 0.2% | 0.5% |
| DNK | 165,000 | 165,000 | 173,000 | 24 | 525 | 1859 | 0.0% | 0.3% | 1.1% |
| EST | 27,000 | 24,000 | | | 257 | | | 1.1% | |
| FIN | 125,000 | 129,000 | 139,000 | 575 | 2157 | 9852 | 0.5% | 1.7% | 7.1% |
| FRA | 1,368,000 | 1,311,000 | 1,268,000 | 277 | 3925 | 7784 | 0.0% | 0.3% | 0.6% |
| DEU | 2,232,000 | 1,969,000 | 2,044,000 | 1308 | 4309 | 11,237 | 0.1% | 0.2% | 0.5% |
| HUN | | | | 24 | 240 | 593 | | | |
| IRL | | | | | 92 | 777 | | | |
| ITA | 711,000 | 788,000 | 816,000 | 7 | 521 | 1157 | 0.0% | 0.1% | 0.1% |
| NLD | 349,000 | 305,000 | 298,000 | 66 | 747 | 1080 | 0.0% | 0.2% | 0.4% |
| NOR | 94,000 | 94,000 | 91,000 | 37 | 3495 | 8588 | 0.0% | 3.7% | 9.4% |
| POL | 598,000 | 544,000 | 615,000 | 127 | 510 | 1193 | 0.0% | 0.1% | 0.2% |
| SVN | 41,000 | 30,000 | 30,000 | 53 | 65 | 387 | 0.1% | 0.2% | 1.3% |
| ESP | 258,000 | 281,000 | 286,000 | | | 408 | 0.0% | 0.0% | 0.1% |
| SWE | 269,000 | 249,000 | 257000 | 5292 | 39,025 | 52,251 | 2.0% | 15.7% | 20.3% |
| CHE | 123,000 | 113,000 | 138,000 | 2287 | 2836 | 7403 | 1.9% | 2.5% | 5.4% |
| GBR | 1,277,000 | 1,296,000 | 1,152,000 | 3 | 50 | 783 | 0.0% | 0.0% | 0.1% |
| Total/average | 8,337,000 | 8,019,000 | 8,021,000 | 11,400 | 61,419 | 110,005 | 0.1% | 0.8% | 1.4% |
| Without climate correction | | | | | | | | | |
| Total/average | 7,462,000 | 7,782,000 | 7,400,000 | 9405 | 57,611 | 96,464 | 0.1% | 0.7% | 1.3% |

### 2.1.13 Potential system and water quality problems

The use of open GSHP systems can be an environmentally safe operation. However, potential water quality and quantity problems include:

1. change in groundwater temperature
2. leakage of chemical additives to the water outflow
3. leakage of machinery pollutants
4. abuse of injection wells by injecting sewage wastes
5. change in the chemical balance of the aquifer
6. over pumping and/or well interference
7. land subsidence

### 2.1.14 Change in Temperature

The returning groundwater will either be warmer or cooler. For GWHP systems, the temperature is usually changed less than 10° F. Whether or not the discharge will have an impact on the water depends on various factors such as the volume discharged, the temperature and flow of the receiving water and other factors. If the cooling and heating water are returned to the same aquifer throughout the seasons, the temperature contrasts will tend to be neutralized. For subsurface disposal, large GWHP systems could possibly introduce a thermal plume that could affect another well. The potential for this should be assessed during the design of a large system.

### 2.1.15 Chemical Additives

Chemical additives for any purpose may not be supplied to the return flow of groundwater. The use of chemical additives changes the classification of the injection well. Before adding anything to the water, the system owner should contact the DEP regional office.

### 2.1.16 Machinery Pollutants

Machinery oils and refrigerants are generally benign sources of pollutants in heat pump systems. In household systems, the volumes of these substances are limited. Also, since the heat pumps are located inside the building, the risk of any type of contaminant reaching the subsurface is minimal. The amount of refrigerant and oils in commercial systems may pose some risk if the substances migrate to the subsurface. Most systems are equipped with automatic shutoff devices activated by pressure drops.

### 2.1.17 Sewage Disposal and Chemical Imbalances

GWHP systems should not be connected in any way to sewage disposal systems. As groundwater flows through the GWHP system, the water may be slightly changed in quality including temperature pressure or dissolved oxygen. Such changes can cause

the precipitation of insoluble materials such as iron oxides, calcium carbonate and silica. This may be the biggest problem with the use of open systems. Scaling, the deposition of a mineral precipitate, can occur in the pipes, valves or heat exchangers and thus reduce the efficiency of the system.
Serious scaling problems are rare. Scaling is most likely to occur during the air-conditioning mode when the heat exchanger gives off heat to the groundwater. Precipitation of minerals can also result in the clogging of the return well and a shutdown of the GWHP system. Return wells are more likely to require maintenance than supply wells. Evidence that precipitation of minerals is occurring includes:

a. a marked decline in the recharge rate;
b. an increase in the amount of pressure needed to maintain the recharge rate;
c. rising water levels around the injection well. Well failure can occur so rapidly that the first symptom may be water flowing out of the return well. Proper design, development and maintenance can prevent injection well failure. Water quality tests and consultation with system designer and equipment suppliers can avoid these types of problems. In addition, improvements such as expandable cupronickel alloy pipes have reduced problems such as scaling. Filters can also help to alleviate the deterioration of valves by removing fine particles in the water.

### 2.1.18 Over pumping and Well Interference

Uncontrolled groundwater development of an area can lead to problems such as aquifer drawdown and well interference. Aquifer drawdown occurs when withdrawal exceeds recharge. Well interference can take place in areas where yields are low, use of groundwater is high or where supply wells are close to each other. The results are lower water levels in wells and smaller yields. In some cases, water levels may drop below pump intake levels resulting in "dry wells." The surface disposal of groundwater could unnecessarily compound a situation where groundwater is in short supply. Groundwater should be conserved by returning it to the aquifer. Whether or not similarly constructed wells will interfere with each other depends mainly on three factors:

1) The transmissivity of the local aquifer;
2) The pumping rates of the wells;
3) The distance between the wells.

An aquifer with a good transmissivity will generally provide enough water for each user. Carbonate, sand, gravel, and highly fractured rocks will typically yield adequate quantities of water. Wells constructed in igneous and metamorphic rocks and shales and sparsely fractured rocks may yield small quantities of water. The demand for groundwater will vary with the size and design of the heat pump system. Over pumping can expand the cone of depression until it interferes with the area of withdrawal of another well. A high volume commercial well could affect nearby wells even in regions with highly transmissivity aquifers. Wells placed too closely to each other may also result in interference. A well should be placed at least 100 feet from an existing well. However, this does not guarantee that there will be no interference. In geologic formations with poor transmissivity, the cone of depression that develops will be deeper with steeper sides than in areas of high transmissivity. The cone of depression will continue to expand until hydrogeological equilibrium is reached when the flow into the aquifer equals the flow out. This process may take weeks or years.

### 2.1.19 Land Subsidence

Natural subsidence is generally restricted to regions of carbonate rocks. Carbonate rocks (limestone and dolomite) are susceptible to dissolution, which may be followed by subsidence of the land above. The factors involved in subsidence include the composition of the carbonate rock, the surface water drainage and the flow of groundwater. Discharging water to the surface or near surface may accelerate the dissolution of limestone or dolomite and therefore activate the formation of sinkholes. Returning water to its original aquifer will tend to lessen this potential problem. However, in all cases the system installer should exercise caution when placing a GWHP over carbonate terrain. However, the transfer of groundwater to or from mine pools is likely to have little impact on the stability of mined areas. Most rocks (sandstone, shale, siltstone) associated

with coal mining are not susceptible to dissolution by flowing groundwater. Subsidence can also occur from the dewatering of an aquifer.

### 2.1.20 Direct utilization of geothermal energy 2015 worldwide review

A geothermal resource can be simply defined as a reservoir inside the Earth from which heat can be extracted economically (cost wise less expensive than or comparable with other conventional sources of energy such as hydroelectric power or fossil fuels) and utilized for generating electric power or any other suitable industrial, agricultural or domestic application in the near future. Estimates of geothermal resources are made on the basis of geological and geophysical data such as:

(i) depth, thickness and extent of geothermal aquifers;
(ii) properties of rock formations;
(iii) salinity and geochemistry of fluids likely present in the aquifers;
(iv) Temperature, porosity and permeability of rock formations (Rummel and Kappelmeyer, 1993).

Direct-use of geothermal energy is one of the oldest, most versatile and common forms of utilizing geothermal energy (Dickson and Fanelli, 2003). The early history of geothermal direct-use has been reviewed for over 25 countries in the Stories from a Heated Earth- Our Geothermal Heritage (Cataldi, et al., 1999), that documents geothermal use for over 2,000 years.

The five countries with the largest direct-use (with heat pumps) installed capacity (MWt) are China, USA, Sweden, Turkey and Germany accounting for 65.8% of the world capacity, and the five countries with the largest annual energy use (with heat pumps) (TJ/year) are China, USA, Sweden, Turkey and Iceland accounting for 63.2% of the world use. The growing awareness and popularity of ground-source (geothermal) heat pumps has had the most significant impact on the direct use of geothermal energy. The annual energy use of these units grew 1,63 times at a compound rate of 10,3% compared to WGC2010. The installed capacity grew 1,52 times at a compound annual rate of 8,69%. This is due, in part, to better reporting and the ability of geothermal heat

pumps to utilize groundwater or ground-coupled temperature anywhere in the world (see Fig. 22).

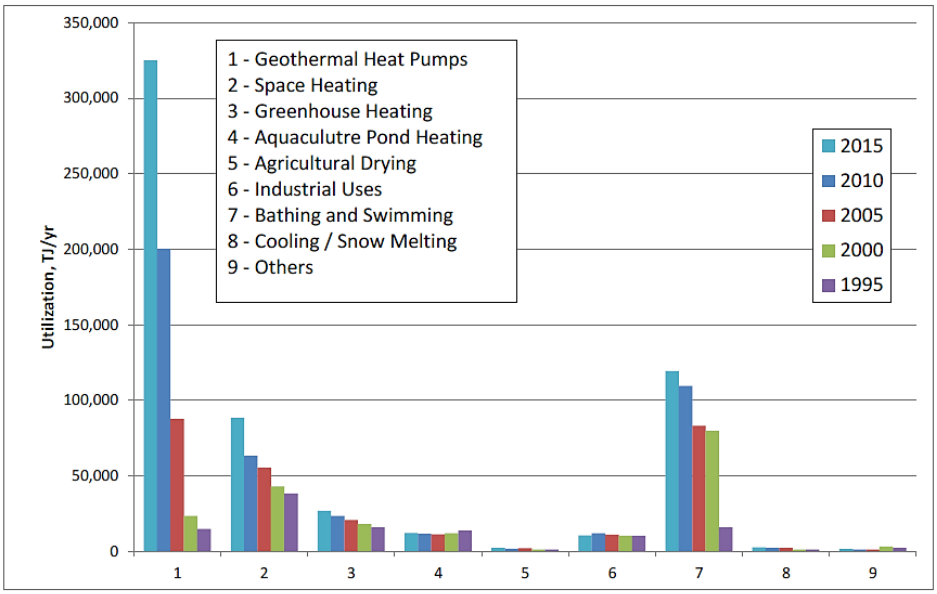


Figure 22 Comparison of worldwide direct-use geothermal energy in TJ/year from 1995, 2000, 2005, 2010 and 2015. (John W. Lund and Tonya L. Boyd, 2015)

The five leading countries in terms of installed capacity (MWt) of just heat pumps are: USA, China, Sweden, Germany and France, and in terms of annual energy use (TJ/year) are: China, USA, Sweden, Finland, and Germany. See Table 9.

Table 8 Worldwide leaders in the installation of geothermal heat pumps (John W. Lund and Tonya L. Boyd, 2015)

| **MWt** | **TJ/year** |
|---|---|
| Usa (16,800) | China (100,311) |
| China (11,781) | Usa (66,670) |
| Sweden (5,600) | Sweden (51,920) |
| Germany (2,590) | Finland (18,000) |
| France (2,010) | Germany (16,200) |

### 2.1.21 Categories of utilization

Table 10 divides the data from 1995, 2000, 2005, 2010 and 2015 among the various uses in terms of capacity, energy utilization and load factor. This distribution can also be viewed as in Fig. 23. Figs. 24–25 presents the 2015 data in pie-chart format as a percentage.

Table 9 Direct-use worldwide for the period 1995–2015.

Summary of the various categories of direct-use worldwide for the period 1995–2015.

| Capacity, MWt | 2015 | 2010 | 2005 | 2000 | 1995 |
|---|---|---|---|---|---|
| Geothermal heat pumps | 50,258 | 33,134 | 15,384 | 5,275 | 1,854 |
| Space heating | 7,602 | 5,394 | 4,366 | 3,263 | 2,579 |
| Greenhouse heating | 1,972 | 1,544 | 1,404 | 1,246 | 1,085 |
| Aquaculture pond heating | 696 | 653 | 616 | 605 | 1,017 |
| Agricultural drying | 161 | 125 | 157 | 74 | 67 |
| Industrial uses | 614 | 533 | 484 | 474 | 544 |
| Bathing and swimming | 9,143 | 6,700 | 5,401 | 3,957 | 1,085 |
| Cooling/snow melting | 360 | 368 | 371 | 114 | 115 |
| Others | 79 | 42 | 86 | 137 | 238 |
| Total | 70,885 | 48,493 | 28,269 | 15,145 | 8,664 |

| Utilization, TJ/year | 2015 | 2010 | 2005 | 2000 | 1995 |
|---|---|---|---|---|---|
| Geothermal heat pumps | 3,26,848 | 2,00,149 | 87,503 | 21,275 | 14,617 |
| Space heating | 88,668 | 63,025 | 55,256 | 42,926 | 38,230 |
| Greenhouse heating | 29,038 | 23,264 | 20,661 | 17,864 | 15,742 |
| Aquaculture pond heating | 11,953 | 11,521 | 10,976 | 11,733 | 13,493 |
| Agricultural drying | 2,030 | 1,635 | 2,013 | 1,018 | 1,124 |
| Industrial uses | 10,454 | 11,745 | 10,868 | 10,220 | 10,120 |
| Bathing and swimming | 1,19,611 | 1,09,410 | 83,018 | 79,546 | 15,742 |
| Cooling/snow melting | 2,506 | 2,126 | 2,012 | 1,063 | 1,124 |
| Others | 1,440 | 955 | 1,045 | 3,034 | 2,249 |
| Total | 5,92,638 | 4,23,830 | 2,73,372 | 1,90,699 | 1,12,441 |

| Cooling/snow melting | 2015 | 2010 | 2005 | 2000 | 1995 |
|---|---|---|---|---|---|
| Geothermal heat pumps | 0.206 | 0.19 | 0.18 | 0.14 | 0.25 |
| Space heating | 0.370 | 0.37 | 0.40 | 0.42 | 0.47 |
| Greenhouse heating | 0.467 | 0.48 | 0.47 | 0.45 | 0.46 |
| Aquaculture pond heating | 0.545 | 0.56 | 0.57 | 0.61 | 0.39 |
| Agricultural drying | 0.400 | 0.41 | 0.41 | 0.44 | 0.53 |
| Industrial uses | 0.540 | 0.70 | 0.71 | 0.68 | 0.59 |
| Bathing and swimming | 0.415 | 0.52 | 0.40 | 0.64 | 0.46 |
| Cooling/snow melting | 0.229 | 0.18 | 0.17 | 0.30 | 0.31 |
| Others | 0.578 | 0.72 | 0.39 | 0.70 | 0.30 |
| Total | 0.265 | 0.28 | 0.31 | 0.40 | 0.41 |

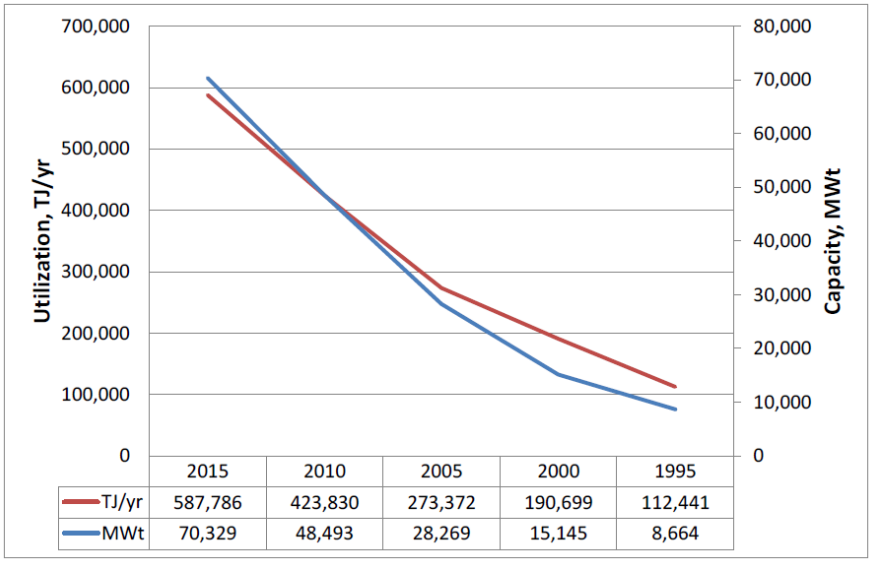


Figure 23 The installed direct-use geothermal capacity and annual utilization from 1995 to 2015. (John W. Lund and Tonya L. Boyd, 2015)

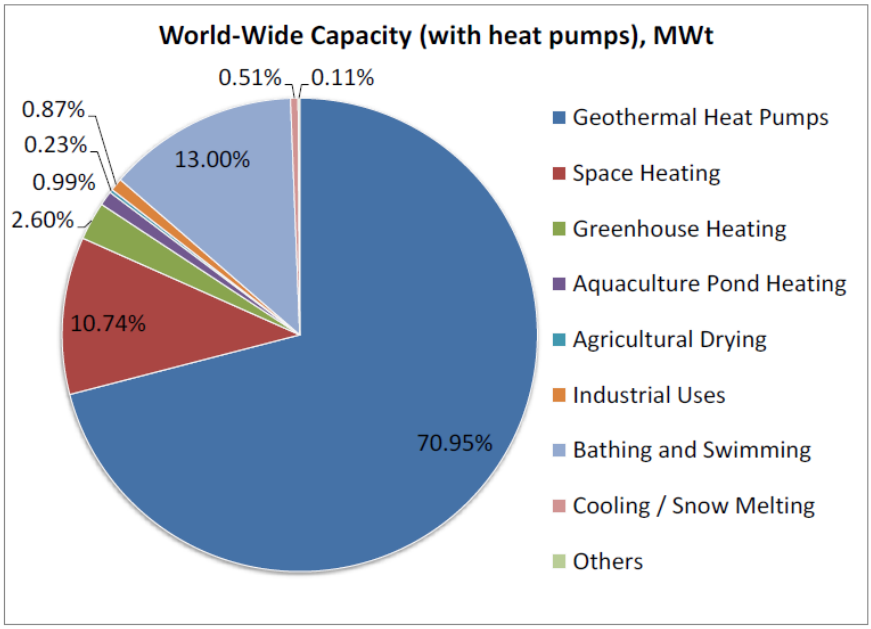


Figure 24 Geothermal direct applications worldwide in 2015, distributed by percentage of total energy used (TJ/year) (John W. Lund and Tonya L. Boyd, 2015).

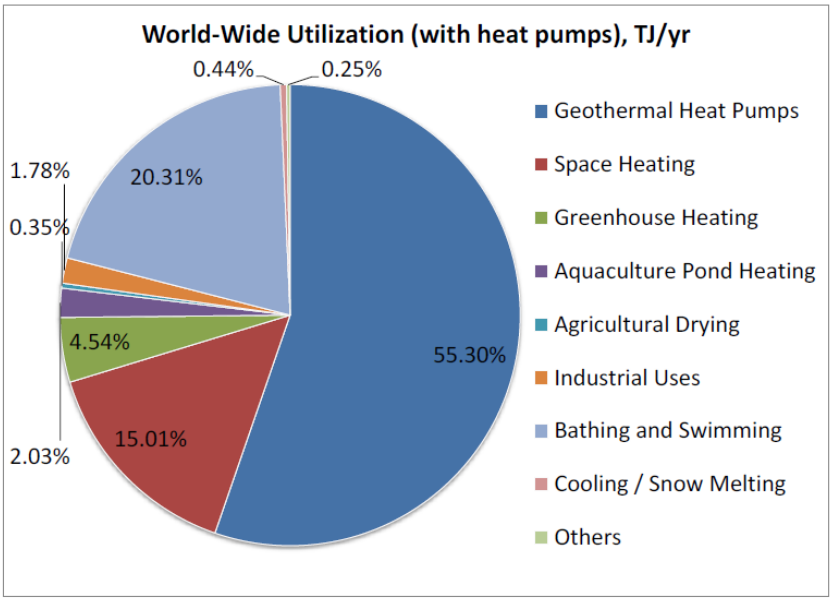


Figure 25 Geothermal direct applications worldwide in 2015 without geothermal heat pumps, distributed by percentage of total installed capacity (MWt) ) (John W. Lund and Tonya L. Boyd, 2015).

An attempt was made to distinguish individual space heating from district heat, but this was often difficult, as the individual country reports did not always make this distinction. Our best estimate is that district heating represents 88% of the installed capacity and 89% of the annual energy use. Snow melting represents the majority of the snow melting/air-conditioning category. “Other” is a category that covers a variety of uses, details of which are not frequently provided, but is known to include animal husbandry and carbonation of soft drinks.

### 2.1.22 Aquaculture pond and raceway heating

Aquaculture use of geothermal energy has increased over WGC2010, amounting to a 6.6% increase in installed capacity and a 3.7% increase in annual energy use. The installed capacity is 696 MWt and the annual energy use is 11,953 TJ/year. Twenty-

one countries report this type of use, the main ones in terms of annual energy use being USA, China, Iceland, Italy and Israel the same as in 2010. These facilities are labour intensive and require well-trained personnel, which are often hard to justify economically, thus, the reason why the growth is slow. Tilapia, salmon and trout seem to be the most common species, but tropical fish, lobsters, shrimp and prawns, as well as alligators are also being farmed. Based on work in the United States, it is estimated that 0,242 TJ/year/tonne of fish (bass and tilapia) are required, using geothermal waters in uncovered ponds. Thus, the reported energy use of 11,953 TJ/year represents an estimated equivalent of 49,393 tonnes of annual production, representing a 3.8% increase over 2010.

### 2.1.23 Agricultural crop drying

Fifteen countries report the use of geothermal energy for drying various grains, vegetables and fruit crops compared to 13 in 2010 and 15 in 2005. Examples include: seaweed (Iceland), onions (USA), wheat and other cereals (Serbia), fruit (El Salvador, Guatemala and Mexico), Lucerne or alfalfa (New Zealand), coconut meat (Philippines), and timber (Mexico, New Zealand and Romania). The largest uses are in China, USA and Hungary. A total of161 MWt and 2030 TJ/year are being utilized, an increase of 28.8% and 24.2% respectively compared to WGC2010.

### 2.1.24 Industrial process heat

This is a category that has applications in 15 countries, the same as in 2010. These operations tends to be large and have high energy consumption, often operating year-around. Examples include: concrete during (Guatemala and Slovenia), bottling of water and carbonated drinks (Bulgaria, Serbia and the United States), milk pasteurization (Romania and New Zealand), leather industry (Serbia and Slovenia), chemical extraction (Bulgaria, Poland and Russia), $CO_2$ extraction (Iceland and Turkey), pulp and paper processing (New Zealand), iodine and salt extraction (Vietnam), and borate and boric acid production (Italy). The installed capacity is 614 MWt and the annual energy use is

10,454 TJ/year, a 15% increase and an 11% decrease, respectively, compared toWGC2010. As expected, because of almost year-around operation, heat use for the industrial processes has one of the highest capacity factors of all direct uses of 0.54, down from 0.70 in 2010. No reason is given for the decrease in annual energy use and capacity factor; however, it may be due to more operations that are efficient and use of energy, or to fewer operating hours per year.

### 2.1.25 Geothermal direct uses in Italy

The use of hot geothermal waters in Italy dates back to prehistoric times and developed intensively during the Roman Antiquity (3rd B.C. - 5 th A.D.). Applications included: thermal baths, cooking food, heating spa facilities in localities with active manifestations, and use of hydrothermal minerals. All these uses declined notably from the 6th to the 12th centuries A.D., but started to grow again from the 13th century onward, reaching a peak in the early 20th century with the production of boron compounds. In that long lapse of time (over 3,000 years), two phases of most intensive development of direct uses occurred: the first during the imperial period of Rome (1st B.C. - 4 th cent. A.D.) with widespread use of thermal balneology, and the second between 1850-1920 with the intensive exploitation of hydrothermal minerals. References on direct applications of geothermal energy in Italy from Prehistory to the end of the second millennium can be found in Ciardi and Cataldi (2005). Almost 325 MWt capacity of direct uses was installed in Italy towards the end of the 20th century (Cappetti et al. 2000). In that period Italy was one of the first five countries of the world (the first in Europe) in terms of annual spa users; as a consequence, thermal balneology has been the main sector of direct uses for a long time. After 2000, other direct uses (especially ground-source heat pumps) started to grow: initially (2000-2005) at small annual rates, and afterwards with moderate or relatively sustained paces.

Concerning geothermal electricity production, we shall limit ourselves here to recall that, following studies, lab experiments and the installation of two demonstration units (20 kWe each), the first industrial power plant in the world (250 kWe ) entered into

operation in September 1913 at Larderello. Since then, two main periods of development occurred: the first until July 1944 when, due to events related to the 2nd World War, the capacity installed (127 MWe ) was totally destroyed; and the second from late 1944 onward, when the installed capacity started to grow unceasingly till reaching 875 MWe at Dec. 2013, with a gross production of 5.66 TWh. For geothermal power generation a specific country report has been prepared by Enel authors for this Congress (Razzano and Cei, 2015).

Direct uses are undergoing continuous growth in Italy and in over 80 other countries in the world. Their importance within the global energy scenario is increasing continuously, especially thanks to the huge development of ground-source heat pump applications. The renewable share of the heat delivered by direct uses is counted within the energy balance of each European country and contributes to reach the EU energy targets mandated by the Directive 2009/28/EC for European Union and by the law Decree 2011/28 for Italy.

To date, at least in Italy, but probably also in many other countries, only a few geothermal operators monitor and declare actual operation data; therefore, it is practically impossible to identify and list all existing systems, especially those with a small capacity (e.g. domestic heating, geothermal heat pumps, fish farming pools, and others). Moreover, even when direct use systems are known, not always the energy data are available, and consequently the final figures of most countries must be estimated. On the other hand, a globally established methodology to assess the final statistics on direct uses does not exist. For these reasons, current values are often an aggregation of fragmentary and incomplete figures, mainly based on simplifying assumptions and personal evaluations by the papers' author(s).

In addition, it is worth recalling that direct applications often combine the geothermal source with other forms of energy, e.g. natural gas, electricity, solar technologies and others; therefore, the use of too simple equations, without a proper energy fluxes analysis, may result in wrong evaluations (for thermal balneology see, for instance, Cataldi and Conti, 2013). Furthermore, regarding terminology, many reports and papers on direct uses show a variety of acronyms and concepts without providing an Conti et al

adequate definition of the terms used. Finally, we must point out that, to date, an established methodology to evaluate the geothermal contribution in "cooling applications" has still not been defined.

### 2.1.26 Geothermal Direct Uses in Apulia

Several large privately owned fish farms installed in the Apulia coast of SE Italy utilise tepid geothermal water for an energy amount in the order of 16,000 TOE/year. Two plants are located at Sannicandro, near Foggia, and use almost 1,500 $m^3$ /h of 25°C saline water from several shallow wells. One farm (AGROITTICA) built in 1985, produces 500 t/y of sea bass, sea breams (80% of total) and eels (20%). The other (EUROQUALITY) grows decorative species (mainly redfish). North of Brindisi PANITTICA PUGLIESE owns a large hatchery-nursery which uses 4,900 $m^3$ /h of 19°C salt water pumped from several 250 m deep wells. Beside fry, some market size fish are also produced. At the southern outskirts of Brindisi ITTICA SUD raises sea bass and sea breams in a plant using almost 400 $m^3$/h of saline water, at a temperature of 25°C, from 200 m deep wells. Production is 200 ton/year.

### 2.1.27 Geological and geothermal Italian background

The Italian territory formed as a result of the collision between the African and European plates, which started in the Upper Cretaceous (80 My ago) and ended in the Upper Miocene (10 My ago). During this long period, a compression regime predominated in the south-western Mediterranean area, with mantle arching, rising of igneous material from deep magma chambers, thinning of the crust, formation of anatectic bodies at shallow depth, and development of large thermal anomalies with high heat flow values (80 - 450 mW/$m^2$ (Fig. 26). A tensional regime followed in the Pliocene and Quaternary, with formation of prevailingly NW-SE horst-graben structures and thick faulting, accentuation of thermal anomalies in areas of up-lifted features, and extrusion of deep and

magmas. These phenomena occurred especially in the pre-Apennines belt from Tuscany to Campania, in the southern Tyrrhenian Sea, in central Sardinia, and in eastern Sicily (Fig. 26).

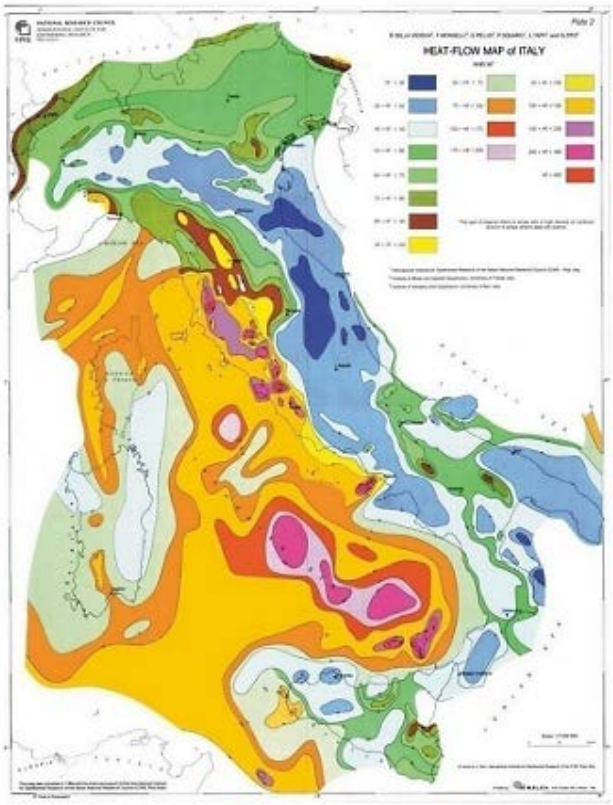


Figure 26 Conductive heat flow of Italian territory (after Buonasorte et al., 2010).

Where permeable complexes overlain by impermeable covers exist at relatively short distance from absorption outcrops through which meteoric water can percolate, confined aquifers formed, with water temperature depending on the depth of the aquifer and the intensity of the local thermal regime. Thus, temperature in such aquifers may range between many tens and few hundreds degrees °C at depths, say, of between several hundreds and few thousands metres. In the latter cases, if favourable hydroge-

ological conditions exist as a result of combined structural and lithostratigraphic situations, a convective circulation may have been triggered inside confined aquifers, with local escapes of hot water along fractures and faults and formation of hot springs in many areas. In particular, where thermal anomaly is strong enough and confined aquifers are found at relatively shallow depths, the water temperature may reach values well above 100°C; therefore, steam caps may have formed at the top of the reservoir with fumarole vents at surface. This type of manifestations, however, occur in few places only, characterized by recent intrusive processes or young and present volcanic activity.

On the contrary, where permeable formations of notable thickness (several hundreds metres, or more) outcrop and overlay impermeable complexes, unconfined aquifers exist, whose water temperature exceptionally exceeds 50 °C within 2 km depth. In these situations too, owing to peculiar hydrogeological conditions (heteropies of facies, fault contacts, lateral barriers with impermeable formations, differential porosity, belts of thick fractures, etc.), the water may escape upwards from unconfined aquifers to form superficial springs with temperature in most cases below 50°C. In particular cases only, where structural situation occur of the "range and basin" type, and the water can rise fastly through faults from depths above 3 km, its surface temperature may reach 70-80°C. However, the sizeable quantity of thermal energy associated to such unconfined aquifers can be harnessed in few cases only, for low-temperature applications. In addition to the factors mentioned above (heteropies of facies, fault contacts, etc.), inversions of lithostratigraphic sequences with doubling of series in many areas of Italy also played an important role on the formation of geothermal fields and manifestations. Such inversions are the result of the compression tectonics (with main north- and eastwards components) occurred during the final orogenetic stage of the Alps and Apennines, characterized by overturned anticlinals, detachments of rock complexes from their basement, and over thrusts of thick nappes over younger terrains. This compression tectonics, preceded the occurrence in the Pliocene and Quaternary of the tensional tectonics cited before, with formation of horst-graben structures and thick faulting.

The tensional tectonics, in turn, affected and modeled the piedmont belt of the southern Alps and of the western Apennines, where the recent igneous processes highlighted in Figure 27 were concurrently happening during the late Pliocene and the Quaternary.

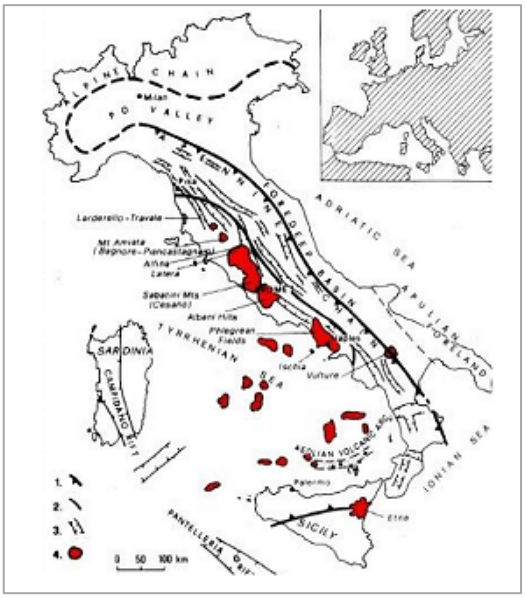


Figure 27 Main geodynamic domains and recent volcanism (after Buonasorte et al., 2010).

And in fact, as result of all the above, the areas with the thickest concentration of thermal anomalies and hot springs in Italy are found in the Euganean district near Padua, in the pre-Apennines belt of Tuscany-Latium-Campania, and in the Ischia island in the southern Tyrrhenian Sea. In short, a wide variety of geological and geodynamic situations can be found in Italy, both at the regional and local scale, in each of which different types of geothermal resources could form. Therefore, Italy is endowed with all types of geothermal resources and systems: high-, moderate-, and low-temperature resources associated with hydrothermal and unconventional geothermal systems. Concerning high-temperature hydrothermal systems at depths $\leq$ 5 km, however, we should point out that the aggregate surface extension of their occurrence areas is 1,500 km$^2$ at most; thus, the resources harness able from them for power generation are intrinsically limited by the slightness of their existence areas. The high-temperature unconventional systems, on the contrary, are found in much larger areas (Cataldi et al., 2015; Proceedings

of this WGC2015). To sum up, the long-term future of geothermal energy in Italy should be envisioned in the light of a much more sustained development of moderate-to-low temperature resources for direct applications, and on the possibility to harness high-temperature unconventional systems for power generation. More detailed information on the geological background of the Italian geothermal resources and manifestations are given in Buonasorte et al. (2011), Cataldi et al. (2013), and Carlino et al. (2013). For thermal springs, in particular, reference can be made to the papers by Cataldi et al. (2010), and Ceccarelli A. and Ceccarelli E. (2010).

### 2.1.28 Italian geothermal development by 2030

In early 2011, a study was initiated to estimate the possible contribution of the Earth's heat to the coverage of national energy requirements by 2030, with steps by 2012, 2015, 2020, 2025 to be periodically updated. The end goal of the study was to provide the Italian Government with factual elements on the possible medium-term deployment of this energy source in Italy, as well as to launch a New Italian Geothermal Manifesto with a wider vision than the one published by UGI almost five years ago. Growth projections were formulated by taking into account:

i) Italy's geological setting and geothermal resources known or supposed to exist down to 5 km depth;
ii) likely sharp increase in fossil fuel prices in the next years; and
iii) expected technological improvements in the utilization of the Earth's heat.

Two different growth scenarios have thus been developed on the following assumptions:

- Scenario I: current economic trend, use of mature production technologies, and prices of crude oil
- Scenario II: economic trend driven by vigorous environmental policies, use of both mature and advanced production technologies, and prices of crude oil.

On this basis, the 2010-2030 growth projections under Scenarios I and II are summarized in Tab. 10 and Fig. 28 for geothermal power generation and in Tab. 11 and Fig.

29 for direct uses. These uses include the energy produced with geothermal heat pumps.

Table 10 2010-2030 development of geothermal power generation, with oil savings and avoided $CO_2$ emissions

| *Anno/Year* | *2010* | *2020* | *2030* |
|---|---|---|---|
| **SCENARIO I** | | | |
| ***Potenza installata (MW)*** *Installed capacity* | 882,5 | 1 080 | 1 500 |
| ***Produzione lorda (TWh/y)*** *Gross generation* | 5,343 | 6,9 | 9,4 |
| ***Olio risparmiato (kTOE/y)*** *Oil saved* | 1 020 | 1 310 | 1 790 |
| ***$CO_2$ evitata (kTonnes/y)*** *Avoided $CO_2$ emissions* | 3 200 | 4 140 | 5 700 |
| **SCENARIO II** | | | |
| ***Potenza installata (MWe)*** *Installed capacity* | 882,5 | 1 150 | 2 000 |
| ***Produzione lorda (TWh/y)*** *Gross generation* | 5,343 | 7,3 | 12,0 |
| ***Olio risparmiato (kTOE/y)*** *Oil saved* | 1 020 | 1 390 | 2 280 |
| ***$CO_2$ evitata (kTonnes/y*** *Avoided $CO_2$ emissions)* | 3 200 | 4 380 | 7 200 |

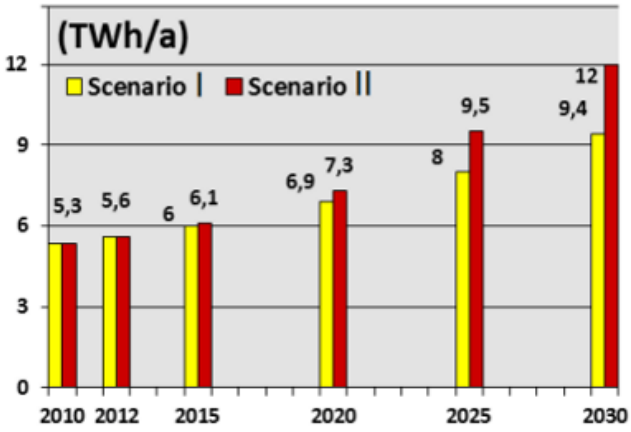

Figure 28 2010-2030 development of geothermal generation under Scenarios I and II

Table 11 Development of indirect uses from 2010-2030

| *Anno/Year* | *2010* | *2020* | *2030* |
|---|---|---|---|
| ***SCENARIO I*** | | | |
| ***Potenza installata*** *(MW$_{th}$)* *Installed capacity* | 1 000 | 2 510 | 7 400 |
| ***Produzione lorda*** *(TJ/y)* *Gross production* | 12 600 | 26 380 | 65 200 |
| ***Olio risparmiato*** *(kTOE/y)* *Oil saved* | 300 | 630 | 1 560 |
| ***$CO_2$ evitata*** *(kTonnes/y)* *Avoided $CO_2$ emissions* | 800 | 1 640 | 4 060 |
| ***SCENARIO II*** | | | |
| ***Potenza installata*** *(MW$_{th}$)* *Installed capacity* | 1 000 | 2 750 | 8 800 |
| ***Produzione lorda*** *(TJ/y)* *Gross production* | 12 600 | 30 660 | 90 000 |
| ***Olio risparmiato*** *(kTOE/y)* *Oil saved* | 300 | 740 | 2 160 |
| ***$CO_2$ evitata*** *(kTonne/y)* *Avoided $CO_2$ emissions* | 800 | 1 920 | 5 620 |

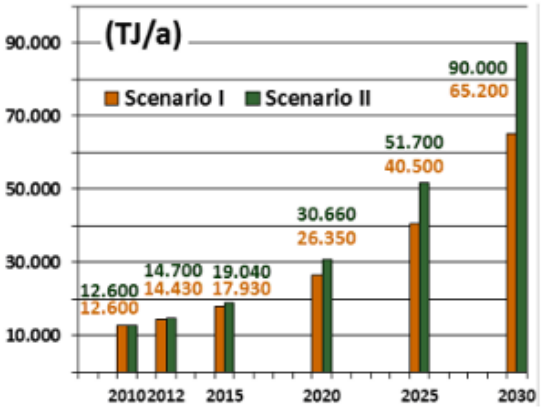


Figure 29 (2010-2030 development of direct uses including heat pumps under Scenarios I and II)

In terms of regional distribution, geothermal power generation is estimated to come from Tuscany, but only until 2015; afterwards, beginning in the second half of this decade, it is expected to start coming also from other Italian Regions. The share of geothermal power generated in the latter Regions may attain by 2030, 18% of the total under Scenario I, and 25% under Scenario II. Concerning direct uses, the share obtained by geothermal heat pumps is estimated to progressively rise from 1,700 TJ/yr in 2010 to nearly 4,700 TJ/yr in 2020 and to 15,000 TJ/yr in 2030 under Scenario II, thus from

13.5% at present to roughly 17% by December 2030. All types of direct uses (space heating and cooling, farming, fisheries, aquaculture, industrial processes and other minor uses) are projected to increase in absolute terms. Space heating and cooling, ranking first in 2010 (38%), will grow faster than other uses, hitting over 60% of the total by 2030.

These are of two main types of Benefits expected from geothermal development until 2030:

i) technical and environmental;
ii) Economic-social and scientific.

The values shown in Tables 12 and 13 for geothermal generation and direct uses quantify as follows the benefits resulting from the exploitation of geothermal resources until 2030.

a) Savings in terms of oil-equivalent;
b) Avoided CO2 emissions:

1. for Scenario I: 5.78 (4.14+1.64) Mtonnes in 2020 and 9.76 (5.7+4.06) Mtonnes in 2030;
2. For Scenario II: 6.30 (4.38+1.92) Mtonnes in 2020 and 12.82 (7.2+5.62) Mtonnes in 2030.

c) Contribution to coverage of total energy consumption Total primary energy consumption (185 MTOE in 2010) is assumed to decrease until 2015 and to increase again in the following years, reaching some 200 MTOE in 2020 and 230 MTOE in 2030. On this assumption, the overall contribution of geothermal energy to savings in terms of oil-equivalent will rise from 0.71% in 2010 to about 1% under both Scenarios I and II in 2020, reaching 1.5% under Scenario I and 2% under Scenario II by 2030. In addition to the above-cited technical and environmental benefits, geothermal development until 2030 is expected to yield the following other benefits.

d) New R&D (in all fields of geothermal energy, including but not limited to the implementation of a major R&D project focused on the development of nonconventional high-temperature systems for power generation):

In particular, the above-said R&D project on non-conventional geothermal systems is aimed at testing their characteristics in Italy's unique geological setting and at making it possible to start their systematic development for power generation 10-12 years from now.

# *CHAPTER 2*
# *PRINCIPAL PROCESSES OF HEAT TRANSFER*

## 2.2.0 Processes of heat transfer

Heat can be transferred by three processes:

1. Conduction;
2. Convection;
3. Radiation.

Conduction governs the thermal conditions in almost entire solid portions of the Earth and plays a very important role in the lithosphere. Convection dominates the thermal conditions in the zones where large quantities of fluids (mostly molten rocks) exist, and thus it governs the heat transport in the fluid outer core and the mantle. On a geological time scale, the mantle behaves like a viscous fluid due to the existence of high temperatures. Convection, which involves transfer of heat by the movement of mass, is a more efficient means of heat transport in the Earth compared to pure conduction. However, in several processes of the Earth's interior, both conductive as well as convective heat transfer play important roles. Radiation is the least important mode of heat transport in the Earth. The process of heat exchange between the Sun and the Earth, through radiation, control the temperatures at the Earth's surface. Inside the Earth, radiation is significant in the hottest parts of the core and the lower mantle only. The loss of Earth's internal heat through the continental and oceanic lithosphere takes place primarily by

conduction, except near the mid-oceanic ridges where convection due to hydrothermal circulation becomes significant. Cooling of magmatic intrusive bodies inside the crust and the upper mantle takes place both by conduction as well as convection. In anomalous geothermal locales such as near geysers, hot water springs and fumaroles, convective heat transfer through circulating hot waters in the shallow subsurface levels far exceeds the background heat conduction. Conduction governs the temperature distribution in the continental lithosphere as well as effects of sedimentation, burial, uplift and erosion on subsurface temperature distribution. Convection dominates heat transfer in the Earth's deep mantle and core. Introduction Direct-use of geothermal energy is one of the oldest, most versatile and common forms of utilizing geothermal energy (Dickson and Fanelli, 2003). The early history of geothermal direct-use has been reviewed for over 25 countries in the Stories from a Heated Earth-Our Geothermal Heritage (Cataldi et al., 1999), that documents geothermal use for over 2000 years.

### 2.2.1 Temperature, heat and its storage

Temperature of an object can be described as the property, which determines the sensation of hotness or coldness felt from contact with it. More unambiguously, using the Zeroth law of thermodynamics, temperature of a system is defined as the property that determines whether or not that system is in thermal equilibrium with any other system with which it is put in thermal contact (Finn, 1993). When two or more systems are in thermal equilibrium, they are said to have the same temperature. Temperature is most commonly measured in the Celsius (°C), Fahrenheit (°F) and Kelvin (K) scales. The first two scales are based on the melting point of ice and the boiling point of water. In the Kelvin scale, the limiting low temperature, called the absolute zero, is taken as the zero of the scale, and the triple point of water-where the ice, water and water vapor phases can co-exist in equilibrium, is equal to 273,16 K. The three scales are related as follows:

$$(K) = (°C) + 273.16$$
$$(°C) = 5/9[(°F) - 32]$$
$$(°F) = 9/5°(C) + 32$$

(2)

Heat is defined as the energy transfer between two systems at different temperatures. Heat energy originates from other kinds of energy according to the first law of thermodynamics. It is important to distinguish between temperature and heat. Temperature is a property of matter, while heat is the energy that is flowing because of a temperature difference. According to the second law of thermodynamics,transmission of heat takes place from a body at a higher temperature to another body at a lower temperature. Under suitable conditions, heat can be transformed into yet other forms of energy. When subjected to heating, a body consumes the heat energy ($\Delta Q$) through the increase of its internal energy ($\Delta U$) and work done in doing so ($\Delta W$), i.e., $\Delta Q = \Delta U + \Delta W$. Thermodynamic processes that occur without the gain or loss of heat to or from the system are called as adiabatic processes.

The calorie was originally considered as the basic unit of heat energy, being equal to the heat required to raise the temperature of 1°C of pure water from 14.5 to 15.5 °C at normal atmospheric pressure. This unit is used even today in several countries. After the widespread adoption of the SI system of units, heat is usually expressed in units of energy, i.e., joule (J), with the relation: 1 cal= 4.184 J.

Storage of heat energy is the change of enthalpy or heat content of a medium in the path of heat transmission. In accordance with the first law of thermodynamics, change of enthalpy ($\Delta Q$) occurs as a result of a change in the temperature ($\Delta T$) of the medium with time. The amount of heat that a body is able to store as a result of change in temperature, called free heat, depends upon its specific heat capacity (c). It is defined as the amount of heat required to raise the temperature of unit mass of a material by 1 °C, and it differs from one material to another. In the case of gases, the distinction between specific heat at constant pressure as well as at constant volume becomes important and it needs to be considered. Specific heat capacities of some common materials are listed in Table 12. The relationship between change in heat content and change in temperature of a body of mass m is generally expressed as:

$$\Delta Q = mC\Delta T \tag{3}$$

Table 12 Specific heat capacities of some commonly used materials at 20 °C (Source: Tipler, 1999)

| Substance | Specific heat capacity J kg$^{-1}$ K$^{-1}$ |
|---|---|
| Aluminum | 900 |
| Bismuth | 123 |
| Copper | 386 |
| Brass | 380 |
| Gold | 126 |
| Lead | 128 |
| Silver | 233 |
| Tungsten | 134 |
| Zinc | 387 |
| Mercury | 140 |
| Alcohol (ethyl) | 2,400 |
| Water | 4,186 |
| Ice (−10 °C) | 2,050 |
| Granite | 790 |
| Glass | 840 |

Several geothermal problems involve fluid filled porous rocks, with water as a common fluid. The specific heat capacity of a rock with $a_1$ kilograms of dry weight and $a_2$ kilograms of water content is given by (after Kappelmeyer and Haenel, 1974)

$$c_{wet} = \frac{a_1 c_{dry} + a_2 c_{water}}{a_1 + a_2} \tag{4}$$

or simply by

$$c_{wet} = a_1 c_{dry} + (1 - a_1) c_{water} \tag{5}$$

when $(a_1+a_2)= 1$, i.e., 1 kg of wet porous rock containing $a_2$ kilograms of water. A typical value of specific heat capacity for dry rocks and soils is ~840 J kg$^{-1}$K$^{-1}$ while that for water is ~ 4184 J kg$^{-1}$K$^{-1}$. Therefore, with the increase of water content, the specific heat of the porous rocks increases.

It should be noted that heat added or removed during phase changes do not change the temperature. Therefore Eq. (5) is not valid when a phase change takes place, for example, from ice to water or from water to vapor. Large amounts of energy are required for such phase change. The amount of energy required to change a unit mass of a substance from the solid to the liquid state without changing its temperature is called the latent heat of fusion. A change from solid to liquid phase involves absorption of energy whereas a change from liquid to solid phase would involve release of energy by the same amount. The energy required to change a unit mass of a liquid into the gaseous state at the boiling point is called the latent heat of vaporization. The expression for change in heat content ($\Delta$Q) in case of phase transformation is given by

$$\Delta Q = L\Delta m \tag{6}$$

where L is the latent heat of vaporization, expressed in kJ $kg^{-1}$, and $\Delta$m the mass of substance (in kg) transformed.

However, several geothermal problems involve change of enthalpy or heat content due to both changes of temperature and phase. In such cases, $\Delta$Q can be expressed as:

$$\Delta Q = \sum mc\Delta T + \sum L\Delta m \tag{7}$$

where the summation is carried out for a system comprising materials of different specific heat capacities and latent heats.

### 2.2.2 Heat Conduction

Thermal conduction takes place by the transfer of kinetic energy of molecules or atoms of a warmer body to those of a colder body. The transfer of kinetic energy takes place through movement of the valence electrons (also called conduction electrons) in an atom, a process analogous to electrical conduction. This type of conduction can take place in both solids and fluids. Inside the Earth, however, conduction of heat takes place mainly through poorly conducting solid rocks constituting the crust and the mantle, which are comprised of minerals having a very few conduction electrons. Another type of conduction, called lattice or phonon conduction, caused by lattice vibrations in the rocks, is primarily responsible for heat transfer in such cases. Detailed treatment of heat conduction is provided in several textbooks (e.g., Carslaw and Jaeger, 1959; Jacob, 1964); applications of heat conduction to problems in geothermic have been dealt by Kappelmeyer and Haenel (1974), Lachenbruch and Sass (1977), Haenel et al. (1988) and others.

### 2.2.3 Fourier's Equation of Heat Conduction

When a temperature gradient exists within a body, heat energy will flow from the region of high temperature to the region of low temperature. This phenomenon is known as conductive heat transfer, and is described by Fourier's equation:

$$\vec{q} = -k\vec{\nabla}T \tag{8}$$

where $\vec{q}$ is the flow of heat per unit area per unit time (called as heat flow), k the thermal conductivity of the body (assumed isotropic) and $\vec{\nabla}T$ is the temperature gradient. The negative sign appears because heat flows in the direction of decreasing temperature. When applied to the heat flow of the Earth, we usually consider the heat flow toward the Earth's surface, i.e., $k(\frac{\delta T}{\delta z})$ , where the z-axis is taken vertically downward.

$(\frac{\delta T}{\delta z})$ is called the geothermal gradient, and is expressed in 1Ckm$^{-1}$ or mKm$^{-1}$. Thermal conductivity depends on the nature of the material through which the heat is flowing and is affected by physical conditions such as the temperature. It is expressed in Wm$^{-1}$K$^{-1}$. From Eq. (8) it follows that within an isotropic body, heat flow is a vector quantity with its direction normal to the surface of constant temperature. Heat flow is expressed in mWm$^{-2}$.

In geothermic, one often has to deal with media having anisotropic thermal properties. This is particularly common while dealing with the problems of heat flow in sedimentary rocks where the properties in the bedding plane (plane of sedimentation) tend to differ from properties perpendicular to it. Similarly, one often has to deal with crystals and rock-forming minerals belonging to different systems, such as the monoclinic (feldspar, mica), orthorhombic (pyroxene, olivine), hexagonal (quartz, ilmenite) and other systems.

In an anisotropic media, the thermal conductivity could be represented by a symmetrical tensor of the second order of the type

$$\begin{pmatrix} k_{11} & k_{12} & k_{13} \\ k_{21} & k_{22} & k_{23} \\ k_{31} & k_{32} & k_{33} \end{pmatrix} \tag{9}$$

Assuming each component of the heat-flow vector to be linearly dependent on all components of the temperature gradient at that point, we could write the heat flow in the three mutually perpendicular directions for an anisotropic media as ( Kappelmeyer and Haenel (1974), Lachenbruch and Sass (1977)):

$$q_x = -(k_{11}\frac{\partial T}{\partial x} + k_{12}\frac{\partial T}{\partial y} + k_{13}\frac{\partial T}{\partial z})$$
$$q_y = -(k_{21}\frac{\partial T}{\partial x} + k_{22}\frac{\partial T}{\partial y} + k_{23}\frac{\partial T}{\partial z})$$
$$q_z = -(k_{31}\frac{\partial T}{\partial x} + k_{32}\frac{\partial T}{\partial y} + k_{33}\frac{\partial T}{\partial z})$$

(10)

In the case of anisotropic layers, conductivity being different in the three mutually perpendicular directions coinciding with the x-, y- and z-axes, Eq. (10) simplifies to

$$q_x = -(k_1\frac{\partial T}{\partial x})$$
$$q_y = -(k_2\frac{\partial T}{\partial y})$$
$$q_z = -(k_3\frac{\partial T}{\partial z})$$

(11)

In Eq. (11), $k_1$, $k_2$ and $k_3$ are conductivities in the x, y and z directions, respectively. In case the conductivity is the same in the xy plane ($k_1 = k_2$) and different in the z direction, a case seen very often in sedimentary rocks, the heat flow could be expressed as

$$q_x = q_y = -(k_1 \frac{\partial T}{\partial x}) = -(k_1 \frac{\partial T}{\partial y})$$

$$q_z = -(k_3 \frac{\partial T}{\partial z}) \qquad \text{(since } \frac{\partial T}{\partial x} = \frac{\partial T}{\partial y}\text{)}$$

(12)

### 2.2.4 Differential Equation of Heat Conduction

Fourier's equation, with the energy conservation law, can be used to derive a differential equation describing the temperature field in a medium. In other words, the equation is the mathematical expression of the fact that the rate of increase of heat content of a small volume should be equal to the sum of the rate of heat generation in it and the rate of flow of heat into it across its surface. For the Earth, the rate of heat generation per unit volume could represent the effects of radioactive decay, phase change, frictional heating or chemical reaction. For a material of constant conductivity (isotropic) with a constant rate of heat generation A per unit time per unit volume, the differential equation can be written as (Carslaw and Jaeger, 1959):

$$\nabla(-k\nabla T) = A - \rho c \frac{\partial T}{\partial t}$$

(13)

where $\rho$ is density, c the specific heat capacity at constant pressure, the product ($\rho$c) is called the volumetric specific heat capacity, t the time. Eq. (12) can be simplified to

$$\nabla T^2 - \frac{1}{\alpha}\frac{\partial T}{\partial t} = -\frac{A}{k}$$

(14)

where $\alpha$= k/$\rho$c is called thermal diffusivity; it is expressed in $m^2\ s^{-1}$. In the one dimensional case, for heat flow in the z direction, Eq. (13) reduces to

$$\frac{\partial^2 T}{\partial z^2} - \frac{1}{\alpha}\frac{\partial T}{\partial t} = -\frac{A}{k}$$

(15)

If there are no heat sources within the small volume, i.e., A = 0, Eq. (14) reduce to the Poisson's equation:

$$\frac{\partial^2 T}{\partial z^2} = \frac{1}{\alpha}\frac{\partial T}{\partial t}$$

(16)

Further, at steady state, $\frac{\partial T}{\partial t} = 0$ , Eq. (15) reduces to the Laplace's equation:

$$\frac{\partial^2 T}{\partial z^2} = 0$$

(17)

The differential equation of heat conduction (14) can be modified in different cases such as variable conductivity, or water flow with a finite velocity, and can be solved for understanding heat transfer processes in a wide variety of situations inside the Earth.

### 2.2.5 Heat Convection

Within fluids, the heat transfer takes place through a combination of molecular conduction and energy transportation created by the motion of fluid particles. This mode of heat transfer is known as convection. The heat exchange rate in fluids by convection is much higher than the heat exchange rate in solids through conduction.

This difference becomes more prominent in geothermic because rocks have very low-thermal conductivities compared to metals and other solids.

Convection processes inside the Earth can be of two broad types: free and forced. Free or natural convection refers to the free motion of a fluid and is solely due to differences in the densities of the heated and cold particles of a fluid. The origin and intensity of

free convection are solely determined by the thermal conditions of the process and depend on the kind of fluid, temperature, potential and volume of the space in which the process takes place. Forced convection occurs under the influence of some external force. Flow of water in hot springs and heat transport due to volcanic eruptions are examples of forced convection (advection). Forced convection depends on the physical properties of the fluid, its temperature, flow velocity, shape and size of the passage in which forced convection of fluid occurs. Forced convection may be accompanied by free convection, and the relative influence of the latter increases with the difference in the temperatures of individual particles of the fluid and decreases with the velocity of the forced flow. The influence of natural convection is negligible at high-flow velocity.
In problems dealing with the transmission of heat through the process of convection, the fluid under consideration is usually bounded on one or more sides by a solid. Let at any given time, $T_s$ be the temperature of the solid at its boundary with the fluid and $T_n$ the fluid temperature at a far-off yet unspecified point. In accordance with Newton's law of cooling, the amount of heat flowing would be proportional to the temperature difference and could be expressed as:

$$q = h(T_s - T_\infty) \tag{18}$$

where h is the heat transfer coefficient. The heat is transferred by convection and consequently the heat transfer coefficient depends, in general, upon the thermal boundary condition at the solid–fluid boundary. However, under many situations, h can be estimated satisfactorily when the fluid dynamics of the flow system is known.

### 2.2.6 Heat radiation

In the previous sections, we have discussed the transfer of heat through conduction and convection, the two processes requiring presence of a medium. The means by

which energy is transmitted between bodies without contact and in the absence of intervening medium is known as radiation. Transmission of energy through radio waves, visible light, X-rays, cosmic rays, etc., all belong to this category, having different frequencies in the spectrum of electromagnetic radiation. Here we are concerned with the type of radiation which is principally dependent on the temperature of the body, known as thermal radiation and belonging mostly to the infrared and to a small extent to the visible portion of the electromagnetic radiation spectrum. The heat transferred into or out of an object by thermal radiation is a function of several components. These include its surface reflectivity, emissivity, surface area, temperature and geometric orientation with respect to other thermally participating objects. In turn, an object's surface reflectivity and emissivity is a function of its surface conditions (roughness, finish, etc.) and composition. To account for a body's outgoing radiation (or its emissive power, defined as the heat flux per unit time), one makes a comparison to a perfect body, which absorbs the entire amount of heat radiation falling on its surface as well as emits the maximum possible thermal radiation at any given temperature. Such an object is known as a black body. The concept of black body is important in understanding the radiation of heat. According to Stefan–Boltzmann's law, heat emitted by a black body at any given temperature, $q_b$ ($Wm^{-2}$), is expressed as follows for a unit area in a unit time:

$$q_b = \sigma T^4 \tag{19}$$

where $q_b$ is the heat flow through radiation from the surface of a black body, T the temperature, and $\sigma$ a constant known as the Stefan–Boltzmann constant, with a theoretical value of 5,67 x$10^{-8}$ $Wm^{-2}K^{-4}$. Because no material ideally fulfils the properties of absorption and emission of the theoretically defined black body, for practical purposes a new constant of emissivity, $\varepsilon$, is defined for real surfaces as

$$\mathrm{q} = \varepsilon \sigma T^4 \tag{20}$$

### 2.2.7 Heat Transfer in Porous Media

The behavior of heat transport in porous media is strongly dependent from the fluid velocity.
For high velocity flow, the interaction between solid and fluid phase is rapid and then solid and fluid phase cannot exchange sufficient amount of energy to establish local thermal equilibrium. At a given location, solid and fluid phases have different temperatures. In this situation, each phase needs an energy equation for the description of heat transport. Assuming that porosity, densities and heat capacities are constant in time, energy equations can be written for the fluid and solid phase:

$$\frac{\partial T_f}{\partial t} = -v\frac{\partial T_f}{\partial x} + \frac{\partial}{\partial x}\cdot\left(\frac{k_{eff}}{\rho_f c_f}\frac{\partial T_f}{\partial x}\right) + \frac{q_{fs}}{\rho_f c_f} \tag{21}$$

$$\frac{\rho_s c_s}{\rho_f c_f}\frac{\partial T_s}{\partial t} = \frac{\partial}{\partial x}\cdot\left(\frac{k_s}{\rho_f c_f}\frac{\partial T_s}{\partial x}\right) - \frac{q_{fs}}{\rho_f c_f} \tag{12}$$

The interaction between the two phases is represented by the sink/source terms $q_{fs}$ given by following equation:

$$q_{fs} = h^* s_f \left(T_s - T_f\right) \tag{23}$$

The convective heat transfer coefficient can be expressed as:

$$h^* = \left( \frac{d_p}{10k_s} + \frac{d_p}{\mathrm{Nu}\left(\mathrm{Pr},\mathrm{Re}\right)k_f} \right)^{-1} \tag{24}$$

Ergun (1952) redefined the Reynolds number to describe non-Darcy flow in porous media as:

$$\mathrm{Re} = \frac{\rho_f d_p v}{\mu} \frac{1}{1-n} \tag{25}$$

Hassanizadeh and Gray (1987) suggest Re = 10 as a critical value for non-Darcy flow. In low velocity, flow regimes the solid phase and fluid phase are in contact for a sufficient period, and there exists the possibility for energy exchange locally and to establish a local thermal equilibrium. In such case, only one energy equation is sufficient for the description of heat transport. The energy equation for the fluid and solid phases are combined into a single equation as:

$$\left( 1 + \frac{1-n}{n} \frac{\rho_s c_s}{\rho_f c_f} \right) \frac{\partial T_f}{\partial t} = \frac{\partial}{\partial x} \left( \frac{k_{eff}}{\rho_f c_f} \frac{\partial T_f}{\partial x} \right) - v \frac{\partial T_f}{\partial x} \tag{26}$$

Damnkholer number *Da* can be used in order to evaluate the presence of local thermal equilibrium. *Da* relates the convection time scale to the exchange time scale between two phases:

$$Da = \frac{hL}{\rho_f c_f v} \tag{27}$$

When $Da >> 1$ the heat exchange between the two phases is rapid and there is the instantaneous equilibrium between the two phases. On the contrary $Da << 1$ the heat exchange velocity between the two phases is very low and it does not influence the heat propagation. When the convection time scale close the exchange time scale $Da \cong 1$ the impact of local thermal non equilibrium behavior of heat transport is stronger and the temperature distribution are characterized by a long tail.

# *II PART*
# *RESEARCH AND EXPERIMENTATION WORK THROUGH LABORATORY AND ON SITE TESTS ABOUT HEAT TRANSPORT IN FRACTURED AND POROUS MEDIA*

During these three years of doctoral several bench scale experiments have been conducted over the past three years of doctorate. The first and the second work have involved the study of heat transport in fractured media. It was therefore constructed a prototype composed of fractured limestone. Several tests were conducted to single fracture and for the network of fractures and were compared in the second work the results obtained with those of the mass transport of a previous publication.
In order to model the obtained thermal breakthrough curves, the Explicit Network Model (ENM) has been used, which is based on an adaptation of a Tang's solution for the transport of the solutes in a semi-infinite single fracture embedded in a porous matrix. Parameter estimation, time moment analysis, tailing character and other dimensionless parameters have permitted to better understand the dynamics of heat transport and the efficiency of heat exchange between the fractures and matrix. The results have been compared with the previous experimental studies on solute transport.
Subsequently, in situ tests were performed on fractured media of chalky nature, at the university's experimental platform La Salle Beauvais. During this test it was carried out a laboratory test to natural gradient using hot water as a tracer. It was later created another prototype to study the heat transport in porous media. Therefore, two works were made from material with different grain size, which in the last work were compared. This study concerned the laboratory investigation of heat transport through a thermally isolated column filled with porous medium. The experiments consisted in injecting hot water flow rates in correspondence of two thermocouples positioned along a porous medium column and recording thermal breakthrough curves (BTCs). Several tests have been carried out, using porous materials with different grain sizes and several flow rates for each grain size of porous medium. This study has permitted to in-

vestigate the critical issues regarding heat transport phenomena such as the relationship between the flow velocity with the thermal dispersion and the validity of the local thermal equilibrium (LTE) and non-local thermal equilibrium (LNTE) to describe the behaviour between the fluid and solid phase.
Some works have been published, others are in review, others waiting to be published.

# *CHAPTER 3*

# *STUDY AND ANALYSIS OF HEAT TRANSPORT IN FRACTURED MEDIA*

## 2.3.0 LITERATURE REVIEW

Fractured geological formations are ubiquitous throughout the world, and are of interest in a number of contexts:

1. Reservoir exploitation for water supply;
2. Contamination from subsurface waste repositories;
3. Petroleum reservoir exploitation;
4. Geothermal reservoir exploitation and heat storage;
5. Mining and mineralization processes (in situ leaching and location of ore bodies);
6. Geotechnical applications (including effects on underground storage reservoirs, tunnels and other structures);
7. Deeper Earth systems, such as earthquakes and ocean floor hydrothermal venting.

Researchers with diverse backgrounds in hydrology, geology, soil science, engineering, physics, chemistry, statistics, and mathematics have undertaken a broad range of theoretical, numerical, laboratory, and field investigations.

The growing interest in geothermal energy source has stimulated attempts 32 to develop methods and technologies for extracting energy also from ground resource at low temperature. An example is the exploitation of low enthalpy geothermal energy that can be obtained at any place with the aid of ground-source heat pump system from the soil, rock and groundwater. In such geothermal systems the fluid movement and thermal behavior in the fractured porous media is very important and critical. In fractured rock formations, the rock mass hydraulic behavior is controlled by fractures. In such aquifers, open and well connected fractures constitute high permeability pathways and are orders of magnitude more permeable than the rock matrix (Cherubini and Pastore, 2011).

There is, therefore, a certain ambiguity associated with fractured media and predictive capabilities relating to flow and transport processes remain severely limited. The specific problems of interest considered here can involve single and multi-phase (miscible or immiscible) flow and transport, in saturated and in partially saturated domains, in fracture networks and in fractured porous formations. Fractures themselves range in size over scales ranging from microns to hundreds of kilo- meters. It is known that throughout this scale range, they have a significant effect on flow and transport processes in the Earth's crust.

In particular manner the transport of heat through geological media is central to many environmental and industrial processes, including heat generation from radioactive waste repositories, energy production in geothermal reservoirs, hydrocarbon extraction from subsurface formations, and hydrothermal flow in the oceanic and continental lithosphere. In many cases, it is assumed that heat transfer by convection and thermal dispersion is governed by a "Fourier" transport equation of the form [Nield and Bejan, 1992]:

$$\frac{\delta T}{\delta t} = \nabla[v_h T + k_e \nabla T] \tag{28}$$

where T is the effective temperature of the domain, $v_h$ represents the effective heat transfer velocity, and $k_e$ represents the effective thermal dispersion tensor; here

$$v_h = (v_n \rho_f c_f) / (\rho_e c_e) \tag{29}$$

where v is the interstitial fluid velocity, n is porosity, $\rho$ is density, c is heat capacity, and the subscripts e and f represent the effective and fluid parameters respectively.
In addition, the product $\rho_e c_e$ is defined as:

$$\rho_e c_e = [n \rho_f c_f + (1-n) \rho_s c_s] \tag{30}$$

where the subscript s indicates the solid phase.
While the standard model of heat transfer can describe the thermal breakthrough curves in some geological systems [e.g., Levec and Carbonell, 1985; Paek et al., 1999, 2001], there is evidence to suggest that significant deviations from Fourier like behavior do occur. An experiment studying heat transport in an artificial aquifer revealed that the inferred thermal dispersion coefficients changed significantly with time [Kim et al., 2005], while studies of thermal transfer in soils have noted that measured break-through curves (BTC's) sometimes exhibit highly non- Fourier behavior [Ochsner et al., 2005]. Such discrepancies between models and measurements are often attributed to inadequate controls over experimental conditions; however, they may also reflect the inherently non-Fourier nature of heat transfer in some systems.
Analogous to the non-Fickian transport of solutes in porous media, non-Fourier heat transfer in geological systems can also arise due to heterogeneities present at different spatial scales, including fractures and lithological and petrographic variations [Berkowitz et al., 2006]. Such features can lead to the transfer of heat parcels along different pathways with spatially varying velocities, which results in a broad spectrum of

transport rates. However, the fundamental difference between solute and heat transport is that heat diffuses about 100 times faster than solutes; in addition, standard models assume heat to be advected at a rate approximately equal to the Darcy velocity, rather than the interstitial pore velocity. Hence, for a given geological medium and flow regime, the difference in rates for heat and solute transport could lead to contrasting behaviours. Still, non-Fourier heat transfer is expected to be characterized by long “tailing” in the temperature breakthrough curves that cannot be captured by a Fourier-type equation (Fig. 30)

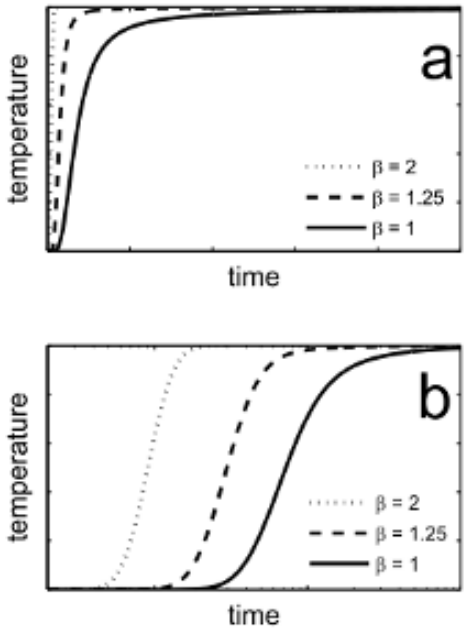


Figure 30 Schematic thermal breakthrough curves in a porous medium in response to a step function at the inlet. (a) Linear time scale and (b) a logarithmic time scale. Trans- port varies from Fourier (b = 2) to highly non-Fourier (b = 1). Note the elevated retardation and the long tailing with lower values of b.

Generally speaking, the more heterogeneous the flow system, the more non-Fourier the transport; consequently, it is expected that highly anomalous thermal transport will be observed in fractured porous media in which transport is often dominated by advection

and the range of transfer rates spans orders of magnitude [Berkowitz and Scher, 1998; Matthäi and Belayneh, 2004; Cortis and Birkholzer, 2008]. To address the problem of non-Fourier thermal transport, Emmanuel and Berkowitz [2007] adopted the Continuous Time Random Walk (CTRW) framework; such an approach has been successful in describing solute transport in heterogeneous subsurface formations [e.g., Berkowitz et al., 2000b; Kosakowski et al., 2001; Berkowitz et al., 2001; Cortis and Berkowitz, 2004], and Emmanuel and Berkowitz [2007] therefore proposed that a similar approach could be used to describe heat transfer in geological systems. While it was demonstrated that CTRW successfully described systems in which thermal disequilibrium existed between the solid and fluid phases, the CTRW framework was not tested on data from heterogeneous geological media, and the physical conditions necessary for non-Fourier transport to dominate were not assessed.

Quantifying solute transport in fractured media has become a very challenging research topic in hydrogeology over the last three decades (Cherubini, 2008, Cherubini et al., 2008, Cherubini et al., 2009, Masciopinto et al., 2010), whereas the literature on heat flow in fractured porous media is somewhat limited.

Hao et al. (2013) developed a dual continuum model for representation of discrete fractures and the interaction with surrounding rock matrix in order to permit a reliable prediction of impacts of fracture – matrix interaction on heat transfer in fractured geothermal formations. In this study single-phase flow and heat transfer processes in fractured geothermal reservoirs are considered. It is assumed that the fracture networks are the major pathways for flow and convective heat transfer, and the solid rock matrix is treated as impermeable but heat conductive. The fracture and matrix systems are treated as two overlapping and interacting continua, as illustrated in Fig. 31.

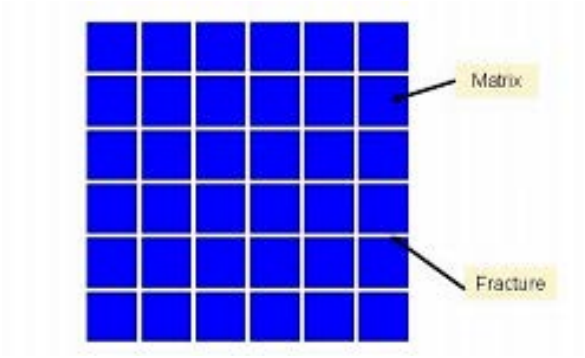

Figure 31 Conceptual schematic of dual-continuum

The mathematical equations used to describe flow and transport processes in porous media are based on the principle of mass, momentum and energy conservation. Darcy's law is the well-known approximate momentum balance for fluid flow through a porous medium.

Commonly used for hydraulic groundwater modelling, the mathematical formulation for mass transport of a single fluid phase in fracture media can be written in a general form as:

$$\phi \frac{\delta \rho}{\delta t} = -\nabla(\rho v) + \Gamma \tag{31}$$

Here t, $\nabla$, and Γ respectively represent time, spatial derivative operator, andsource/sink terms. Φf is the porosity of the fracture, ρ is the fluid density, and the
Darcy flux vector v is expressed as

$$v = -K \times \nabla h \tag{32}$$

in which h is piezometric head, and K denotes effective hydraulic conductivity tensor.

For a non-isothermal system the energy balance equations are expressed as

$$\frac{\delta}{\delta t}[\phi_f \rho C_p T_f + (1-\phi_f)\rho_s C_p T_f] + \nabla(\rho C_p T_f v) = \nabla(K_T \nabla T_f) - T_{fm} + Q_f \tag{33}$$

for the fracture continuum, and

$$\frac{\delta}{\delta t}[\phi_m \rho C_p T_m + (1-\phi_m)\rho_s C_p Tm] = \nabla(K_T \nabla T_m) - T_{fm} + Q_m \tag{34}$$

for the matrix continuum, in which the subscripts f and m denote fracture and matrix continuum, and T, $C_p$, $C_{ps}$, $\rho_s$, $K_T$ and Q denote temperature, specific heat of fluid and solid phases, solid phase density, thermal conductivity, and heat source term, respectively. The energy coupling term between fracture and matrix, $\Gamma_{fm}$, is defined as:

$$\Gamma_{fm} = h_t A_{fm}(T_f - T_m) \tag{35}$$

with $h_T$ denoting heat transfer coefficient between fracture and matrix, and $A_{fm}$ interfacial fracture matrix specific area. Both $h_T$ and $A_{fm}$ are important parameters, influencing fracture-matrix interactions.

While $A_{fm}$ can be estimated based on geometric relations between fractures and matrix blocks $h_T$ is typically computed by harmonic averaging of matrix/fracture thermal conductivities (e.g. Lichtner, 2000), in the form of

$$h_t = \frac{KT_f KT_m}{l_m K_{Tf} + l_f K_{Tm}} \tag{36}$$

In this study the fracture continuum methodology proposed by Botros et al. (2008) and Reeves et al. (2008a, b) was employed to transform the discrete fracture network into hydraulic properties on a uniform Cartesian grid in a two-dimensional continuum model. The scheme of grid-based effective hydraulic conductivity calculation (Botros et al., 2008; Reeves et al., 2008a, b) is briefly summarized as follows, and also depicted in Fig. 32.

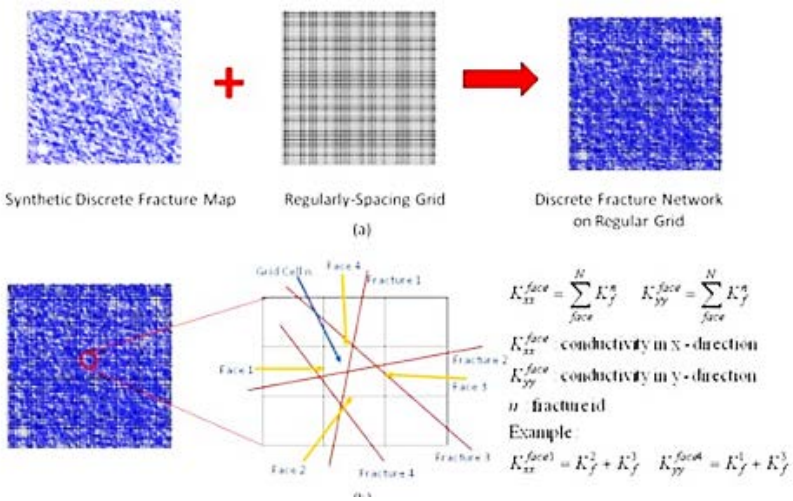


Figure 32 Conceptual schematic for grid-based effective hydraulic conductivity calculation (Botros et al., 2008; Reeves et al., 2008a, b) (a) The discrete fractures are mapped onto a Cartesian finite difference grid; (b) The effective hydraulic conductivity between grid cells in each principle direction is determined based on the intersections between fractures and grid cell faces in order to preserve the main fracture geometry/anisotropy.

In numerical implementation, $l_f$ and $l_m$ are taken as $\delta/2$ and $L/2$, with $\delta$ denoting fracture aperture width and L matrix block length.

Moonen et al. (2011) introduced the concept of cohesive zone which represents a transition zone between the fracture and undamaged material. They proposed a model to adequately represent the influences of fractures or partially damaged material interfaces on heat transfer phenomena.

The framework employs the partition of unity concept and captures the change from conduction-dominated transfer in the initial continuum state to convection and radiation-dominated transfer in the damaged state. The underlying model can be directly linked to a mechanical cohesive zone model, governing the initiation and subsequent growth and coalescence of micro-cracks. The methodology proved to be applicable for quasi-static, periodic, and transient problems.

Geiger and Emmanuel (2010) found that matrix permeability plays an important role on thermal retardations and attenuation of thermal signal. At high matrix permeability, poorly connected fractures can contribute to the heat transport, resulting in heterogeneous heat distributions in the whole matrix block. For lower matrix permeability heat transport occurs mainly through fractures that form a fully connected pathway between the inflow and outflow boundaries, that results in highly non – Fourier behavior, characterized by early breakthrough and long tailing. They conducted high-resolution finite element–finite volume numerical simulations of heat transfer in two geologically realistic fractured porous domains. They calculated thermal breakthrough curves at various locations in the domains and analysed them with a CTRW model adapted for heat transfer.

Numerous field observations (Tsang and Neretnieks, 1998) show that flow in fractures is being organized in channels due to the small scale will have a strong influence on the transport characteristics of a fracture variations in the fracture aperture.

Flow channelling causes dispersion in fractures. Such chare, such as, for instance, its thermal exchange area, crucial for geothermal applications (Auradou et al., 2006). Highly channelized flow in fractured geologic systems has been credited with early thermal breakthrough and poor performance of geothermal circulation systems (Adam at al., 2012).

Lu et. Al (2012) conducted experiments of saturated water flow and heat transfer 63 in a regularly fractured granite at meter scale. The experiments indicated that the heat advection due to water flow in vertical fracture nearest to the heat sources played a major role in influencing the spatial distributions and temporal variations of the temperature, impeding the heat conduction in transverse direction; such effect increased with

larger water fluxes in the fractures and decreased with higher heat source and/or larger distance of the fracture from the heat source. Kepikova et al. (2013) and Neuville (2010) showed that fracture – matrix thermal exchange is highly affected by the fracture wall roughness. Natarajan et. al (2010) conducted numerical simulation of thermal transport in sinusoidal fracture matrix coupled system. They affirmed that this model presents a different behavior respect to the classical parallel plate fracture matrix coupled system. The sinusoidal curvature of the fracture provides high thermal diffusion into the rock matrix.

Ouyang (2014) developed a three-equation local thermal non-equilibrium model to predict the effective solid-to-fluid heat transfer coefficient in the geothermal system reservoirs. They affirmed that due to the high rock-to-fracture size ratio, the solid thermal resistance effect in the internal rocks could not be neglected in the effective solid-to fluid heat transfer coefficient. Furthermore, the results of this study show that it is not efficient to extract the thermal energy from the rocks without a large enough fracture density.

There exist analytical and semi analytical models of heat transport in fractured rock. Such model are amenable to the same mathematical treatment as their counterparts developed for mass transport (Martinez et al., 2014). An example of the latter includes the analytical solution derived by Tang et al. (1981). While the equations of solute and thermal transport have the same basic form, the fundamental difference between mass and heat transport is that:

1) Solutes are transported through the fractures only, whereas heat is transported through both the fractures and the matrix,

2) Heat diffusion in rocks is large compared to molecular diffusion, implying that fracture-matrix exchange is more significant for heat than mass tracers.

Thus, thermal breakthrough curves (BTCs) are strongly controlled by matrix thermal diffusivity (Becker and Shapiro, 2003).

On the contrary, the advective transport of heat is slower than solute transport since the heat capacity of the solids will retard the advance of the thermal front (Rau et al.,

2012). Another issue that has not been properly addressed experimentally is the quantification of thermal dispersivity as far as heat transport and its relationship with velocity. In fact the literature contains conflicting descriptions of the thermal dispersivity coefficient (Ma et al, 2012).

The hydrodynamic component of thermal dispersion is often neglected because thermal diffusion is more efficient than molecular diffusion by several orders of magnitude (Bear 1972).

It has been suggested that thermal dispersivity is important due to enhanced spreading of thermal energy caused by forced convection and thus should be part of the mathematical description, in analogy to solute dispersivity [e.g., de Marsily, 1986]. Accordingly, a number of authors have incorporated this term into their models in a similar manner to solute dispersivity (e.g., Smith and Chapman, 1983; Hopmans et al., 2002; Niswonger and Prudic, 2003).

Other authors claim that as heat propagates through both phases, the hydrodynamic dispersivity mechanism is inappropriate because the enhanced thermal spreading is either negligible or can be described simply by increasing the effective diffusivity [Bear, 1972; Ingebritsen and Sanford, 1998].

Many researchers (e.g., Smith and Chapman, 1983, Ronan et al., 1998, Constantz et al., 2002, Su et 106 al., 2004) suggest thermal dispersivities are significant and include the thermomechanical.

Dispersion tensor representing mechanical mixing caused by unspecified heterogeneities within the porous medium, while others (e.g., Bravo et al., 2002, Keery et al, 2007) argue that dispersivity is negligible.

Constantz et al. (2003) and Vandenbohede et al. (2009) found that thermal dispersivity was significantly smaller than the solute dispersivity. Others (de Marsily , 1986, Molina-Giraldo et al., 2011) found that thermal and solute dispersivity were on the same order of magnitude.

Tracer tests of both solute and heat at Bonnaud, Jura, France, gave thermal dispersivity of the same order of magnitude as solute dispersivity (deMarsily 1986), leading some researchers to set thermal dispersivity equal to solute dispersivity.

Smith and Chapman (1983) regional values of longitudinal and transverse thermal dispersivity are given, respectively, as 100 and 10 m; in table 1 of Niswonger and Prudic 2003, longitudinal thermal dispersivity for ground water exchange with streams is given as 0.01 to 1 m. Analysis of heat transport under natural gradients has commonly neglected hydrodynamic dispersion (e.g., Bredehoeft and Papadopulos 1965; Domenico and Palciauskas 1973; Taniguchi et al. 1999; Reiter 2001; Ferguson et al. 2006). In models of relatively large systems and modest fluid flow rates, dispersive heat transport is often assumed to be represented by thermal conductivity and/or to have little influence (Bear, 1972, Woodbury and Smith, 1985).

Bear (1972), Ingebritsen and Sanford (1998), and Hopmans et al. (2002), among others, concluded that the effects of thermal dispersion are negligible compared to conduction and set a* to zero.

However, Hopmans et al (2002) showed that dispersivity is increasingly important at higher flow water velocities, since it is only then that the thermal dispersion term is of the same order of magnitude or larger than the conductive term.

Sauty et al. (1982) provided the strongest argument for the inclusion of a hydrodynamic dispersion term in advective – conductive modeling, suggesting that there was a correlation between the apparent thermal conductivity and Darcy velocity.

Other similar formulations of this concept are present in the literature (e.g., Papadopulos and Larson 1978; Smith and Chapman 1983; Molson et al. 1992). Such treatments have not explicitly distinguished between the components of hydrodynamic dispersion that occur due to variations in velocity at the pore scale and macro dispersion, which occurs due to variations in permeability over larger scales.

The literature contains conflicting descriptions of the thermal dispersivity and the relationship between thermal dispersivity and fluid velocity with one group of authors suggesting a linear relationship (e.g., de Marsily, 1986; Anderson, 2005; Hatch et al., 2006; Keery et al., 2007; Vandenbohede et al., 2009; Vandenbohede and Lebbe, 2010; Rau et al., 2010), while others working in the chemical engineering field have identified the possibility of a nonlinear relationship (Green et al., 1964).

In previous studies by Cherubini et al. (2012, 2013a, 2013b, 2013c and 2014) the presence of nonlinear flow and non-Fickian transport in a fractured rock formation was analyzed at bench scale in laboratory tests. The effects of nonlinearity in flow have been investigated by analysing hydraulic tests on an artificially created fractured limestone block of parallelepiped ($0.6 \times 0.4 \times 0.8$ $m^3$) shape. The experimental results show evidence of a non Darcy relationship between flow rate and hydraulic head differences that is best described by a Forchheimer law. A power law has been detected between the Forchheimer terms and the tortuosity factor, which means that the latter influences flow dynamics. The non-Fickian nature of transport were investigated by means of tracer tests. The observed experimental BTCs of solute transport were proven to be better modelled by the 1D single rate Mobile Immobile model (MIM) and the 2D explicit network model (ENM). Unlike the former, the latter expressly takes the fracture network geometry into account.

The ENM model may allow to understand the physical meaning of flow and transport phenomena (i.e., the meaning of long-time behavior of BTCs that characterize fractured media) and permits one to obtain a more accurate estimation of flow and transport parameters. In this model the fractures are represented as 1-D pipe elements and they form a 2-D pipe network.

In this study, in order to investigate the behavior of heat transport in a fractured network, thermal tracer tests have been carried out on the same artificially created fractured rock sample.

A better development of the Explicit Network Model (ENM) based on a Tang's solution developed for solute transport in a single semi-infinite fracture inside a porous matrix has been used for the fitting of the thermal BTCs.

In analogous way the ENM model has been used in order to fit the observed BTCs obtained from previous experiments on mass transport. The obtained thermal BTCs show a more enhanced early arrival and long tailing than solute BTCs.

The travel time for solute transport is an order of magnitude lower than for heat transport experiments. Thermal convective velocity is thus more delayed respect to solute

transport. The thermal dispersion mechanism dominates heat propagation in the fractured medium in the carried out experiments and thus cannot be neglected.
For mass transport the presence of the secondary path and the nonlinear flow regime are the main factors affecting non – Fickian behavior observed in experimental BTCs, whereas for heat transport non - Fickian nature of the experimental BTCs is governed mainly by the heat exchange mechanism between the fracture network and the surrounding matrix. The presence of a nonlinear flow regime gives rise to a weak growth on heat transfer phenomena.
Furthermore the estimation of the average effective thermal conductivity suggests that there is a solid thermal resistance in the fluid to solid heat transfer processes due to the rock – fracture size ratio. This result matches previous analyses (Pastore et al., 2015) in which a lower heat dissipation respect to the Tang's solution in correspondence of the single fracture surrounded by a matrix with more limited heat capacity has been found.

### 2.3.1 Flow in fractured media

In fractured media flow is generally focused along a few preferred pathways. This phenomenon is referred to as flow channelling. It is recognized that flow channeling, arising on all scales, significantly complicates flow and transport prediction. The issue is to properly describe heterogeneous characteristics of fractured media. Throughout this section, flow within individual fractures and within multi-fracture networks is discussed.

### 2.3.2 Single fracture

At the fracture scale, flow patterns are influenced by the fracture aperture variability and the roughness of the facing aperture surfaces. For a laminar flow in sufficiently open fractures, the cubic law provides a good estimates of the flowrate q per a unit fracture length [e.g. Moreno et al., 1988]

$$q = -\frac{d^3}{6\eta}\nabla P$$

(37)

The geometrical heterogeneity of the fracture walls results in variable hydraulic behavior of fractures [e.g. Berkowitz, 2002; Meheust and Schmittbuhl, 2001; Tsang and Neretnieks, 1998]. Numerous studies demonstrate that due to heterogeneous characteristics of the fracture aperture, flow channeling occurs [e.g. Moreno et al., 1990; Tsang and Neretnieks, 1998].of a fracture aperture is shown in 33 a. The hydraulic flow computed in- side this morphology, shown in Fig.33, exhibits a strong channeling as previously described by Meheust and Schmittbuhl [2001]. Moreover, this study demonstrates that depending on the orientation of the hydraulic gradient (relative to heterogeneities in wall roughness), flow can be either enhanced or inhibited in comparison to a parallel wall fracture.

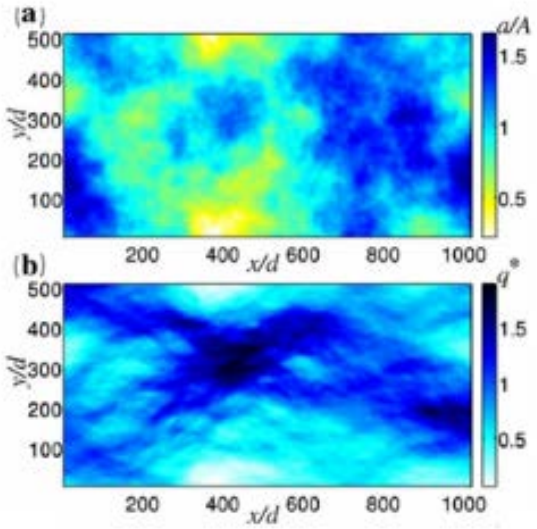


Figure 33 Example of self-affine fracture aperture (a) and dimensionless hy- draulic flow norm computed with this aperture (b) (from Neuville et al. [2010]).

### 2.3.3 Fracture networks

In addition to flow in individual fractures being organized in channels, flow chan- neling or preferential flowpaths in fracture networks has been demonstrated by numerous field observations [Tsang and Neretnieks, 1998]. For example, in a fractured granitic rock at Stripa mine, 80% of the total flow arrived in one of the tunnel is produced by a single fracture [Olsson, 1992] (Fig. 34). At the Mirror Lake site, the major part of flow was shown to be channelized in a few fractures (Fig.35a). Hsieh [1998] demonstrates that at the Mirror Lake site high degree of heterogeneity arises from a large variability of hydraulic permeability at the fracture network scale (Fig. 35b). Several other studies show that fractured rocks are generally characterized by spatial variability of permeability on all scales [Clauser, 1992; Hsieh, 1998] (Fig. 36). The causes of this variability and permeability scaling are still debated [e.g. Illman, 2006].

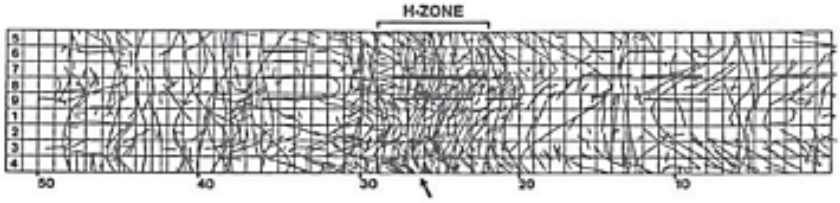


Figure 34 Fracture map from one of the Stripa mine tunnel, showing H-zone, which produces 80 % of the total flow (from Olsson [1992]).

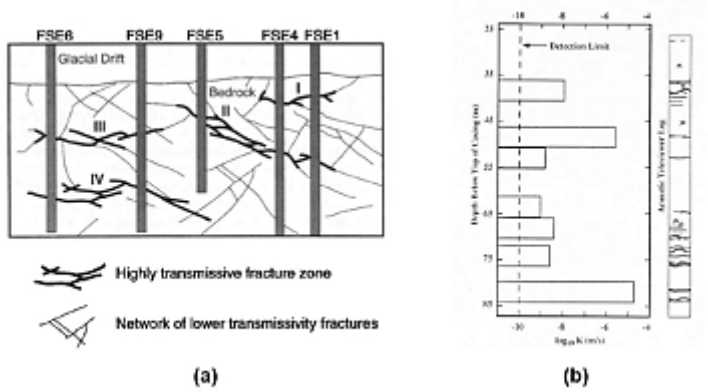


Figure 35 Fracture distribution at Mirror Lake site, transmissive fractures are shown with a bold line, from Day-Lewis et al. [2000] (a). Distribution of hydraulic conductivity measured in one borehole at Mirror Lake site, from Hsieh [1998] (b).

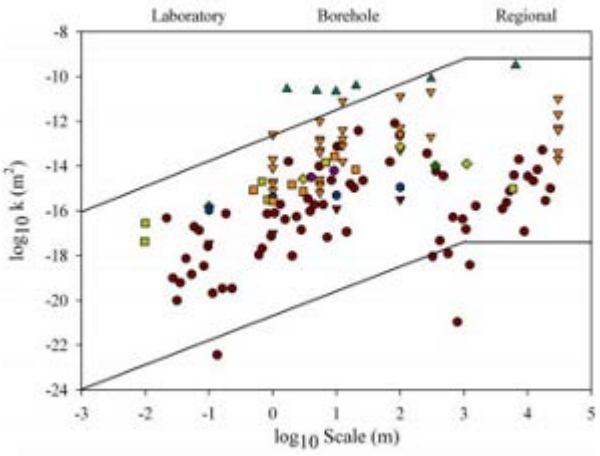


Figure 36 Permeability data from different fractured field sites plotted against measurement scale. (from Illman [2006]).

The experimental evidence of flow channelling stimulated a series of numerical and theoretical studies. Fig. 37 presents an example of channelled flow obtained on a synthetic 2D fracture network, where a total flow is carried only by a few among all generated fractures. This is explained by the fact that the key characteristic controlling fluid flow at the network scale is the connectivity of fractures [Bour and Davy, 1997]. Fracture connectivity, in turn, depends on geometrical properties of fracture network. The influence of geometrical fracture network characteristics such as fracture density, fracture length distribution, distribution of fracture orientations and apertures on fracture-network connectivity and on the permeability scaling is the subject of numerous experimental and numerical studies [e.g. Berkowitz, 2002; Berkowitz et al., 2000; Bour and Davy, 1998; Darcel et al., 2003; de Dreuzy et al., 2001; Margolin et al., 1998].

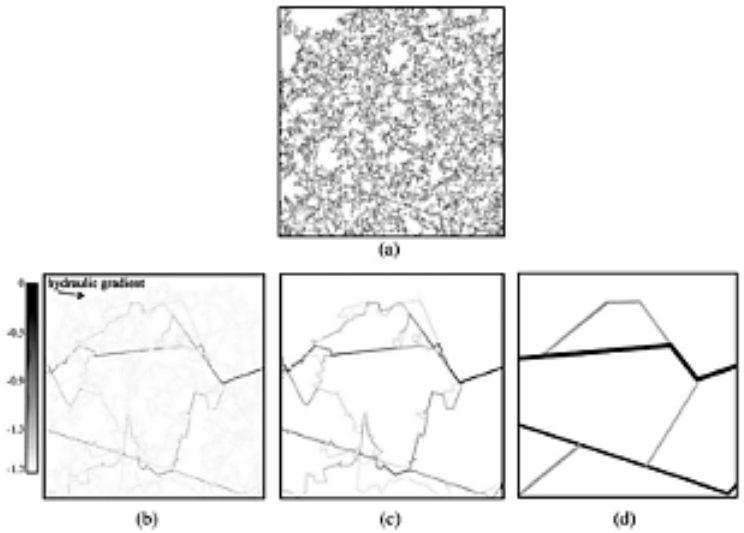


Figure 37 Example of flow in fractured network from Le Goc et al. [2010]. (a) Synthetic fracture network. (b) Flows computed with a constant sub-horizontal hydraulic gradient of direction given by the arrow. All fractures have the same transmissivity.

In order to characterize fracture network connectivity, percolation theory was shown to be an efficient approach [Stauffer and Aharony, 1985]. Thus, for in- finitely large systems, consisting of a uniformly distributed cracks of constant length, there exists a critical density of elements pC (the percolation threshold) below which systems are not connected, and above which systems are always connected whatever the scale of investigation. For a widely scattered length distribution systems ($N(l) = \alpha l^{-a}$), the challenge is to find a parameter of percolation that is a right measure of network connectivity, i.e., that does not depend on scale at connectivity threshold [Berkowitz et al., 2000; Bour and Davy, 1997, 1998; Darcel et al., 2003]. Thus, Bour and Davy [1997] demonstrate that for widely scattered length distribution systems even for a low density of elements there always exists a scale for which the percolation threshold is reached (Fig. 38). These studies demonstrate that while channeling in single-fractures is due to heterogeneity of the fracture aperture, flow channeling at the field-scale is con- trolled by distribution of fracture conductivities and by connectivity of fractures [Berkowitz, 2002].

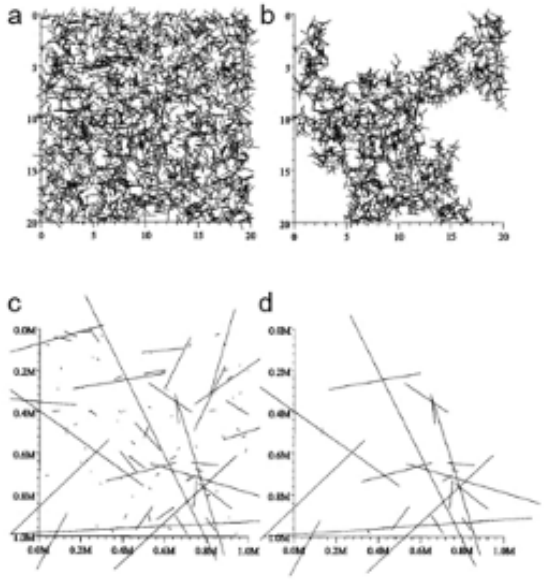


Figure 38(a) Example of a constant-length (l = 1) fault network at the percolation threshold; (b) the infinite cluster of the network presented in (a); (c) fault networks at the percolation threshold in the case of power law fault lengths distribution (N(l) = αl−a, a = 1.5); (d) largest cluster of the network presented in (c). From Bour and Davy [1997].

### 2.3.4 Transport in fractured media

Flow heterogeneities in fractured media influence transport behavior by inducing a broad range of transport rates. The coexistence of high velocity flow paths and immobile zones complicates the prediction of transport pattern. A basic transport model which can be used to describe the tracer migration in homogeneous media is the advection-dispersion model accounting for advection of the solute in the fracture plane and hydrodynamic dispersion.

The equation is given by

$$\frac{\delta C}{\delta t} = -\nabla(Cv) + \nabla[D\nabla C] \tag{38}$$

where C is concentration, t is time, D is the hydrodynamic dispersion tensor and v is average fluid velocity.

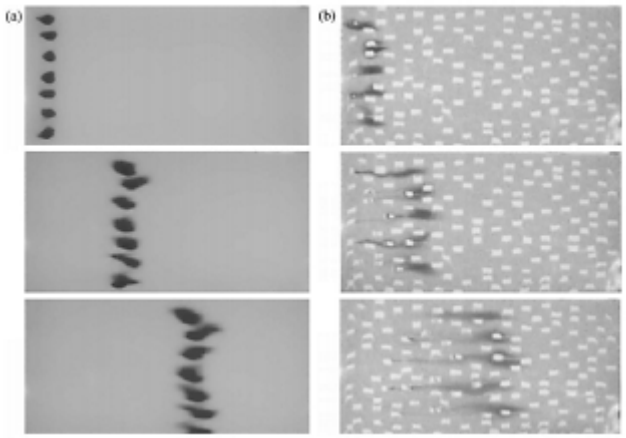


Figure 39 Photographies of tracer propagation through homogeneous (a) and heterogeneous (b) media from Levy and Berkowitz [2003].

The experimental results from Levy and Berkowitz [2003], shown in Figure 40, demonstrate the difference in transport behavior in homogeneous and heterogeneous media. Figure 39 a, corresponding to homogeneous media, shows tracer plume that disperses uniformly around average tracer velocity. In contrast, irregular shapes of tracer plume in heterogeneous media reflect mass spreading related to preferential flowpaths (Fig. 39b). Consequently, the classical advection- dispersion theory cannot effectively describe transport in heterogeneous media. The investigation of processes involving in transport in fractured media is a subject of numerous studies [e.g. Becker and Shapiro, 2003; Bodin et al., 2003a; Gelhar and Welty, 1992]. Additional processes involved in transport in fractured media have been well identified and one can synthesize them as follows [Bodin et al., 2003a]:

- Dispersion at fracture scale related to fracture roughness and fracture aperture variability [Detwiler et al., 2000].
- Dispersion at the scale of a fracture network due to transport in different flow paths [Moreno and Neretnieks, 1993].
- Diffusion of the solute in the fracture plane and in the rock matrix [Novakowski and Lapcevic, 1994].
- Physico-chemical reactions between the solute and the solid material of the matrix and the fracture walls [Smellie and Karlsson, 1999].

The principal equations describing these processes for a single fracture are described in Bodin et al. [2003b].

In order to model flow and transport in fractured media, two large classes of approaches were developed: continuum approaches and discrete fracture models. In either case, deterministic or stochastic frameworks can be considered. In contrast to deterministic concept, stochastic models provide a range of values rather than a unique solution. Furthermore, the 'hybrid' approach was proposed as a combination of stochastic continuum approach with known deterministic fractures [Berkowitz, 2002; de Dreuzy, 1999].

Continuum approaches (Fig. 40), including equivalent porous continuum concept, dual porosity model, dual permeability model [Ando et al., 2003; Hao et al., 2008; Illman et al., 2009; Y.W.Tsang et al., 1996], aim to describe the averaged hydraulic behavior of the system, while their simplicity allows us to constrain the model with the available set of data. Nevertheless, Long et al. [1982] demonstrate that the application of a continuum approach is credible only for high density fracture networks with uniform aperture distribution and nonuniform orientation distribution.

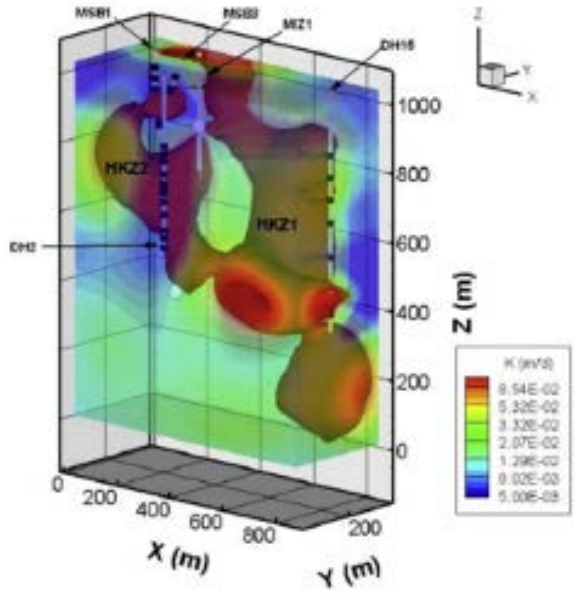


Figure 40 Example of application of stochastic continuum approach to hydraulic tomography data. Hydraulic conductivity K tomogram (m/d) obtained from the inversion of two cross-hole tests from Illman et al. [2009].

Instead of capturing the effect of heterogeneity on hydraulic properties, the discrete approach represents heterogeneity (as fractures) themselves based on in situ measurements [Cacas et al., 1990; Frampton and Cvetkovic, 2010; Le Goc et al., 2010] (Figure 41). The advantage of the discrete fracture approach is that it can account explicitly for the effects of individual fractures on fluid flow and solute transport. However, the discrete fracture approach demands detailed field data including fracture geometries and spatial distribution that limits its practical application. For a detailed overview of different numerical approaches, see de Dreuzy [1999]

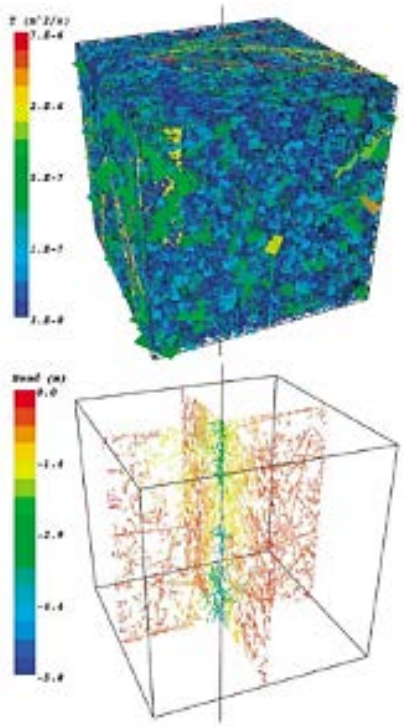

Figure 41 An example of the application of a stochastic discrete fracture net- work (DFN) approach to borehole flow rates data measured during extraction pumping, from Frampton and Cvetkovic [2010]. One DFN realization colored by transmissivity and the corresponding pressure field (drawdown).

Numerous applications demonstrate that both the continuum and discrete fracture models can capture the main flow and transport patterns [e.g. Cacas et al., 1990; Hao et al., 2008; Illman et al., 2009]. To date, images of fractured hydraulic properties obtained with continuum approaches are characterized by a high smoothness and low resolution. On the other hand, available data content are generally limited, resulting in high uncertainties in individual fracture characterization with DFN models [e.g. Le Goc et al., 2010]. The choice of the most suitable conceptual model for characterization of fractured media is still highly debated [Neuman, 2005]. On the basis of these models, a wide variety of experimental methods has been reported in the literature. In the next part, we discuss the existing field methods for imaging of fractured media in between boreholes.

### 2.3.5 Theory of Continuous Time Random Walks (CTRW)

The CTRW formalism was developed to account for electron hopping in disordered solids [Montroll and Scher, 1973; Scher and Montroll, 1975], although it has more recently been used to describe anomalous solute transport in geological systems [Berkowitz et al., 2000b; Kosakowski et al., 2001; Berkowitz et al., 2001; Cortis and Berkowitz, 2004]. As detailed descriptions of CTRW [e.g., Cortis et al., 2004; Berkowitz et al., 2006] and its application to heat transport can be found elsewhere [Emmanuel and Berkowitz, 2007], only a brief summary will be given here. In the CTRW framework, the processes of heat conduction and advection are generalized by considering heat packets that move between different sites or positions in a series of discrete transitions. To model transport in a given system, the CTRW framework can be extended to a continuum formulation, which adopts a partial differential equation (PDE) form [Berkowitz et al., 2002; Dentz et al., 2004]; in Laplace space the PDE form is given as:

$$u\bar{T}(s,u) - T_0(s) = \bar{M}(u)[v_\varphi \nabla \tilde{T}(s,u) + k_\varphi : \nabla\nabla \tilde{T}(s,u) \tag{39}$$

where the Laplace transform of a function f (t) is denoted by $\tilde{f}(u)$ , and u is the Laplace variable with dimensions of inverse time; s indicates the spatial location. In addition, M(u) is a memory function given by:

$$\tilde{M}(u) = t_1 u \frac{\tilde{\varphi}(u)}{1 - \tilde{\varphi}(u)} \tag{40}$$

where $\tilde{\varphi}(u)$ is the Laplace transform of the probability rate for a transition time t [Berkowitz et al., 2002; Dentz et al., 2004; Cortis et al., 2004] and the $t_1$ parameter is a characteristic time for transitions between sites. It is important to recognize that when $\tilde{M}(u) = 1$, when equation (39) has a form identical to equation (28). However, the "transport velocity" ($v_\varphi$) in equation (39) is distinct from the heat transfer velocity ($v_h$)

in equation (28), and similarly, $k_\varphi$ is not directly comparable to the $k_e$ parameter adopted in the standard heat transfer model. An in-depth analysis relating the CTRW parameters to the parameters of the standard heat transfer equation is beyond the scope of this paper. The memory function, M(u) is essentially determined by the functional form of $\tilde{\varphi}(u)$ [Cortis et al., 2004; Dentz et al., 2004]; of the various functions proposed for $\tilde{\varphi}(u)$, the truncated power law (TPL) has been shown to be particularly versatile, being capable of capturing a wide spectrum of transport behavior [Cortis et al., 2004; Berkowitz et al., 2006]. In the time domain, the TPL defines y(t) as:

$$\varphi(t) = [t_1 / (\frac{t_1}{t_2})^{\beta} \exp(\frac{t_1}{t_2})\Gamma(-\beta(\frac{t_1}{t_2}))]^{-1} * \frac{\exp\frac{t_1}{t_2}}{(1+\frac{t}{t_1})^{1+\beta}} \qquad 0<\beta<2 \qquad (41)$$

where b, $t_1$, and $t_2$ are three model parameters, and G is the incomplete Gamma function [Abramowitz and Stegun, 1970]. Here, $t_2$ is the time after which transport becomes Fourier-like, while the b parameter characterizes the system's heterogeneity with respect to heat transfer [Emmanuel and Berkowitz, 2007]. In systems with a low degree of heterogeneity, heat transfer may be Fourier-like, corresponding to $\beta \geq 2$. However, when a high degree of spatial variability in the flow field exists, such as often occurs in fractured systems, thermal transport is expected to become anomalous, with $\beta<2$.
While the TPL functional form adopted in the present study is often adequate to describe the distribution of waiting times, techniques can be used to extract the distribution of waiting times directly from breakthrough curves without assuming a specific functional form [Cortis, 2007]. Although not adopted here such a general approach could offer an important tool for the interpretation of solute and thermal breakthrough data in future studies. Analytical solutions to the equations described above are available for common boundary conditions [Dentz et al., 2004], and the solutions can be transformed from

the Laplace domain to the time domain with a numerical Laplace inversion algorithm [de Hoog et al., 1982].

### 2.3.6 Heat tracer test

Using thermal tracer tests for characterizing fracture properties may provide more constraints compared to classical tracer tests. The fundamental difference be- tween solute and heat transport is that heat diffusion in rocks is large compared to molecular diffusion of solutes, implying that fracture-matrix exchange is much more significant for heat than for solute tracers. Several theoretical and numerical studies investigated the movement of fluid of contrast temperature through fractures. Thus, Lauwerier [1955] proposed an analytical solution for injection of hot fluid into a confined layer. By using this model Bodvarsson and Tsang [1982] presented type curves that can be used to predict the time of thermal breakthrough during interwell heat tracer tests through fractures. These theoretical works as well as numerical studies of hydrothermal coupling at different scales [Geiger and Emmanuel, 2010; Kolditz, 1995; Molson et al., 2007; Neuville et al., 2010] show that heat transfer from rocks to fluids through the available fracture-matrix interface area results in high thermal retardations and significantly attenuates thermal signals.
An example of heat transport simulations in two-dimensional realistic fracture networks (Fig. 42) show how the change in fracture-matrix interface area influences the heterogeneity of the temperature field. Thus, at high matrix permeability, poorly connected fractures can contribute to the heat transport, resulting in heterogeneous heat distribution in the whole matrix block (Fig.42 a). In contrast, for a lower matrix permeability (Fig. 43 b and c) heat transport occurs mainly through fractures that form a fully connected pathway between the inflow and outflow boundaries, that results in highly non-Fourier behaviour, characterized by early breakthrough and long tailing [Geiger and Emmanuel, 2010].

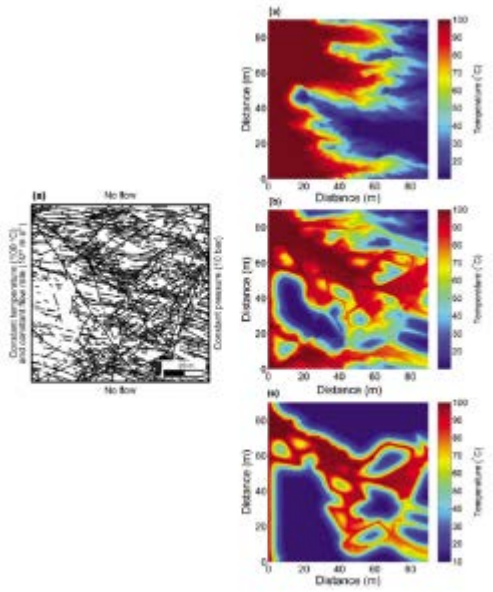

Figure 42 Temperature field computed for a realistic fracture geometry(a) at a matrix permeability of (b) $10^{-11}$ $m^2$, (c) $10^{-13}$ $m^2$, (d) $10^{-15}$ $m^2$. The temperature field for the high matrix permeability case ($10^{-11}$ $m^2$) is after 50 days; all other fields are after 100 days. From Geiger and Emmanuel [2010]

The desire for obtaining test results quickly thus promoted the idea of using 'push-pull' heat tracer tests [Kocabas, 2005; Kocabas and Horne, 1990]. Numerical simulations of Pruess and Doughty [2010] demonstrated that 'push-pull' heat tracer tests are strongly sensitive to changes in fracture-matrix interface area, while insensitive to changes in effective fracture aperture. Recently, Jung and Pruess [2012] proposed an analytical solution for 'push-pull' tracer test including a quiescent period. This solution implies that the effect of fracture aperture on temperature signal during push-pull tracer tests is weak. However, by applying different flow velocities for injection and withdrawal the sensitivity of thermal breakthrough curves to the fracture aperture can be increased [Jung and Pruess, 2013]. It was also demonstrated that while flow rate influence both the cooling rate during injection and the heating rate during pumping. As a result these effects are compensated at the fracture inlet. Thus, the question of what information can be extracted from heat tracer tests and what parameters are likely to be difficult to determine should to be addressed. Moreover, it is necessary to verify and validate the

models by heat tracer tests in real fractures networks in their natural environment i.e. by in situ experiments.

Keplikova et al have been proposed a traditional inversion methods that have been developed for porous aquifers whose hydraulic properties vary smoothly in space. Their objective was to develop new inversion methods that are adapted for fractured media. They then have been proposed an inverse model framework for interpreting cross-borehole data providing an inverse solution to fracture connectivity and transmissivities As they have shown, temperature data can be used to deduce flow patterns. Thus, these results provide new insights on how to include temperature profiles in inverse problem for imaging heterogeneous fracture properties at the site-scale. As discussed in this section, the characterization of transport fracture properties from tracer tests is a strongly under-constrained inverse problem (Fig. 43).

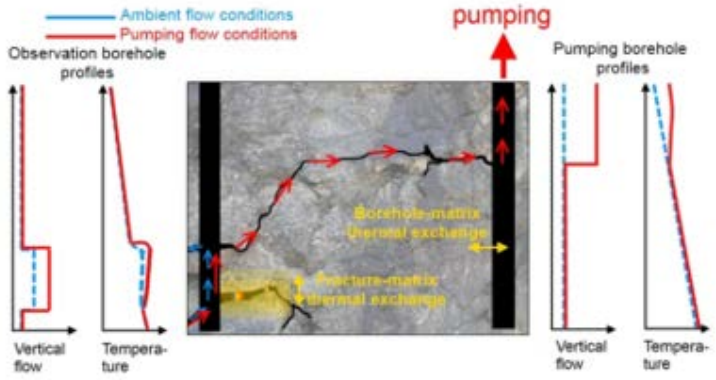


Figure 43 Schema of flow and temperature measurements during cross-borehole pumping test. Two scales of investigation are shown. Small-scale study considers borehole-matrix thermal exchange. Large-scale investigations concerns to flow paths connecting the pair of 'pumping-observation' boreholes. Hot water movement in fractures is controlled by fracture-matrix thermal exchange.

### 2.3.7 Heat transfer experiments in fractured media: material and methods

The heat transfer tests have been carried out on the experimental apparatus previously employed to perform flow and tracer transport experiments at bench scale (Cherubini et al. 2012, 2013a, 2013b, 2013c and 2014). However, the apparatus has been modified in order to analyze heat transport dynamics (Fig. 44).

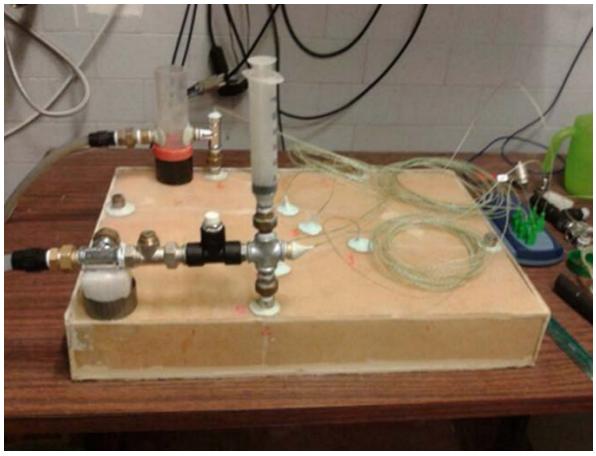

Figure 44 New configuration of fractured limestone block

In first test only two thermocouples have been placed at the inlet and the outlet of a selected fracture path of the limestone block with parallelepiped shape ($0.6 \times 0.4 \times 0.08$ $m^3$) described in previous studies. A TC- 08 Thermocouple Data Logger (PicoLog Technology) with a sampling rate of 1 second has been connected to the thermocouples. In a second test more thermocouples. An extruded polystyrene panel with thermal conductivity equal to 0.034 $Wm^{-1}K^{-1}$ and thickness 0.05 m has been used to thermally insulate the limestone block which has then been connected to a hydraulic circuit (Fig. 45-46-47).

Figure 45 Thermal insulate fractured limestone block

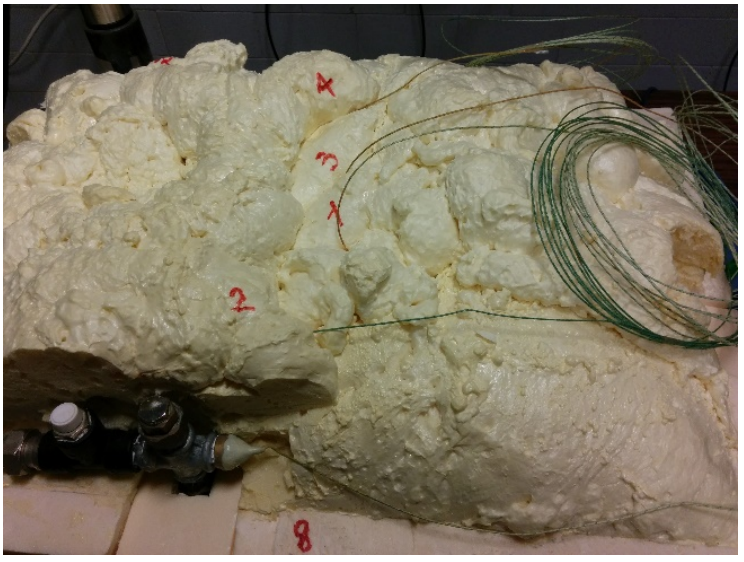


Figure 46 Particular of thermal insulate fractured limestone block.

The difference in hydraulic head between the upstream tank connected to the inlet port and the downstream tank connected to the outlet port drives flow of water through the

fractured block (Fig. 48). An ultrasonic velocimeter (DOP3000 by Signal Processing) has been adopted to measure the instantaneous flow rate that flows across the block.

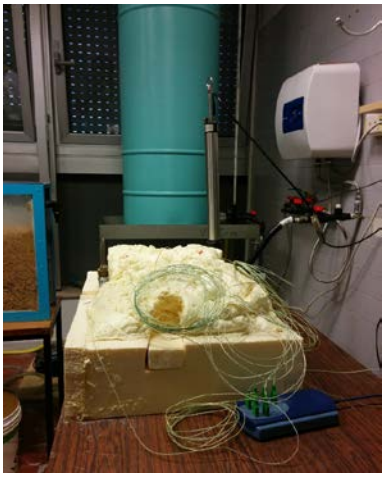

Figure 47 Thermal insulate fractured limestone block with thermocouple

Figure 48 Configuration of experiment.

An electric boiler with a volume of $10^{-2}$ $m^3$ has been used to heat the water. In a flow cell located in correspondence of the outlet port, a multiparametric probe is positioned

for the instantaneous measurement of pressure (dbar), temperature (°C) and electric conductivity (μS $cm^{-1}$). The schematic diagram of the experimental apparatus is shown in Fig. 49.

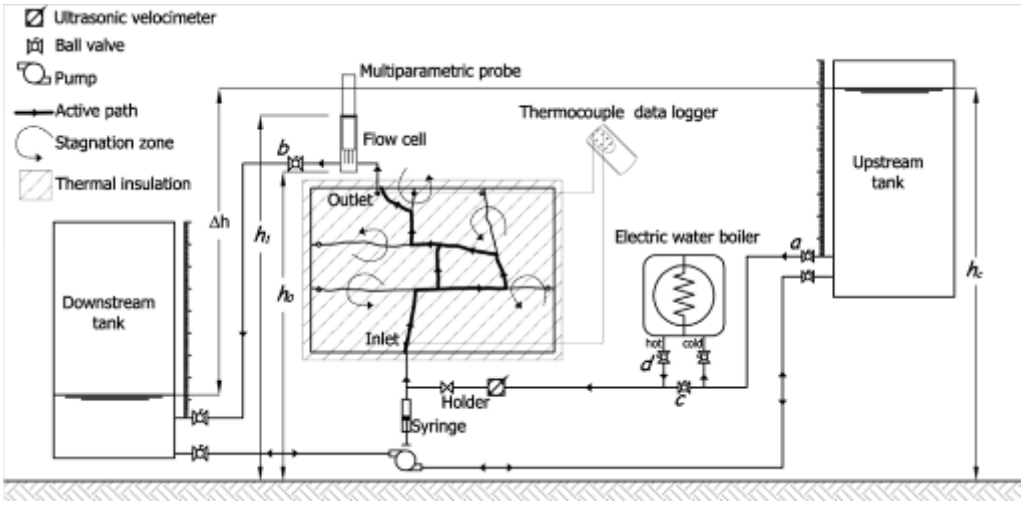


Figure 49 Schematic diagram of the experimental setup.

### 2.3.8 First test:"Experimental study of heat transport in fractured network"

(N. Pastore , C. Cherubini , C. I. Giasi , N. M. Allegretti , J. M. Redondo , A. M. Tar-quis Experimental study of heat transport in fractured network. Energy Procedia · Volume 76, August 2015, Pages 273–281)


**Abstract**

Fractured rocks play an important role in transport of natural resources through subsurface systems. In recent years, interest has grown in investigating heat transport by means of tracer tests, driven by the important current development of geothermal applications. Geothermal energy is one of the largest sources of renewable energies that are extracted from the earth. In the geothermal systems the fluid movement and thermal behavior in the fractured porous media is very important and critical. Existing theory of fluid flow and heat transport through porous media is of limited usefulness when applied to fractured rocks. Many field and laboratory tracer tests in fractured media show that fracture –matrix exchange is more significant for heat than mass tracers, thus thermal breakthrough curves (*BTCs*) are strongly controlled by matrix thermal diffusivity. In

this study, the behaviour of heat transport in a fractured network, at bench laboratory scale, has been investigated.

## Introduction

The aim of this paper is understand the behaviour of heat transport in fractured media. The laws that governs the heat transport in fractured media are still little known and there are not many experiences in literature about these phenomena. Existing theory of fluid flow and heat transport through porous media is of limited usefulness when applied to fractured rocks.

Fractured rocks play an important role in transport of natural resources or contaminants transport through subsurface systems. In recent years, interest has grown in investigating heat transport by means of tracer tests, driven by the important current development of geothermal applications. In recent years, interest has grown in investigating heat transport by means of tracer tests, driven by the important current development of geothermal applications. The interest about this topic has grown in particular manner because this allows improving the exploitation of Geothermal resource.

In particular way low enthalpy geothermal resource is an optimal renewable resource because is always available and that is possible used for the heating and cooling of private buildings, industries, public buildings which represents the largest share of world energy consumption. In particular way low enthalpy geothermal resource is an optimal renewable resource because is always available and that is possible used for heating and cooling of private buildings, industries, public buildings which represents the largest share of world energy consumption. From knowledge of the behavior of heat in the fractured medias, that characterize the majority of the media of the World, it is possible understand the possible advantages and disadvantages resulting from the use of low enthalpy geothermal systems in the presence of that type of media. A laboratory study, at bench scale, has been conducted on an artificially created fractured limestone block of parallelepiped ($0.6 \times 0.4 \times 0.8$ $m^3$ ) shape. Some holes have been drilled on

the block, inside, which have been, included the temperature probe. The observed thermal BTCs have been modeled with the ENM based an adaptation of Tang's solution developed for solute transport in a semi-infinite single fracture embedded in a porous matrix.
Characteristic time scale has been compared in order to evaluate the dominant mechanism on heat propagation in fractured media.

### 2.3.9 Theoretical background

#### Nomenclature

a linear coefficient of Forchheimer's law ($TL^{-3}$)
b inertial coefficient of Forchheimer's law ($T^2L^{-6}$)
BTC thermal breakthrough curve
C conductance term ($L^2\ T^{-1}$)
Cw specific heat capacity of the water ($L^2T^2K^{-1}$)
Cm specific heat capacity of the matrix ($L^2T^2K^{-1}$)
d distance along z axis from fracture – matrix interface (L)
$\delta$ thickness of boundary layer (L)
ENM explicit network model
Df thermal dispersion coefficient ($L^2T^{-1}$)
h hydraulic head (L)
j single vertical fracture index
$k_e$ effective thermal conductivity of the matrix ($MLT^{-3}K^{-1}$)
L length of single fracture or characteristic length of fracture network (L)
$L^{-1}$ inverse Laplace transform operator
nf number of single fracture
Np number of paths
PQ probability of water distribution of shorter parallel branch
PDF probability of density function of residence time
Q flow rate ($L^3T^{-3}$)

Q0 injection flow rate ($L^3T^{-3}$)
$\rho_w$ density of water ($ML^{-3}$)
$\rho_m$ density of the matrix ($ML^{-3}$)
Re Reynolds number (-)
s Laplace parameter (-)
SF vertical single fracture
$t_u$ convective time scale (T)
$t_d$ dispersion time scale (T)
$t_e$ transfer time scale (T)
$T_f$ fracture temperature (K)
$T_m$ matrix temperature (K)
$T_0$ initial temperature (K)
$T_{inj}$ injection temperature (K)
$u_f$ thermal convective velocity ($LT^{-1}$)
x coordinate parallel to the axis of vertical single fracture
$w_f$ fracture aperture (L)
z coordinate perpendicular to the fracture axis (L)
* convolution operator

**Flow and heat transport in single fractures**

A fracture can be depicted as two rough surfaces in contact. Cross sectional solid areas representing asperities in contact are similar to the grains of porous media. It is therefore possible to apply the general equations describing flow and heat transport in porous as well as in fractured media.
In most studies examining hydrodynamic processes in fractured media, it is assumed that flow is described by Darcy's law, which expresses a linear relationship between pressure gradient and flow rate (Cherubini C, Pastore N., 2000). Darcy's law has been

demonstrated to be valid at low flow regimes (Reynolds number (Re) < 1). For Re > 1 a nonlinear flow behavior is likely to occur.

In the literature different laws are reported that account for the nonlinear relationship between velocity and pressure gradient. In case of higher Reynolds numbers (Re >> 1) the pressure losses pass to a strong inertial regime, described by the Forchheimer equation. The relationship between flow rate and hydraulic head gradient can be written as:

$$-\frac{dh}{dx} = a \cdot Q + b \cdot Q^2 \tag{48}$$

A *SF* is subject to fluid flow with an averaged velocity, heat will migrate by convection and diffusion phenomena along the fracture. Furthermore they will also undergo dispersion caused by small scale variations in fracture aperture.

One dimensional advective - dispersive transport along the fracture axis is considered, as well as one – dimensional diffusion in the rock matrix, in direction perpendicular to the axis of the fracture. Assuming that density and heat capacity are constant in time, conservation equation can be written for heat transport in a semi-infinite fracture as:

$$\frac{\partial T_f}{\partial t} + u_f \frac{\partial T_f}{\partial x} = \frac{\partial}{\partial x}\left( D_f \frac{\partial T_f}{\partial x} \right) - \frac{k_e}{\rho_w C_w \delta} \frac{\partial T_m}{\partial z}\bigg|_{z=w_f/2} \tag{49}$$

Whereas the conservation equation for heat transport in the matrix is:

$$\rho_m C_m \frac{\partial T_m}{\partial t} = k_e \frac{\partial^2 T_m}{\partial z^2} \tag{50}$$

[Cherubini C et al, 2013] and [Forchheimer P, 1901] proposed a thermal dispersion coefficient similar to the solute transport, where the thermal dispersion term is related to the heterogeneity and it is a linear function of velocity.

[Sauty JP, et al 1982] present a solution for solute transport in semi – infinite single fracture surrounded by porous matrix for a constant concentration at the fracture inlet (x = 0) equal to c0 (ML-3) and for initial concentration equal to zero everywhere. They give the expression for the solute concentration in the fracture and in the matrix as function of time. On the basis of these analytical solutions the PDF in the single fracture in the Laplace space can be written as:

$$\overline{\Gamma}(s) = \exp(vL)\exp\left[-vL\left\{1+\beta^2\left(\frac{s^{1/2}}{A}+s\right)\right\}^{1/2}\right] \tag{51}$$

Whereas the PDF in the matrix in the Laplace space assumes the following expression:

$$\overline{\Gamma}'(s) = \overline{\Gamma}(s)\cdot\exp\left(-Bs^{1/2}d\right) \tag{52}$$

The coefficients $v$, $A$, $\beta^2$ and $B$ assume the following expressions:

$$v = \frac{u_f}{2D_f};\ \beta^2 = \frac{4D_f}{u_f};\ B = \frac{1}{\sqrt{D_e}} \tag{53}$$

$$A = \frac{\delta}{\sqrt{\theta D_e}};\quad \theta = \frac{\rho_m C_m}{\rho_f C_f},\quad D_e = \frac{k_e}{\rho_w C_w} \tag{54}$$

### 2.3.10 Explicit network model

A vertical *SF* can be viewed as 1d pipe element in which head loss is described by Forchheimer law. The conductance to flow of the generic *SFj* can be written as:

$$C_j = \left[ L_j \left( a_j + b_j Q_j \right) \right]^{-1}$$

(55)

The flow field in the fracture network can be solved in analytical way through the application of the first and second Kirchhoff's laws. The flow rate crossing generic SF*j* can be obtained as the product between the total discharge flow $\Sigma Q_i$ evaluated for the fracture intersection located at the inlet bond of the SF*j* and the probability of flow distribution of SF*j* $P_{Q,j}$. The latter is equal to the ratio between the conductance to flow of *SFj* and the sum of conductance to flow of each discharge *SF* connected at the inlet bond of *SFj*, as well as $P_{Q,j}$ should be proportional to the relative discharge flow rates:

$$P_{Q,j} = \frac{C_j}{\sum_{i=1}^{n} C_i} = \frac{Q_j}{\sum_{i=1}^{n} Q_i}$$

(56)

The PDF at a generic node can be obtained as the summation of PDFs of each elementary path that reach the node That is equal to the convolution product of the PDFs of each single fracture belonging the elementary path.

The BTC that described the temperature in the fracture at the generic node of the fracture network is:

$$T_f \left( t \right) = T_0 + T_{inj} \left( t \right) * L^{-1} \left[ \sum_{i=1}^{N_p} \prod_{j=1}^{n_{f,i}} P_{Q,j} \overline{\Gamma}_j \left( s \right) \right]$$

(57)

Whereas the temperature in the matrix evaluated at distance *d* along z axis from fracture – matrix interface at the generic node is:

$$T_m(t) = T_0 + T_{inj}(t) * L^{-1}\left\{\left[\sum_{i=1}^{N_p}\prod_{j=1}^{n_{f,i}} P_{Q,j}\,\overline{\Gamma}_j(s)\right]\exp\left(-Bs^{1/2}d\right)\right\} \tag{58}$$

### 2.3.11 Material and methods: experimental setup

The experiments have been performed on the laboratory physical model used to study flow and solute transport at bench scale (Sauty JP, 1982, deMarsily G. 1986, Tang DH, 1981, Cherubini C, 2012).

In order to analyze the heat transport dynamics in the fractured sample, some modifications have been made. The same sealed fractured limestone block with parallelepiped shape ($0.6\times0.4\times0.08$ m$^3$) described in previous work has been used. A hole of 2 mm diameter has been opened up to the depth of 1 cm along the center of some discontinuities by means of a percussion drill. Inside of each opened hole a thermocouple has

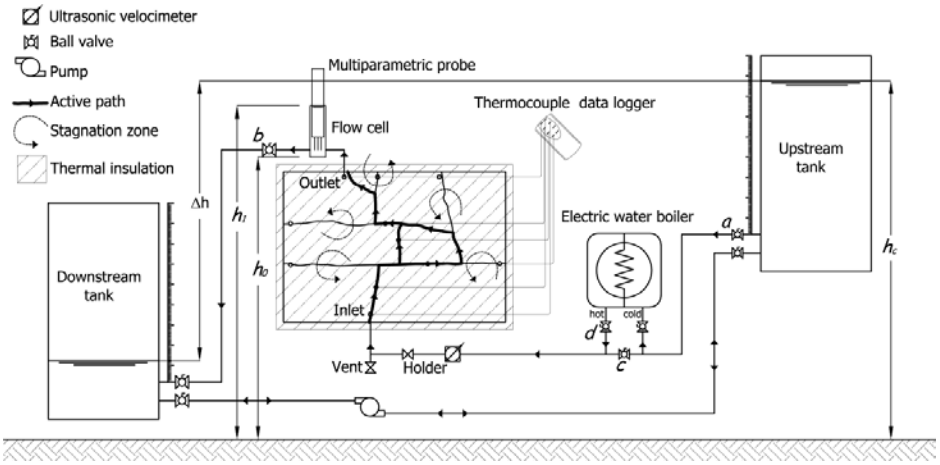


Figure 50 Schematic diagram of the experimental setup

been placed and welded to the block by means of rapid – hardening epoxy resin.

Furthermore at the inlet and the outlet of the selected path other two thermocouples have been placed. All thermocouples have been connected to a TC-08 Thermocouple Data Logger (Pico Technology) and a sampling rate of 1 second has been used.
The limestone block has been thermally insulated using extruded polystyrene panel with thermal conductivity equal to 0.034 $Wm^{-1}K^{-1}$ and thickness 0.05 m. Finally the sample has been connected to a hydraulic circuit. Water inside the sample flows according to the hydraulic head difference between upstream tank connected to the inlet port and downstream tank connected to the outlet port. The instantaneous flow rate that flows across the block is measured by an ultrasonic velocimeter (DOP3000 by Signal Processing). Water that enters into the sample is heated by an electric water boiler with a volume of $10^{-2}$ $m^3$. In correspondence of outlet port there is a flow cell in which a multiparametric probe is positioned for instantaneous measurement of pressure (dbar), temperature (°C) and electric conductivity ($\mu S\ cm^{-1}$). In Fig. 50 are reported the schematic diagram of the experimental setup.

### 2.3.12 Temperature tracer tests

The study of heat transport dynamics has been carried out through a selected path. Initially a hydraulic head difference between the upstream tank and downstream tank is imposed. At time $t = 0$ the valve "*a"* is closed and hydrostatic head inside the block is equal to the downstream tank. At time $t = 10$ s the valve "*a"* is opened while at time $t = 60$ s valve "*d*" is opened and in the same time valve "*c"* is closed. In this manner a step temperature function in correspondence of the inlet port $T_{inj}$(t) is imposed and measured by the thermocouple inside the inlet port. At time $t = 1000$ s the valve "*d"* and valve "*c"* is reclosed and reopened respectively. The flow rate entering the system is measured by means of the ultrasonic velocimeter. For different flow rates BTC curves can be recorded at the inlet and output ports and inside the sample in correspondence of some discontinuities.

### 2.3.13 Results and discussion

The Forchheimer parameters representative of the whole fracture network was derived. The estimated Forchheimer parameters are respectively $a = 7.345 \times 10^4$ $sm^{-3}$ and $b = 11.65 \times 10^9$ $s^2m^{-6}$. The critical flow rate corresponding to the ratio between the linear and nonlinear term equal to the unit in which the inertial force dominate viscous one is equal to $Q_{crit} = 6.30 \times 10^{-6}$ $m^3s^{-1}$. The probability of water distribution of each *SF* is equal to one except for the parallel branches. The probability of water distribution of the shorter parallel branch $P_Q$ decreases as the injection flow rate increases because, due to the nonlinear nature of flow, the conductance term of the shorter parallel branch decreases faster than the conductance term of the longer parallel branch.

The observed BTCs have been fitted by ENM based on Tang's solution. The parameters $u_f$, $D_f$, $D_e$ and $\delta$ are supposed equal for the all branches except for the parallel branches in which $u_f$ and $D_f$ become $u_f P_Q$ and $D_f P_Q$ for the shorter branch and $u_f(1 - P_Q)$ and $D_f(1 - P_Q)$ for the longer branch. The thermal BTC in correspondence of the outlet port is fitted using equation (57), whereas the thermal BTCs at the position inside the block is fitted by equation (58) using a distance along z axis from fracture – matrix interface *d* equal to the dimension of thermocouple (2 mm).

Fig. 51 shows the fitting results of thermal BTCs at different positions along the fracture network for the injection flow rate equal to $Q_0 = 4.03 \times 10^{-6}$ $m^3/s$. The fitting was satisfactory, except for the positions 2 and 3 in which the ENM model underestimate the observed thermal BTCs curves. The ENM model is able to represent the behavior of observed heat transport except where the configuration of the fracture network gives rise to a fracture block characterized by a limited capability to store heat. In this configuration, the Tang solution fail to model the observed thermal transport in correspondence of parallel branch, because the porous matrix surrounding the single fracture cannot be considered infinite in size. In this configuration the thermal BTCs are influenced each other. As consequence the observed BTCs show a lower heat dissipation then ENM model. Initially the hypothesis of porous matrix infinite is still valid, the ENM model reaches observed BTCs, subsequentely the observed BTCs begin to influenced each

other giving rise to lower heat dissipation outcoming that the ENM model underestimate the observed BTCs.

According to Kacabas (2004) can be defined the following three transport time scale:

$$t_u = \frac{L}{u_f};\ t_d = \frac{L^2}{D_f};\ t_e = \frac{\delta^2}{\theta D_e} \tag{59}$$

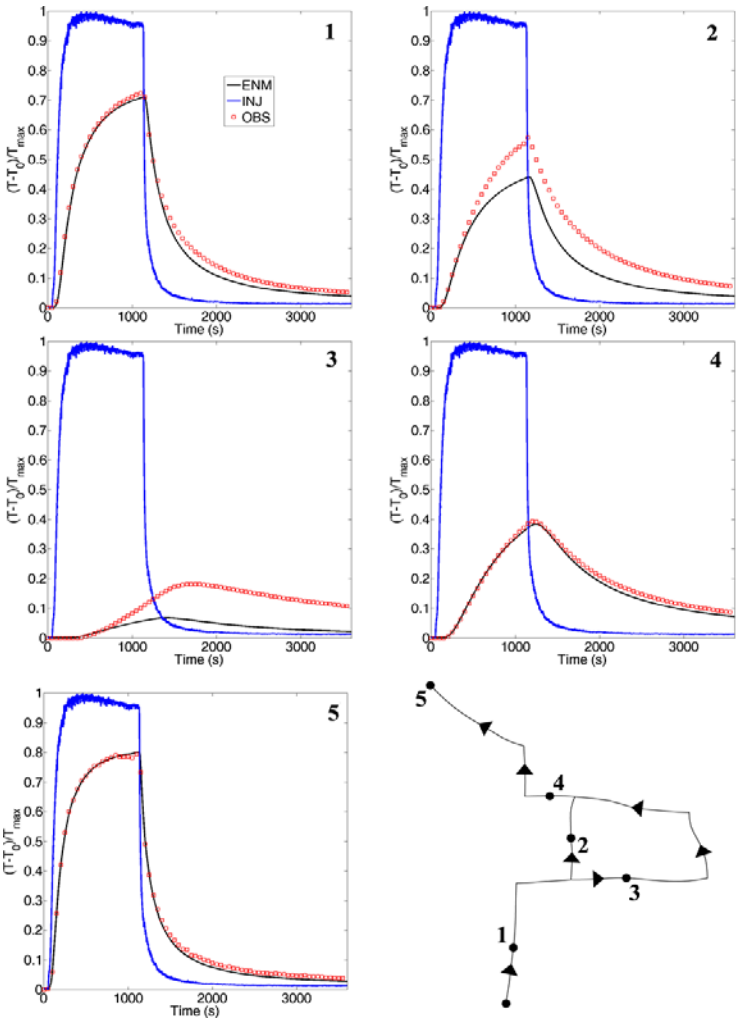


Figure 51 Fitting of BTCs at different positions in the fracture netowork using ENM with Tang solution for heat transport with injection flow rate equal to $Q_0 = 4.03 \times 10^{-6}$ m$^3$/s.

Table 13 shows the estimated transport time scale at different injection flow rates. According to previus work the characteristic lengthof fractured media is equal to $L$ = 0.601 m. Convective transport time is the same order of magnitude of the exchange time, the impact of the fracture matrix exchange is very strong giving rise to a strong retardation effect on the convective velocity.

Table 13 Estimated values of parameters for ENM with Tang solution at different injection flow rates.

| $Q_0$ ($m^3s^{-1}$)$\times10^{-6}$ | $t_u$ (s) | $t_d$ (s) | $t_e$ (s) |
|---|---|---|---|
| 1.84 | 240 | 182 | 297 |
| 2.32 | 251 | 190 | 240 |
| 2.68 | 234 | 198 | 273 |
| 2.85 | 245 | 178 | 256 |
| 3.00 | 231 | 157 | 317 |
| 4.00 | 226 | 54 | 879 |
| 4.22 | 143 | 40 | 349 |
| 7.06 | 72 | 35 | 318 |
| 7.96 | 61 | 19 | 164 |
| 8.97 | 44 | 15 | 115 |
| 12.36 | 53 | 16 | 352 |
| 12.59 | 40 | 14 | 164 |

The thermal dispersion plays an important role on heat transport dominating on convective transport although the injection flow rate is relatively high. In fact dispersion time scale is always less than convective time scale. Furthermore dispersion time scale and exchange time scale are comparable, however the latter is always less than the former. The comparison with previous studies on solute transport carried out in fractured media shows that thermal BTCs are characterized by a more enhanced early arrival and long tailing than solute BTCs. The residence time for heat transport is an order

of magnitude higher than for solute transport experiments. Fig. 52 shows the comparison of the observed residence time versus the injection flow rates both solute and heat transport. This results highlight that the heat transport is more retarted than mass transport.

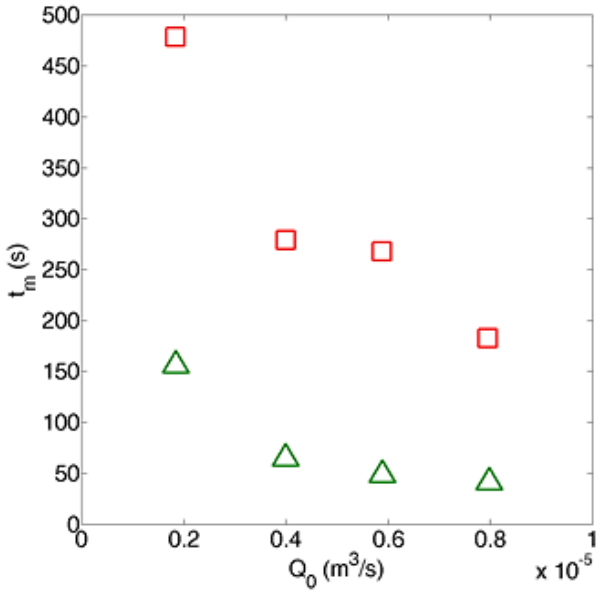


Figure 52 Comparison between the residence time $t_m$ of heat transport (red square) and solute transport (green triangle) at different injection flow rate $Q_0$.

### 2.3.14 Conclusion

Several features on behaviour of heat transport have been observed by the conducted experiments and their interpretation.

Heat transport dynamics has been fitted with explicit network model with Tang's solution. ENM model exhibit a satisfactory fitting except in correspondence of the parallel branch in which the porous matrix surrounding the single fracture cannot be considered infinite in size. Parallel branch are influenced each other as a consequence the observed BTCs show a lower heat dissipation than ENM model.

Heat transfer time scale is comparable with convective time scale the dual porosity behaviour is very strong giving rise to a delay on heat propagation in fracture network.

Thermal BTCs are characterized by a more enhanced early arrival and long tailing than solute BTCs observed in previous experiments. The residence time of heat transport is an order of magnitude higher than the residence time of solute transport.
Thermal dispersion time scale is always less than both thermal convective time scale and thermal exchange time scale. This results confirms that thermal dispersion play an important role on the heat transport ant its effect cannot be neglected.
The results encourage further experimental work to increase the knowledge of the key parameters that govern the heat propagation in fractured media, and therefore developing the best strategies for installation of devices for heat recovery and heat dissipation in fractured media.

### 2.3.15 Second test: "Laboratory experimental investigation of heat transport in fractured media" (Claudia Cherubini, Nicola Pastore, Concetta I. Giasi, Nicoletta Maria Allegretti (2017))

**Abstract**

Low enthalpy geothermal energy is a renewable resource that is still underexploited nowadays, in relation to its potential for development in the society worldwide. Most of its applicability have already been investigated, such as: heating and cooling of private and public buildings, roads defrost, cooling of industrial processes, food drying systems, desalination.
One of the major limitations related to the choice of installing low enthalpy geothermal power plants regards the initial investment costs.
In order to increase the optimal efficiency of installations which use groundwater as geothermal resource, flow and heat transport dynamics in aquifers need to be well characterized. Especially in fractured rock aquifers these processes represent critical elements that are not well known. Therefore there is a tendency to oversize geothermal plants.
In literature there are very few studies on heat transport especially in fractured media.

This study is aimed to deepen the understanding of this topic through heat transport experiments in fractured network and their interpretation.
The heat transfer tests have been carried out on the experimental apparatus previously employed to perform flow and tracer transport experiments, which has been modified in order to analyze heat transport dynamics in a network of fractures. In order to model the obtained thermal breakthrough curves, the Explicit Network Model (ENM) has been used, which is based on an adaptation of a Tang's solution for the transport of the solutes in a semi-infinite single fracture embedded in a porous matrix.
Parameter estimation, time moment analysis, tailing character and other dimensionless parameters have permitted to better understand the dynamics of heat transport and the efficiency of heat exchange between the fractures and matrix. The results have been compared with the previous experimental studies on solute transport.

### 2.3.16 Theoretical background: Nonlinear flow

With few exceptions, any fracture can be envisioned as two rough surfaces in contact. In cross section the solid areas representing asperities might be considered as the grains of porous media.
Therefore, in most studies examining hydrodynamic processes in fractured media, the general equations describing flow and transport in porous media are applied, such as Darcy's law, that depicts a linear relationship between the pressure gradient and fluid velocity (Whitaker, 1986; Cherubini and Pastore, 2010a)
However, this linearity has been demonstrated to be valid at low flow regimes (Re $<$ 1). For Re $>$ 1 a nonlinear flow behavior is likely to occur (Cherubini, 2013d).
When Re $>>$ 1, a strong inertial regime develops, that can be described by the Forchheimer equation (Forchheimer, 1901):

$$-\frac{dp}{dx} = \frac{\mu}{k} \cdot u_f + \rho\beta \cdot u_f^2 \tag{60}$$

Where $\beta$ ($L^{-1}$) is called the inertial resistance coefficient, or non – Darcy coefficient. It is possible to express Forchheimer law in terms of hydraulic head (h):

$$-\frac{dh}{dx} = a' \cdot u_f + b' \cdot u_f^2 \tag{61}$$

The coefficients *a* ($TL^{-1}$) and *b* ($TL^{-2}$) represent the linear and inertial coefficient respectively equal to:

$$a' = \frac{\mu}{\rho g k};\ b' = \frac{\beta}{g} \tag{62}$$

The relationship between hydraulic head gradient and flow rate *Q* ($L^3T^{-1}$) can be written as:

$$-\frac{dh}{dx} = a \cdot Q + b \cdot Q^2 \tag{63}$$

The coefficients *a* ($TL^{-3}$) and *b* ($T^2L^{-6}$) can be related to *a'* and *b'*:

$$a = \frac{a'}{\omega_{eq}}; b = \frac{b'}{\omega_{eq}} \tag{64}$$

Where $\omega_{eq}$ ($L^2$) is the equivalent cross sectional area of fracture.

### 2.3.17 Heat transfer by water flow in single fractures

Fluid flow and heat transfer in a single fracture (*SF*) undergo advective, diffusive and dispersive phenomena. Dispersion is caused by small-scale fracture aperture variations. Flow channeling is one example of macro dispersion caused by preferred flow paths, in that mass and heat tend to migrate through the portions of a fracture with the largest apertures.

In fractured media another process is represented by diffusion into surrounding rock matrix. Matrix diffusion attenuates the mass and heat propagation in the fractures.

According to the boundary – layer theory (Fahien, 1983), solute mass transfer $q_m$ ($ML^{-2}$) per unit area at the fracture-matrix interface (Wu et al., 2010) is given by:

$$q_M = \frac{D_m}{\delta}\left(c_f - c_m\right)$$

(25)

Where $c_f$ ($ML^{-3}$) is the concentration across fractures, $c_m$ ($ML^{-3}$) is the concentration of the matrix block surfaces, $D_m$ ($LT^{-2}$) is the molecular diffusion coefficient, and $\delta$ (m) is the thickness of boundary layer (Wu et al., 2010). For small fractures, $\delta$ may become the aperture $w_f$ (m) of the *SF.*

In analogous manner the specific heat transfer flux $q_H$ ($MT^{-3}$) at the fracture – matrix interface is given by:

$$q_H = \frac{k_m}{\delta}\left(T_f - T_m\right)$$

(66)

Where $T_f$ (K) is the temperature across fractures, $T_m$ (K) is the temperature of the matrix block surfaces, $k_m$ ($MLT^{-3}K^{-1}$) is the thermal conductivity.

The continuity conditions at the fracture – matrix interface requires a balance between mass transfer rate and mass diffused into the matrix described as:

$$q_M = -D_e \left.\frac{\partial C_m}{\partial z}\right|_{z=w_f/2}$$

(67)

Where $z$ (m) is the coordinate perpendicular to the fracture axis and $w_f$ is the aperture of the fracture.

In the same way the specific heat flux must be balanced by heat diffused into the matrix described as:

$$q_H = -k_e \frac{\partial T_m}{\partial z}\bigg|_{z=w_f/2} \tag{68}$$

The effective diffusion coefficient takes into account the fact that diffusion can only take place through pore and fracture openings because mineral grains block many of the possible pathways. The effective thermal conductivity of a formation consisting of multiple components depends on the geometrical configuration of the components as well as on the thermal conductivity of each.

The effective terms ($D_e$ instead of $D_m$ and $k_e$ instead of $k_m$) have been introduced in order to include the effect of various system parameters such as fluid velocity, porosity, surface area, roughness, that may enhance mass and heat transfer effect. For instance, when large flow velocity occurs, convective transport is stronger along the centre of the fracture, enhancing the concentration or temperature gradient at the fracture matrix interface. As known roughness plays an important role in increasing mass or heat transfer because of increasing turbulent flow conditions.

According to Bodin (2007) the governing equation for the one dimensional advective - dispersive transport along the axis of a semi-infinite fracture with one – dimensional diffusion in the rock matrix, in perpendicular direction to the axis of the fracture is:

$$\frac{\partial c_f}{\partial t} + u_f \frac{\partial c_f}{\partial x} = \frac{\partial}{\partial x}\left( D_f \frac{\partial c_f}{\partial x} \right) - \frac{D_e}{\delta} \frac{\partial c_m}{\partial z}\bigg|_{z=w_f/2} \tag{69}$$

Where $x$ (m) is the coordinate parallel to the axis of *SF*, $u_f$ ($LT^{-1}$) is the convective velocity, $D_f$ ($L^2T^{-1}$) is the dispersion coefficient. The latter mainly depends on two processes: Aris – Taylor dispersion and geometrical dispersion. Previous experiments (Cherubini et al., 2013) show that, due to the complex geometrical and topological

characteristics of the fracture network that create tortuous flow paths, Aris – Taylor dispersion may not develop. A linear relationship has been found between velocity and dispersion so geometrical dispersion is mostly responsible for the mixing process along the fracture:

$$D_f = \alpha_{LM} u_f \tag{70}$$

Where $\alpha_{LM}$ (L) is the dispersion coefficient for mass transport.

Assuming that fluid flow velocity in the surrounding rock matrix is equal to zero, the equation for the conservation of heat in the matrix is given by:

$$\frac{\partial C_m}{\partial t} = D_a \frac{\partial^2 C_m}{\partial z^2} \tag{71}$$

Where $D_a$ is the apparent diffusion coefficient of the solute in the matrix expressed as function of $\vartheta_m$ (-) the matrix porosity $D_a = D_e / \theta_m$ (Bodin et al., 2007). Tang et al. (1981) presented an analytical solution for solute transport in semi – infinite single fracture embedded in a porous rock matrix with a constant concentration at the fracture inlet ($x = 0$) equal to $c_0$ ($ML^{-3}$) and with an initial concentration equal to zero. The solute concentration in the fracture $\overline{c}_f$ and in the matrix $\overline{c}_m$ has been given as function of time in Laplace space.

$$\overline{c}_f = \frac{c_0}{s} \exp(vL) \exp\left[ -vL \left\{ 1 + \beta^2 \left( \frac{s^{1/2}}{A} + s \right) \right\}^{1/2} \right] \tag{72}$$

$$\overline{c}_m = \overline{c}_f \exp\left[ -Bs^{1/2} \left( z - w_f / 2 \right) \right] \tag{73}$$

Whereas the gradient of $\overline{c}_m$ at the interface $z = w_f/2$ is:

$$\left.\frac{d\overline{c}_m}{dx}\right|_{x=w_f/2} = -\overline{c}_f B s^{1/2} \tag{74}$$

The $v$, $A$, $\beta^2$ and $B$ coefficients are expressed as follows:

$$v = \frac{u_f}{2D_f} \tag{75}$$

$$A = \frac{\delta}{\sqrt{\theta D_e}};\ \theta = \theta_m \tag{76}$$

$$\beta^2 = \frac{4D_f}{u_f^2} \tag{77}$$

$$B = \frac{1}{\sqrt{D_e}} \tag{78}$$

Defined the residence time as the average amount of time that the solute spends in the system, on the basis of these analytical solutions the probability density function of the solute residence time (*PDF*) in the single fracture in the Laplace space can be expressed as:

$$\overline{\Gamma}(s) = \exp(vL)\exp\left[-vL\left\{1+\beta^2\left(\frac{s^{1/2}}{A}+s\right)\right\}^{1/2}\right] \tag{79}$$

Assuming that density and heat capacity are constant in time, the heat transport conservation equation in *SF* can be expressed as follows:

$$\frac{\partial T_f}{\partial t} + u_f \frac{\partial T_f}{\partial x} = \frac{\partial}{\partial x}\left( D_{fH} \frac{\partial T_f}{\partial x} \right) - \frac{k_e}{\rho_w C_w \delta} \frac{\partial T_m}{\partial z}\bigg|_{z=w_f/2}$$

(80)

Where $\rho_w$ ($ML^{-3}$), $C_w$ ($L^2T^2K^{-1}$) represent the density, the specific heat capacity of the fluid within *SF* respectively. $D_f$ for heat transport assumes the following expressions:

$$D_{fH} = \frac{\lambda_L}{\rho_w C_w}$$

(81)

Where $\lambda_L$ is the thermodynamic dispersion coefficient ($MLT^{-3}K^{-1}$). Sauty et al. (1982) and de Marsily (1986) proposed an expression for the thermal dispersion coefficient where the thermal dispersion term varies linearly with velocity and depends on the heterogeneity of the medium, as for solute transport:

$$\lambda_L = k_0 + \alpha_{LH} \rho_w c_w u_f$$

(82)

Where $k_0$ is the bulk thermal conductivity ($MLT^{-3}K^{-1}$) $\alpha_{LH}$ (L) is the longitudinal thermal dispersivity.

The heat transport conservation equation in the matrix is expressed as follows:

$$\rho_m C_m \frac{\partial T_m}{\partial t} = k_e \frac{\partial^2 T_m}{\partial z^2}$$

(83)

Note that the governing equations of heat and mass transport highlight similarities between the two processes, thus Tang's solution can be used also for heat transport.
In terms of heat transport, the coefficients $v$, $A$, $\beta^2$ and $B$ are expressed as follows:

$$v = \frac{u_f}{2D_{fH}};$$

(84)

$$A = \frac{\delta}{\sqrt{\theta D_e}}; \quad \theta = \frac{\rho_m C_m}{\rho_f C_f}, \quad D_e = \frac{k_e}{\rho_w C_w}$$

(85)

$$\beta^2 = \frac{4D_f}{u_f^2}$$

(86)

$$B = \frac{1}{\sqrt{D_e}}$$

(86)

Three characteristic time scales can be defined:

$$t_u = \frac{L}{u_f}; \quad t_d = \frac{L^2}{D_f}; \quad t_e = \frac{\delta^2}{D_e}$$

(87)

Where $L$ (L) is the characteristic length, $t_u$ (T), $t_d$ (T) and $t_e$ (T) represent the characteristics time scales of convective transport, dispersive transport and loss of the mass or heat into the surrounding matrix.
The relative effect of dispersion, convection and matrix diffusion on mass or heat propagation in the fracture can be evaluated by comparing the correspondent time scale.

Peclet number $P_e$ is defined as the ratio between dispersive ($t_d$) and convective ($t_u$) to transport times:

$$Pe = \frac{t_d}{t_u} = \frac{u_f L}{D_f} \tag{88}$$

At high Peclet numbers transport processes are mainly governed by convection, whereas at low Peclet numbers it is mainly dispersion that dominates.
Another useful dimensionless number, generally applied in chemical engineering, is the Damköhler number that can be used in order to evaluate the influence of matrix diffusion on convection phenomena. The Damköhler number is based on the exchange rate coefficient corresponding to:

$$\alpha = \frac{D_e}{\delta^2} \tag{89}$$

Note that the inverse of $t_e$ has the same meaning of the exchange rate coefficient $\alpha$ ($T^{-1}$). $D_a$ relates the convection time scale to the exchange time scale.

$$Da = \frac{t_u}{t_e} = \frac{\alpha L}{u_f} \tag{90}$$

When $t_e$ values are of the same order of magnitude as the transport time $t_u$ ($D_a \cong 1$), diffusive processes in the matrix are more relevant. In this case concentration or temperature distribution profiles are characterized by a long tail.
When $t_e \gg t_u$ ($D_a \ll 1$) the fracture – matrix exchange is very slow and it does not influence mass or heat propagation. On the contrary when $t_e \ll t_u$ ($D_a \gg 1$) the

fracture matrix exchange is rapid, there is instantaneous equilibrium between fracture and matrix and they have the same concentration or temperature. These two circumstances close the standard advective – dispersive transport equation.
The product between $P_e$ and $D_a$ represents another dimensionless group which is a measure of transport processes:

$$Pe \times Da = \frac{t_d}{t_e} = \frac{\alpha L^2}{D_f} \tag{91}$$

When $Pe \times Da$ increases $t_e$ decreases more rapidly than $t_d$, and subsequently the mass or heat diffusion into the matrix may be dominant on the longitudinal dispersion.

### 2.3.18 Explicit network model (ENM)

With the assumption that a *SF j* can be schematized by a 1d-pipe element, the Forchheimer model can be used to write the relationship between head loss $\Delta h_j$ (L) and flow rate $Q_j$ ($L^3T^{-1}$) in finite terms:

$$\frac{\Delta h_j}{L_j} = aQ_j + bQ_j^2 \Rightarrow \Delta h_j = \left[ L_j \left( a + bQ_j \right) \right] Q_j \tag{92}$$

Where $L_j$ (L) is the length of *SF j*, $a$ ($TL^{-3}$) and $b$ ($T^2L^{-6}$) represent the Forchheimer parameters written in finite terms. The term in the square brackets constitutes the resistance to flow $R_j\left(Q_j\right)$ ($TL^{-2}$) of *SF j*.
In case of steady-state conditions and for a simple 2D fracture network geometry, a straightforward manner can be applied to obtain the solution of flow field by applying the first and second Kirchhoff's laws.

In a 2D fracture network, fractures can be arranged in series and/or in parallel. Specifically, in a network in which fractures are set in a chain, the total resistance to flow is calculated by simply adding up the resistance values of each single fracture. The flow in a parallel fracture network breaks up, with some flowing along each parallel branch and re – combining when the branches meet again. In order to estimate the total resistance to flow the reciprocals of the resistance values have to be added up and then the reciprocal of the total has to be calculated. The flow rate $Q_j$ across the generic fracture *j* of the parallel network can be calculated as (Cherubini et al., 2014):

$$Q_j = \sum Q \left[ \frac{1}{R_j} \left( \sum_{i=1}^{n} \frac{1}{R_i} \right)^{-1} \right] \tag{93}$$

Where $\sum Q$ ( $LT^{-3}$) is the sum of the mass flow rates at fracture intersections in correspondence of the inlet bond of *j* fracture, whereas the term in square brackets represents the probability of water distribution of *j* fracture $P_{Q,j}$.

Once known the flow field in the fracture network, to obtain the *PDF* at a generic node the *PDFs* of each elementary path that reaches the node have to be summed up. They can be calculated as the convolution product of the *PDFs* of each single fracture composing the elementary path.

Definitely the BTC describing the concentration in the fracture as function of time at the generic node, using the convolution theorem, can be obtained as follows:

$$c_f(t) = c_0 + c_{inj}(t) * L^{-1} \left[ \sum_{i=1}^{N_p} \prod_{j=1}^{n_{f,i}} P_{M,j} \overline{\Gamma}_j(s) \right] \tag{94}$$

Where $c_0$ ($ML^{-3}$) is the initial concentration and $c_{inj}$ ($ML^{-3}$) is the concentration injection function, (∗) is the convolution operator, $L^{-1}$ represents the inverse Laplace transform operator, $N_p$ is the number of the paths that reach the node, $n_{f,i}$ is the number of the *SF* belonging to the elementary path $i^{th}$, $P_{M,j}$ and $\overline{\Gamma}(s)$ are the mass distribution probability

and the *PDF* in the Laplace space of the generic $j^{th}$ *SF* respectively. Inverse Laplace transform $L^{-1}$ can be solved numerically using Abate et al. (2006) algorithm.
At the same way the BTC $T_f$ which describes the temperature in the fracture as function of time at the generic node can be written as:

$$T_f(t) = T_0 + T_{inj}(t) * L^{-1}\left[\sum_{i=1}^{N_p}\prod_{j=1}^{n_{f,i}} P_{H,j}\overline{\Gamma}_j(s)\right] \tag{95}$$

Where $T_0$ (K) is the initial temperature and $T_{inj}$ (K) is the temperature injection function, $P_{H,j}$ is the heat distribution probability.

$P_{\mathrm{M},j}$ and $P_{\mathrm{H},j}$ can be estimated as the probabilities of the mass and heat distribution at the inlet bond of each individual *SF* respectively. The mass and heat distribution is proportional to the correspondent flow rates:

$$P_{\mathrm{M},j} = P_{H,j} = \frac{Q_j}{\sum Q} \tag{96}$$

Where $Q_j$ is the flow rate in the *j SF* and $\sum Q$ is the sum of the flow rate calculated at the fracture intersection in correspondence of the inlet bond of *j* fracture. Note that if Equation 95 is valid, the probability of water distribution is equal to the probabilities of mass and heat distribution (term in square brackets in Equation 93). Definitely the ENM model regarding each *SF* can be described by four parameters ($u_{f,j}$, $D_{f,j}$, $\alpha_j$, $P_{Q,j}$).

### 2.3.19 Flow experiments.

The average flow rate through the selected path can be evaluated as:

$$\overline{Q} = \frac{S_1}{t_1 - t_0}(h_1 - h_0) \tag{97}$$

Where $S_1$ ($L^2$) is the cross section area of the flow cell, $\Delta t = t_1 - t_0$ is the time for the flow cell to be filled from $h_0$ (L) and $h_1$ (L). To calculate the average hydraulic head differences between the upstream tank and the flow cell the following expression is adopted:

$$\Delta h = h_c - \frac{h_0 + h_1}{2} \tag{98}$$

Where $h_c$ is the hydraulic head measured in the upstream tank. Several tests have been carried out varying the control head, and in correspondence of each value of the average flow rate and head differences, the average resistance to flow has been determined as:

$$\overline{R}\left(\overline{Q}\right) = \left[\frac{S_1}{t_1 - t_0} \ln\left(\frac{h_0 - h_c}{h_1 - h_c}\right)\right]^{-1} \tag{99}$$

### 2.3.20 Solute and temperature tracer tests

Solute and temperature tracer tests have been conducted through the following steps. As initial condition, a specific value of hydraulic head difference between the upstream tank and downstream tank has been assigned. At $t = 0$ the valve *a* is closed so as the hydrostatic head inside the block assumes the same value to the one in the downstream tank. At $t = 10$ s the valve *a* is opened.

For solute tracer test at time $t = 60$ s by means of a syringe, a mass of $5 \times 10^{-4}$ kg sodium chloride is injected into the inlet port. Due to the very short source release time, the instantaneous source assumption can be adopted (the solute is released instantaneously at the source in units of mass). The multiparametric probe located within the flow cell measures the solute BTC.

As concerns thermal tracer tests at the time $t = 60$ s the valve *d* is opened while the valve c is closed. In such a way a step temperature function in correspondence of the

inlet port $T_{inj}(t)$ is imposed and measured by the first thermocouple. The other thermocouple located inside the outlet port is used to measure the thermal BTC.
The ultrasonic velocimeter is used in order to measure the instantaneous flow rate, whereas a multiparametric probe located at the outlet port measures the pressure and the electric conductivity.

### 2.3.21 Results and discussion

**Flow characteristics**

The Kirchhoff laws have been used in order to estimate the flow rates flowing in each single fracture. In figure 53 a sketch of the 2D pipe conceptualization of the fracture network is reported.

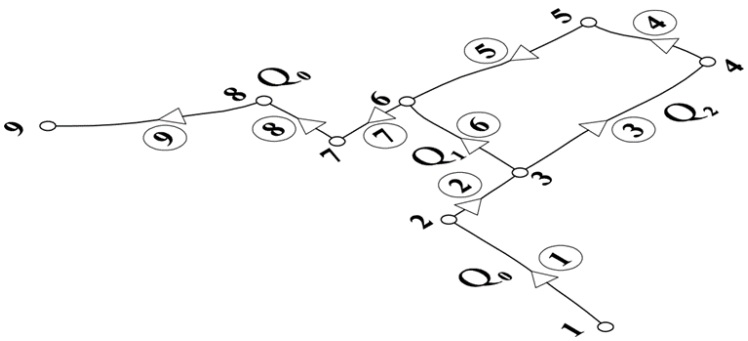


Figure 53 Two dimensional pipe network conceptualization of the fracture network.

The linear and nonlinear terms have been assumed equal for each single fracture of the fracture network and have been estimated matching the average experimental resistance to flow resulting from Equation (99) with resistance to flow estimated as:

$$\bar{R}\left(\bar{Q}\right) = R_1\left(Q_0\right) + R_2\left(Q_0\right) + \left(\frac{1}{R_6\left(Q_1\right)} + \frac{1}{R_3\left(Q_2\right) + R_4\left(Q_2\right) + R_5\left(Q_2\right)}\right)^{-1} + \\ + R_7\left(Q_0\right) + R_8\left(Q_0\right) + R_9\left(Q_0\right) \tag{100}$$

The flow rate $Q_1$ is determined using the following iterative equation:

$$Q_1^{k+1} = Q_0 \left[ \frac{R_3\left(Q_0 - Q_1^k\right) + R_4\left(Q_0 - Q_1^k\right) + R_5\left(Q_0 - Q_1^k\right)}{R_3\left(Q_0 - Q_1^k\right) + R_4\left(Q_0 - Q_1^k\right) + R_5\left(Q_0 - Q_1^k\right) + R_6\left(Q_1^k\right)} \right] \tag{101}$$

Whereas the flow rate $Q_2$ is determined merely as:

$$Q_2 = Q_0 - Q_1 \tag{102}$$

The linear and nonlinear term are equal respectively to $a = 7.345 \times 10^4$ sm$^{-3}$ and $b = 11.65 \times 10^9$ s$^2$m$^{-6}$. Inertial forces dominate viscous ones when the Forchheimer number is higher than one. The critical flow rate $Q_{crit}$ can be determined in correspondence of Fo = 1 as the ratio between $a$ and $b$ resulting $Q_{crit} = 6.30 \times 10^{-6}$ m$^3$s$^{-1}$.

Because of the nonlinearity of flow, varying the inlet flow rate $Q_0$ the ratio between the flow rates $Q_1$ and $Q_2$ flowing respectively in the branches 6 and 3 – 5 is not constant. When $Q_0$ increases $Q_2$ increases faster than $Q_1$. The probability of water distribution of the branch 6 $P_{Q,6}$ is evaluated as the ratio between $Q_0$ and $Q_1$, whereas the probability of water distribution of the branch 3 – 5 is equal to $P_{Q,3\text{-}5} = 1 - P_{Q,6}$.

### 2.3.22 Fitting of breakthrough curves and interpretation of estimated model parameters

The behavior of mass and heat transport has been compared varying the injection flow rates. In particular 21 tests in the range $1.83 \times 10^{-6}$ - $1.26 \times 10^{-5}$ m$^3$s$^{-1}$ for heat transport have been made and compared with the 55 tests in the range $1.32 \times 10^{-6}$ - $8.34 \times 10^{-6}$ m$^3$s$^{-1}$ for solute transport presented in previous studies.

The observed heat and mass BTCs for different flow rates have been individually fitted using the ENM approach presented in the previous section. The transport parameters $u_f$, $D_f$ and $\alpha$ are assumed equal for all branches of the fracture network. The probability of mass and heat distribution are assumed equal to the probability of water distribution. The experimental BTCs are fitted using Equation 93 and Equation 94 for mass and heat transport respectively. Note that for mass transport $c_{inj}(t)$ supposing the instantaneous injection condition becomes a Dirac delta function.

The determination coefficient ($r^2$) and the root mean square error (*RMSE*) have been used in order to evaluate the goodness of fit.

Table 14 Estimated values of parameters, RMSE, and determination coefficient $r^2$ for ENM with Tang's solution at different injection flow rates for mass transport.

| $Q_0$ ($m^3s^{-1}$)$\times10^{-6}$ | $u_f$ ($ms^{-1}$)$\times10^{-3}$ | | $D_f$ ($ms^{-2}$)$\times10^{-3}$ | | $\alpha$ ($s^{-1}$)$\times10^{-6}$ | | RMSE | $r^2$ |
|---|---|---|---|---|---|---|---|---|
| 1.319 | 4.38 | 4.47 | 0.68 | 0.70 | 4.80 | 5.06 | 0.0053 | 0.9863 |
| 1.843 | 6.21 | 6.28 | 0.57 | 0.58 | 2.86 | 3.01 | 0.0026 | 0.9954 |
| 2.234 | 6.54 | 6.59 | 0.66 | 0.67 | 3.09 | 3.13 | 0.0017 | 0.9976 |
| 2.402 | 7.64 | 7.68 | 0.67 | 0.67 | 2.65 | 2.68 | 0.0015 | 0.9983 |
| 2.598 | 9.88 | 9.94 | 0.80 | 0.82 | 2.76 | 2.84 | 0.0015 | 0.9987 |
| 2.731 | 8.27 | 8.35 | 0.75 | 0.76 | 2.80 | 2.91 | 0.0018 | 0.9977 |
| 2.766 | 8.35 | 8.41 | 0.84 | 0.85 | 2.65 | 2.69 | 0.0021 | 0.9978 |
| 3.076 | 11.33 | 11.43 | 0.89 | 0.91 | 2.53 | 2.59 | 0.0029 | 0.9982 |
| 3.084 | 10.86 | 10.95 | 0.87 | 0.89 | 3.11 | 3.18 | 0.0022 | 0.9982 |
| 4.074 | 15.88 | 16.02 | 1.19 | 1.21 | 2.89 | 2.94 | 0.0048 | 0.9979 |
| 4.087 | 15.07 | 15.20 | 1.11 | 1.13 | 3.75 | 3.83 | 0.0045 | 0.9976 |
| 4.132 | 14.71 | 14.82 | 1.08 | 1.09 | 2.93 | 2.98 | 0.0028 | 0.9985 |
| 4.354 | 15.63 | 15.77 | 1.14 | 1.16 | 3.24 | 3.30 | 0.0052 | 0.9979 |
| 4.529 | 17.05 | 17.21 | 1.30 | 1.32 | 2.88 | 2.94 | 0.0055 | 0.9978 |
| 5.852 | 19.26 | 19.38 | 1.44 | 1.46 | 4.21 | 4.25 | 0.0042 | 0.9983 |
| 5.895 | 19.38 | 19.54 | 1.37 | 1.39 | 3.77 | 3.82 | 0.0058 | 0.9981 |
| 6.168 | 18.98 | 19.17 | 1.36 | 1.39 | 2.87 | 2.92 | 0.0091 | 0.9973 |
| 7.076 | 20.64 | 20.86 | 1.36 | 1.39 | 3.33 | 3.39 | 0.0123 | 0.9963 |
| 7.620 | 20.47 | 20.75 | 1.52 | 1.55 | 2.33 | 2.39 | 0.0180 | 0.9951 |
| 7.983 | 21.33 | 21.58 | 1.61 | 1.64 | 2.92 | 2.98 | 0.0137 | 0.9965 |
| 8.345 | 21.71 | 21.97 | 1.65 | 1.68 | 2.81 | 2.86 | 0.0136 | 0.9964 |

Table 15 Estimated values of parameters, RMSE, and determination coefficient $r^2$ for ENM with Tang's solution at different injection flow rates for heat transport.

| $Q_0$ ($m^3s^{-1}$)$\times10^{-6}$ | $u_f$ ($ms^{-1}$) $\times10^{-3}$ | | $D_f$ ($ms^{-2}$)$\times10^{-3}$ | | $\alpha$ ($s^{-1}$)$\times10^{-3}$ | | RMSE | $r^2$ |
|---|---|---|---|---|---|---|---|---|
| 1.835 | 2.20 | 2.91 | 1.91 | 1.95 | 6.27 | 6.59 | 0.0065 | 0.9997 |
| 2.325 | 1.74 | 2.73 | 1.82 | 1.91 | 5.39 | 9.26 | 0.0098 | 0.9992 |
| 2.462 | 0.35 | 0.52 | 2.42 | 2.57 | 2.25 | 2.33 | 0.0138 | 0.9984 |
| 2.605 | 0.44 | 0.54 | 2.33 | 2.40 | 0.74 | 0.77 | 0.0073 | 0.9995 |
| 2.680 | 2.18 | 2.95 | 1.77 | 1.83 | 5.68 | 8.31 | 0.0030 | 0.9998 |
| 2.800 | 0.36 | 0.79 | 2.53 | 2.68 | 3.54 | 3.72 | 0.0213 | 0.9982 |
| 2.847 | 1.73 | 3.16 | 1.98 | 2.06 | 4.95 | 13.45 | 0.0283 | 0.9978 |
| 3.003 | 2.34 | 2.87 | 2.24 | 2.32 | 5.33 | 6.55 | 0.0033 | 0.9998 |
| 3.998 | 2.56 | 2.75 | 6.63 | 6.80 | 2.05 | 2.11 | 0.0150 | 0.9993 |
| 4.030 | 2.60 | 2.83 | 7.18 | 7.36 | 1.42 | 1.52 | 0.0147 | 0.9993 |
| 4.217 | 3.85 | 4.56 | 8.92 | 9.29 | 4.86 | 5.77 | 0.0228 | 0.9945 |
| 4.225 | 2.43 | 2.64 | 7.53 | 7.84 | 1.64 | 1.80 | 0.0251 | 0.9987 |
| 4.471 | 2.30 | 3.13 | 9.18 | 9.50 | 1.06 | 1.33 | 0.1115 | 0.9957 |
| 5.837 | 3.51 | 4.13 | 4.95 | 5.36 | 0.61 | 0.79 | 0.2360 | 0.9872 |
| 5.880 | 2.71 | 3.10 | 4.23 | 4.60 | 0.04 | 0.05 | 0.1997 | 0.9926 |
| 6.445 | 4.71 | 5.12 | 6.18 | 6.81 | 1.49 | 1.54 | 0.2156 | 0.9863 |
| 7.056 | 8.15 | 8.46 | 10.05 | 10.74 | 5.63 | 6.00 | 0.0694 | 0.9951 |
| 7.959 | 9.64 | 10.11 | 18.40 | 19.47 | 10.92 | 11.55 | 0.0662 | 0.9971 |
| 8.971 | 13.40 | 13.79 | 24.57 | 25.82 | 15.35 | 15.85 | 0.0303 | 0.9985 |
| 12.364 | 11.01 | 11.67 | 21.97 | 22.63 | 5.23 | 5.25 | 0.0631 | 0.9939 |
| 12.595 | 13.71 | 14.26 | 26.65 | 27.61 | 9.26 | 9.41 | 0.0426 | 0.9955 |

Tables 14 and 15 show the values of transport parameters, the *RMSE* and $r^2$ for mass and heat transport respectively.

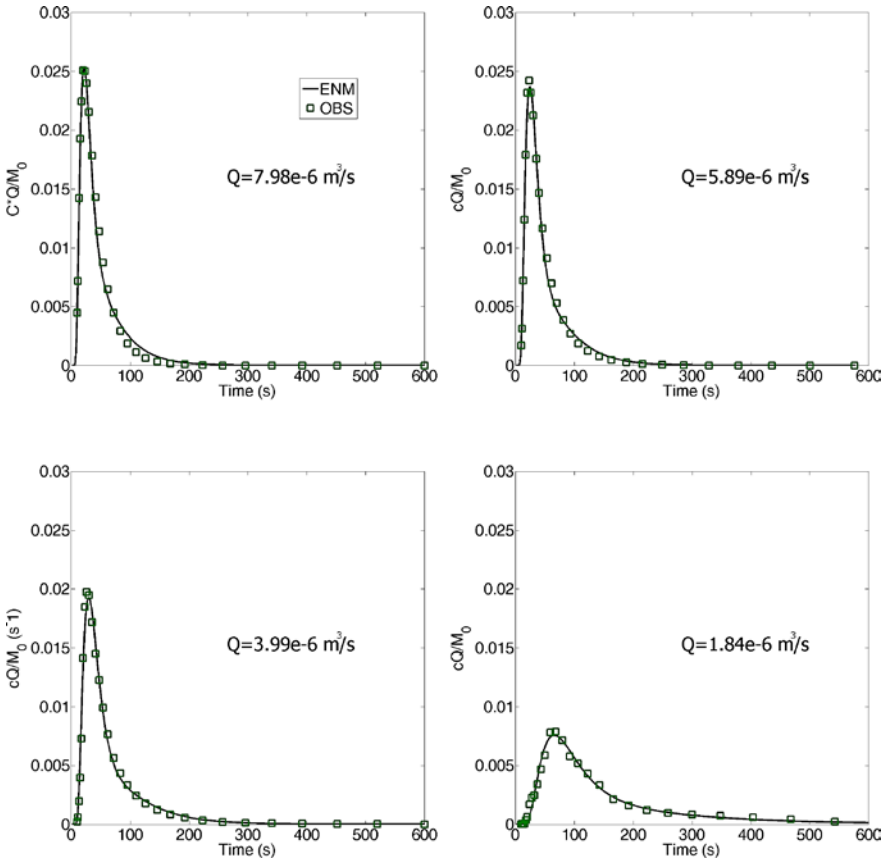


Figure 54 Fitting of BTCs at different injection flow rates using ENM with Tang's solution for mass transport.

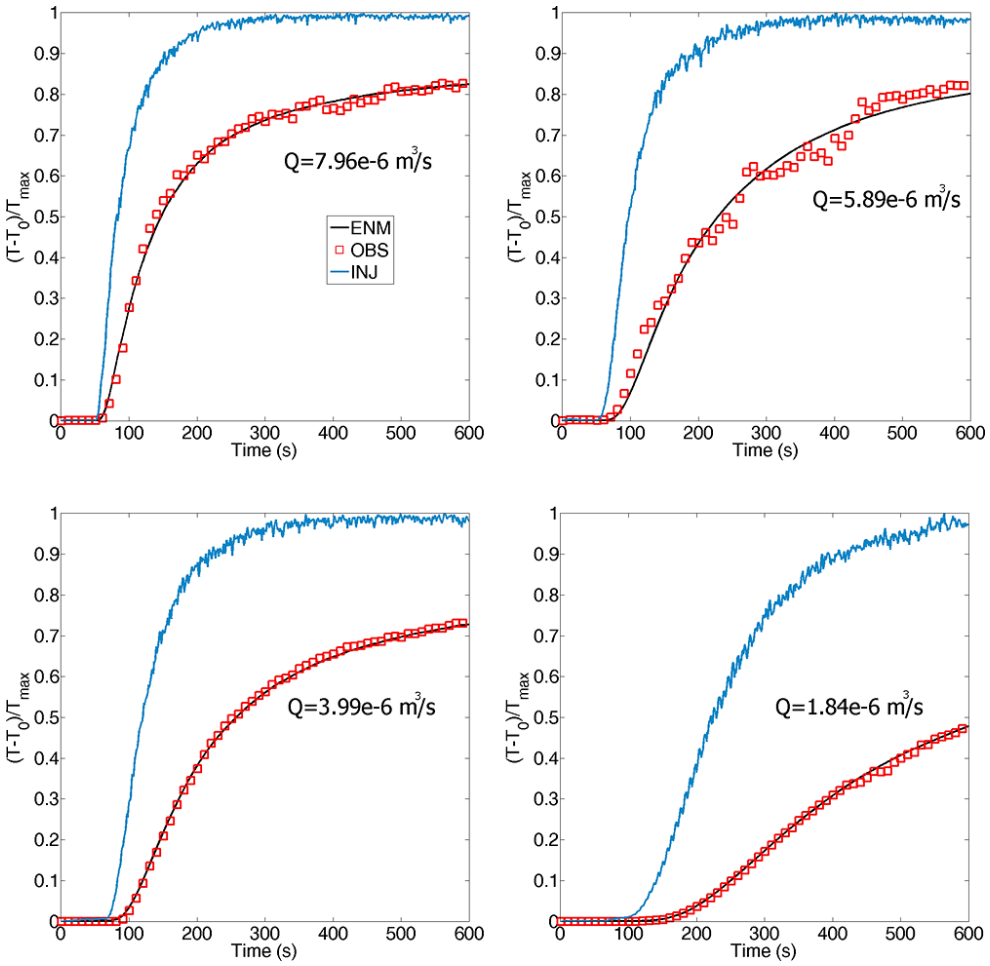


Figure 55 Fitting of BTCs at different injection flow rates using ENM with Tang's solution for heat transport.

Furthermore Figure 54 and Figure 55 show the fitting results of BTCs for some values of $Q_0$.

The estimated convective velocities $u_f$ for heat transport are lower than for mass transport. Whereas the estimated dispersion coefficients $D_f$ for heat transport are higher than for mass transport. Regarding the transfer rate coefficient $\alpha$, it assumes very low values for mass transport relatively to the convective velocity. Instead for heat transport the exchange rate coefficient is of the same order of magnitude of the convective velocity and, considering a characteristic length equal to $L = 0.601$ m, the effect of dual

porosity is very strong and cannot be neglected relatively to the investigated injection flow range.

Both mass and heat transport show a satisfactory fitting. In particular manner, *RMSE* varies in the range 0.0015 – 0.0180 for mass transport and in the range 0.0030 – 0.236 for heat transport, whereas $r^2$ varies in the range 0.9863 – 0.9987 for mass transport and in the range 0.0963 – 0.9998 for heat transport.

In order to investigate the different behavior between mass and heat transport, the relationships between injection flow rate and the transport parameters have been analyzed.

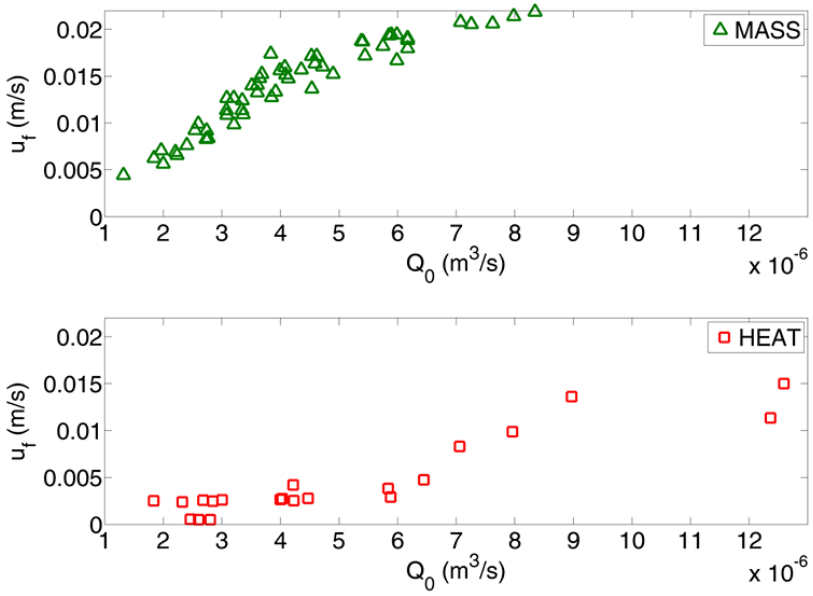


Figure 56 Velocity $u_f$ (m $s^{-1}$) as function of the injection flow rate $Q_0$ (m3$s^{-1}$) for ENM with Tang's solution for both mass and heat transport.

In Figure 56 the relationship between $u_f$ and $Q_0$ is reported. Whereas in figures 57 and 58 are reported the dispersion coefficient $D_f$ and the exchange term $\alpha$ as function of $u_f$. The figures show a very different behavior between mass and heat transport.

Regarding mass transport experiments according to previous studies (Cherubini at al., 2013 and 2014) the figure 5 shows that for values of $Q_0$ higher than $4\times10^{-6}$ $m^3s^{-1}$ $u_f$

increases less rapidly. This behavior was due to the presence of inertial forces that gave rise to a retardation effect on solute transport.

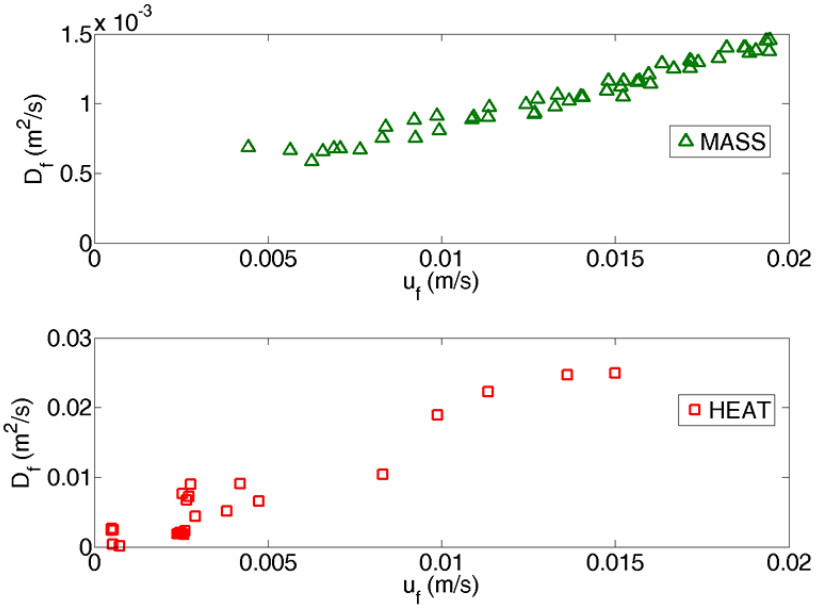


Figure 57 Dispersion Df (m $s^{-2}$) as function of velocity uf (m $s^{-1}$) for ENM with Tang's solution for both mass and heat transport.

Instead figure 57 shows a linear relationship between $u_f$ and $D_f$ suggesting that inertial forces didn't exert any effect on dispersion and that geometrical dispersion dominates the Aris – Taylor dispersion.

The estimated exchange rate coefficient $\alpha$ is much lower than the convective velocity. These results suggest that in the case study fracture – matrix exchange is very slow and it may not influence mass transport. Non Fickian behavior observed in the experimental BTCs is therefore dominated mainly by the presence of inertial forces and the parallel branches.

A very different behavior is observed for heat transport. Heat convective velocity does not seem to be influenced by the presence of the inertial force whereas $u_f$ is influenced by fracture matrix exchange phenomena resulting in a significant retardation effect.

In the same way as for mass transport, for heat transfer a linear relationship is evident between dispersion and convective velocity. Even if heat convective velocity is lower than solute advective velocity, the longitudinal thermal dispersivity assumes higher values than the longitudinal solute dispersivity. Also for heat transport experiments a linear relationship between $u_f$ and $D_f$ has been found.

Once the model parameters for each flow rate have been determined, the unit response function ($f_{URF}$), corresponding to the *PDF* obtained from impulsive injection of both solute and temperature tracers, is obtained. The unit response function can be characterized using the time moments and tail character analysis (Fig. 58).

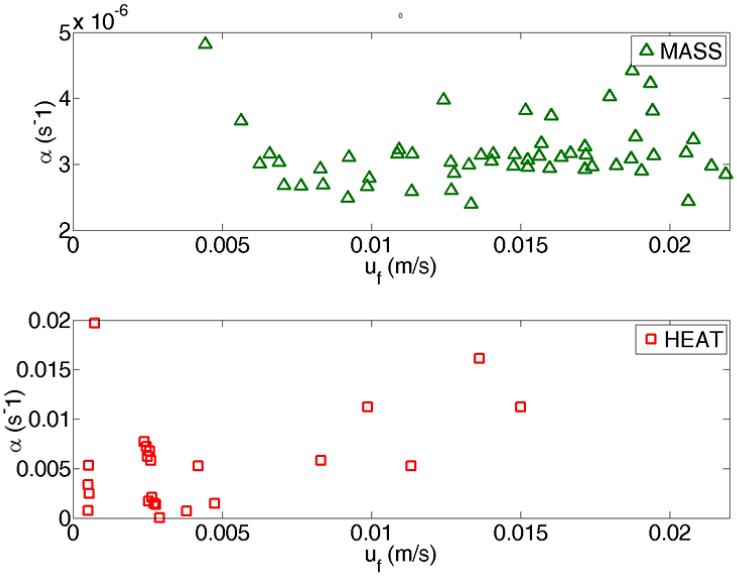


Figure 58 Transfer coefficient α ($s^{-1}$) as function of velocity $u_f$ ($ms^{-1}$) for both mass and heat transport.

The mean residence time $t_m$ assumes the following expression:

$$t_m = \frac{\int_0^\infty t f_{URF}(t)\,dt}{\int_0^\infty f_{URF}(t)\,dt} \qquad (103)$$

Whereas the n[th] normalized central moment of distribution of the $f_{URF}$ versus time can be written as:

$$\mu_n = \frac{\int_0^\infty \left(t - t_m\right)^n f_{URF}\left(t\right) dt}{\int_0^\infty f_{URF}\left(t\right) dt}$$

(104)

The second moment $\mu_2$ can be used in order to evaluate the dispersion relative to $t_m$, whereas the skewness is a measure of the degree of asymmetry and it is defined as follows:

$$S = \mu_3 / \mu_2^{3/2}$$

(105)

The tailing character $t_c$ can be described as:

$$t_c = \frac{\Delta t_{fall}}{\Delta t_{rise}}$$

(106)

Where $\Delta t_{fall}$ denotes the duration of the falling limb defined as the time interval from the peak to the tail cutoff which is the time when the falling limb first reaches a value that is 0.05 times the peak value. $\Delta t_{rise}$ is defined as the time interval from the first arrival to the peak. This quantity provides a measure of the asymmetry between the rising and falling limbs. A value of $t_c$ significantly higher than 1 indicates an elongated tail compared to the rising limb (Cherubini et al., 2010b).

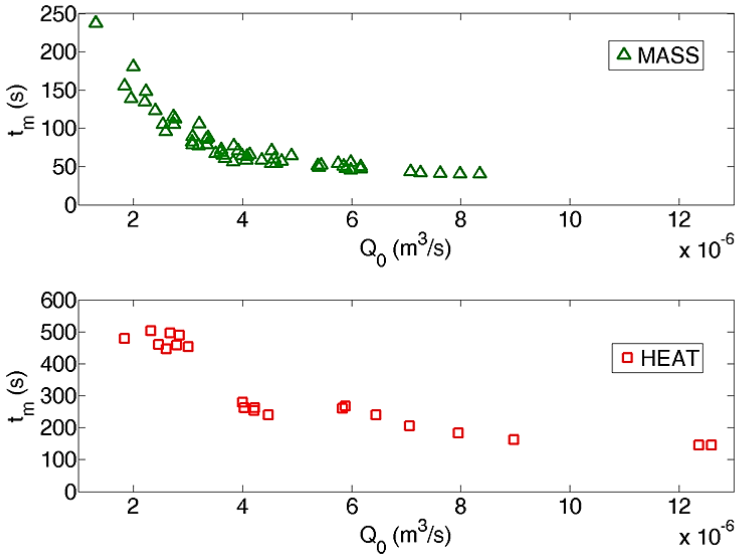


Figure 59 Mean travel time $t_m$ (s) as function of injection flow rate for both mass and heat transport.

In Figure 59 is reported the mean travel time versus the injection flow rates. The figure highlights that $t_m$ for heat transport is about 3 times higher than for mass transport. In particular way $t_m$ varies in the range 40. 3 - 237.1 *s* for mass transport and in the range 147.8 – 506.9 *s* for heat transport. This result still highlights that heat transport is more delayed than mass transport.

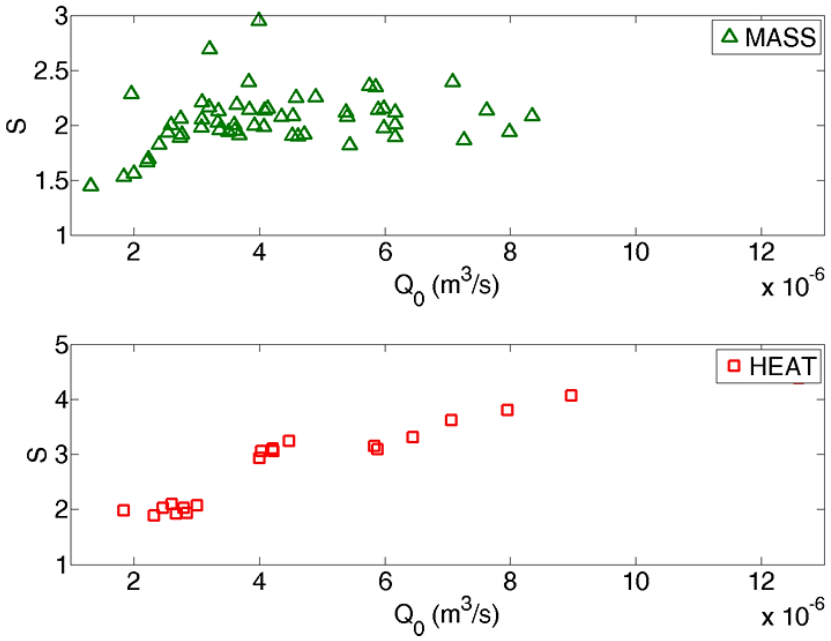


Figure 60 Skewness as function of injection flow rate for both mass and heat transport.

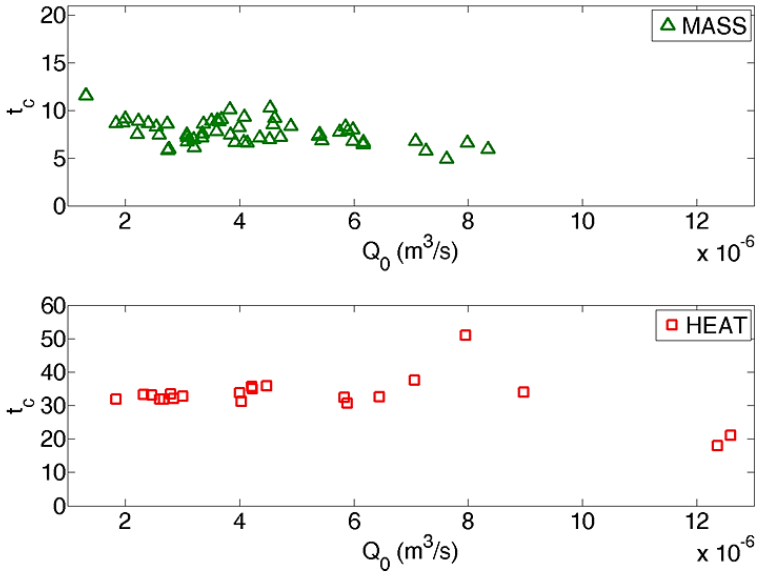


Figure 61 Tailing character tc as function of injection flow rate for both mass and heat transport.

In same way the skewness $S$ (Fig.60) and tailing character $t_c$ (Fig. 61) are reported as function of $Q_0$.

A different behavior for heat and mass transport is observed for the skewness coefficient. For heat transfer the skewness shows a growth trend which seems to decrease after $Q_0 = 3\times10^{-6}$ $m^3s^{-1}$. Its mean value is equal to 2.714. For solute transport the S does not show a trend, and assumes a mean value equal to 2.018.

The tailing character does not exhibit a trend for both mass and heat transport. In either cases $t_c$ is significantly higher than 1, specifically 7.70 and 30.99 for mass and heat transport respectively.

In order to explain the transport dynamics, the trends of dimensionless numbers $P_e$ and $D_a$ varying the injection flow rate have been investigated.

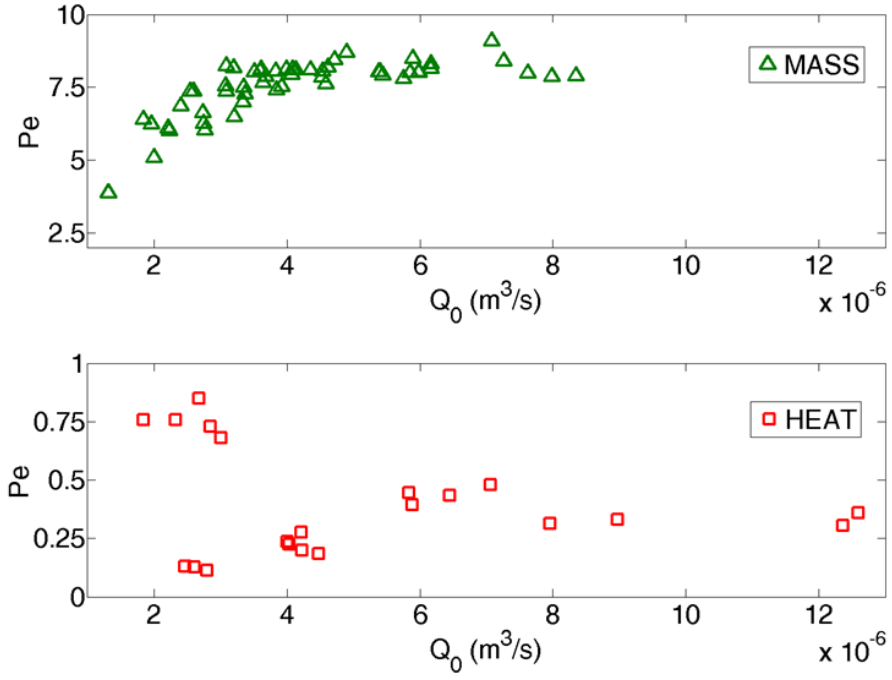


Figure 62 Peclet number as function of injection flow rate $Q_0$ ($m^3s^{-1}$) for both mass and heat transport.

The Figure 62 shows the $P_e$ as function of $Q_0$ for both mass and heat experiments. As concerns mass experiments $P_e$ increases as $Q_0$ increases, assuming a constant value for high values ($Pe = 7.5$) of $Q_0$. For heat transport a different behavior is observed, $P_e$ showing a constant trend and being always lower than one. Even if the injection flow rate is relatively high, thermal dispersion is the dominating mechanism in heat transfer.

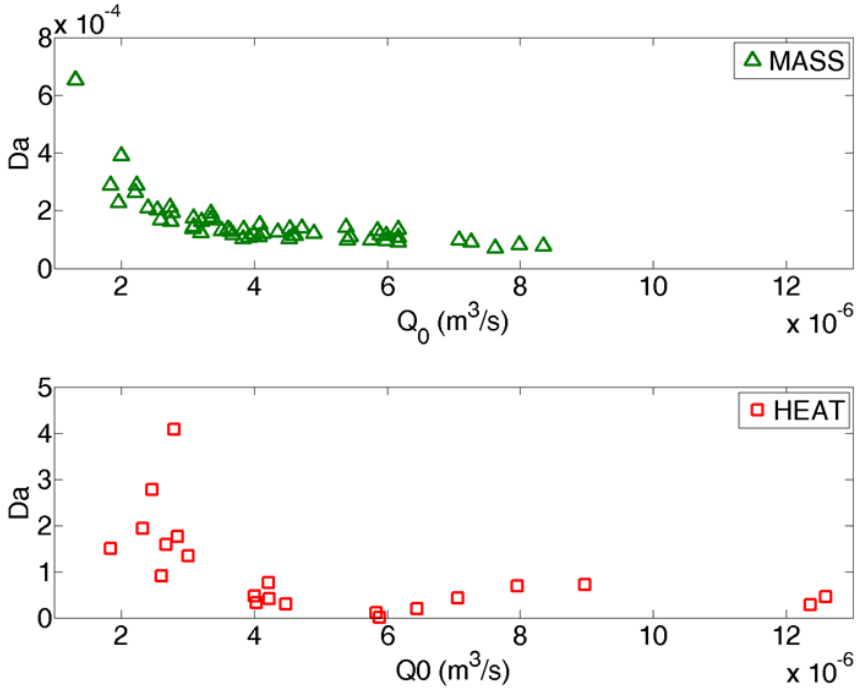


Figure 63 $D_a$ number as function of injection flow rate $Q_0$ ($m^3s^{-1}$) for both mass and heat transport.

Figure 63 reports $D_a$ as function of $Q_0$. For mass transport $D_a$ assumes very low values, of the order of magnitude of $10^{-4}$.

The convective transport scale is very low respect to the exchange transport scale, thus the mass transport in each single fracture can be represented with the classical advection dispersion model.

As regards heat transport $D_a$ assumes values around the unit showing a downward trend as injection flow rate increases switching from higher to lower values than the

unit. As injection flow rate increases the convective transport time scale reduces more rapidly than the exchange time scale.

These arguments can be explained because the relationships between $Q_0$ and $u_f$ show a change of slope when $D_a$ becomes lower than the unit. In other words when $D_a$ is higher than the unit the exchange between fracture and matrix dominates on the convective transport giving rise to a more enhanced delay on heat transport, conversely when $D_a$ is lower than one convective transport dominates on fracture- matrix interactions and the delay effect is reduced.

Furthermore this effect is evident also on the trend observed in the graph $S - Q_0$ (Figure 61). For values of $D_a$ lower than the unit a change of slope is evident, the skewness coefficient increases more slowly. Thus for $D_a > 1$ the early arrival and the tail effect of *BTC* increase more rapidly than for $D_a < 1$.

Note that even if $D_a$ presents a downward trend as $Q_0$ increases, when the latter exceeds $Q_{crit}$ a weak growth trend for $D_a$ is detected, that however assumes values lower than the unit.

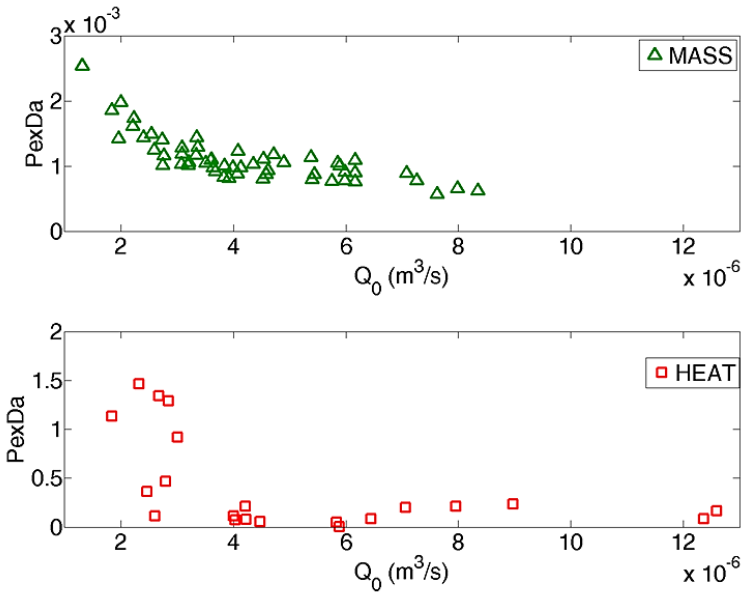


Figure 64. $P_e \times D_a$ number as function of injection flow rate $Q_0$ ($m^3s^{-1}$) for both mass and heat transport.

The Figure 64 shows the dimensionless group $Pe \times D_a$ varying the injection flow rate. Regarding mass transport $P_e \times D_a$ is of the order of magnitude of $10^{-3}$ confirming the fact that the fracture – matrix interaction can be neglected relatively to the investigated range of injection flow rates. For heat transport $P_e \times D_a$ assumes values just below the unit, with a downward trend as $Q_0$ increases. $t_d$ and $t_e$ have the same order of magnitude.

In order to find the optimal conditions for heat transfer in the analyzed fractured medium the thermal power exchanged per unit temperature difference $\dot{Q} / \left( T_{inj} - T_0 \right)$ ($ML^2T^{-1}K^{-1}$) for each injection flow rate in quasi steady state conditions can be estimated. The thermal power exchanged can be written as:

$$\dot{Q} = \rho C_p Q_0 \left( T_{inj} - T_{out} \right) \tag{107a}$$

The outlet temperature $T_{out}$ can be evaluated as function of the $f_{URF}$ using the following expression:

$$T_{out} = T_0 + \left( T_{inj} - T_0 \right) \int_0^\infty f_{URF} \left( t \right) dt \tag{107b}$$

Substituting the Equation (107a) in the Equation (107b) the thermal power exchanged per unit temperature difference is:

$$\frac{Q}{\left( T_{inj} - T_0 \right)} = \left( 1 - \int_0^\infty f_{URF} \left( t \right) dt \right) \rho C_p Q_0 \tag{108}$$

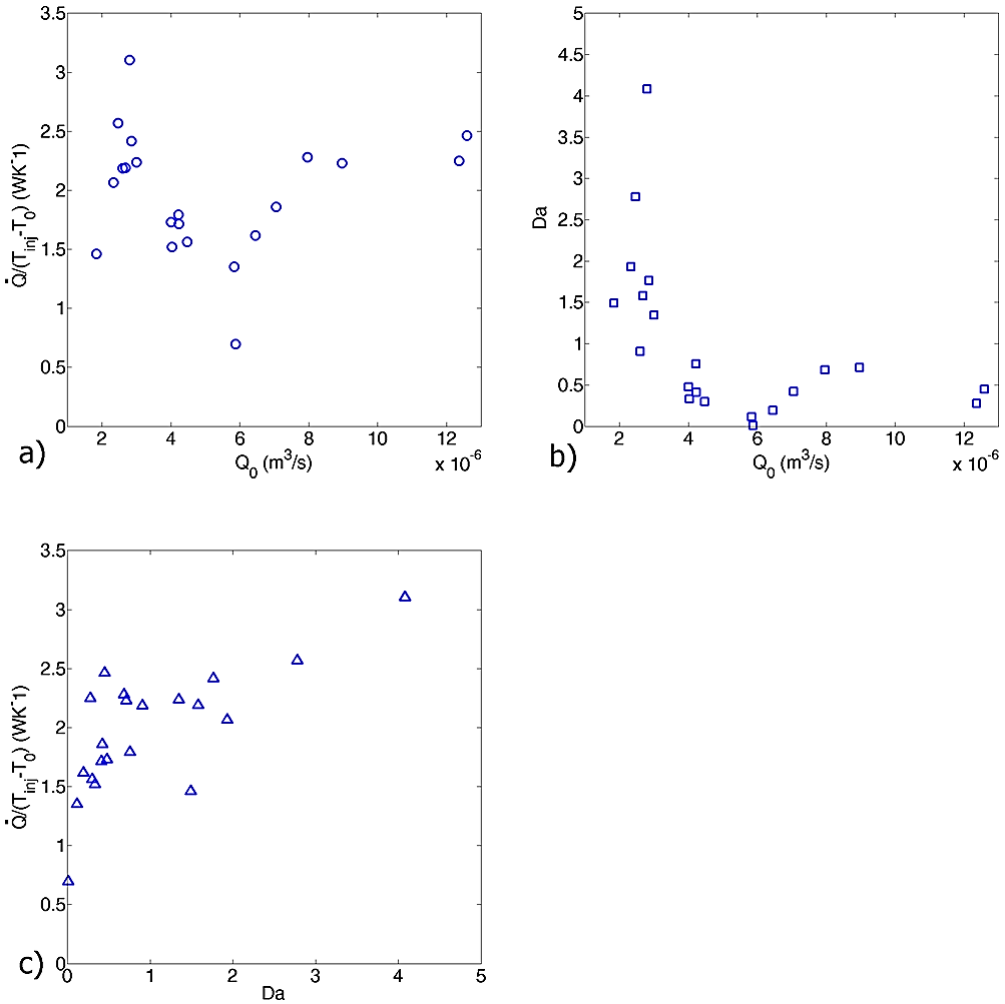


Figure 65 Heat power exchanged per difference temperature unit $\dot{Q}/(T_{inj}-T_0)$ as function of injection flow rate $Q_0$ ($m^3s^{-1}$) (a), Damköhler number *Da* as function of injection flow rate (b), power exchanged per difference temperature unit as function of Damköhler number (c).

Figure 65 shows the similarities between the relationship $\dot{Q}/\left(T_{inj}-T_0\right)$ - $Q_0$ (Figure 65 a) and $D_a$ – $Q_0$ (Figure 65 b). Higher $D_a$ values correspond to higher values of $\dot{Q}/\left(T_{inj}-T_0\right)$. The thermal power exchanged increases as the Damköhler number increases as shown in Figure 65c. These results highlight that for the observed case study the optimal condition for thermal exchange in the fractured medium is obtained

when the exchange time scale is lower than the convective transport scale or rather when the dynamics of fracture – matrix exchange are dominant on the convective ones. Moreover in a similar way to $D_a$, $\dot{Q}/\left(T_{inj}-T_0\right)$ shows a weak growth trend when $Q_0$ exceeds $Q_{crit}$. This means that the nonlinear flow regime improves the fracture – matrix thermal exchange, however at high values of injection flow rates convective and dispersion time scales are less than the exchange time scale. Nevertheless these results have been observed in a small range of $D_a$ numbers close to the unit. In order to generalize these results a larger range of $D_a$ numbers should be investigated.

In order to estimate the effective thermal conductivity coefficient $k_e$, the principle of conservation of heat energy can be applied to the whole fractured medium. Neglecting the heat stored in the fractures, the difference between the heat measured at the inlet and at the outlet must be equal to the heat diffused into the matrix:

$$\rho C_p Q_0 \left(T_{inj}-T_{out}\right)=\int_{A_f} k_e \left.\frac{dT_m}{dz}\right|_{z=wf/2} dA_f \tag{109}$$

where $A_f$ is the whole surface area of the whole active fracture network and the gradient of $T_m$ can be evaluated according to Equation (84). Then the average effective thermal conductivity $\overline{k_e}$ can be obtained as:

$$\overline{k_e}=\frac{\rho C_p Q_0 \left(T_{inj}-T_{out}\right)}{\int_{A_f} k_e \left.\frac{dT}{dz}\right|_{z=wf/2} dA_f} \tag{110}$$

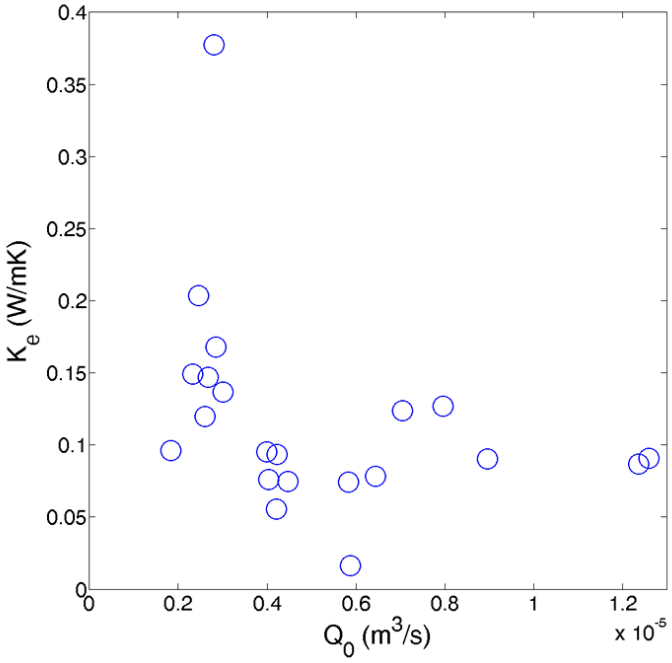


Figure 66 Effective thermal conductivity $k_e$ ($Wm^{-1}K^{-1}$) as function of injection flow rate $Q_0$ ($m^3s^{-1}$).

The average effective thermal conductivity has been estimated for each injection flow rate (Fig. 66) and assumes a mean value equal to $\overline{k}_e = 0.1183\ \mathrm{Wm^{-1}K^{-1}}$. The estimated $\overline{k}_e$ is one order of magnitude lower than the thermal conductivity coefficient reported in the literature (Robertson, 1988). Fractured media have a lower capacity for diffusion as opposed to the Tang's model which has unlimited capacity. There is a solid thermal resistance in the fluid to solid heat transfer processes, which depends on the rock – fracture size ratio.

This result is coherent with previous analyses on heat transfer carried out on the same rock sample (Pastore et al. 2015). In this study Pastore et al. (2015) found that the ENM model failed to model the behavior of heat transport in correspondence of parallel branches where the hypothesis of Tang's solution of single fracture embedded in a porous medium having unlimited capacity cannot be considered valid. In parallel

branches the observed BTCs are characterized by less retardation of heat propagation as opposed to the simulated BTCs.

### 2.3.23 Conclusions

Aquifers offer a possibility of exploiting geothermal energy by withdrawing the heat from groundwater by means of a heat pump and subsequently supplying the water back into the aquifer through an injection well. In order to optimize the efficiency of the heat transfer system and minimize the environmental impacts it is necessary to study the behavior of convective heat transport especially in fractured media, where flow and heat transport processes are not well known.

Laboratory experiments on the observation of mass and heat transport in a fractured rock sample have been carried out in order to analyse the contribution of thermal dispersion in heat propagation processes, the contribution of nonlinear flow dynamics on the enhancement of thermal matrix diffusion and finally the optimal heat recovery and heat dissipation strategies.

The parameters that control mass and heat transport have been estimated using the ENM model based on Tang's solution.

Heat transport shows a very different behavior compared to mass transport. The estimated transport parameters show differences of several orders of magnitude. Convective thermal velocity is lower than solute velocity, whereas thermal dispersion is higher than solute dispersion, mass transfer rate assumes a very low value suggesting that fracture – matrix mass exchange can be neglected. Non - Fickian behavior of observed solute BTCs is mainly due to the presence of the secondary path and nonlinear flow regime. Contrarily heat transfer rate is comparable with convective thermal velocity giving rise to a retardation effect on heat propagation in the fracture network.

The discrepancies detected in transport parameters are moreover observable through the time moment and tail character analysis which demonstrate that the dual porosity behavior is more evident in the thermal BTCs than in the solute BTCs.

The dimensionless analysis carried out on the transport parameters proves that as the injection flow rate increases thermal convection time scale decreases more rapidly than

the thermal exchange time scale, explaining the reason why the relationship $Q_0 - u_f$ shows a change of slope for $D_a$ lower than the unit.

Thermal dispersion dominates heat transport dynamics, the Peclet number and the product between Peclet number and Damköhler number is almost always less than the unit.

The optimal conditions for thermal exchange in a fracture network have been investigated. The power exchanged increases in a potential way as $D_a$ increases in the observed range.

The rock – fracture size ratio plays an important role in the fluid to solid heat transfer processes. It represents a key parameter in order to design devices for heat recovery and head dissipation that exploit the convective heat transport in fractured media. The estimation of the average effective thermal conductivity coefficient shows that it is not efficient to store thermal energy in rocks with high fracture density because the fractures are surrounded by a matrix with more limited capacity for diffusion giving rise to an increase in solid thermal resistance.

# *CHAPTER 4*
# *HEAT TRANSPORT IN FRACTURED MEDIA: EXPERIENCE ON SITE AT UNIVERSITY OF LA SALLE DE BEAUVAIS (FRANCE)*

## 2.4.0 Introduction and aims

Geothermal energy is one of the largest sources of renewable energies that are extracted from the earth. In the geothermal systems the fluid movement and thermal behavior in the fractured porous media is very important and critical. In particular way, low enthalpy geothermal resource is an optimal renewable resource because is always available and it is possible used for the heating and cooling of private buildings, industries, public buildings, representing the largest share of world energy consumption. Fractured rocks play an important role in transport of natural resources through subsurface systems. In recent years, interest has grown in investigating heat transport by means of tracer tests, driven by the important current development of geothermal applications. Existing theory of fluid flow and heat transport through porous media is of limited usefulness when applied to fractured rocks. Many field and laboratory tracer tests in fractured media show that fracture – matrix exchange is more significant for heat than mass tracers, thus thermal breakthrough curves (BTCs) are strongly controlled by matrix thermal diffusivity. In this study, the behaviour of heat transport in a fractured network, at bench laboratory scale, has been investigated. (N. Pastore, Cherubini, C. I. Giasi, N. M. Allegretti, J. M. Redondo, and M. Tarquis, “Experimental Study

of Heat Transport in Fractured Network," *Energy Procedia*, vol. 76, pp. 273–281, 2015).

The aim of this research study is to evaluate the fractured aquifers behavior towards heat. In particular, the first step is to assess, by making small changes in temperature in the system, how a fractured aquifer manages to retain or dissipate heat in a specified period. This information may be useful to understand the feasibility and the heat efficiency of a fractured system compared to a porous system. This would allow in the future, continuing the topic of studies, to avoid oversizing or undersized geothermal exchangers, and to assess, in advance, an engineering solution specifically for each type of aquifer.

### 2.4.1 Research activities at Institut Polytechnique LaSalle Beauvais

During the last two weeks of June, at the hydrogeological platform of Institut Polytechnique LaSalle Beauvais, the natural gradient tests were carried out, using hot water as a tracer.

Figure 67 *Experimental platform of Institut Polytechnique LaSalle Beauvais*

The city of Beauvais is in the Oise, about 80 km North of Paris, is bounded by the Mont of Saint-Adrien and the cities of Troissereux, Fouquenies, Goncourt, Therdonne and Tillé. Here the agricultural activities are critical and require a good management planning of water resources. It is located to the southeast of the country of Bray anticline where the series Cretaceous are flush. The Institut Polytechnique LaSalle Beauvais, located north of Beauvais, matches early Picardy plateau. This plateau is composed exclusively of a Senonian chalk white and tender, topped by flint clay, silt and flint plateau but with some silt mounds scattered Thanetian sands. The aquifer Beauvais (aquifer of the Upper Cretaceous) flows through a network of joints (Pomerol & FEUGUEUR, 1974) in the turo-Senonian chalk. It is based on clays Gault, impermeable formation, which is the bedrock of the hydrogeological chalk layer. (Translate by : Pascale Lutz, Lahcen Zouhri "hydrogeophysique sur le site experimental de lasalle beauvais : resultats et perspectives," 2014)

The study area is located in the city of Beauvais, the French department of Oise, (Figure 70a). It covers 33.31 $km^2$, is bounded by the Mont of Saint-Adrien and the cities of Troissereux, Fouquenies, Goncourt, Therdonne and Tillé. The area is drained by several rivers taking place in the Thérain valley (Fig. 68b), the most important one being the Oise river (L. Zouhri, 2009). The water is used to provide drinking water for the city of Beauvais and its suburbs mainly Troissereux and Fouquenies (about 60000 $m^3$/day), for irrigation in valley and for industry purpose. Indeed, the increasing demand of groundwater supply is explained by the development of agricultural activity and the growth of the population. Therefore, land use is primarily agricultural (60%), forest-prairies (36%), industrial and urban use (4%). The morphology of the study area varies between 57 m and 170 m with an average elevation of 100 m a.s.l (Figure 68b). The region receives an annual precipitation ranging between 600 - 800 mm/year and the annual average temperature ranges between 8°C and 15°C. Runoff is taking place by rivers with permanent flow and a general flow is observed to the south, more locally to the Oise river valley, the main drainage valley (L. Zouhri and P. Lutz, 2010).

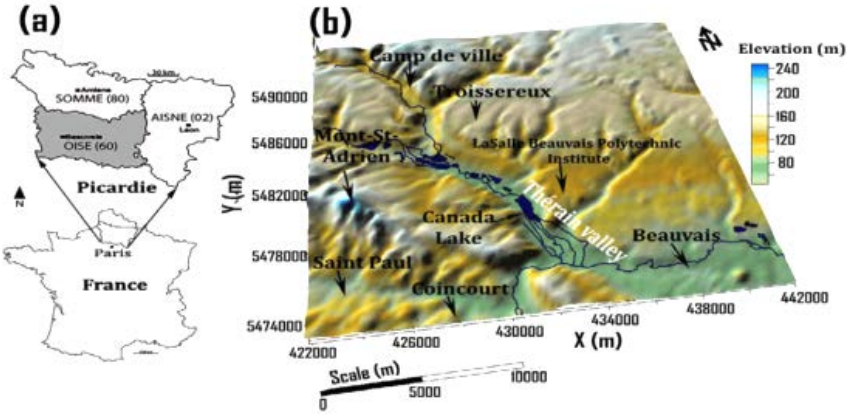


Figure 68 Map location (a) of Oise department and (b) topographic framework of Beauvais.

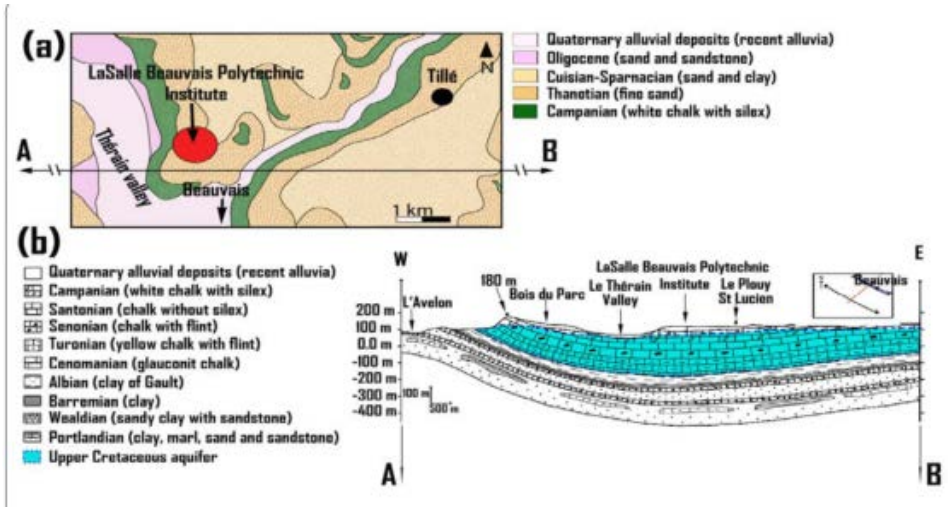


Figure 69 (a) Geological map and (b) simplified geological cross-section (A-B) through the chalk aquifer of Beauvais (N France) BRGM (2008) Carte géologique à différentes échelles de la ville de Beauvais.

### 2.4.2 Hydraulic parameters

The hydraulic conductivity considered in the regional conceptual model are mapped in Figure 70. The value of these parameters originate from several data investigation campaigns performed at the regional scale, involving borehole testing, pumping tests, laboratory test of the core plugs and geophysical methods .

In addition, the hydraulic conductivity range between $5 \times 10^{-4}$ and $5 \times 10^{-5}$.

m/s (Figure 70).

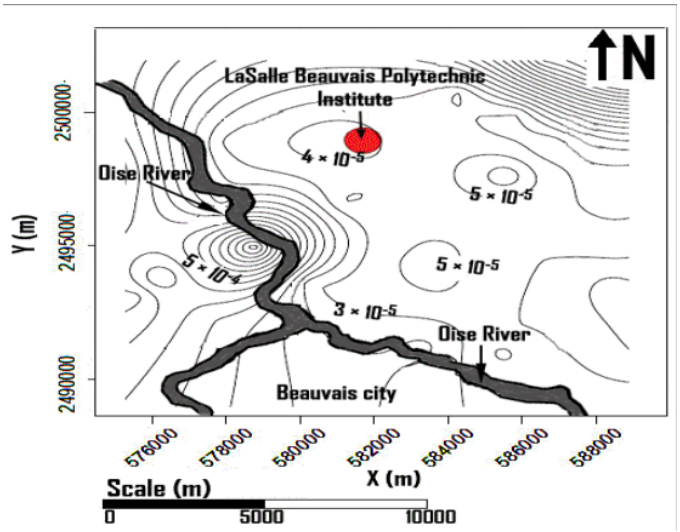


Figure 70 Hydraulic conductivity distribution of the chalk aquifer of Beauvais.

The higher values of hydraulic conductivity reaching $2 \times 10^{-4}$ m/s are found around the Oise river and surrounding the lakes of the Thérain valley. These higher hydraulic conductivity values are due to the development of solution-enhanced fractures in the chalk. The hydraulic transmissivity range between $10^{-3}$ and $10^{-2}$ $m^2$ /s and the specific storage varies between 0.01 and 0.63 l/s.

A hydraulic conductivity value was assigned to each model cell to represent the heterogeneous nature of the materials in the model layer. Within each model cell, the horizontal hydraulic conductivity (Kx) was assumed to be homogeneous.

The vertical hydraulic conductivity values were established by a variable anisotropy ratio Kx/Kz ranging between 3 and 13.

### 2.4.3 Natural gradient test

The tests have been divided into two main phases:

1) Hydrogeological knowledge site

2) Natural gradient tests

During the first phase (Hydrogeological knowledge site) the level of the water table have been measured by a phreatimeters.

Figure 71 Well where the measurements were carried out on experimental platform at the University La Salle de Beauvais.

Stages of natural gradient test:

1) Recovery of the materials for the test:
   - Nr. 2 clean containers of 20 liters each;
   - Nr. 2 long thermocouples 100 meters each;
   - Nr. 1 datalogger;
   - Nr. 1 personal computer.

Figure 72 Equipment with which the test was carried out

2) Placement of the fixture on the field:

Thermocouples have been placed in the well and are subsequently connected to the data logger, who in turn was connected to the personal computer.

Figure 73 Natural gradient test

3) Natural gradient test

Two clean plastic containers were filled with drinking water at a temperature around 42°C.

The hot water has been inserted within the selected well, timing the injection time to calculate the flow rate. The thermal BTCs were obtained. In particular, two wells to make the tests were chosen.

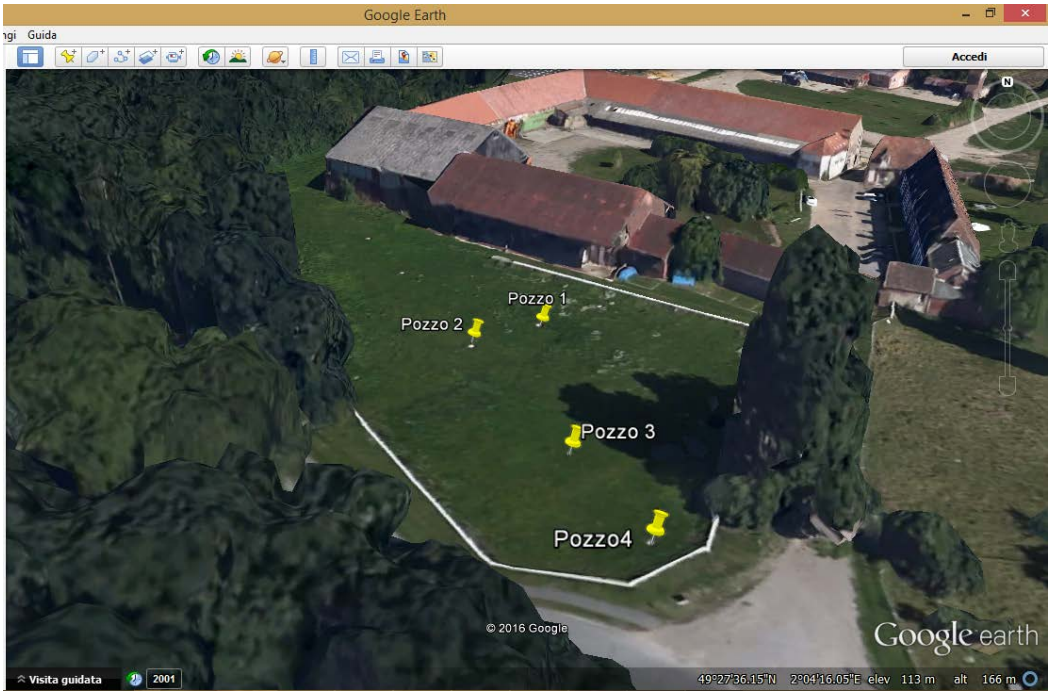


Figure 74 Experimental platform at the University La Salle de Beauvais

Curves obtained from the well nr. 1:

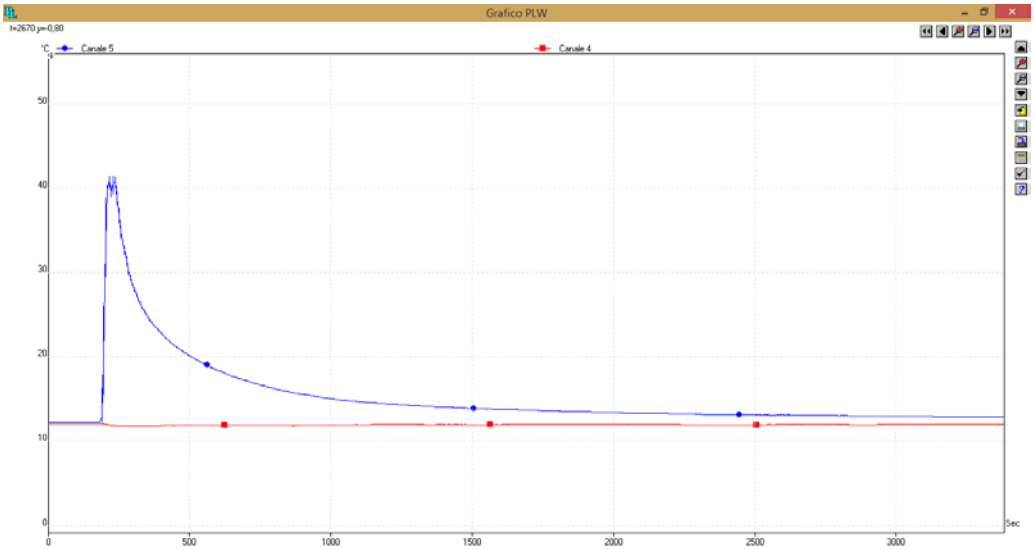


Figure 75 Thermal BTC (thermal breakthrough curve) nr.1, well nr.1

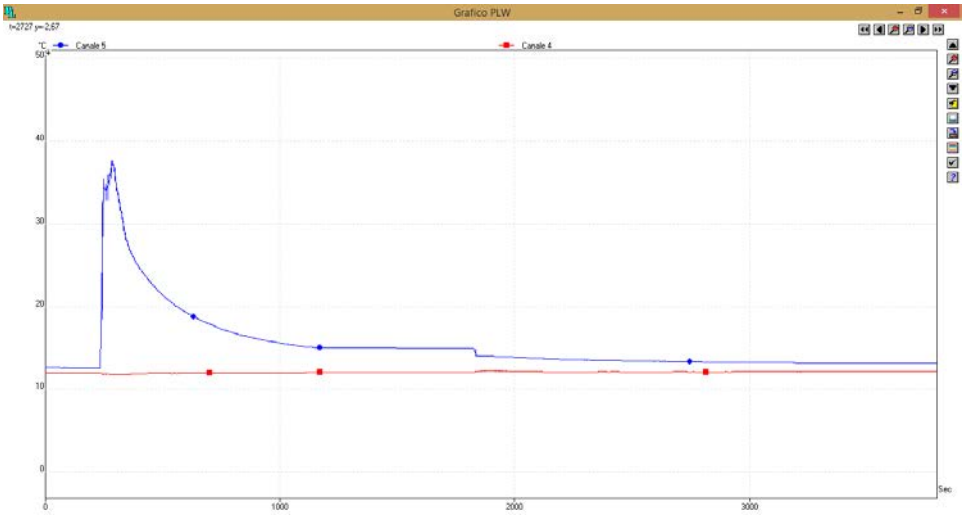


Figure 76 Thermal BTC (thermal breakthrough curve) nr.1, well nr. *1*

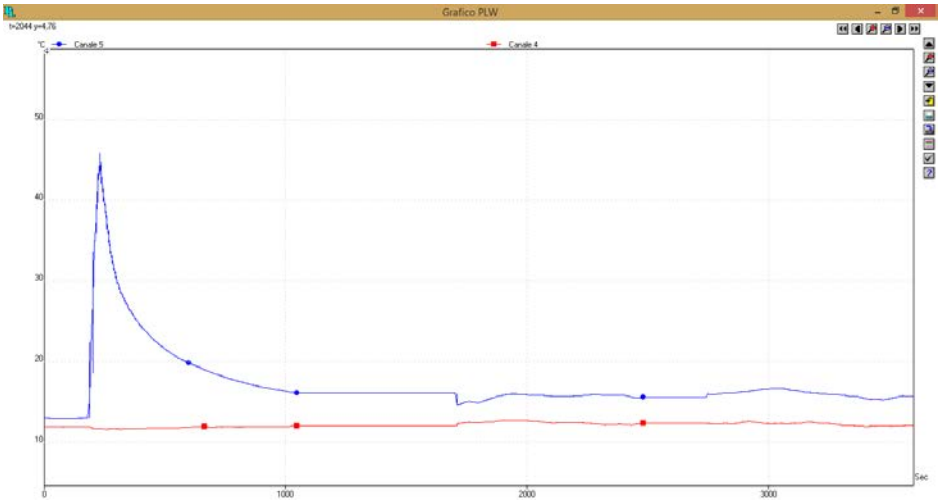


Figure 77 BTC (thermal breakthrough curve) nr.3, well nr. 1

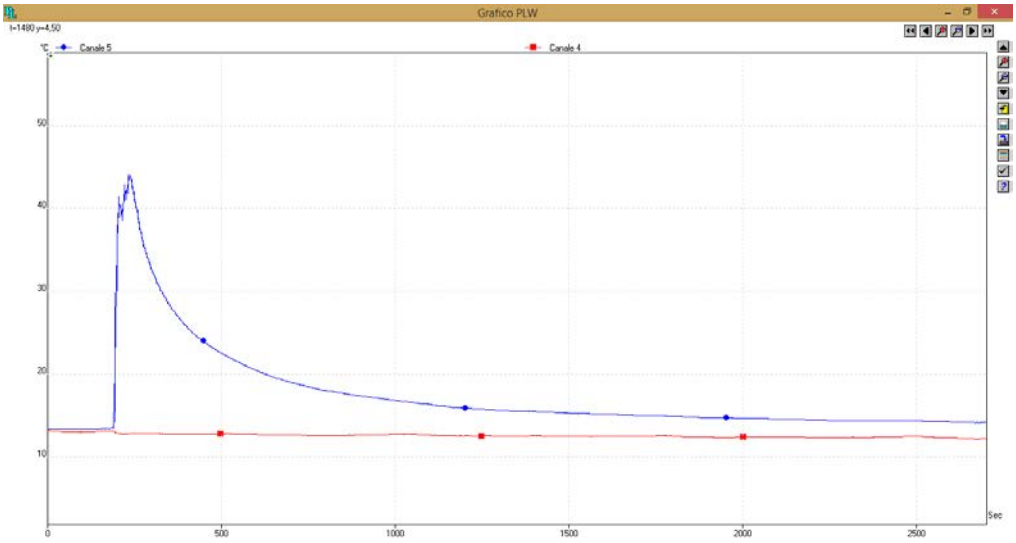


Figure 78 Thermal BTC (thermal breakthrough curve) nr.4, well nr. 1

Curves obtained from the well Nr. 2:

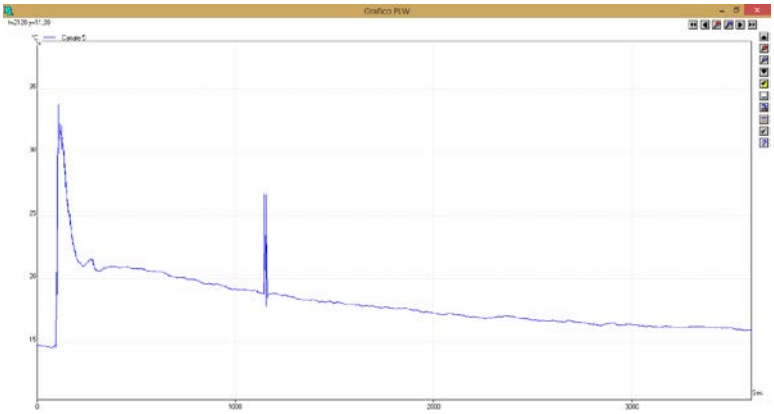

Figure 79 BTC (thermal breakthrough curve) nr.1, well nr. 2

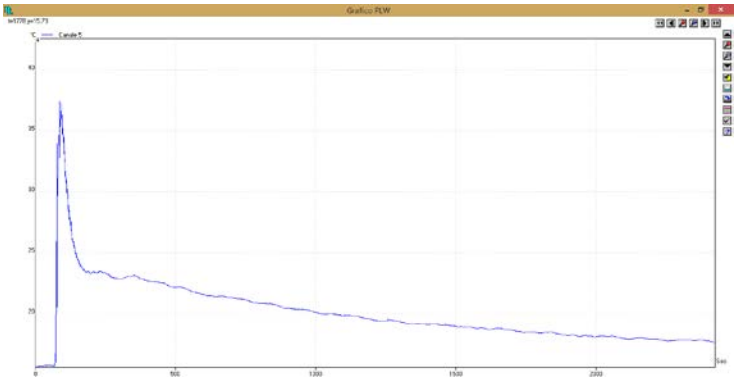

Figure 80 BTC (thermal breakthrough curve) nr.2, well nr. 2

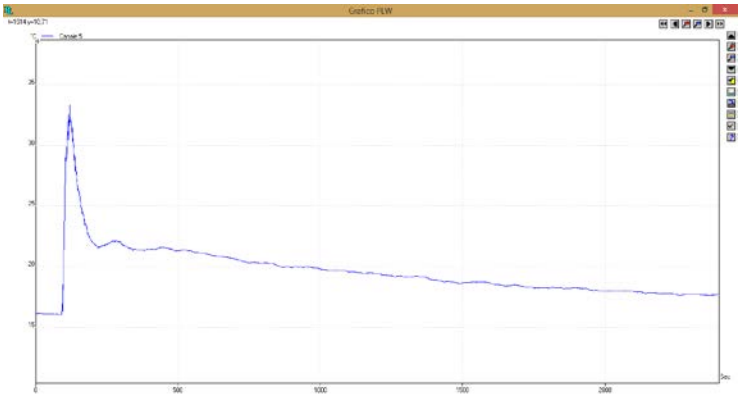

Figure 81 BTC (thermal breakthrough curve) nr.3, well nr. 2

The thermal BTCs are characterized by a more enhanced early arrival and long tailing, and have a very smiley trends than those observed during laboratory tests on fractured limestone.

### 2.4.4 Conclusions

The aim has been to compare the results obtained in the laboratory with those obtained in site. It 'was therefore carried out in punctual gradient tests that already has demonstrated behaviour consistent with that obtained in the laboratory with regard to the fractured. Have to do other tests such as push and pull to deepen the knowledge on heat transport in fractured.

# *CHAPTER 5*
# *ANALYSIS OF DYNAMICS OF HEAT TRANSPORT IN POROUS MEDIA*

## 2.5.0 LITERATURE REVIEW

The study of heat transport in porous media has received widespread attention in recent years due its important applications in fields such as in petroleum engineering, and geothermal systems, drying, insulation technology, nuclear waste disposal and in the control of pollutant spread in ground water.

Low enthalpy geothermal resources are underdeveloped with regard to their potentiality worldwide. One of the biggest limits on the development of low-enthalpy geothermal systems concerns the economic aspect. In fact, the initial investment costs often exceed the expectations of depreciation expense, so the investment is therefore inconvenient and the economic benefits can only occur after a long time. One solution could be to investigate more about the behaviour of hydrological systems in the presence of heat. This study is aimed at studying the dynamics of heat transfer in porous media allowing the understanding of the real performance of low-enthalpy geothermal installations. In particular, the present study involves the experimental investigation of heat transport through a thermally isolated column filled with porous medium. Several tests have been carried out, using porous media with different grain sizes.

Studying heat transfer phenomena takes the advantage of the fact that the governing partial differential equations used to describe flow and transport processes in porous media are based on the same form of mass and/or energy conservation laws.

Several studies have been already carried out in this context with the aim of enhancing heat transfer phenomena in porous media for engineering processes. Theoretical and numerical research on convection heat transfer in porous media has used two different models for the energy equation: the local thermal equilibrium model and the local thermal non-equilibrium model.

Most of the studies have been focussed on investigating on the validity of the local thermal equilibrium assumption (LTE) between the solid and fluid phase, the influence of nonlinear flow patterns, and the existing relationship between thermal dispersion and flow velocity.

Koh and colony (1974) and Koh and Stevens (1975) studied forced convection in a porous channel filled with a high conductivity porous material by using the Darcy flow model. They reported that the wall temperature and the wall-to-coolant temperature difference decrease drastically in the channel with a constant heat flux.

Vafai and Tien (1981) have formulated a general mathematical model that takes into consideration the boundary and inertial (non Darcian) effects on flow and heat transfer in porous media. In analyzing these effects, they considered three flow resistances: the bulk damping resistance due to the porous structure, the viscous resistance due to the boundary, and the resistance due to the inertial forces.

Later, Vafai and Tien (1982) investigated the boundary and inertial effects on convective mass transfer in porous media. Kaviany (1985) studied the flow through a constant porosity medium bounded by isothermal parallel plates using the Brinkman-extended flow model and constant matrix porosity. Vafai and Kim (1989) used the Brinkman-Forchheimer-extended Darcy model to obtain a closed-form analytical solution for completely generated flow in a porous channel, subject to constant heat flux boundary conditions. Lauriat and Vafai (1991) presented a comprehensive study of forced convective heat transfer in porous media through a channel or over a flat plate.

Hadim (1994) performed a numerical study to analyse steady forced convection in a channel filled or partially filled with a porous medium and containing discrete heat sources. He modelled the flow in the porous medium using the Brinkman-Forchheimer extended Darcy model. Kamuto and Saitoh (1994) examined numerically the fully developed forced convection heat transfer in cylindrical packed beds with constant wall temperatures based on a two-dimensional model incorporating the effects of non-Darcy, variable porosity and radial thermal dispersion. [194, 195] Hwang et al. (1994, 1995) found that the value of the heat transfer coefficient between the solid and the fluid phases might affect seriously the estimation of the heat transfer performance in a high conductivity porous channel.

A review of literature indicates that the local thermal equilibrium assumption (LTE) between the solid and fluid phase is used in the majority of heat transfer applications involving porous media (Mikowycz et al., 1999). An in-depth analysis of non-thermal equilibrium is provided by [197, 198] Amiri & Vafai (1994, 1998).

Amiri &Vafai (1994) carried out a steady-state analysis of incompressible flow through a bed of uniform solid sphere particles packed randomly. The investigation was aimed at exploring the influence of a variety of phenomena such as the inertial effects, boundary effects, and the effect of the porosity variation model together with the thermal dispersion effect on the momentum and energy transport in a confined porous bed. They also proved the validity of LTE assumption the two-dimensionality effects on transport processes in porous media.

In a subsequent study, Amiri &Vafai (1998) realised a rigorous and flexible model to explore the heat transfer aspects in a packed bed made of randomly oriented spherical particles. Along with the generalized momentum equatio they used a two-energy equation model to describe the thermal response of a packed bed. They explored the temporal impact of the non Darcian terms and the thermal dispersion effects on energy transport. In addition, they investigated on the LTE condition and the one dimensional approach under transient condition by formulating dimensionless variables that will serve as instruments in depicting the pertinent characteristics of energy transport in a packed bed.

Wu and Hwang (1998) investigated experimentally and theoretically flow and heat transfer dynamics inside an artificial porous matrix by using a modified version of the local thermal nonequilibrium model (LTNE) which neglected the effects of thermal dispersion in both fluid and solid. The results showed a highly non-Fourier behaviour which combined rapid thermal breakthrough with extremely long-tailing, that was attributed to disequilibrium between the fluid and the porous matrix. However, the adopted model was unable to fully capture the thermal breakthrough observed in some experimental runs. Their results show that the heat transfer coefficient increases with the decrease in porosity and the increase in the particle Reynolds number.

Khalil et al. (2000) presented a numerical investigation of forced convection heat transfer through a packed pipe with constant heat flux showing the effects of particle Reynolds number, pipe-to-particle diameter ratios and Prandtl number.

Emmanuel and Berkowitz (2007) were able to successfully fit the thermal breakthrough curves obtained by Wu and Hwang (1998) by applying the continuous time random walk (CTRW) which provided an alternative description of heat transport in porous media. They argued that larger scale spatial heterogeneities in porous media present obstacles to both the equilibrium and the LTNE models and that CTRW would be particularly applicable to the quantification of heat transfer in naturally heterogeneous geological systems, such as soils and geothermal reservoirs.

Geological media are typically characterized by heterogeneities on many scales, resulting in a wide range of fluid velocities, porosities, and effective thermal conductivities.

Heterogeneity in geologic media is the principal responsible of thermal dispersion, which takes place as a result of the no uniformity of the pore level temperature and velocity, and the effects of hydrodynamic mixing on the temperature field [202] (Özgümüş et al., 2013)

Several studies addressed the effects of thermal dispersion in porous media and different approaches have been developed to describe it (Hsu and Cheng, 1990; Anderson, 2005; Molina-Giraldo et al.,2011).

Thermal dispersion is generally defined as a function of fluid velocity and grain size (Lu et al., 2009, Sauty et al., 1982, Nield and Bejan, 2006).

Sauty et al.(1982) described the thermal dispersion as a linear function of velocity.
Recently, Rau et al. (2012) suggested a dispersion model as a function of the square of the thermal front velocity.
The literature also contains conflicting theories about the magnitude of thermal dispersivity. Smith and Chapman (1983) assert that thermal dispersion has the same order of magnitude as solute dispersivities, while Ingebritsen and Sanford (1999) ignore it. Vandenbohede et al. (2009) suggested that thermal dispersivities are less scale-dependent and are small in comparison to solute dispersivity values.
Experimental results from Mori et al. (2005) showed that thermal dispersion effects were insignificant and independent of water fluxes ranging between $0.6\times10^{-6}$ and $0.3\times10^{-3}$ [m/s].
Metzger et al. (2004) introduced a dispersion model based on the thermal Peclet number.
Rau et al. (2012) found that the effect of thermal dispersion on heat transport is significant when the Peclet number, the ratio of conduction to convection, is relatively large.
Koch et al. (1989) obtained an analytical expression for the dispersion tensor for a regular arrangement of cylinders or spheres. They found that for high values of Peclet numbers, the ratio of longitudinal total thermal diffusivity to the fluid thermal diffusivity was proportional to the square of the Peclet number while maintaining the transverse dispersion constant. The analytic finding was in good concordance with the experimental measurements of Gunn and Pryce (1969).
Eidsath et al. (1983) quantified the longitudinal thermal dispersion and stressed that the stream wise ratio of longitudinal total thermal diffusivity to the fluid thermal diffusivity was proportional to Pe1.7.
Ait Saada et al (2006) investigated the behavior of microscopic inertia and thermal dispersion in a porous medium with a periodic structure by using a local approach at the pore scale to evaluate the velocity and temperature fields as well as their intrinsic velocity and temperature fluctuations in a typical unit cell of the porous medium under study. They concluded that non-linear effects characterizing the microscopic inertia

might be the definitive cause of thermal dispersion depending on the nature of the porous medium and in certain situations can exceed 50% toward the contribution of thermal dispersion. Particularly for a highly conducting fluid moving with high Peclet numbers, microscopic inertial effects showed to take a great part in the heat transfer duty. They concluded that a considerable interaction between the velocity and thermal fields exists.

Traditionally, the empirical Darcy's law has been applied for flows through porous media when the Reynolds number based on the pore size (or particle diameter, *d*p*)* is very small. Under this circumstance, the momentum equation for fluid flows passing through an isotropic media is described by

$$-\nabla P = \frac{\mu \mathbf{U}}{k} \tag{111}$$

where $P$ is the pore pressure, $\mu$ the fluid viscosity, and U the Darcy velocity. Here, Darcy velocity is taken as a superficial velocity by regarding the media as a continuum and ignoring the details of porous structures. In Eq. (112), the permeability, $k$, takes the well-known form of

$$K = \frac{\varphi^3 d^2{}_p}{a(1-\varphi)^2} \tag{112}$$

where $\varphi$ is the porosity of porous media and $a$ is a constant to parameterize the microscopic geometry of the porous materials.

More lately, engineering practices require the operation of flows in porous media at high Reynolds number, such as those in packed-bed reactors. Experimental evidences showed that Eq.(112) was unable to describe the flows at high Reynolds number. By fitting to experimental data, a nonlinear term was added to Eq.(112) to correct for the advection inertia effect (Forchheimer ). Thus, Eq.(112) was modified empirically into

$$-\nabla P = \frac{\mu U}{K} + \frac{F_p \,|U|\, U}{\sqrt{K}} \tag{113}$$

where $\rho$ is the fluid density. According to Ergun, the Forchheimer coefficient $F$ is given by $F = b/\sqrt{a}\varphi 3$ where $b$ is again a constant to parameterize the microscopic geometry of the media. Although Eq. (111) had been used by researchers with some success in predicting flows in porous media, Hsu and Cheng showed theoretically that in addition to the two terms on the right-hand side of Eq.(113), there is a need to include a term proportional to $|U|^{1/2}U$, to account for the viscous boundary layer effect at the intermediate
Reynolds number. As a result, Eq. (113) was then modified into:

$$-\nabla P = \frac{\mu U}{k} + \frac{H\sqrt{\rho\mu\,|U|}U}{k^{3/4}} + \frac{F_p\,|U|}{k^{1/2}} \tag{114}$$

where the dimensionless coefficient $H$, like $F$, is a function of porosity and microscopic solid geometry. Equation (114) was confirmed by Hsu et al. who performed experiments for flows through porous media over a wide range from low to high Reynolds numbers.
Equation (114) was constructed based on the experiments and theory for steady flows. Therefore, Eq. (114) is anticipated to apply only for steady flows over all range of Reynolds number. Unsteady flows in porous media have recently received great attention.

One example is the oscillating flow in the regenerators used in Stirling engines and catalytic converters. Others are the transient processes in the start-up and shutdown of a capillary heat pipe in mechanical engineering, and the well-bore pumping in hydraulic and petroleum engineering. Because of the lack of adequate equations to describe the unsteady flows in porous media, Eq.(113) sometimes was used indiscriminately without justification. For coastal engineers to study the ocean waves acting on sand sea beds or porous breakwaters, the common practice is to incorporate into Eq.(111) the terms corresponding to transient inertia and viscous diffusion (Liu et al.), based on the classical works of Biot and Dagan .The resultant equations had neglected the virtual mass and viscous-diffusion memory effects and are expected to be valid only for low Reynolds number flows of waves at long period. There remains the task to construct a model for unsteady flows through porous media, which to the first-order approximation is valid over the entire ranges of time scale and Reynolds number.

In recent years, considerable interest has been given to the study of heat transfer through porous media because of its wide applications in many fields like crude oil extractions, petroleum reservoirs, agricultural engineering, coal combustors, solar collectors, electronic cooling, energy storage units and nuclear waste repositories (Singh, 2015). Since Darcy's pioneering experimental study of porous medium flow, a great number of analytical, numerical, and experimental works have been carried out to provide qualitatively and quantitatively macroscopic descriptions of the overall viscous resistance or heat transfer across the porous media.

For the subject of flow and heat transfer through porous media, there have been extensive investigations covering broad ranges of applications since the early work of Darcy in the nineteenth century. Darcy correlated the pressure drop and flow velocity experimentally by defining a special constant property of the medium called permeability. However, it is only applicable to low speed (creeping) flow and low porosity saturated medium. It is well known that in flow through porous media the pressure drop caused by the frictional drag is proportional to the velocity at the low Reynolds number range. In addition, this famous Darcy's law also neglects the effects of solid boundary and the inertial forces on fluid flow and heat transfer. Fluid transport is usually modeled using

the continuum approach in terms of appropriate averaged parameters in which the real pore structure and the associated length scales are neglected. Moreover, those averaged parameters can only be obtained by experiments and are strongly influenced by the types of microstructure and operating conditions. Fundamentally, they are limited to the scope of macroscopic phenomena. Specifically, the microscopic (pore scale) dispersion effect has significant impacts on the mass, momentum, and thermal transports. Hence, modeling transport behavior at the pore-scale for real engineering processes is desirable. In this study, an alternative numerical approach is proposed and used for microscopic transport in porous media.

The study of heat transfer phenomena in the subsurface is also relevant for geothermal energy extraction.

Mass and thermal transport in porous media, such as ceramics, rocks, soils and catalytic channels in fuel cells, play an important role in many engineering and geological processes. There are two interesting aspects that arise in the research of porous media. They are hydrodynamic and thermal effects. The dynamics of fluids flow through a porous medium is a relatively old topic. Since the nineteenth century, Darcy's law has traditionally been used to obtain quantitative information on flow in porous medium. This law is reliable when the representative Reynolds number is low whereas the viscous and pressure forces are dominant. As the Reynolds number increases, deviation from Darcy's law grows due to the contribution of inertial terms to the momentum balance [Bear, 1972; Kaviany, 1991]. Following a continuum approach, Hassanizadeh and Gray (1980) developed a set of equations to describe the macroscopic behaviour of fluid flow through porous media. It is shown that for all investigated media, the axial pressure drop is represented by the sum of two terms, one being linear in the velocity (viscous contribution) and the other being quadratic in velocity (inertial contributions). The inertial contribution is known as Forchheimer's modification of the Darcy's law [Reynolds, 1900].

Basically, the pressure drop occurring in a porous medium is composed of two terms. Later Beavers and Sparrow [1969] proposed a similar model for fibrous porous media.

A general expression can be obtained from Bear [1972] and is widely accepted in the following formula,

$$\frac{dp}{dx} = -\frac{\mu u}{k} \tag{115}$$

It is seen that the pressure drop is directly proportional to the fluid viscosity μ and inversely proportional to the permeability of the porous medium. Lage et al. [1997] suggested that an additional cubic term of fluid velocity be included in the above equation in the regime of higher speed. Another significant work for predicting momentum transport in porous media is by Brinkman [1947]. Brinkman first introduced a term which superimposed the bulk and boundary effects together for flows with bounding walls. In Brinkman's model, an effective viscosity was postulated from experiments performed on beds of spheres to replace the viscosity of fluid by taking into account of the porosity effect,

$$\mu_{eff} = \mu[1 + 2.5(1 - \varepsilon)] \tag{116}$$

where ε is the porosity.

The following sections include discussions of these subjects: validation tests, numerical setup for studying the pressure drop with respect to pore structure, and numerical results reporting the fluid's hydrodynamic behaviors in porous media.

Table 16 Summary of some works in evaluating viscous resistance (pressure drop) in porous media

| Assumption | References | Formulation and Method | Major results |
|---|---|---|---|
| Periodic porous media, low Reynolds number flow | Larson & Higdon, 1992 | Solving Stokes flow with a periodic grain consolidation model, collocation method used | Excellent accuracy, moderate computational effort |
| Incompressible, low Reynolds number flow | Verberg & Ladd, 1999 | Solving Stokes flow, Lattice-Boltzmann method used | Study of the convergence of the permeability as a function of grid resolution for random arrays of spheres - a second order approach. |
| Periodic porous media, low Reynolds number flow | Chapman & Higdon, 1992 | Solving unsteady Stokes equations, oscillatory pressure gradient imposed | A study in the dynamic permeability and acoustic propagation in porous medium |
| Incompressible, low Reynolds number flow | Martys & Hagedorn, 2002 | Solving Brinkman equation for Stokes flow, Lattice-Boltzmann method used | Evaluating permeability in multiple pore size material - low porosity, using parallel computing technique |
| Incompressible, Low Reynolds number, Suspended random arrays cir-cular cylinders | Sangani & Yao, 1988 | Stokes flow equation number, Suspended random arrays cir-cular cylinders | Longitudinal permeability a weak function of po-rosity if the arrays porosity $\leq$ 0.7; transverse permea-bility also insensi-tive of porosity if porosity $\leq$ 0.5.Solving actual flow gives better es-timation of permea-bility than solving disturbance of flow. |
| Incompressible | Fand et al., 1987 | Experiment | providing a simple method to characterizing the behavior of porous media in the transition region between Darcy and Forchheimer and between Forchheimer and turbulent flow. |
| Compressible, high Reynolds number | Masha et al., 1974 | Experiment | Incompressible Forchheimer resistance law still valid for subsonic flow with significant density changes. |

There have been modifications on the above function to describe different types of porous media [Lundgren, 1972; Sahraoui, 1992]. More recently, computational modeling

has been used to provide detailed flow fields. There are also results obtained by the asymptotic solutions [Chapman & Higdon, 1992].

While study of porous media flow is an old topic in fluid mechanics, the convective heat transfer of flows through porous medium has emerged as a new interest due to new technologies developments. Forced convection in porous media arises wherever the energy is delivered, controlled, utilized, converted or produced. The recent widely used cellular microstructure materials have found implementation in the technologies of thermal dissipation media, impact absorbers and compact heat exchangers. Their thermal attributes enable applications as heat dissipation media and as recuperation elements. Consequently, these enable high heat transfer rates and can be effectively used for either cooling or efficient heat exchange. Hence, it has become important to understand the interaction between mass and thermal transports and the resulting effects on the thermomechanical characteristics of porous media.

Oztop et al.studied numerically free convection in a partially opened square cavity of length H filled with a fluid saturated porous medium using the Darcy-Brinkman Forchheimer model. The heated wall was under constant temperature boundary conditions (isothermal wall) and remaining impermeable walls were adiabatic. The effects of changes location center (OC) of the opened cavity depends on the cases considered with Grashof number, Darcy number, length of the heated wall h and porosity were investigated. The results appear that Nusselt number was an increasing function of the Rayleigh number so, Nusselt number increases with increasing of porosity and heater length. Higher Nusselt number was observed for OC $=0.75$ at low porosity values but Nusselt number was increased for OC $=0.25$ at higher values of porosity.

Basak et al. studied numerically free convection flows in a square cavity filled with a fluid saturated porous medium, with uniformly and non-uniformly heated bottom wall, and adiabatic top wall, keeping constant temperature of cold vertical walls. Darcy-Forchheimer model was used to simulate the momentum transfer in the porous medium. The effect of Rayleigh number, Darcy number, and Prandtl number with respect to continuous and discontinuous thermal boundary conditions were investigated. The results appear that the thermal boundary layer is developed approximately 75% within

the cavity for uniform heating whereas the boundary layer is approximately 60% for non-uniform heating.

Varol et al. studied numerically free convection in diagonally divided square enclosures filled with porous media. Vertical walls were kept at isothermal conditions, while horizontal walls were insulated. The effects of the Rayleigh number, thermal conductivity ratio and position of the divided plate inside the cavity (Case I $45^o$, and Case II $135^o$ ) were investigated. The results appear that, Nusselt number was attenuated when the plate was positioned at $45^o$; the Nusselt number was less than when it was at $135^o$. Varol studied numerically free convection in partially divided porous trapezoidal cavity. Bottom wall was nonuniformly heated while two vertical walls were insulated and the top wall was maintained at constant cold temperature. The effect of Rayleigh number, thickness of the horizontal partition, location of the horizontal partition, and thermal conductivity ratio were investigated. The results appear that, the Nusselt number decreases with increasing of partition thickness due to domination of conduction mode of heat transfer. Haghshenas et al. studied free convection in an open-ended cavity with and without porous medium. Left wall was at a constant temperature and the right side was open. The effect of Rayleigh number and porosity were investigated. The results appear that heat transfer increased with Rayleigh number and porosity increasing.

Forced convection is type of heat transport in which fluid motion is generated by an external source like a (pump, fan, suction device, etc.). It should be considered as one of the main methods of useful heat transfer as significant amounts of heat energy can be transported very efficiently. In this context, forced convection heat transfer in porous media are actively under investigation. Porous media effects on forced convection received a great deal of attention in recent years, because found very commonly in everyday life, such as steam coil air heater, water treatment filter, heat exchangers and so on. Comprehensive literature survey concerned with this subject is given by: [239] Wu and Wang studied a numerically two-dimensional unsteady state forced convection heat transfer and laminar, incompressible flow across a porous square cylinder with a uniform heat generation mounted on the non-permeable cylinder bottom surface in the middle of the channel. Darcy Brinkman-Forchheimer model was adopted for the porous

region. The top and bottom walls of the channel were assumed to be adiabatic. The effects of Reynolds number, porosity, Darcy number and cylinder to-channel height ratio B/H were investigated. The results appear that heat transfer increased with Reynolds number, Darcy number and porosity increasing.

Zehforoosh and Hossainpour studied numerically two dimensional, single phase, incompressible, steady, and laminar forced convection heat transfer in a partially porous channel, with four dissimilar porous-blocks, attached to the strip heat sources at the bottom wall. The effects of variations of different parameters such as porous blocks Darcy numbers, arrangements of dissimilar blocks, Forchheimer coefficient, Reynolds number, thermal conductivity and Prandtl number were investigated. The results appear that when the blocks sorted from the lowest Darcy numbers in first block up to highest in fourth. The Nusselt number enhancement was almost the same as in the similar porous channel (Nu/Nusimilar=92%), while the total pressure drop was considerably lower (P/Psimilar= 28%).

Li et al. [240] studied numerically laminar fluid flow and forced convection heat transfer characteristics in a channel with staggered porous blocks. The fluid flows into the channel at lower temperature, so the temperatures of two walls for channel were higher. The effects of Darcy number, Reynolds number, porous block height and width, the thermal conductivity ratio and the associated local heat transfer in channel with staggered porous blocks were studied. The results appear that heat transfer was significantly enhanced with the decrease of Darcy number at the expense of high pressure drop. When increased the thermal conductivity ratio between the porous blocks and fluid, the heat transfer at the locations of the porous blocks can be greatly increased.

Jen and Yan studied numerically three-dimensional fluid flow and forced convection heat transfer in a channel with constant wall temperature partially filled with porous medium. The effects of Reynolds number, porous media ratio, on the velocity fields, temperature distributions, friction factors and Nusselt numbers were investigated. The results appear that there exists one pair of strong counter- rotating secondary flow vortices in the channel cross-section in the entrance flow region. These vortices greatly alter the axial velocity profiles and the temperature distributions in the composite square

channel. It was found that as the porous ratio, increases, the flow velocity in fluid layer was increased, and friction factor and Nusselt number were increased.

Shokouhmand and Salimpour studied numerically the effect of porous insert position on enhanced heat transfer in a parallel-plate channel partially filled with a fluid-saturated porous medium. The walls of the channel were subject to a uniform constant temperature. The flow field and thermal performance of the channel were investigated and compared for two configurations:

1. first the porous insert was attached to the channel walls;
2. second the same amount of the porous material was positioned in the channel core.

The effects of porous media thickness, Darcy number, and thermal conductivity ratio between porous media and fluid were investigated and compared for both cases. The results appear that with a porous layer located in the channel core, pressure loss was higher than that of the case with porous medium adjacent to the walls. When the thermal conductivity and Darcy number of porous media were high, locating the inserts near the walls was superior. In lower Darcy numbers, inserting porous layer in the channel core results in higher Nusselt numbers.

The effects of fluid velocity, particle diameter, type of porous media (sintered or non-sintered), and fluid properties on the Heat transfer dynamics in porous media are substantially different from solutes transport in that conduction is through both the matrix and the fluid and therefore conductive heat transport is more rapid than diffusive solute transport. On the contrary, the advective transport of heat (convection) is slower than advective solute transport since the heat capacity of the solid grains will retard the advance of the thermal front (Bodvarsson, 1972, Oldenburg and Pruess, 1998).

Thermal dispersion is analogous to hydrodynamic dispersion and results from local velocity variations due to the mechanical interaction of the fluid with the porous medium structure (Bear, 1972). But the hydrodynamic component of thermal dispersion is often neglected because thermal diffusion is more efficient than molecular diffusion by several orders of magnitude (Bear 1972). However, the literature contains conflicting descriptions of the thermal dispersivity coefficient (Rau et al., 2012). An issue that has

not been properly addressed experimentally is the quantification of thermal dispersivity as far as heat transport and its relationship with velocity.
Another issue to take into account is that the structure and porosity of the porous medium may affect the flow patterns and thermal transport phenomena in the porous channels [199] (Wu and Hwang, 1998). In the aspect of porosity, numerous works consider various problems of flow and heat transfer through a constant porosity medium [Beckermann & Viskanta, 1987; Nield et al., 1996; Poulikakos & Kazmierczak; 1987; Kim et al., 1994; Kaviany, 1987; Nakayama et al., 1990; Ould-amer et al., 1998]. But porous systems with variable porosity near the bounding walls have been shown in a number of experimental studies [Okuyama et al., 2000; Sederman et al., 1997] that variable porosity plays a vital effect in velocity field and results in flow accelerating at the region next to the impermeable bounding walls.

### 2.5.1 Local Thermal Non-Equilibrium (LTNE)

Traditionally, the assumption of local thermal equilibrium has been used in analysis of heat convection in porous media. That is, any temperature differences between the solid and fluid phases are neglected. Thus, the problem of flow in porous media can be simplified from a two phase to a single phase one. However, under certain situations, the local thermal equilibrium is not valid where a substantial temperature difference exists between solid and fluid phases. Thus, a two-medium treatment is necessary. Kaviany [1991] proposed a heuristic two-temperature approach to deal with a condition when there is an internal heat source in one of the media, or if the thermal conductivities of the fluid and solid are disparate, such as the air versus metal foams.
There have been studies on convection in packed beds and open cellular metal foams [Hunt, 1988, Sathe, 1990; Sozen, 1993; Hwang, 1994; Amiri, 1994; Hwang, et al., 1995] to account for local thermal non-equilibrium.

### 2.5.2 Experimental Setup: Heat transport laboratory experiment in porous media in 1d cylinder: material ad methods

The test on convective heat transport in porous medium has been conducted on a laboratory physical model. Figure 82 shows a sketch of the experimental apparatus.

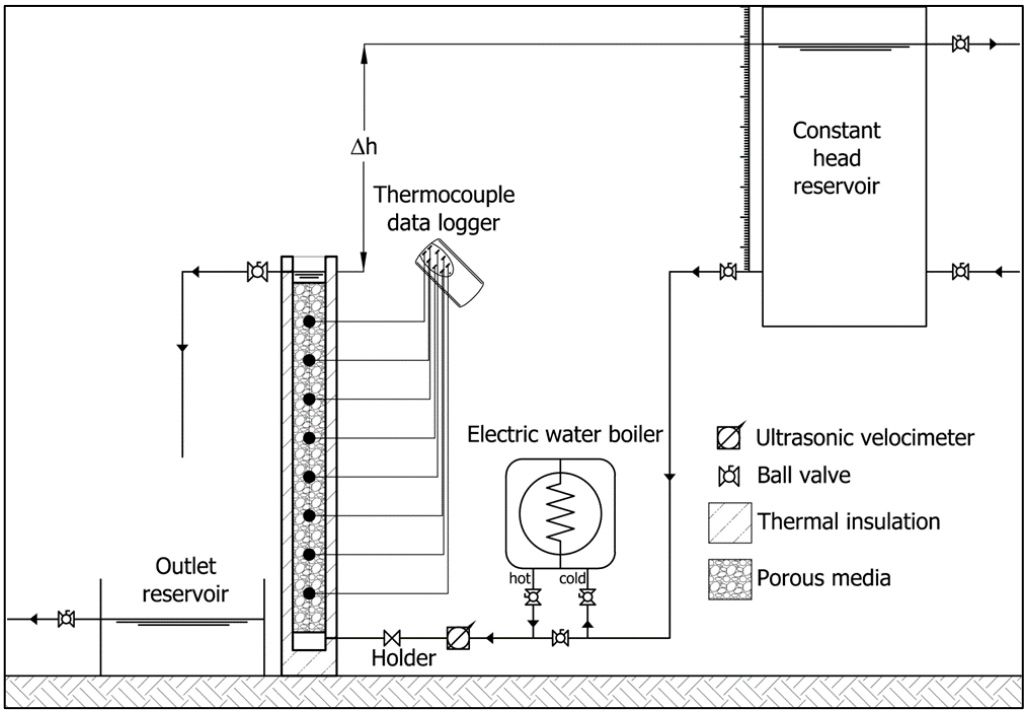


Figure 82 Experimental setup.

A plastic circular pipe characterized by a diameter of D = 0.11 m and height of H = 1.66 m has been thermally insulated ( Fig. 84) using a roll of elastomeric foam with a thickness of s = 0.02 m and a thermal conductivity of $\lambda$ = 0.037 $Wm^{-1}K^{-1}$(Table 18) The pipe can be filled with different porous media with different grain size and hydrothermal properties.

Table 17 Properties of porous medium

| Property | Value |
|---|---|
| Porosity (-) | 0.47 |
| Average grain size (mm) | 9.21 |
| Average specific surface ($m^{-1}$) | 337.90 |
| Soil density ($Kg \cdot m^{-3}$) | 2210 |
| Soil heat capacity ($J \cdot Kg^{-1} \cdot K^{-1}$) | 840 |
| Soil thermal conductivity ($W \cdot m^{-1} K^{-1}$) | 2.15 |

Eight thermocouple have been equally placed along the axis of the pipe (Fig 83-84).

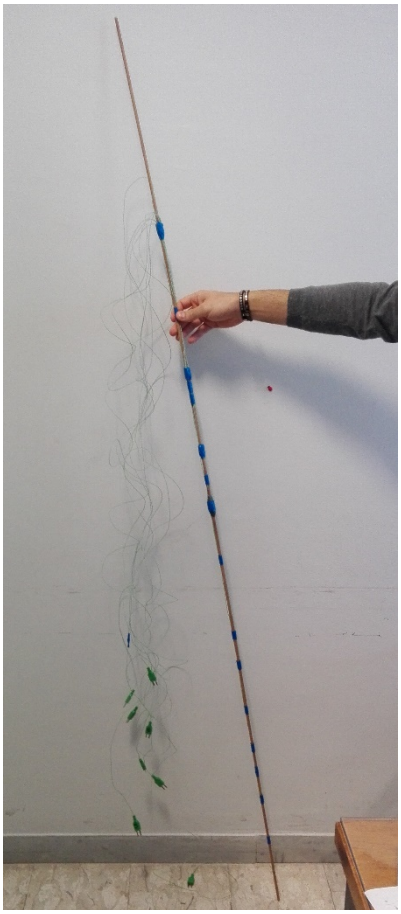

Figure 83 Eight thermocouple have been equally placed along the axis of the pipe

TC08 Thermocouple Data Logger (pico Thecnology) with sampling rate equal to 1 second has been connected with the thermocouples. An adaptable constant head reservoir and an outlet reservoir permit to maintain a constant head during the test and water within the pipe flows from the bottom to the top. An ultrasonic velocimeter (DOP3000 by Signal Processing) is used to measure the instantaneous flow rate. An electric water boiler characterized by a volume equal to 0.01 $m^3$ has been used to heat the water flowing through the pipe.

Figure 84 Thermocouple that have been equally placed along the axis of the pipe.

Two porous materials having different grain sizes have been used. Figure 89 shows the tested materials whereas in Table 18 are reported the hydraulic and the thermal parameter of the samples.

Figure 85 Thermal Insulated cylinder


Figure 86 Sample of the material used for the experiments with different average grain size $d_p$. a) $d_p$ = 9.2 mm b) $d_p$ = 41.6 mm.

The temperature tracer tests involve the observation of the thermal breakthrough curves (BTCs) monitored by the eight thermocouples. Initially cold water flows through the pipe filled with porous material in order to have a constant temperature $T_0$ along the pipe. Subsequently, hot water flows through the pipe, maintaining the constant head conditions during the test.

### 2.5.3 First test: Experimental investigations of heat transport dynamics in a 1d porous medium column

**Abstract**

The present study involves the experimental investigation of heat transport due to the forced convective flow through a thermally isolated porous medium column.

A laboratory physical model has been set up to analyse the forced convective flow and the related heat transport dynamics through a 1d porous medium column. In particular, the experiments regard the observation of thermal breakthrough curves obtained through a hot flow injection in correspondence of two thermocouples positioned along a thermally isolated column of porous medium. The experiment has been carried out for three flow rates in order to investigate the critical issues regarding heat transport phenomena such as the relationship between the thermal dispersion with the flow velocity and the validity of the local thermal equilibrium assumption between the fluid and solid phase.

The results put into evidence the magnitude of the errors between the estimated and the theoretical values of the key parameters that govern heat transport in order to evaluate the goodness of the commonly used assumptions in the numerical modelling of heat transport in porous media.

### 2.5.4 Introduction

In recent years, considerable interest has been given to the study of heat transfer through porous media because of its wide applications in many fields like crude oil extractions, petroleum reservoirs, agricultural engineering, coal combustors, solar collectors, electronic cooling, energy storage units and nuclear waste repositories (Singh, 2015).

The study of heat transfer phenomena in the subsurface is also relevant for geothermal energy extraction.

Heat transfer dynamics in porous media are substantially different from solutes transport in that conduction is through both the matrix and the fluid and therefore conductive heat transport is more rapid than diffusive solute transport. On the contrary, the advective transport of heat (convection) is slower than advective solute transport since the heat capacity of the solid grains will retard the advance of the thermal front (Bodvarsson, 1972, Oldenburg and Pruess, 1998).

Thermal dispersion is analogous to hydrodynamic dispersion and results from local velocity variations due to the mechanical interaction of the fluid with the porous medium structure (Bear, 1972). However, the hydrodynamic component of thermal dispersion is often neglected because thermal diffusion is more efficient than molecular diffusion by several orders of magnitude (Bear 1972). However, the literature contains conflicting descriptions of the thermal dispersivity coefficient (Rau et al., 2012). An issue that has not been properly addressed experimentally is the quantification of thermal dispersivity as far as heat transport and its relationship with velocity. Another issue to take into account is that the structure and porosity of the porous medium may affect the flow patterns and thermal transport phenomena in the porous channels (Wu and Hwang, 1998).

Few authors have carried out laboratory experiments on heat transfer in porous media. Among those, the principal investigated issues have been the influence of non-linear flow regime, the relationship between the thermal dispersion with the flow velocity and the validity of the local thermal equilibrium assumption between the fluid and solid phase.

Wu and Hwang (1998) investigated experimentally and theoretically the flow and heat transfer characteristics inside packed and fluidized beds. The purpose of their study was to study the heat transfer performance of the porous channels by using a modified version of the local thermal non equilibrium model (LTNE) which neglected the effects of thermal dispersion in both fluid and solid. The results showed a highly non-Fourier behaviour which combined rapid thermal breakthrough with extremely long-tailing, that was attributed to disequilibrium between the fluid and the porous matrix. However, the adopted model was unable to fully capture the thermal breakthrough observed in some experimental runs. Emmanuel and Berkowitz (2007) applied the continuous time random walk (CTRW) to three of the experiments carried out by Wu and Hwang (1998) over a range of different flow rates. CTRW is capable of quantifying both local equilibrium and non equilibrium heat transfer in heterogeneous domains, and showed to successfully capture the observed non equilibrium thermal breakthrough curves.

Rau et al (2012) carried out laboratory experiments on heat transfer in a specifically designed hydraulic tank containing well-sorted saturated sand. The experiments were aimed at analysing heat and solute transport behaviour separately, but under the same conditions, representative of naturally occurring groundwater flow systems.

They found that the thermal dispersion behavior for Darcy-related velocities in natural porous media did not exceed beyond a transition regime. The thermal dispersion can be approximated by a thermal dispersivity coefficient and a square dependency on the thermal front velocity. This result deviates from the linear description of thermal dispersion, which is assumed in analogy to solute transport. The difference can be explained with the different characteristics of heat and solute transport in porous media as expressed by the respective transport Peclet numbers.

The results indicated that for relatively uniform coarse sand the thermal dispersivity term in the thermal dispersion equation can be neglected for $Pe < 0.5$.

This study is aimed at investigating the critical issues regarding heat transport phenomena in porous media by means of laboratory experiments. A physical model has been realised to analyse the forced convective flow and the related heat transport dynamics through a 1d porous medium column.

### 2.5.5 Experimental setup

The experiments have been performed on a laboratory physical model constituted by a thermal insulated plastic circular pipe with diameter of 0.11 m and height of 1.66 m filled with a porous medium with hydraulic and thermal parameters described in the Table 19.

Water inside the column flows from the bottom to the top according to the hydraulic head difference between the upstream tank connected to the inlet port positioned at the bottom and the outlet port positioned at the top. Water that enters into the column is heated by an electric water boiler with a volume of $10^{-2}$ $m^3$. The instantaneous flow rate that flows across the block is measured by an ultrasonic velocimeter (DOP3000 by Signal Processing). Two thermocouples have been positioned at the center of the circular section of the pipe at the height of 0.25 m and 1.55 m respect to the inlet port. They have been connected to a TC – 08 Thermocouple Data Logger (pico Technology) and a sampling rate of 1 second has been used.

Table 18 Properties of porous medium.

| Property | Value |
|---|---|
| Porosity (-) | 0.47 |
| Average grain size (mm) | 9.21 |
| Average specific surface ($m^{-1}$) | 337.90 |
| Soil density ($Kg \cdot m^{-3}$) | 2210 |
| Soil heat capacity ($J \cdot Kg^{-1} \cdot K^{-1}$) | 840 |
| Soil thermal conductivity ($W \cdot m^{-1}K^{-1}$) | 2.15 |

**2.5.6**

### 2.5.7 Heat transport tests

Temperature tracer tests have been conducted through the following steps.

First a hydraulic head difference between the upstream tank and the outlet port has been imposed. At time t = 0 s the cold water valve has been opened. At time t = 60 s

the cold-water valve has been closed and at the same time the hot water valve has been opened. In this manner, the thermal breakthrough curves (BTCs) are measured by the thermocouples. The BTC measured by the first thermocouple located at the height of 0.25 from the inlet port is used as the injection temperature function $T_{inj}(t)$ whereas the BTC measured by the second thermocouple located at the height of 1.55 m from the inlet port is used as the observed temperature function $T_{obs}(t)$.

### 2.5.8 Theoretical background: Heat transport in one dimensional porous medium column

(N. Pastore, C. Cherubini, C. I. Giasi, N. M. Allegretti (2016). Experimental investigations of heat transport dynamics in a 1d porous medium column. Energy Procedia.)

**Nomenclature**

$\alpha L$ Longitudinal dispersion coefficient (m)
*cf* Specific heat capacity of the fluid phase ($JKg^{-1}K^{-1}$)
*cs* Specific heat capacity of the solid phase ($JKg^{-1}K^{-1}$)
*cs* Specific heat capacity of the solid phase ($JKg^{-1}K^{-1}$)
*dp* Average particle diameter (m)
*Da* Damnkhöler number (-)
*D0* Thermal diffusion ($m^2s^{-1}$)
*Deff* Effective thermal dispersion ($m^2s^{-1}$)
*keff* Effective thermal conductivity of the fluid phase ($Wm^{-1}K^{-1}$)
*ks* Thermal conductivity of the solid phase ($Wm^{-1}K^{-1}$)
*h** Convective heat transfer coefficient ($Wm^{-2}K^{-1}$)
*n* Porosity (-)
*Nu* Nusselt number (-)
$\mu$Viscosity ($Kgs^{-1}m^{-1}$)
*L* Characteristic length ($Kgs^{-1}m^{-1}$)
*q* specific discharge ($ms^{-1}$)
*qfs* Heat flux between from fluid to solid phase ($Wm^{-2}$)
*Pr* Prandtl number (-)

*Re* Reynolds number (-)
*R* Retardation factor (-)
$\rho f$ Density of the fluid phase (kg/m$^3$)
$\rho s$ Density of the solid phase (kg/m$^{3)}$
*sf* specific surface of the grain (m$^{-1}$)
*t* time (s)
*Tf* Temperature of the fluid (K)
*Ts* Temperature of the solid phase (K)
*v* Fluid velocity (m/s)
*x* coordinate along the direction of the flow (m)

The behavior of heat transport in porous media is strongly dependent from the fluid velocity. For high velocity flow, the interaction between the solid and fluid phase is rapid and then the solid and fluid phase cannot exchange sufficient amount of energy to establish local thermal equilibrium. At a given location, the solid and fluid phases have different temperatures. In this situation, each phase needs an energy equation for the description of heat transport. Assuming that porosity, densities and heat capacities are constant in time, energy equations can be written for the fluid and solid phase:

$$\frac{\partial T_f}{\partial t} = -v\frac{\partial T_f}{\partial x} + \frac{\partial}{\partial x}\cdot\left(\frac{k_{eff}}{\rho_f c_f}\frac{\partial T_f}{\partial x}\right) + \frac{q_{fs}}{\rho_f c_f} \tag{117}$$

$$\frac{\rho_s c_s}{\rho_f c_f}\frac{\partial T_s}{\partial t} = \frac{\partial}{\partial x}\cdot\left(\frac{k_s}{\rho_f c_f}\frac{\partial T_s}{\partial x}\right) - \frac{q_{fs}}{\rho_f c_f} \tag{118}$$

The interaction between the two phases is represented by the sink/source terms $q_{fs}$ given by following equation:

$$q_{fs} = h^* s_f \left(T_s - T_f\right)$$

(119)

The convective heat transfer coefficient can be expressed as:

$$h^* = \left( \frac{d_p}{10 k_s} + \frac{d_p}{\mathrm{Nu}\left(\mathrm{Pr}, \mathrm{Re}\right) k_f} \right)^{-1}$$

(120)

Ergun (1952) redefined the Reynolds number to describe non-Darcy flow in porous media as:

$$\mathrm{Re} = \frac{\rho_f d_p v}{\mu} \frac{1}{1-n}$$

(121)

Hassanizadeh and Gray (1987) suggest Re = 10 as a critical value for non-Darcy flow. In low velocity flow regimes the solid and fluid phase are in contact for a sufficient period, and there exists the possibility for energy exchange locally and to establish a local thermal equilibrium. In such a case, only one energy equation is sufficient for the description of heat transport. The energy equation for the fluid and solid phase are combined into a single equation as:

$$\left( 1 + \frac{1-n}{n} \frac{\rho_s c_s}{\rho_f c_f} \right) \frac{\partial T_f}{\partial t} = \frac{\partial}{\partial x} \left( \frac{k_{eff}}{\rho_f c_f} \frac{\partial T_f}{\partial x} \right) - v \frac{\partial T_f}{\partial x}$$

(122)

Damköhler number *Da* can be used in order to evaluate the presence of local thermal equilibrium. *Da* relates the convection time scale to the exchange time scale between the two phases:

$$Da = \frac{h^* s_f L}{\rho_f c_f v}$$

(123)

When Da>>1 the heat exchange between the two phases is rapid and there is instantaneous equilibrium between the two phases. On the contrary for Da<<1 the heat exchange velocity between the two phases is very low and it does not influence the heat propagation. When the convection time scale approaches the exchange time scale Da≅1, the impact of local thermal non-equilibrium behavior of heat transport is stronger and the temperature distribution is characterized by a long tail.

### 2.5.9 Results and discussion

Fitting thermal breakthrough curves and interpretation of estimated parameter models

Three tests have been conducted at different flow rates. As shown in the Table 19 for the range of velocity investigated the Damnkhöler number is much higher than the unit and then local thermal equilibrium model can be used to describe the behavior of heat transport.

Table 19 Specific discharge, fluid velocity, Reynolds number, heat transfer rate coefficient and Damköhler.

| **Q ($m^3s^{-1}$)×$10^{-6}$** | **q (m/s)×$10^{-3}$** | **v (m/s)×$10^{-3}$** | **Re (-)** | **$hs_f/\rho_f c_f$ ($s^{-1}$)** | **Da (-)** |
|---|---|---|---|---|---|
| 2.32 | 2.45 | 5.69 | 42.2 | 0.1847 | 23.56 |
| 1.60 | 1.68 | 3.61 | 29.0 | 0.1824 | 33.93 |
| 0.99 | 1.04 | 2.23 | 17.9 | 0.1774 | 53.30 |

Using the analogy with solute transport the Equation 122 can be rewritten as:

$$R\frac{\partial T_f}{\partial t} = \frac{\partial}{\partial x}\left( D_{eff}\frac{\partial T_f}{\partial x}\right) - v\frac{\partial T_f}{\partial x} \tag{124}$$

Where:

$$R = 1 + \frac{1-n}{n} \frac{\rho_s c_s}{\rho_f c_f}$$

(125)

$$D_{eff} = D_0 + \alpha_L v$$

(126)

On the basis of the analytical solution for the instantaneous temperature injection of the Equation 124 the probability density function of the residence time (*PDF*) for the temperature in the one dimensional column of porous medium can be written as:

$$PDF\left(x,t\right) = \frac{1}{\sqrt{\pi D_{eff} R^{-1} t}} \exp\left(\frac{x - vR^{-1}t}{4D_{eff} R^{-1} t}\right)$$

(127)

Using the convolution theorem the $T_{obs}$(t) can be related to $T_{inj}$(t) as:

$$T_{obs}\left(t\right) = T_{inj}(t) * PDF(t)$$

(128)

The observed BTCs for different flow rates have been individually fitted using the Equation 126. Figure 26 shows the fitting results.

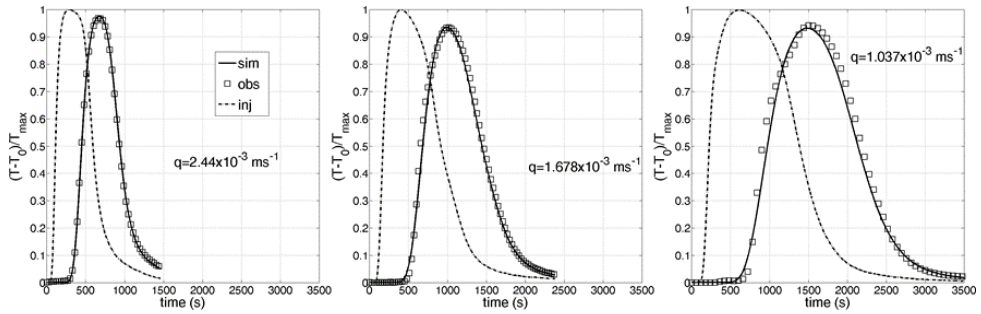


Figure 26 Fitting BTCs at different specific discharge.

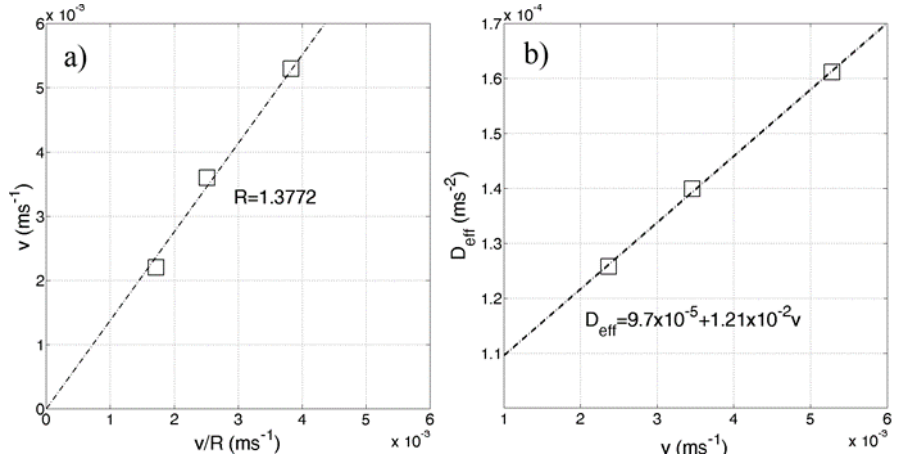


Figure 27 a) Relationship between the transport parameter $v/R$ and the fluid velocity $v=q/n$. b) relationship between fluid convective velocity $v$ and the effective thermal dispersion $D_{eff}$.

Figure 27a shows the relationship between the transport parameter $v/R$ and the convective velocity evaluated as $v=q/n$. The estimated value of the retardation factor is $R = 1.3772$ and it is close to the theoretical value that is equal to $R = 1.5084$. Figure 2b shows the relationship between $v$ and $D_{eff}$. A linear relationship is evident between the thermal convective velocity and the effective thermal dispersion for the investigated range of velocity with a longitudinal dispersion coefficient equal to $\alpha_L = 0.0121$ m. The estimated value of thermal diffusion is equal to $D_0 = 9.74\times10^{-5}$ m$^2$/s and it is much higher than the theoretical value equal to $D_0 = 2.82\times10^{-7}$ m$^2$/s.

### 2.5.10 Conclusions

Experimental investigations have been carried out to analyze the behavior of heat transport through a one-dimensional porous medium column. For the investigated range of velocity the fluid and solid phases are in thermal equilibrium. *Da* is much higher than the unit, varying in the range between 23.5 – 53.3.
In a previous study that analyzed heat transfer dynamics in a fractured limestone block the heat transfer velocity between the fluids in the fracture, the matrix was comparable with transport velocity, and a non-local thermal equilibrium has been detected.
This puts into evidence that $s_f$ plays an important role on heat transport behavior. When $s_f$ reduces, *h* reduces consequently and then the heat transfer velocity between the fluid and solid phases could be comparable with the convective velocity-giving rise to a strong local thermal non-equilibrium effect.
Assuming valid the local thermal equilibrium model, the thermal BTCs have been fitted using the analytical solution of the 1d advection dispersion model. The estimated thermal convective velocity approaches the fluid convective velocity with an error in the range of 0.58% - 6.38% whereas regarding the effective thermal dispersion the results put into evidence a discrepancy between the estimated and theoretical values of the thermal diffusion coefficient.
The obtained results encourage further experimental work to increase the knowledge of the key parameters that govern heat propagation in porous media.

### 2.5.11 Second test: heat transport in porous media for different porous diameter

**Abstract**
The present study concerns the laboratory investigation of heat transport through a thermally isolated column filled with porous medium.
The experiments consisted in injecting hot water flow rates in correspondence of two thermocouples positioned along a porous medium column and recording thermal breakthrough curves (BTCs). Several tests have been carried out, using porous mate-

rials with different grain sizes and several flow rates for each grain size of porous medium. This study has permitted to investigate the critical issues regarding heat transport phenomena such as the relationship between the flow velocity with the thermal dispersion and the validity of the local thermal equilibrium and non-local thermal equilibrium to describe the behaviour between the fluid and solid phase.

### 2.5.12 Theoretical background: Flow in one dimensional porous medium column

The basic law governing the flow of fluids through porous media is Darcy's law, which describes a linear relation between flow velocity and pressure gradients in the reservoir, an assumption that is adequate for low-velocity or laminar flow.
However, at higher flow velocities, deviations from Darcy's law are observed because of inertial effects. In order to account for these high velocity inertial effects, Forchheimer (1901) suggested to add an inertial term representing the kinetic energy of the fluid to the Darcy equation (Teng & Zhao, 2000). The Forchheimer equation for one-dimensional flow is given as follows:

$$-\frac{dp}{dx} = \frac{\mu}{k} q + \beta \rho q^2 \tag{129}$$

Where $x$ (L) is the coordinate along the fracture axis, $p$ ($ML^{-1}T^{-2}$) is the pressure, $k$ ($L^2$) is the permeability, $\mu$ ($ML^{-1}T^{-1}$) is the viscosity, $\rho$ ($ML^{-3}$) is the density, $q$ ($LT^{-1}$) is the darcian velocity and $\beta$ ($L^{-1}$) is called the non –Darcy coefficient.
Ergun (1952) derived a model for high velocity pressure loss in a porous medium from the Forchheimer equation by correlating the permeability and inertial resistance dimensionally to the porosity and the equivalent sphere diameter of rough particles. The permeability and inertial coefficient are interpreted in terms of spatial parameters as follows:

$$k = \frac{{d_p}^2 n^3}{A\left(1-n\right)^2} \tag{130}$$

$$\beta = \frac{B(1-n)}{d_p n^3}$$

(131)

Where $d_p$ (L) is the average particle diameter, n (-) is the porosity and the coefficients A = 180 and B = 1.8 are empirical and were derived by averaging the Navier – Stokes equations for a cubic representative unit volume.

In literature two types of criteria have been used for identifying non – Darcy flow, the Reynolds number and the Forchheimer number. The former represents the ratio of inertial forces to viscous ones and the latter the ratio of non-linear to linear pressure losses.

Ergun (1952) redefined the Reynolds number to describe non-Darcy flow in porous media as:

$$\mathrm{Re} = \frac{\rho D v}{\mu} \frac{1}{1-n}$$

(132)

Where $v$ ($LT^{-1}$) is the true velocity of the fluid.

Hassanizadeh and Gray (1987) suggest Re = 10 as a critical value for non – Darcy flow.

The Forchheimer number can be expressed:

$$\mathrm{Fo} = \frac{k \beta \rho q}{\mu}$$

(133)

The Forchheimer number represents the ratio of pressure drop consumed by liquid-solid interactions to that by viscous resistance, and has a direct relation to non-Darcy effect (Zeng &Grigg, 2006).

A good reference for the critical Forchheimer number is 0.11, which corresponds to a 10% non-Darcy effect.

**Heat transport in one-dimensional porous medium column**

The behavior of convective heat transport in porous media is strongly dependent from the fluid velocity and the kinetics of heat transfer process between fluid and solid phases.

If the solid phase and fluid phase are in contact for a sufficient period, there is the possibility to establish a local thermal equilibrium (LTE) condition. In such case, only one energy equation is sufficient for the description the convective heat transport through porous media. Assuming that porosity, densities and heat capacities are constant in time the energy equation for the fluid and solid phases are combined into a single equation as:

$$\left(\rho c\right)_{sf} \frac{\partial T_f}{\partial t} = \frac{\partial}{\partial x} \cdot \left[ -v \rho_f c_f T_f + k_{sf} \frac{\partial T_f}{\partial x} \right] \tag{134}$$

With:

$$\left(\rho c\right)_{sf} = \left(1-n\right) \rho_s c_s + n \rho_f c_f \tag{135}$$

$$k_{sf} = \left(1-n\right) k_s + n k_f \tag{136}$$

Where $T_f$ (K) is the temperature of the fluid, $\rho_f$ ($ML^{-3}$) is the density of the fluid, $\rho_s$ ($ML^{-3}$) is the density of the solid, $c_f$ ($LT^2K^{-1}$) is the thermal capacitance of the fluid, $c_s$ ($LT^2K^{-1}$) is the thermal capacitance of the solid, $k_f$ ($MLT^{-3}K^{-1}$) is the thermal conductivity of the fluid, $k_s$ ($MLT^{-3}K^{-1}$) is the thermal conductivity of the solid, whereas $\left(\rho c\right)_{sf}$ and $k_{sf}$ represent the equivalent thermal capacitance and thermal conductivity of the porous domain respectively including porosity and thermal properties of solid and fluid.

If the interaction between solid and fluid phase is rapid the solid and fluid phases cannot exchange sufficient amount of energy to establish local thermal equilibrium. At a given location solid and fluid phases have different temperatures. In this situation, each phase needs an energy equation for the description of heat transport. Assuming that porosity,

densities and heat capacities are constant in time, energy equations can be written for the fluid and solid phase:

$$n\rho_f c_f \frac{\partial T_f}{\partial t} = \frac{\partial}{\partial x} \cdot \left[ -vn\rho_f c_f T_f + nk_f \frac{\partial T_f}{\partial x} \right] + q_{fs}$$

(137)

$$(1-n)\rho_s c_s \frac{\partial T_s}{\partial t} = \frac{\partial}{\partial x} \cdot \left[ (1-n) k_s \frac{\partial T_s}{\partial x} \right] - q_{fs}$$

(138)

The interaction between the two phases is represented by the sink/source terms $q_{fs}$ given by following equation:

$$q_{fs} = h^* s_f \left( T_s - T_f \right)$$

(139)

Where $h^*$ is the convective heat transfer coefficient ($MT^{-3}K^{-1}$) and $s_f$ ($L^{-1}$) is the specific surface area.

The convective heat transfer coefficient can be expressed as:

$$h^* = \left( \frac{d_p}{\Gamma k_s} + \frac{d_p}{\mathrm{Nu}\left(\mathrm{Pr}, \mathrm{Re}\right) k_f} \right)^{-1}$$

(140)

Where Nu= Nusselt number that represents the ratio of convective to conductive heat transfer across a surface within a fluid.

$$Nu_L = \frac{q''_w(convection)}{q''_w(conduction)} = hL/k.$$

(141)

The Prandtl Number is a dimensionless number approximating the ratio of momentum diffusivity (kinematic viscosity) to thermal diffusivity and can be expressed as:

$$\mathrm{Pr} = \nu / \alpha$$

(142)

Where

Pr = Prandtl's number

v = momentum diffusivity ($m^2/s$)

$\alpha$ = thermal diffusivity ($m^2/s$)

Several Nusselt number correlations are available in literature. Kuwahara et al. (2001) presents the following correlation expression for the Nusselt number:

$$Nu = \left(1 + \frac{4(1-n)}{n}\right) + \frac{1}{2}(1-n)^{1/2}\,\mathrm{Re}^{0.6}\,\mathrm{Pr}^{1/3} \tag{3}$$

The correlation expression are valid in the range of porosities $0.36 \leq n \leq 0.96$ and Reynolds number and Prandtl number in the ranges $3\times10^{-3} \leq \mathrm{Re} \leq 5\times10^{5}$ and $10^{-2} \leq \mathrm{Pr} \leq 10^{2}$ respectively.

The hydrodynamic mixing of the interstitial fluid at the pore scale gives rise to significant thermal dispersion phenomena. Generally, the hydrodynamic mixing is due to the presence of obstruction, flow restriction and turbulent flow. Therefore, the equivalent thermal conductivity in equation (134) and thermal conductivity in equation (137) is replaced with the effective thermal conductivity $k_{eff}$ which is the sum of the thermal conductivity and the thermal dispersion conductivity. The effective thermal conductivity depends on various parameters such as mass flow rate, porosity, shape of pores, temperature gradient, and solid and fluid thermal properties (Kaviany, 1995). The following equation can be used to estimate $k_{eff}$.

$$\frac{k_{eff}}{k_f} = \frac{k}{k_f} + K\left(\mathrm{Re}\,\mathrm{Pr}\right)^{n} \tag{44}$$

### 2.5.13 Experimental setup

The test on convective heat transport in porous medium has been conducted on a laboratory physical model. Figure 1 shows a sketch of the experimental apparatus. A

plastic circular pipe characterized by a diameter of D = 0.11 m and height of H = 1.66 m has been thermally insulated using a roll of elastomeric foam with a thickness of s = 0.02 m and a thermal conductivity of $\lambda = 0.037\ Wm^{-1}K^{-1}$. The pipe can be filled with different porous media with different grain size and hydrothermal properties. Eight thermocouple have been equally placed along the axis of the pipe. TC08 Thermocouple Data Logger (pico Thecnology) with sampling rate equal to 1 second has been connected with the thermocouples. An adaptable constant head reservoir and an outlet reservoir permit to maintain a constant head during the test and water within the pipe flows from the bottom to the top. An ultrasonic velocimeter (DOP3000 by Signal Processing) is used to measure the instantaneous flow rate. An electric water boiler characterized by a volume equal to 0.01 $m^3$ has been used to heat the water flowing through the pipe.


Figure 87 Sample of the material used for the experiments with different average grain size $d_p$. a) $d_p$ = 9.2 mm b) $d_p$ = 41.6 mm.

Two porous materials having different grain sizes have been used. Figure 87 shows the tested materials whereas in Table 20 are reported the hydraulic and the thermal parameter of the samples.

Table 20. Properties of the porous media

| | $M_1$ | $M_2$ |
|---|---|---|
| Porosity (-) | 0.47 | 0.53 |
| Average grain size (mm) | 9.21 | 41.65 |
| Average specific surface ($m^{-1}$) | 675.80 | 148.4 |
| Soild density ($Kg \cdot m^{-3}$) | 2210 | 2210 |
| Soil heat capacity ($J \cdot Kg^{-1} \cdot K^{-1}$) | 840 | 840 |
| Soil thermal conductivity ($W \cdot m^{-1} \cdot K^{-1}$) | 2.15 | 2.15 |

The temperature tracer tests involve the observation of the thermal breakthrough curves (BTCs) monitored by the eight thermocouples. Initially cold water flows through the pipe filled with porous material in order to have a constant temperature $T_0$ along the pipe. Subsequently, hot water flows through the pipe, maintaining the constant head conditions during the test.

### 2.5.14 Discussion

Using the analogy with solute transport the equation (134) can be written as:

$$R\frac{\partial T_f}{\partial t} = \frac{\partial}{\partial x}\left( D_f \frac{\partial T_f}{\partial x} \right) - v\frac{\partial T_f}{\partial x} \tag{5}$$

With:

$$R = 1 + \frac{1-n}{n}\frac{\rho_s c_s}{\rho_f c_f} \tag{6}$$

$$D_f = \frac{k_{eff}}{\rho_f C_f} \tag{7}$$

Where R (-) is the retardation factor and Df ($L^2T^{-1}$) is the thermal dispersion.

The analytical solution of Equation (146) describing 1D heat transport in infinite domain for instantaneous temperature injection $T_{inj}$ is given by Crank (1956). The probability density function $PDF_{eq}$ of the residence time for local thermal equilibrium condition can be written as:

$$PDF_{eq}\left(x,t\right)=\frac{1}{\sqrt{\pi D_{eff}R^{-1}t}}\exp\left(\frac{x-vR^{-1}t}{4D_{eff}R^{-1}t}\right)$$

(8)

The energy equation representative of the local thermal non equilibrium can be written as:

$$\frac{\partial T_f}{\partial t}=-v\frac{\partial T_f}{\partial x}+D_f\frac{\partial^2 T_f}{\partial x}+\alpha\left(T_s-T_f\right)$$

(9)

$$\frac{1-n}{n}\frac{\rho_s c_s}{\rho_f c_f}\frac{\partial T_s}{\partial t}=\frac{1-n}{n}\frac{k_s}{\rho_f c_f}\frac{\partial^2 T_s}{\partial x}-\alpha\left(T_s-T_f\right)$$

(150)

With:

$$\alpha=\frac{h^* s_f}{\rho_f C_f}$$

(1051)

$\alpha$ ($T^{-1}$) is the exchange coefficient. Neglecting the first term in the right hand side of the Equation 149, the analytical solution of the system equations describing 1D heat transport in infinite domain for instantaneous temperature injection $T_{inj}$ is given by Goltz and Robertz, 1986. The probability density function $PDF_{neq}$ of the residence time for local thermal equilibrium condition can be written as:

$$PDF_{neq}\left(x,t\right)=e^{\alpha t}c_0\left(x,t\right)+\alpha\int_0^t H\left(t,\tau\right)c_0\left(x,t\right)d\tau$$

(152)

With:

$$c_0(x,t) = \frac{1}{\sqrt{\pi D_{eff} t}} \exp\left(\frac{x - vt}{4 D_{eff} t}\right) \tag{11}$$

$$H(t,\tau) = e^{-\frac{\alpha}{\beta}(t-\tau)-\alpha\tau} \frac{\tau I_1\left(\frac{2\alpha}{\beta}\sqrt{\beta(t-\tau)\tau}\right)}{\sqrt{\beta(t-\tau)\tau}} \tag{154}$$

$$\beta = \frac{1-n}{n}\frac{\rho_s c_s}{\rho_f c_f} \tag{12}$$

Where $I_1$ is the modified Bessel function of order 1.

The thermal BTC measured by the first thermocouple located at the height of 0.25 m from the inlet port is used as the injection temperature function $T_{inj}(t)$. Then the observed temperature function $T_{obs}(t)$ at a generic distance $x$ from the first thermocouple can be obtained using the convolution theorem:

$$T_{obs}(t) = T_{inj}(t) * PDF(t) \tag{156}$$

For each tested material four thermal tracer tests have been carried out varying the injection flow rate in the range $0.531 \times 10^{-5}$ – $2.404 \times 10^{-5}$ $m^3 s^{-1}$. The thermal BTCs have been fitted using both LTE (for the first test) and LTNE model for the second test with the other porosity dimension.

## CONCLUSIONS

The study has been developed for low enthalpy geothermal open systems that operate within the same geothermal well. This type of system has been designed to reduce the environmental impact given by the injection of water at a temperature higher than temperature taken wing.

In this way, in fact, it is able to reduce thermal variations within a same area of interest.

The first study: “Experimental Study of Heat Transport in Fractured Network” has given, in summary, the following results.

Heat transfer time scale is comparable with convective time scale, the dual porosity behaviour is very strong giving rise to a delay on heat propagation in fracture network.

Thermal BTCs are characterized by a more enhanced early arrival and long tailing than solute BTCs observed in previous experiments. The residence time of heat transport is an order of magnitude higher than the residence time of solute transport.

Thermal dispersion time scale is always less than both thermal convective time scale and thermal exchange time scale. This results confirms that thermal dispersion play an important role on the heat transport ant its effect cannot be neglected.

The second study: ‘’Laboratory experimental investigation of heat transport in fractured media’’ confirms the results of the first study, and develops other, very interesting.

Heat transport shows a very different behavior compared to mass transport. The estimated transport parameters show differences of several orders of magnitude. Convective thermal velocity is lower than solute velocity, whereas thermal dispersion is higher than solute dispersion, mass transfer rate assumes a very low value suggesting that fracture – matrix mass exchange can be neglected. Non - Fickian behavior of observed solute BTCs is mainly due to the presence of the secondary path and nonlinear flow regime. Contrarily heat transfer rate is comparable with convective thermal velocity giving rise to a retardation effect on heat propagation in the fracture network.

The discrepancies detected in transport parameters are moreover observable through the time moment and tail character analysis which demonstrate that the dual porosity behavior is more evident in the thermal BTCs than in the solute BTCs.

The dimensionless analysis carried out on the transport parameters proves that as the injection flow rate increases thermal convection time scale decreases more rapidly than the thermal exchange time scale, explaining the reason why the relationship $Q_0 - u_f$ shows a change of slope for *Da* lower than the unit.

Thermal dispersion dominates heat transport dynamics, the Peclet number and the product between Peclet number and Damköhler number is usually less than the unit.

The optimal conditions for thermal exchange in a fracture network have been investigated. The power exchanged increases in a potential way as *Da* increases in the observed range.

This study has permitted to detect the key parameters to design devices for heat recovery and heat dissipation that exploit the convective heat transport in fractured media.

Heat storage and transfer in fractured geological systems is affected by the spatial layout of the discontinuities.

Specifically, the rock – fracture size ratio which determines the matrix block size is a crucial element in determining matrix diffusion on fracture – matrix surface.

The studies about the analysis of heat transport in fracture network: "Experimental investigations of heat transport dynamics in a 1d porous medium column'' and ''Experimental investigations of heat transport dynamics in a column filled by different grain size of porous media'' have given the following results:

For the investigated range of velocity the fluid and solid phases are in thermal equilibrium. *Da* is much higher than the unit, varying in the range between 23.5 – 53.3.

In a previous study that analyzed heat transfer dynamics in a fractured limestone block the heat transfer velocity between the fluid in the fracture and the matrix was comparable with transport velocity and a non-local thermal equilibrium has been detected.

This puts into evidence that $s_f$ plays an important role on heat transport behavior. When $s_f$ reduces *h* reduces consequently and then the heat transfer velocity between the fluid and solid phases could be comparable with the convective velocity giving rise to a strong local thermal non equilibrium effect.

Assuming valid the local thermal equilibrium model, the thermal BTCs have been fitted using the analytical solution of the 1d advection dispersion model. The estimated thermal convective velocity approaches the fluid convective velocity with an error in the range of 0.58% - 6.38% whereas regarding the effective thermal dispersion the results put into evidence a discrepancy between the estimated and theoretical values of the thermal diffusion coefficient.

The obtained results encourage further experimental work to increase the knowledge of the key parameters that govern heat propagation in porous media.

From this study showed that the specific surface of the medium plays an extremely important role. By varying the specific surface area, the subsurface reservoir formations is able to retain more or less heat due to variation of thermal dispersion. From the present studies, have been found, in fact, that an subsurface reservoir formations characterized by a low specific surface, at the same flow rate, at the same hydraulic and thermal properties, presents high capability to store heat respect to the subsurface reservoir formations characterized by a high specific surface system that has better properties to dissipate heat In fact, if the fractures in the reservoir have a high density and are well connected, such that the matrix blocks are small, the optimal conditions for thermal exchange are not reached as the matrix blocks have a limited capability to store heat. Therefore, subsurface reservoir formations with large porous matrix blocks will be the optimal geological formations to be exploited for geothermal power development. In fact, if the fractures in the reservoir have a high density and are well connected, such that the matrix blocks are small, the optimal conditions for thermal exchange are not reached as the matrix blocks have a limited capability to store heat.

The estimation of the average effective thermal conductivity coefficient shows that it is not efficient to store thermal energy in rocks with high fracture density because the fractures are surrounded by a matrix with more limited capacity for diffusion giving rise to an increase in solid thermal resistance.

On the other hand, isolated permeable fractures will tend to lead to the more distribution of heat throughout the matrix.

The study could help to improve the efficiency and optimization of industrial and environmental systems, and may provide a better understanding of geological processes involving transient heat transfer in the subsurface.

Future developments of the current study will be carrying out investigations and experiments aimed at further deepening the quantitative understanding of how fracture arrangement and matrix interactions affect the efficiency of storing and dissipation thermal energy in aquifers. This result could be achieved by means of using different formations with different fracture density and matrix porosity.

ACKNOWLEDGEMENTS

In primis ringrazio la tutor del mio dottorato la Prof. Ing. Giasi che mi ha permesso di raggiungere questo traguardo. La ringrazio per aver messo a mia disposizione la sua professionalità e per avermi permesso di crescere come professionista. La ringrazio per avermi trattata con umanità e per avermi compresa nei momenti di difficoltà. Le sono grata per avermi coinvolta nel suo team di ricerca e di aver creduto in me. Grazie per tutte le esperienze in ambito universitario che mi ha permesso di fare e che mi hanno consentito anche di affrontare la mia timidezza. Grazie alla Prof. Cherubini che mi ha permesso di svolgere due anni del mio dottorato in cotutela con l'università Francese La Salle di Beauvais. La ringrazio per tutto l'aiuto nei lavori di pubblicazione e nei convegni e per avermi aiutata con la lingua inglese. Ringrazio il prof. Pastore perché è a lui che devo moltissimo. Per avermi guidata, aiutata, indirizzata in questi tre anni. Per avermi insegnato che significa lavorare in laboratorio, quanta attenzione bisogna metterci nelle prove, quanto è importante la precisione nel riportare i dati. Grazie perché hai compreso i miei tempi e grazie per la tua amicizia, per i confronti e per i consigli. Ringrazio la mia famiglia per aver compreso la mia scelta di intraprendere questo percorso, di essermi sempre stata vicina. Ringrazio il mio papà per tutto ciò che ha fatto per me, per essersi messo a disposizione ed avermi aiutata e compresa. Ringrazio la mia mamma per la sua dolcezza, per la sua comprensione e per aver condiviso con me le mie tante soddisfazioni e i miei sacrifici. Ringrazio Francesco per essermi stato sempre accanto e per avermi spronata e sostenuta, per avermi ascoltata e sopportata nei momenti no e per aver creduto in me, per non aver permesso che io mollassi. Grazie alle mie amiche e ai miei amici di sempre per i momenti di spensieratezza e di confronto, persone essenziali nella mia vita. Grazie alle persone speciali che ho avuto la fortuna di conoscere in questi anni con i quali condivido tutti i giorni le mie passioni e i sacrifici per obiettivi comuni. Grazie per tutte quelle volte in cui mi avete aiutata a superare con un sorriso i momenti no, per tutte le volte che ci siete stati, per i momenti di spensieratezza dopo una lunga e dura giornata. Perché è anche grazie a voi se adesso ho le idee più chiare sul mio percorso professionale.

REFERENCES

Adviser, T. and Greber I., (2005). A Numerical Study of Transport Phenomena in Porous Media by Submitted in partial fulfillment of the requirements For the degree of Doctor of Philosophy May-Fun Liou.

Ait Saada, M., Chikh, A.S., Campo, A. (2006). Analysis of hydrodynamic and thermal dispersion in porous media by means of a local approach. Heat Mass Transfer 42: 995–1006.

Ait Saada, M., Chikh, A.S., Campo, A. (2006).Analysis of hydrodynamic and thermal dispersion in porous media by means of a local approach Heat Mass Transfer (2006) 42: 995–1006 DOI 10.1007/s00231-005-0061-y

Amiri A. and Vafai K. (1994) Analysis of dispersion effects and non-thermal equilibrium, non- Darcian, variable porosity incompressible flow through porous media , International Journal of Heat and Mass Transfer . Vol. 37, No. 6, pp. 939-954.

Amiri, A., Vafai, K. (1998). Transient analysis of incompressible flow through a packed bed. International Journal of Heat and Mass Transfer 41 4259-4279.

Anderson, M.P. (2005). Heat as a ground water tracer. Ground Water 43, no. 6: 951-968.

Anderson, M.P. (2005). Heat as a ground water tracer. Ground Water 43, no. 6: 951–968.

Barhoum, S., Valdès, D., Guérin, R., Marlin, C., Vitale, Q., Benmamar, J., and Gombert, P. (2014). Spatial heterogeneity of high-resolution Chalk groundwater geochemistry-Underground quarry at Saint Martin-le-Noeud, France. Journal of Hydrology, vol. 519, pp. 756–768.

Bayer, P., Saner, D., Bolaya, S., Rybachc, L., Blumd, P. (2012). Renewable and Sustainable Energy Reviews 16, 1256–1267.

Beavers, G.S. and Sparrow, E.M. (1969). Non-Darcy flow through fibrous porous media. *J. Appl. Mech* 36(4), 711-714.

Becker, M.W. and Shapiro, A. M. (2003). Interpreting tracer breakthrough tailing from different forced gradient tracer experiment configurations in fractured bedrock. Water Resources Research. 39(1):1024.
Bertani, R., (2012). Geothermal power generation in the world 2005–2010 update report. Geothermics 41, 1–29.
Bertani, R., Geothermal Power Generation in the World 2010-2014 Update Report
Biot, A. (1941). General theory of three dimensional consolidation. *J. Appl. Phys.* 12:155–164.
Blum, P., Campillo, G., Münch, W., Kölbel, T. (2010). $CO_2$ savings of ground source heat pump systems – a regional analysis. Renew Energy; 35:122–7.
Blum, P., Campillo, G., Kölbel, T. (2011). Techno-economic and spatial analysis of vertical ground source heat pump systems in Germany. Energy; 36:3002–11.
Blumsack, S., Brownson J., Witmer L. (2009). Efficiency, economic and environmental assessment of ground-source heat pumps in Central Pennsylvania. In: International Conference on System Sciences.
Boait, P.J., Fan, D., Stafford, A. (2011). Performance and control of domestic ground-source heat pumps in retrofit installations. Energy Buildings; 43:1968–76.
Bodvarsson, G. (1972). Thermal Problems in Siting of Reinjection Wells. Geothermics, 1(2), pp. 63-66.
Botteghi, S., Chiesa, S., Destro, E., Di Sipio, E., Galgaro, A., Manzella, A., Montanari, D. (2012). VIGOR: Prime indicazioni tecnico-prescrittive in materia di impianti di climatizzazione geotermica. Progetto VIGOR – Valutazione del Potenziale Geotermico delle Regioni della Convergenza POI Energie Rinnovabili e Risparmio Energetico 2007 2013. CNR – IGG. ISBN: 9788879580106.
Bredehoeft, J. H. and. Papadopulos, I. S. S. (1965). Rates of vertical groundwater movement estimated from the earth thermal profile. Water Resource Research, 1:325–328.
Bristow, D., Kennedy, C. A., (2010). Potential of building-scale alternative energy to alleviate risk from the future price of energy. Energy Policy; 38:1885–94.

Buzăianu, A.; Csáki, I.; Moţoiu, P.; Popescu, G.; Thorbjornsson, I.; Ragnarsodottir, K.R.; Guðlaugsson, S.; Goubmunson, D. (2015). Recent advances of the basic concepts in geothermal turbines of low and high enthalpy. Adv. Mater. Res., 1114, 233–238.

Caird, S., Roy, R. (2010). Adoption and use of household microgeneration heat technologies. Low Carbon Econ; 1:61–70.

Carmo, C.; Elmegaard, B.; Nielsen, M.P.; Detlefsen, N. (2015). Empirical platform data analysis to investigate how heat pumps operate in real-life conditions. In Proceedings of the 24th Iir International Congress of Refrigeration (ICR2015), Yokohama, Japan, 16–22.

Carslaw, H. S., and J. C. Jaeger (1952). Conduction of Heat in Solids, 386 pp., Oxford University Press, New York, 1959. Ergun.

Castello, M., 2004. La géothermie. In Les enjeux des geosciences. ADEME & BRGM, 44p.

Cherubini, C., (2008). A modeling approach for the study of contamination in a fractured aquifer. Geotechnical and geological engineering 26 (5), 519-533

Cherubini, C., Giasi, C. I., and Pastore, N. (2009). Application of Modelling for Optimal Localisation of Environmental Monitoring Sensors, Proceedings of the Advances in sensor and Interfaces (IWASI), Trani, Italy, 222–227.

Cherubini, C., Giasi, C. I., Pastore, N. (2012). Bench scale laboratory tests to analyze non-linear flow in fractured media. Hydrology and Earth System Sciences, 16, 2511-2622.

Cherubini, C., Giasi, C. I., Pastore, N. (2013b). Laboratory tests to analyze solute transport behavior in fractured media. Rendiconti Online Società Geologica Italiana, 24, 55-57.

Cherubini, C., Giasi, C. I., Pastore, N. (2013c). Un modello fisico di laboratorio per analizzare dinamiche di flusso e trasporto in un campione di roccia fratturata a scala di banco [A laboratory physical model to analyse flow and transport processes in fractured rock sample at bench scale level]. Italian Journal Engineering Geology and Environment. 19-32.

Cherubini, C., Giasi, C..I, Pastore, N. (2013). Evidence of non-Darcy flow and non-Fickian transport in fractured media at laboratory scale. Hydrology and Earth System Sciences 2013; 17 p. 2599-2611.
Cherubini, C., Giasi, C.I., Pastore, N. (2013). Fluid flow modelling of a coastal fractured karstic aquifer by means of a lumped parameter approach. Environmental Earth Sciences, 70 (5) p. 2055-2060.
Cherubini, C., Giasi, C.I., Pastore, N. (2013). Laboratory tests to analyze solute transport behaviour in fractured media. Rendiconti Online Società Geologica Italiana, 24 p. 55-57.
Cherubini, C., Giasi, C..I, Pastore, N. (2013). Un modello fisico di laboratorio per analizzare dinamiche di flusso e trasporto in un campione di roccia fratturata a scala di banco [A laboratory physical model to analyse flow and transport processes in fractured rock sample at bench scale level]. Italian Journal Engineering Geology and Environment, (1) p. 19-32.
Cherubini, C., Giasi, C.I., Pastore, N. (2013a). Evidence of non-Darcy flow and non-Fickian transport in fractured media at laboratory scale. Hydrology and Earth System Sciences 17, 2599-2611.
Cherubini, C., Giasi, C.I., Pastore, N. (2014). On the reliability of analytical models to predict solute transport in a fracture network. Hydrology and Earth System Sciences 18, 2359-2374.
Cherubini, C., Giasi, C.I., Pastore, N. (2014). On the reliability of analytical models to predict solute transport in a fracture network. Hydrology and Earth System Sciences; 18 p. 2359-2374.
Cherubini, C., Pastore N., Francani, V. (2008). Different approaches for the characterization of a fractured karst aquifer. WSEAS Transactions On Fluid Mechanics 1, 29-35
Cherubini, C., Pastore, N. (2000). Modeling contaminant propagation in a fractured and karstic aquifer. Fresenius Environmental Bulletin, 19 (9) p. 1788-1794.

Cherubini, C., Pastore, N. (2011). Critical stress scenarios for a coastal aquifer in southeastern Italy. Natural Hazards and Earth System Science. 11 (5) p. 1381-1393.
Curtis, R., Lund, J., Sanner, B., Rybach, L., Hellström, G. (2005). Ground source heat pumps-geothermal energy for anyone, anywhere: current worldwide activity. In: World Geothermal Congress, p. 24–9.
Dagan (1979). The generalization of Darcy's law for non-uniform flows. *Water Resour. Res.* 15:1–7.
Darcy, H. (1856). *Les fontaines publiques de la ville de Dijon*. Paris: Victor Dalmont.
deMarsily, G. (1986). Quantitative Hydrogeology: Groundwater Hydrology for Engineers. Academic Press.
Dickson, M.H. and Fanelli, M. (2003). Geothermal energy: Utilization and technology. UNESCO, 205 pp.
Droulia, F.; Lykoudis, S.; Tsiros, I.; Alvertos, N.; Akylas, E.; Garofalakis, I. (2009). Ground temperature estimations using simplified analytical and semi-empirical approaches. *Solar Energy*, *83*, 211–219.
EC, (2006). Action Plan for Energy Efficiency: Realising the Potential. Commission of the European Communities, COM, 545 final, Brussels, Belgium, 26 pp.,
EHPA action plan, (2007). European Heat Pump Association.
Eidsath, A., Carbonell, R.G., Whitaker, S., Herrmann, L.R. (1983). Dispersion in pulsed systems. Part III, comparison between theory and experiments in packed beds. Chem Eng Sci 38: 1803–1816
Emmanuel, S., Berkowitz, B. (2007). Continuous time random walks and heat transfer in porous media. Transport in Porous Media; 67 p. 413-430.
Enerdata. (2011). ODYSSEE database on energy efficiency data & indicators. Grenoble, FR: Enerdata.
Ergun. Fluid flow through packed columns. *Chem. Eng. Prog.* 48:89–94, 1952.

Esen, H., Inalli, M., Esen, M. (2006). Techno economic appraisal of a ground source heat pump system for a heating season in eastern Turkey. Energy Convers Manage; 47:1281–97.
EURISPES (2010). Rapporto Italia 2010. Eurispes.
European Commission (2000). Conclusions of the Lisbon European Council. SN 100/00, 23–24 March.
European Commission (2009). Decision no 406/2009/EC of the European Parliament and of the Council on the effort of member states to reduce their greenhouse gas emissions to meet the community's greenhouse gas emission reduction commitments up to 2020. Off Eur Union, 5.
European Commission (2010). Directive 2010/31/EU of the European Parliament and of the Council of 19 May 2010 on the energy performance of buildings.
European Commission (2010). Europe 2020 – a strategy for smart, sustainable and inclusive growth. COM (2010) 2020 final. 2010. p. 35.
European Commission (2011). Communication from the commission to the European Parliament, the council, the European economic and social committee and the committee of the regions energy efficiency plan 2011. COM/2011/0109 final 2011. p. 16
Ferguson, G. (1985). Perturbation of ground surface temperature reconstructions by groundwater flow. Geophys. Res. Lett., 33, 2006. XVI, 22, 23, 24.
Florides, G. and Kalogirou, S. (2007). Ground heat exchangers - A review of systems, models and applications. Renewable Energy 32, 2461–2478.
Forchheimer P. (1901). Wasserbewegung durch Boden. Z. Ver. Dtsch. Ing. 45 p. 1781-1788.
Forchheimer, H. (1901). *Z. Ver. Dtsch. Ing.* 45:1782–1788,.
Fridleifsson, I.B., Bertani, R., Huenges, E., Lund, J.W., Ragnarsson, A., Rybach, L. (2008). The possible role and contribution of geothermal energy to themitigation of climate change. Lübeck, Germany: IPCC Geothermal; p. 59–80.
Frischknecht, R., Stucki, M. (2010). Scope-dependent modelling of electricity supply in life cycle assessments. Int J Life Cycle Assess 806–16.

Gehlin, S., (2002). Thermal response test. Method development and evaluation. Doctoral thesis, Lulea University of Technology, 186p.

Geiger, S. and Emmanuel, S. (2010). Non-fourier thermal transport in fractured geological media. Water Resources Research, 46, XVII, 26, 27, 168.

Gemelli, A., Mancini, A., Longhi, S., Mencucci, D., Menichetti, M.(2009). Definizione del potenziale geotermico a bassa entalpia su supporto GIS: un caso applicativo per la bassa valle del Fiume Metauro (Marche). In: AA.VV. e advanced manufacturing systems for geothermal energy, Energy Resources. Ancona; p. 171 e 86.

Genchi, Y., Kikegawa, Y., Inaba, A. (2002). $CO_2$ payback-time assessment of a regionalscale heating and cooling system using a ground source heat-pump in a high energy-consumption area in Tokyo. Appl Energy, 71:147–60.

Graf, S.; Lanzerath, F.; Sapienza, A.; Frazzica, A.; Freni, A.; Bardow, A. (2015). Prediction of scp and cop for adsorption heat pumps and chillers by combining the large-temperature-jump method and dynamic modelling. Appl. Therm. Eng., *98*, 900–909.

Gudmundsson, J.S., (1988). The elements of direct uses. Geothermics, 17,119-136.

Gunn, D.G., Pryce, C, (1969), Dispersion in packed beds. Trans Inst Chem Eng 47:341–350

Hadim, A., (1994). Forced Convection in a Porous Channel With Localized Heat Sources. ASME J. Heat Transfer, 116, pp. 465–472.

Hähnlein. S-, Molina-Giraldo. N-, Blum. P., Bayer, P., Grathwohl, P. (2010). Ausbreitung von Kältefahnen im Grundwasser bei Erdwärmesonden. Grundwasser; 15:123–33.

Hao, Y., Fu, P., Carrigan, C. R. (2013). Application of a dual-continuum model for simulation of fluid flow and heat transfer in fractured geothermal reservoir. Proceedings, Thirty-Eighth Workshop on Geothermal Reservoir Engineering Stansford University, Stanford, California 11-12 SGP-TR-198.

Harsh K.G., Sukanta, R. (2006). Geothermal Energy: An Alternative Resource for the 21st Century

Hawkins, A.J. and Becker, M.W. (2012). Measurement of the Spatial Distribution of Heat Exchange in a Geothermal Analog Bedrock Site Using Fiber Optic Distributed Temperature Sensing.

Hikari, F., Tadasuke, I., Ryuichi, I., Youhei, U. (2007). Development of suitability maps for ground-coupled heat pump systems using groundwater and heat transport models. Geothermics 36, 459–472.

Howard, J. H. (1975). Present Status and Future Prospects for Non-Electrical Uses of Geothermal Resources." Lawrence Livermore Laboratory (prepared for the U.S. Energy Research and Development Administration), University of California, Livermore, CA, 162 p.

Howard, J.H. (Ed.) (1975). Present status and future prospects for non-electrical uses of geothermal resources. NATO CCMS Report, No. 40. Lawrence Livermore Laboratory, University

Hsu C.T. and Cheng. P. (1990). Thermal dispersion in a porous medium. *Int. J. Heat Mass Transfer* 33:1587–1597, 1990.

Hsu, C.T., Cheng, P. (1990). Thermal dispersion in a porous medium. International Journal of Heat and Mass Transfer, 33(8), 1587-1597.

Hsu, C.T., Fu, H.L. and Cheng. P.(1999). On pressure-velocity correlation of steady and oscillating flows in regenerators made of wire-screens. *ASMEJ. Fluids Eng.*121:52–56.

Hughes, L., Chaudhry, N. (2011). The challenge of meeting Canada's greenhouse gas reduction targets. Energy Policy; 39:1352–62.

Hunt, M. L. and Tien, C. L., (1988a). Effects of Thermal Dispersion on Forced Convection in Fibrous Media. Int. J. Heat Mass Transfer, 31, No. 2, 301-309.

Huttrer, G.W. (1997). Geothermal heat pumps: an increasingly successful technology. Renew Energy,10:481–8.

Hwang ,G. l and Chao, C. H. (1994). Heat Transfer Measurement and Analysis for Sintered Porous Channels'', ASME Journal of Heat Transfer, Vol. 116, pp. 456-464.

Hwang, G. l, Wu, C. c., and Chao, C. H. (1995). Investigation of Non-Darcian Forced Convection in an Asymmetrically Heated Sintered Porous Channel'', ASME Journal of Heat Transfer, Vol. 117, pp. 725-732.

Ingebritsen, S.E., Stanford, W.E.(1999). Groundwater in geologic processes. Cambridge University Press.

J. Bear. (1972). Dynamics of Fluids in Porous Media. American Elsevier Publishing Company Inc., New York.

Jakob, M., Volkart, K., Widmer, D. (2009). $CO_2$ Intensität des Stromabsatzes an Schweizer Endkunden. Zurich, CH.

Kamiuto, K and Saitoh, S. (1994). Fully Developed Forced-Convection Heat Transfer in Cylindrical Packed Beds With Constant Wall Temperatures. JSME International Journal, Series B. Vol. 37, No.3, pp. 554-559.

Kaviany, M. (1995). Principles of Heat Transfer in Porous Media, 2nd Edition, New York, Springer-Verlag.

Kaviany, M.(1987). Boundary layer Treatment of Forced Convection Heat Transfer from a Semi-finite Flat Plate Embedded in Porous Media. ASME J. Heat Transfer, 109, 345- 349.

Kaviany, M., (1985). Laminar flow through a porous channel bounded by isothermal parallel plates. Int. J. Heat Mass Transf., 28, pp. 851–858.

Kaviany, M., (1991). Principles of Heat Transfer in Porous Media, Springer-Verlag, New York.

Khalil, R. A, El-Shazly, K M. and Assasa, G. R. (2000). Heat Transfer and Fluid Flow Characteristics of Forced Convection Through a Packed Pipe. 11th Int. Mechanical power Engineering Conference, Cairo, Vol. 1, pp. HI86-H200.

Kim, S. J., and Choi, C. Y., (1996).Convective Heat Transfer in Porous and Overlying Fluid Layers Heated From Below. Int. J. Heat Mass Transf., 39, pp. 319–329.

Klepikova, M. (2013). Imaging of fractured rock properties from flow and heat transport : field experiments and inverse modelling Maria Klepikova rock properties from.

Kocabas I. (2005). Geothermal reservoir characterization via thermal injection backflow and interwork tracer testing. Geothermics, 34 p. 27- 46.
Koch, D.L., Cox, R.G., Brenner, H., Brady, J.F. (1989). The effect of order on dispersion in porous media. J Fluid Mech 200:173–188 12.
Koh, J.C.Y. and Colony, R. (1974). Analysis of cooling effectiveness for porous material in a coolant passage. ASME J. Heat Transfer 96, 324-330.
Koh, J.C.Y., Stevens, R. (1975). Enhancement of cooling effectiveness by porous materials in coolant passage. Trans. ASME. J. Heat Transfer 97, 309-311.
Kuwahara, F., Shirota, M., Nakayama, A. (2001). A numerical study of interfacial convective heat transfer coefficient in two-equation model for convection in porous media, International Journal of Heat and Mass Transfer 44 1153–1159.
Lachenbruch, A. H., and J. H. Sass (1977). Heat flow in the United States and the thermal regime of the crust, in The Earth's Crust. Geophys. Monogr. Ser., vol. 20, edited by J. G Heacock, pp. 626-675, AGU, Washington, D.C.
Lantschner, N.( 2005) Casa Clima: Vivi in più. Bolzano. Edition Raetia.
Lauriat, G., and Vafai, K., (1991). Forced Convective Flow and Heat Transfer Through a Porous Medium Exposed to a Flat Plate or a Channel. Convective Heat and Mass Transfer in Porous Media, S. Kacac, B. Kilikis, F. A. Kulacki, and F. Arnic, eds., Kluwer Academic, Dordrecht, pp. 289–328.
Li, T. Q., Seymour, J. D., Powell, R. L., McCarthy, M. J., McCarthy, K. L., and Odberg, L., (1994). Visualization of Flow Patterns of Cellulous Fiber Suspensions by NMR Imaging. AIChE J., 40.
Liu, L.F., Davis, M.H. and Downing,S.(1996). Wave-induced boundary layer flows above and in a permeable bed. *J. Fluid Mech.* 325:195–218.
Lo Russo, S., Civita, M., V. (2009). Open-loop groundwater heat pumps development for large buildings: A case study. *Geothermics*, 38(3), pp.335–345.
Lu, W., Xiang, Y. (2012). Experiments and sensitivity analyses for heat transfer in a meter-scale regularity fracture granite model with water flow. Journal of Zhejiang University-SCIENCE A (Applied Physics & Engineering). 13 (12) 958-968.Martinez,

A. R., Roubinet, D., Tartakovsky, D. M. (2014). Analytical models of heat conduction in fractured rocks. J. Geophys. Res. Solid Earth, 119.
Lu, X., Ren, T., Gong, Y. (2009). Experimental investigation of thermal dispersion in saturated soils with one-dimensional water flow. Soil Science Society of America Journal, 73(6), 1912-1920.
Lubimova, E.A., (1969). Thermal history of the Earth. In: Hart, P.J. (Ed.), The Earth's Crust and Upper Mantle. AGU Monograph, 13, 63–77.
Lund JW, Freeston D., H., Boyd, T., L. (2010). Direct utilization of geothermal energy 2010 Worldwide Review. In: World Geothermal Conference. p. 25–9.
Lund, J. W., D. H. Freeston and T. L. Boyd (2005a). Worldwide Direct-Uses of Geothermal Energy 2005. Geothermics, Vol. 34, No. 6 (Dec.), Elsevier, Amsterdam, Netherlands, pp. 691-727.
Lund, J.W., Lienau, P.J., Lunis, B.C. (1998). Geothermal direct-use engineering and design guidebook, Geo-Heat Center, Klamath Falls, Oregon, 470pp.
Lund, J.W., Freeston, D.H. (2001). Worldwide direct uses of geothermal energy 2000. Geothermics, 30,29–68.
Lund, J., Sanner, B., Rybach, L., Curtis, G., Hellstrom, G.( 2004). Heat pumps e a world overview. GHC Bulletin.
Luzzini, F., (2012). L'industria principesca. Piero Ginori Conti e l'impianto geotermico di Larderello. Acque Sotterr. (Ital. J. Groundw.) 3, 97–98
Ma, R.C., Zheng, J.M., Zachara, and Tonkin, M. (2012). Utility of bromide and heat tracers for aquifer characterization affected by transient flow conditions, Water Resources Research, 48(June), doi: 10. 1029/2011WR011281.
Mands, E. and Sanner, B. (2001). In-situ-determination of underground thermal parameters. Proc. IGD Germany Bad Urach, Suppl. pp. 45-54.
Márquez, J.M.A., Bohórquez, M.Á.M, and. Melgar, S.G. (2016). Ground thermal diffusivity calculation by direct soil temperature measurement. Application to very low enthalpy geothermal energy systems, *Sensors (Switzerland)*, vol. 16, no. 3,
Masciopinto, C., Volpe, A., Palmiotta, D., Cherubini, C., A., (2010). Combined PHREEQC-2/parallel fracture model for the simulation of laminar/non-laminar flow

and contaminant transport with reactions Journal of contaminant hydrology 117 (1), 94-108.
Menichetti, M., Renzulli, A., Piscaglia, F., Blasi, A. (2001). Geotermia a bassa entalpia: temperatura e conducibilità termica del sottosuolo. In: AA.VV. e advanced manufacturing systems for geothermal energy, Energy Resources. Ancona. p. 39e80
Metzger, T., Didierjean, S., Maillet, D. (2004). Optimal experimental estimation of thermal dispersion coefficients in porous media.", International Journal of Heat and Mass Transfer, 47(14), 3341-3353.
Minkowycz, W.J., Haji-Sheikhb, A., Vafai K. (1999). On departure from local thermal equilibrium in porous media due to a rapidly changing heat source: the Sparrow number. International Journal of Heat and Mass Transfer 42 3373-3385.
Molina-Giraldo, N., Bayer, P., Blum, P. (2011). Evaluating the influence of thermal dispersion on temperature plumes from geothermal systems using analytical solutions. International Journal of Thermal Sciences, 50(7), 1223-1231.
Molson, J.W., E.O. Frind, and C.D. Palmer. (1992). Thermal energy storage in an unconfined aquifer 2. Model development, validation and application. Water Resources Research 28, no. 10: 2857–2867.
Moonen, P., Sluys, L. J., Carmeliet, J. (2011). A continuous - Discontinous Approach to simulate heat transfer in fractured media. Transp. Porous Med. 89 399-419.
Mori, Y., Hopmans, J.W., Mortensen, A.P., Kluitenberg, G.J. (2005). Estimation of vadose zone water flux from multi-functional heat pulse probe measurements. Soil Science Society of America Journal, 69(3), 599-606.
Nakayama, A., Kokudai, T., and Koyama, H. (1990). Non-Darcian Boundary layer Flow and Forced Convection Heat Transfer over a Flat Plate in A Saturated Porous Medium. ASME J. Heat Transfer, 112, 157-162, [251].
Neuville, A., Toussaint, R. and Schmittbuhl. J. (2010). Hydrothermal coupling in a self- affine rough fracture. PHYSICAL REVIEW E, 82:036317. XV, 4, 26, 134, 136, 154, 158, 168.

Nield, D. A., Porleana, D. C., and Lage, J. L., (1999). A Theoretical Study, with Experimental Verification of the Viscous Effect on the Forced Convection Through a Porous Medium Channel," ASME J. Heat Transfer, 121, 500-503.
Nield, D.A., Bejan, A. (2006). Convection in porous media. Springer.
Ogola, P.F.A., Davidsdottir, B., Fridleifsson, I.B. (2012). Potential contribution of geothermal energy to climate change adaptation: A case study of the arid and semi-arid eastern Baringo lowlands, Kenya, Renewable and Sustainable Energy Reviews,16, 6,4222-4246, Elsevier.
Okuyama, M. and Abe, Yutaka, (2000). Measurement of Velocity and Temperature Distributions in a Highly Porous Medium. J. of Porous Media, 3, No. 3, 193-206.
Omer, A., M. (Rev 2008) Ground-source heat pumps systems and applications. Renew Sustain Energy; 12:344–71.
Ondreka, J., Rusgen, M.I., Stoberb, I., Czurda, K. (2007). GIS-supported mapping of shallow geothermal potential of representative areas in south-western Germany possibilities and limitations. Renewable Energy, 32 (13):2186 e 200.
Özgümüş, T., Mobedi, M., Özkol, Ü. and Nakayama, A. (2013). Thermal Dispersion in Porous Media-A Review on the Experimental Studies for Packed Beds Appl. Mech. Rev 65(3), 031001 (Jul 15, 2013) doi: 10.1115/1.4024351
Poulikakos, D., and Renken, K.(1987). Forced Convection in a Channel Filled with Porous Medium, Including the Effects of Flow Inertia, Variable Porosity, and Brinkman Friction. ASME J. Heat Transfer, 109, 880-888.
Rafferty, K.A. (1995). Capital cost comparison of commercial ground-source heat pump systems. Oregon Institute of Technology, Geo Heat Center.
Rau, G. C., Andersen, M. S. and Acworth, R. I. (2012). Experimental investigation of the thermal dispersivity term and its significance in the heat transport equation for flow in sediments. *Water Resources Research*, vol. 48, no. 3, pp. 1–21.
Ryan, G.P. (1981). Equipment used in direct heat projects. In: Geothermal Resources Council Transactions, 5, 483–485.
Rybach, L. (2005). The advance of geothermal heat pumps world-wide. IEA Heat Pump Centre Newslett; 23:13–8.

Rybach, L. (2008). $CO_2$ emissions savings by GSHPs in Europe. Presented at the Workshop for Decision Makers on Direct Heating Use of Geothermal Resources in Asia. UNU-GTP, TBLRREM and TBGMED, Tianjin, China.

Saleh, F., Flipo, N., Habets, F., Ducharne, A., Oudin, L., Viennot, P. and Ledoux, E. (2011). Modeling the impact of in-stream water level fluctuations on stream-aquifer interactions at the regional scale. Journal of Hydrology, vol. 400, no. 3–4, pp. 490–500.

Sathe, S.B., Peck, R. E., and Tong, T. W., (1990). A numerical Analysis of Heat Transfer and Combustion in Porous Radiant Burners. Int. J. Heat Mass Transfer, 33, 1331-1338, 1990.Sathe.

Sauty, J., Gringarten, A., Menjoz, A., and Landel, P., (1982). Sensible energy storagein aquifers: 1. Theoretical study, 18(1), 245-252.

Sauty, J.P., Gringarten, A.C., Fabris, H., Thiery, D., Menjoz, A., and Landel, P.A. (1982). Sensible energy storage in aquifers 2. Field experiments and comparison with theoretical results. Water Resources Research; 18 (2) p. 253–265.

Sauty, J.P., A.C. Gringarten, H. Fabris, D. Thiery, A. Menjoz, and P.A. Landel. (1982a). Sensible energy storage in aquifers 2. Field experiments and comparison with theoretical results. Water Resources Research 18, no. 2: 253–265.

Schellschmidt, R., Sanner, B., Pester, S., Schulz,R. (2010). Geothermal energy use in Germany.

Schimschar, S., Blok, K., Boermans, T., Hermelink, A. (2011). Germany's path towards nearly zero-energy buildings—enabling the greenhouse gas mitigation potential in the building stock. Energy Policy; 39(6):3346–60.

Sederman, A. J., Johns, M. L., Alexander, P., and Gladden, L. F., (1997). Magnetic Resonance Imaging of Liquid flow and Pore Structure within Packed Beds ," Chem. Eng. Sci., 52.

Seyboth. K., Beurskens, L., Langniss., O., Sims, R.E.H. ( 2008). Recognising the potential for renewable energy heating and cooling. Energy Policy; 36:2460–3

Signorelli, S., Kohl, T. (2004). Regional ground surface temperature mapping from meteorological data. Global and Planetary Change; 40(3): 267e84.

Smith, L., Chapman, D.S. (1983). On the thermal effects of groundwater flow: 1.Regional scale systems. Journal of Geophysical Research, 88(B1), 593-608.
Sozen, M., and Vafai, K., (1901). Longitudinal Heat Dispertion in Porous Beds with Real-Gas Flow. J. Thermophysics Heat Transfer, 7, 153-157.
Tang, D.H., Frind, E.O., Sudicky, E.A. (1981). Contaminant transport in fractured porous media: analytical solutions for a single fractures. Water Resources Research, Vol. 17, No 3, pp. 555-564.
Tang, D.H., Frind, E.O., Sudicky, E.A. (1981). Contaminant transport in fractured porous media: analytical solutions for a single fractures. Water Resources Research 1981; 17 (3) p. 555-564.
Teng, H. and Zhao, T. S. (2000). An extension of Darcy's law to non-Stokes flow in porous media. Chemical Engineering Science, 55(14):2727 – 2735.
Thorsteinsson, H.H., Tester, J.W. (2010). Barriers and enablers to geothermal district heating system development in the United States. Energy Policy; 38: 803–13.
Tsang, C. F. and Neretnieks, I. (1998). Flow channeling in heterogeneous fractured rocks. Reviews of Geophysics, 36 257-298.
Turner, J.A. (1999). A realizable renewable energy future. Science; 285:687–9.
US DoE. (2004). Energy efficiency and renewable energy, Geothermal Technologies Program. U.S. Department of Energy.
Vafai, K. and Tien, C.L. (1981). Boundary and inertia effects on flow and heat transfer in porous media. International Journal of Heat and Mass Transfer, Vol 24 pp 195-203.
Vafai, K., and Kim, S. J., (1989). Forced Convection in a Channel Filled With a Porous Medium: An Exact Solution. ASME J. Heat Transfer, 111, pp. 1103–1106.
Vafai, K., and Tien, C. L., (1982). Boundary and Inertia Effects on Convective Mass Transfer in Porous Media. Int. J. Heat Mass Transf., 25, pp. 1183– 1190.
Vandenbohede, A., Louwyck, A., Lebbe, L. (2009). Conservative solute versus heat transport in porous media during push-pull tests. Transport in porous media, 76(2), 265-287.

Verein Deutscher Ingenieure (2001). Thermische Nutzung des UntergrundeseBlatt 2: erdgekoppelte Warmepumpenanlagen. Beuth Verlag. VDI-Richtlinie 4640.
Verhoogen, J., (1980). Temperatures within the Earth. In: Enegetics of the earth, National Academy of Sciences, Washington, DC, USA, pp. 29-66.
White, D. E., (1973). Characteristics of geothermal resources. In: Kruger, P. and Otte, C., eds., Geothermal Energy, Stanford University Press, Stanford, pp. 69-94.
Woodbury and Smith, Hopmans, J.W., Simunek, J. and Bristow, K.L. (2002). Indirect estimation of soil thermal properties and water flux using heat pulse probe measurements: Geometry and dispersion effects. Water Resources Research 38, no. 1: 1–14.
Wu, C.C., Hwang, G.J. (1998). Flow and heat transfer characteristics inside packed and fluidized beds. J. Heat Trans; 120 p. 667–673.
Yu Xing, C., (2011). Research on low carbon city development. Appl Mech Mater; 52–54:1953–7.
Zeng, Z., Grigg, R. (2006). A criterion for non-Darcy flow in porous media. Trans. Porous Media 63 57–69.
Zervos, A., Lins, C., Tesnière, L., (2011). Mapping Renewable, Energy Pathways Towards 2020. European Renewable Energy Council.
Zhu, K., Blum, P., Ferguson, G., Balke, K.D., Bayer, P. (2010). The geothermal potential of urban heat islands. Environ Res Lett, 5:044002.
Zouhri, L. and Lutz, P.(2010). A comparison of peak and plate electrodes in electrical resistivity tomography: Application to the chalky groundwater of the Beauvais aquifer (northern part of the Paris basin, France)," Hydrological Processes, vol. 24, no. 21, pp. 3040–3052.
Zouhri, L., Smaoui, H., Carlier, E. and Ouahsine A. (2009). Modelling of hydrodispersive processes in the fissured media by flux limiters schemes (Chalk aquifer, France)," Mathematical and Computer Modelling, vol. 50, no. 3–4, pp. 516–525.

CURRICULUM

**Education**

**PhD student** in Risk, environmental development, land and building (XXIX cycle) in Environmental Geoengineering, DICATECh - Politecnico di Bari, Via Edoardo Orabona, 4-70125 Bari, Italy

Topic of PHD: heat transport in fractured and porous media.

Tutor: Prof. Eng. Concetta I. Giasi.

**Master**: Technologies of depuration and disinfection of waste water for reuse in agriculture. (1500 h: 660h Training course, 770-company internship, 70 project work)

University of Bari, Department of Agro-Environmental and Territorial Sciences, Bari (Italy)

**Lead Auditor for management and quality systems (40 ore)**

Dasa-Ragister S.P.A., Bari (Italia)

**Training course RSPP (responsible for security Mod. C (24 ore)**

Plip srl (Certificato An.fo.s.), Andria (Italia)

**Competent technician in environmental acoustics** (240 hours)

**M. Sc.,** Enviromental engineering (17/04/2012) (110/110)

Thesis: "Study of the performance of a low enthalpy geothermal plant for summer cooling".

**Erasmus,** RWTH, Aachen (Germany)

Exams: Municipal waste management (management of municipal waste), Plannig of waste water treatment plants (designing of wastewater treatments systems), Trasporting planning (Transportation Planning), Introduction to CAD (introduction to CAD).

German course A1 basis.

**B. Sc.,** Enviromental engineering **(23/07/2009) (105/110)**

Thesis: " Environmental aspects of the territory of Barletta: interconnection between the groundwater and the river Ofanto "

**Research and Work experience**

**Project Manager, Environmental Engineer,** in Biotec, Molfetta(Bari), Italy

**Environmental Engineer**

Patto territoriale nord barese Ofantino, Km. 24.500 Via Andria, Barletta, BT 76121, 76121

Finnovaregio, Rue de la Science 14b, First Floor, Brussels 1040, BE

EPA, European projet Association asbl , square Marie-Louise, 2 1000 Bruxelles, Belgium. Search for innovative projects in the environmental field: energy, water treatment and recovery, biomass energy. Looking for partnerships for environmental projects in Europe with universities of other nationalities. Use of European platforms for sharing innovative projects EPA (European project association).

**Publications**

N. Pastore , C. Cherubini , C. I. Giasi , N. M. Allegretti , J. M. Redondo , A. M. Tarquis Experimental study of heat transport in fractured network. Energy Procedia · Volume 76, August 2015, Pages 273–281.

N. Pastore, C. Cherubini, C. I. Giasi, N. M. Allegretti (2016). Experimental investigations of heat transport dynamics in a 1d porous medium column. Energy Procedia

N. Pastore, C. Cherubini, C. I. Giasi, N. M. Allegretti (2017). Laboratory experimental investigation of heat transport in fractured media. NPG (Nonlinear Processes in Geophysics)

C. Cherubini, N. Pastore, C. I. Giasi, N. M. Allegretti. (2016). Groundwater recharge dynamics in unsaturated fractured chalk : a case study.18, p.10145.( waiting to Be Published)

Articles almost complete

N. Pastore, C. Cherubini, C. I. Giasi, N. M. Allegretti (2016). Experimental investigations of heat transport dynamics in a column filled by different grain size of porous media.

**Conference Acts**

N. Pastore, C. Cherubini, C. I. Giasi, N. M. Allegretti., (2015). Experimental Study of Heat Transport in Fractured Network. *Energy Procedia*, 76, pp.273–281. Available at: http://linkinghub.elsevier.com/retrieve/pii/S1876610215016367.

N. Pastore, C. Cherubini, C. I. Giasi, N. M. Allegretti., (2016). Experimental investigations of heat transport dynamics in a 1D porous medium column. , 18, p.11145.

C. Cherubini, N. Pastore, C. I. Giasi, N. M. Allegretti., (2016). Groundwater recharge dynamics in unsaturated fractured chalk : a case study.18, p.10145.

**Other academic experiences**

Supervisor for some Thesis of degree in B. Sc. Environmental Engineering:

1) "Studio delle potenzialità e limitazioni dei test di risposta termica per lo sfruttamento dei sistemi geotermici a bassa entalpia"

2) ''Descrizione e valutazione degli aspetti idro geomorfologici e ambientali del territorio compreso tra Ceglie e Carbonara"

3) "Studio delle performance di fito-tecnologie per la bonifica di siti contaminati e depurazione delle acque"

Teaching assistant in the following courses of study of Environmental Engineering:

- Geologia Applicata alla difesa ambientale (B.Sc)
- Geoigegneria Ambientale (M.Sc)

Geophysical Research Abstracts
Vol. 17, EGU2015-2279, 2015
EGU General Assembly 2015


# Experimental Study of Heat Transport in Fractured Network

Nicola Pastore (1), Claudia Cherubini (2), Concetta I. Giasi (1), Nicoletta M. Allegretti (1), Jose M. Redondo (4,5), Ana Maria Tarquis (3,4)

(1) Polytechnic of Bari, DICATECh, Bari, Italy (nicola.pastore@poliba.it), (2) Hydrise, LaSalle Beauvais, France, (3) CEIGRAM, Univ. Politecnica Madrid, Spain, (4) PELNoT, ERCOFTAC, Instituto Plridisciplinar, Madrid, Spain, (5) Dept. Fisica Aplicada, Univ. Politecnica de Cataluña, Barcelona, Spain

Fractured rocks play an important role in transport of natural resources or contaminants transport through subsurface systems. In recent years, interest has grown in investigating heat transport by means of tracer tests, driven by the important current development of geothermal applications. In literature different methods are available for predicting thermal breakthrough in fractured reservoirs based on the information coming from tracer tests. Geothermal energy is one of the largest sources of renewable energies that are extracted from the earth. The growing interest in this new energy source has stimulated attempts to develop methods and technologies for extracting energy also from ground resource at low temperature. An example is the exploitation of low enthalpy geothermal energy that can be obtained at any place with the aid of ground-source heat pump system from the soil, rock and groundwater. In such geothermal systems the fluid movement and thermal behavior in the fractured porous media is very important and critical. Existing theory of fluid flow and heat transport through porous media is of limited usefulness when applied to fractured rocks. Many field and laboratory tracer tests in fractured media show that fracture –matrix exchange is more significant for heat than mass tracers, thus thermal breakthrough curves (BTCs) are strongly controlled by matrix thermal diffusivity. In this study the behaviour of heat transport in a fractured network at bench scale has been investigated. Heat tracer tests on an artificially created fractured rock sample have been carried out.
The observed thermal BTCs obtained with six thermocouple probes located at different locations in the fractured medium have been modeled with the Explicit Network Model (ENM) based an adaptation of Tang's solution for solute transport in a semi-infinite single fracture embedded in a porous matrix. The ENM model is able to represent the behavior of observed heat transport except where the configuration of the fracture network gives rise to a fracture block characterized by a limited capability to store heat. As a consequence the observed BTCs show a greater penetration of heat in the system than ENM model. Furthermore the results show that heat transport in fractures is dominated also by thermal dispersion attributable to flow channeling inside them. The comparison with previous studies on solute transport carried out in fractured media shows that thermal BTCs are characterized by a more enhanced early arrival and long tailing than solute BTCs.
The residence time for heat transport is an order of magnitude higher than for solute transport experiments.
The results show that it is not possible to neglect the dispersion factor as well as the interaction between matrix and fractures in the study of heat transport in fractured media.

Available online at www.sciencedirect.com

ScienceDirect

Energy Procedia 76 (2015) 273 – 281

Energy Procedia

European Geosciences Union General Assembly 2015, EGU

Division Energy, Resources & Environment, ERE

# Experimental study of heat transport in fractured network

N. Pastore[a]*, C. Cherubini[b], C. I. Giasi[a], N. M. Allegretti[a,b], J. M. Redondo[d,e], A. M. Tarquis[c,d]

[a]*DICATECh - Politecnico di Bari, via E. Orabona, 70125 Bari, ITALY*
[b]*Hydrise, Institut Polytechnique LaSalle Beauvais, 19 rue Pierre Waguet, 60026 Beauvais Cedex, France*
[c]*CEIGRAM, Universitad Politécnica de Madrid - iudad Universitaria Madrid, 28040 Spain*
[d]*PELNoT, ERCOFTAC, Instituto Pluridisciplinar, Paseo Juan XXIII, 1, 28040, Madrid, Spain*
[e]*Dept. Fisica Aplicada, Univ. Politecnica de Cataluña, 08034, Barcelona, Spain*

**Abstract**

Fractured rocks play an important role in transport of natural resources through subsurface systems. In recent years, interest has grown in investigating heat transport by means of tracer tests, driven by the important current development of geothermal applications. Many field and laboratory tracer tests in fractured media show that fracture - matrix exchange is more significant for heat than mass tracers, thus thermal breakthrough curves are strongly controlled by matrix thermal diffusivity. In this study, the behaviour of heat transport in a fractured network, at bench laboratory scale, has been investigated.


Peer-review under responsibility of the GFZ German Research Centre for Geosciences

*Keywords:* heat transport; fractured rock, physical model

## 1. Introduction

The aim of this paper is investigate the behaviour of heat transport in fractured media. The laws that govern the heat transport in fractured media are still little known and there are not many experiences in literature about these

* Corresponding author. Tel.: +39-080-596-3371 ; fax: +39-080-596-3414 .
*E-mail address:* nicola.pastore@poliba.it


Peer-review under responsibility of the GFZ German Research Centre for Geosciences
doi:10.1016/j.egypro.2015.07.860

phenomena. Existing theory of fluid flow and heat transport through porous media is of limited usefulness when applied to fractured rocks.

**Nomenclature**

| | |
|---|---|
| $a$ | linear coefficient of Forchheimer's law ($TL^{-3}$) |
| $b$ | inertial coefficient of Forchheimer's law ($T^2L^{-6}$) |
| $BTC$ | thermal breakthrough curve |
| C | conductance term ($L^2T^{-1}$) |
| $C_w$ | specific heat capacity of the water ($L^2T^2K^{-1}$) |
| $C_m$ | specific heat capacity of the matrix ($L^2T^2K^{-1}$) |
| $d$ | distance along $z$ axis from fracture – matrix interface (L) |
| $\delta$ | thickness of boundary layer (L) |
| $ENM$ | explicit network model |
| $D_f$ | thermal dispersion coefficient ($L^2T^{-1}$) |
| $h$ | hydraulic head (L) |
| $j$ | single vertical fracture index |
| $k_e$ | effective thermal conductivity of the matrix ($MLT^{-3}K^{-1}$) |
| $L$ | length of single fracture or characteristic length of fracture network (L) |
| $L^{-1}$ | inverse Laplace transform operator |
| $n_f$ | number of single fracture |
| $N_p$ | number of paths |
| $P_Q$ | probability of water distribution of shorter parallel branch |
| $PDF$ | probability of density function of residence time |
| $Q$ | flow rate ($L^3T^{-3}$) |
| $Q_0$ | injection flow rate ($L^3T^{-3}$) |
| $\rho_w$ | density of water ($ML^{-3}$) |
| $\rho_m$ | density of the matrix ($ML^{-3}$) |
| Re | Reynolds number (-) |
| $s$ | Laplace parameter (-) |
| $SF$ | vertical single fracture |
| $t_u$ | convective time scale (T) |
| $t_d$ | dispersion time scale (T) |
| $t_e$ | transfer time scale (T) |
| $T_f$ | fracture temperature (K) |
| $T_m$ | matrix temperature (K) |
| $T_0$ | initial temperature (K) |
| $T_{inj}$ | injection temperature (K) |
| $u_f$ | thermal convective velocity ($LT^{-1}$) |
| $x$ | coordinate parallel to the axis of vertical single fracture |
| $w_f$ | fracture aperture (L) |
| $z$ | coordinate perpendicular to the fracture axis (L) |
| $*$ | convolution operator |

Fractured rocks play an important role in transport of natural resources or contaminants transport through subsurface systems. In recent years, interest has grown in investigating heat transport by means of tracer tests, driven by the important current development of geothermal applications.

In particular way low enthalpy geothermal resource is an optimal renewable resource because is always available and it is possible used for the heating and cooling of private buildings, industries, public buildings, representing the largest share of world energy consumption.

The study of heat transport in fractured aquifers, which represent the 75% of the earth's surface, is crucial in order to understand the possible advantages and disadvantages resulting from the use of aquifers as low enthalpy geothermal resources.

A laboratory study, at bench scale, has been conducted on an artificially created fractured limestone block of parallelepiped shape. Some holes have been drilled on the block, inside which the temperature probe has been inserted. The observed thermal *BTCs* have been modeled with the explicit network model (*ENM*) based on an adaptation of Tang's solution, developed for solute transport in a semi – infinite single fracture embedded in a porous matrix.

Characteristic transport time scale has been compared in order to evaluate the dominant mechanism on heat propagation in fractured media.

## 2. Theoretical background

### *2.1. Flow and heat transport in single fractures*

A fracture can be depicted as two rough surfaces in contact. Cross sectional solid areas representing asperities in contact are similar to the grains of porous media. It is therefore possible to apply the general equations describing flow and heat transport in porous as well as in fractured media.

In most studies examining hydrodynamic processes in fractured media, it is assumed that flow is described by Darcy's law, which expresses a linear relationship between pressure gradient and flow rate [1]. Darcy's law has been demonstrated to be valid at low flow regimes ($Re < 1$). For $Re > 1$, a nonlinear flow behaviour is likely to occur [2].

In the literature different laws are reported that account for the nonlinear relationship between velocity and pressure gradient. In case of higher Reynolds numbers ($Re >> 1$) the pressure losses pass to a strong inertial regime, described by the Forchheimer's law [3]. The relationship between flow rate and hydraulic head gradient can be written as:

$$-\frac{dh}{dx} = a \cdot Q + b \cdot Q^2 \tag{1}$$

A *SF* is subject to fluid flow with an averaged velocity, heat will migrate by convection and diffusion phenomena along the fracture. Furthermore they will also undergo dispersion caused by small scale variations in fracture aperture.

One dimensional advective - dispersive transport along the fracture axis, as well as one – dimensional diffusion in the rock matrix, in direction perpendicular to the axis of the fracture is considered. Assuming that density and heat capacity are constant in time, conservation equation can be written for heat transport in a semi - infinite fracture as:

$$\frac{\partial T_f}{\partial t} + u_f \frac{\partial T_f}{\partial x} = \frac{\partial}{\partial x}\left( D_f \frac{\partial T_f}{\partial x} \right) - \frac{k_e}{\rho_w C_w \delta} \frac{\partial T_m}{\partial z}\bigg|_{z=w_f/2} \tag{2}$$

Whereas the conservation equation for heat transport in the matrix is:

$$\rho_m C_m \frac{\partial T_m}{\partial t} = k_e \frac{\partial^2 T_m}{\partial z^2} \tag{3}$$

[4] and [5] propose a thermal dispersion coefficient similar to the solute transport, where the thermal dispersion term is related to the heterogeneity and it is a linear function of velocity.

[6] presents a solution for solute transport in semi – infinite single fracture surrounded by porous matrix for a constant concentration at the fracture inlet ($x = 0$) and for initial concentration equal to zero everywhere. They give the expression for the solute concentration in the fracture and in the matrix as function of time. On the basis of this analytical solution, the *PDF* in the single fracture in the Laplace space can be written as:

$$\overline{\Gamma}(s) = \exp(vL)\exp\left[-vL\left\{1+\beta^2\left(\frac{s^{1/2}}{A}+s\right)\right\}^{1/2}\right] \tag{4}$$

Whereas the *PDF* in the matrix in the Laplace space assumes the following expression:

$$\overline{\Gamma}'(s) = \overline{\Gamma}(s)\cdot\exp\left(-Bs^{1/2}d\right) \tag{5}$$

The coefficients $v$, $A$, $\beta^2$ and $B$ assume the following expressions:

$$v = \frac{u_f}{2D_f};\ \beta^2 = \frac{4D_f}{u_f};\ B = \frac{1}{\sqrt{D_e}} \tag{6}$$

$$A = \frac{\delta}{\sqrt{\theta D_e}};\ \ \theta = \frac{\rho_m C_m}{\rho_f C_f},\ \ D_e = \frac{k_e}{\rho_w C_w} \tag{7}$$

*2.2. Explicit network model*

A vertical *SF* can be viewed as one dimensional pipe element in which head loss is described by Forchheimer's law. The conductance to flow of the generic *SF j* can be written as:

$$C_j = \left[L_j\left(a_j + b_j Q_j\right)\right]^{-1} \tag{8}$$

The flow field in the fracture network can be determined in analytical way through the application of the first and the second Kirchhoff's laws. The flow rate crossing generic *SF j* can be obtained as the product between the total discharge flow $\Sigma Q_i$, evaluated for the fracture intersection located at the inlet bond of the *SF j*, and the probability of flow distribution of *SF j* $P_{Q,j}$. The latter is equal to the ratio between the conductance to flow of *SF j* and the sum of conductance to flow of each discharge *SF* connected at the inlet bond of *SF j*, as well as $P_{Q,j}$ should be proportional to the relative discharge flow rates:

$$P_{Q,j} = \frac{C_j}{\sum_{i=1}^{n} C_i} = \frac{Q_j}{\sum_{i=1}^{n} Q_i} \tag{9}$$

The *PDF* at a generic node can be obtained as the summation of *PDFs* of each elementary path that reach the node. The latter is equal to the convolution product of the *PDFs* of each single fracture along the elementary path.

The *BTC* that describe the temperature in the fracture at the generic node of the fracture network is:

$$T_f(t) = T_0 + T_{inj}(t) * L^{-1}\left[\sum_{i=1}^{N_p}\prod_{j=1}^{n_{f,i}} P_{Q,j}\bar{\Gamma}_j(s)\right] \tag{10}$$

Whereas the temperature in the matrix evaluated at distance $d$ along $z$ axis from fracture – matrix interface at the generic node is:

$$T_m(t) = T_0 + T_{inj}(t) * L^{-1}\left\{\left[\sum_{i=1}^{N_p}\prod_{j=1}^{n_{f,i}} P_{Q,j}\bar{\Gamma}_j(s)\right]\exp\left(-Bs^{1/2}d\right)\right\} \tag{11}$$

## 3. Material and methods

### *3.1. Experimental setup*

The experiments have been performed on the laboratory physical model used to study flow and solute transport at bench scale [7, 8, 9, 10, 11]. In Fig. 1 is reported the schematic diagram of the experimental setup.

In order to analyze the heat transport dynamics in the fractured sample, some modifications have been made. The same sealed fractured limestone block with parallelepiped shape (0.6×0.4×0.08 $m^3$), described in previous work, has been used. A hole of 2 mm diameter has been opened up to the depth of 1 cm along the center of some discontinuities by means of a percussion drill. Inside of each opened hole a thermocouple has been placed and welded to the block by means of rapid – hardening epoxy resin. Furthermore at the inlet and the outlet of the selected path other two thermocouples have been placed. All thermocouples have been connected to a TC-08 Thermocouple Data Logger (Pico Technology) and a sampling rate of 1 second has been used.

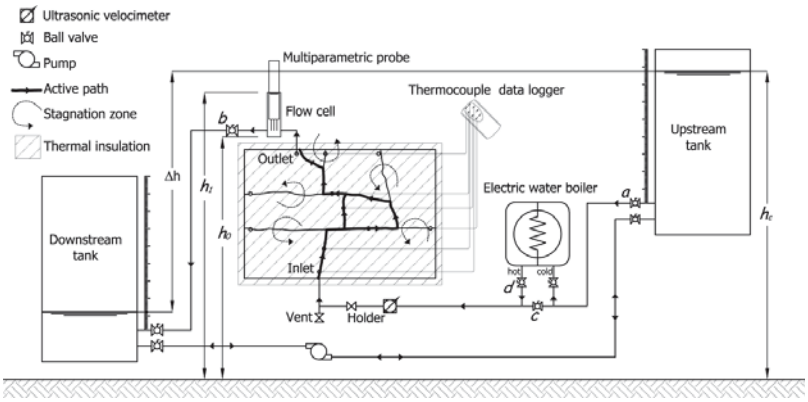


Fig. 1. Schematic diagram of the experimental setup.

The limestone block has been thermally insulated using extruded polystyrene panel with thermal conductivity equal to 0.034 $Wm^{-1}K^{-1}$ and thickness 0.05 m. Finally the sample has been connected to a hydraulic circuit. Water inside the sample flows according to the hydraulic head difference between the upstream tank connected to the inlet port and the downstream tank connected to the outlet port. The instantaneous flow rate that flows across the block is measured by an ultrasonic velocimeter (DOP3000 by Signal Processing). Water that enters into the sample is heated by an electric water boiler with a volume of $10^{-2}$ $m^3$. In correspondence of outlet port there is a flow cell in which a multiparametric probe is positioned for instantaneous measurement of pressure (dbar), temperature (°C) and electric conductivity (μS $cm^{-1}$).

### 3.2. Temperature tracer tests

The study of heat transport dynamics has been carried out through a selected path. Initially a hydraulic head difference between the upstream tank and the downstream tank is imposed. At time $t = 0$ the valve "*a*" is closed and hydrostatic head inside the block is equal to the downstream tank. At time $t = 10$ s the valve "*a*" is opened while at time $t = 60$ s the valve "*d*" is opened and in the same time the valve "*c*" is closed. In this manner, a step temperature function is imposed in correspondence of the inlet port $T_{inj}$ (t) and it is measured by the thermocouple inside the inlet port. At time $t = 1000$ s the valve "*d*" and the valve "*c*" are reclosed and reopened respectively. For different flow rates *BTCs* curves have been recorded at the inlet and output ports and inside the sample in correspondence of some discontinuities.

## 4. Results and discussion

The Forchheimer parameters representative of the whole fracture network were derived in [11]. The estimated Forchheimer parameters are respectively $a = 7.345\times10^{4}$ $sm^{-3}$ and $b = 11.65\times10^{9}$ $s^{2}m^{-6}$. The critical flow rate corresponding to the ratio between the linear and nonlinear term equal to the unit in which the inertial force dominate viscous one is equal to $Q_{crit} = 6.30\times10^{-6}$ $m^{3}s^{-1}$. The probability of water distribution of each *SF* is equal to one except for the parallel branches. The probability of water distribution of the shorter parallel branch $P_Q$ decreases as the injection flow rate increases because, due to the nonlinear nature of flow, the conductance term of the shorter parallel branch decreases faster than the conductance term of the longer parallel branch.

The observed *BTCs* have been fitted by *ENM* based on Tang's solution. The parameters $u_f$, $D_f$, $D_e$ and $\delta$ are supposed equal for the all branches except for the parallel branches in which $u_f$ and $D_f$ become $u_f P_Q$ and $D_f P_Q$ for the shorter branch and $u_f (1 - P_Q)$ and $D_f (1 - P_Q)$ for the longer branch. The thermal *BTC* in correspondence of the outlet port is fitted using equation (10), whereas the thermal *BTCs* at the position inside the block is fitted by equation (11) using a distance along z - axis from fracture - matrix interface $d$ equal to the dimension of thermocouple (2 mm).

Fig. 2 shows the fitting results of thermal *BTCs* at different positions along the fracture network for the injection flow rate equal to $Q_0 = 4.03\times10^{-6}$ $m^{3}/s$. The fitting was satisfactory, except for the positions 2 and 3 in which the *ENM* model underestimates the observed thermal *BTCs* curves. The *ENM* model results able to represent the behaviour of observed heat transport except where the configuration of the fracture network gives rise to a fracture block characterized by a limited capability to store heat. In this configuration, the Tang's solution fails to model the observed thermal transport in correspondence of parallel branch, because the porous matrix surrounding the single fracture cannot be considered infinite in size. The thermal *BTCs* in parallel branches are influenced each other. As a consequence the observed *BTCs* show a lower heat dissipation then *ENM* model. Initially the hypothesis of infinite porous matrix is still valid, the *ENM* model reaches observed *BTCs*. Subsequently the observed *BTCs* begin to influenced each other giving rise to lower heat dissipation, resulting that the *ENM* model underestimate the observed *BTCs*.

According to [12] the following three characteristics transport time scale can be defined as:

$$t_u = \frac{L}{u_f};\ t_d = \frac{L^2}{D_f};\ t_e = \frac{\delta^2}{\theta D_e} \tag{12}$$

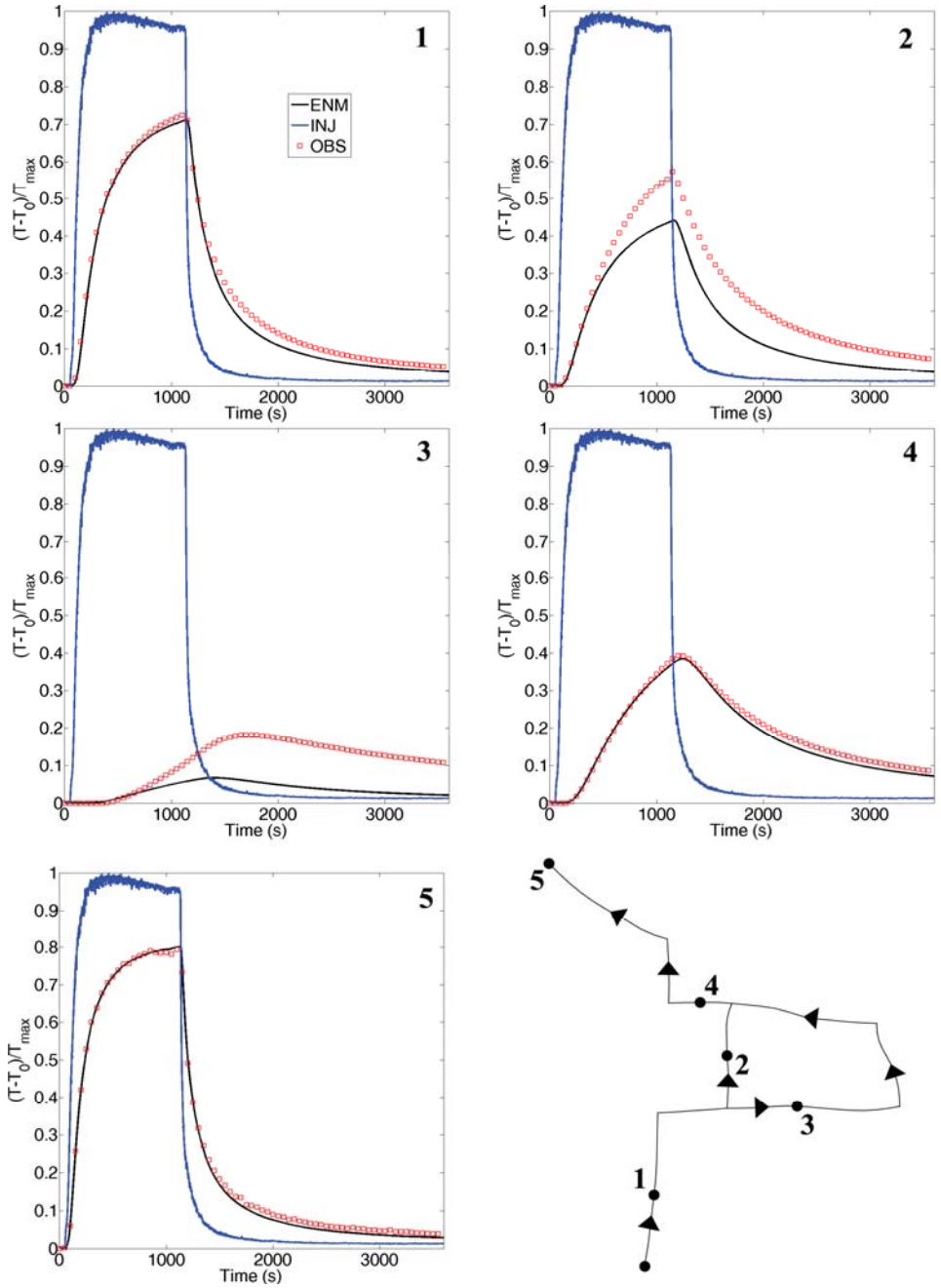


Fig. 2. Fitting of BTCs at different positions in the fracture network using ENM with Tang solution for heat transport with injection flow rate equal to $Q_0 = 4.03 \times 10^{-6}$ m$^3$/s.

Table 1 shows the estimated transport time scale at different injection flow rates.

According to previous works the characteristic length of fractured media is equal to $L$ = 0.601 m. Convective transport time scale is the same order of magnitude of the exchange time scale, the impact of the fracture matrix exchange is very strong giving rise to a strong retardation effect on the convective velocity.

Table 1. Estimated values of parameters for ENM with Tang solution at different injection flow rates.

| $Q_0$ ($m^3s^{-1}$)×$10^{-6}$ | $t_u$ (s) | $t_d$ (s) | $t_e$ (s) |
|---|---|---|---|
| 1.84 | 240 | 182 | 297 |
| 2.32 | 251 | 190 | 240 |
| 2.68 | 234 | 198 | 273 |
| 2.85 | 245 | 178 | 256 |
| 3.00 | 231 | 157 | 317 |
| 4.00 | 226 | 54 | 879 |
| 4.22 | 143 | 40 | 349 |
| 7.06 | 72 | 35 | 318 |
| 7.96 | 61 | 19 | 164 |
| 8.97 | 44 | 15 | 115 |
| 12.36 | 53 | 16 | 352 |
| 12.59 | 40 | 14 | 164 |

The thermal dispersion plays an important role on heat transport dominating on convective transport, although the injection flow rate is relatively high. Infact, dispersion time scale is always less than convective time scale. Furthermore, dispersion time scale and exchange time scale are comparable. However, the latter is always less than the former.

The comparison with previous studies on solute transport carried out in fractured media shows that thermal *BTCs* are characterized by a more enhanced early arrival and long tailing than solute *BTCs*. The residence time $t_m$ for heat transport is an order of magnitude higher than for solute transport experiments. Fig. 2 shows the comparison of the observed residence times versus the injection flow rates both solute and heat transport. These results highlight that the heat transport is more retarted than mass transport.

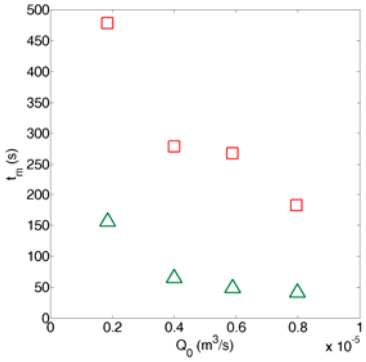


Fig. 2. Comparison between the residence time $t_m$ of heat transport (red square) and solute transport (green triangle) at different injection flow rate $Q_0$.

## 5. Conclusion

Several features on the behaviour of heat transport have been observed by the conducted experiments and their interpretation.

Heat transport dynamics have been fitted by the explicit network model with Tang's solution. *ENM* model exhibits a satisfactory fitting except in correspondence of the parallel branch in which the porous matrix surrounding the single fracture cannot be considered infinite in size. The Parallel branches are influenced by each other as a consequence the observed *BTCs* show lower heat dissipation than *ENM* model.

Heat transfer time scale is comparable with convective time scale because the dual porosity behaviour is very strong, giving rise to a delay on heat propagation in fracture network.

Thermal *BTCs* are characterized by a more enhanced early arrival and long tailing than solute *BTCs* observed in previous experiments. The residence time of heat transport is an order of magnitude higher than the residence time of solute transport.

Thermal dispersion time scale is always less than both thermal convective time scale and thermal exchange time scale. These results confirm that thermal dispersion plays an important role on heat transport and its effect cannot be neglected.

The results encourage further experimental work to increase the knowledge of the key parameters that govern the heat propagation in fractured media, and therefore developing the best strategies for installation of devices for heat recovery and heat dissipation in fractured media.

## References

[1] Cherubini C, Pastore N. Modeling contaminant propagation in a fractured and karstic aquifer. Fresenius Environmental Bulletin 2000; 19 (9) p. 1788-1794.

[2] Cherubini C, Giasi CI, Pastore N. Fluid flow modeling of a coastal fractured karstic aquifer by means of a lumped parameter approach. Environmental Earth Sciences 2013; 70 (5) p. 2055-2060.

[3] Forchheimer P. Wasserbewegung durch Boden. Z. Ver. Dtsch. Ing. 1901; 45 p. 1781-1788.

[4] Sauty JP, Gringarten AC, Fabris H, Thiery D, Menjoz A, and Landel PA. Sensible energy storage in aquifers 2. Field experiments and comparison with theoretical results. Water Resources Research 1982; 18 (2) p. 253–265.

[5] deMarsily G. Quantitative Hydrogeology: Groundwater Hydrology for Engineers. Academic Press; 1986.

[6] Tang DH, Frind EO, Sudicky EA. Contaminant transport in fractured porous media: analytical solutions for a single fractures. Water Resources Research 1981; 17 (3) p. 555-564.

[7] Cherubini C, Giasi CI, Pastore N. Bench scale laboratory tests to analyze non-linear flow in fractured media. Hydrology and Earth System Sciences 2012; 16 p. 2511-2622.

[8] Cherubini C, Giasi CI, Pastore N. Evidence of non-Darcy flow and non-Fickian transport in fractured media at laboratory scale. Hydrology and Earth System Sciences 2013; 17 p. 2599-2611.

[9] Cherubini C, Giasi CI, Pastore N. Laboratory tests to analyze solute transport behaviour in fractured media. Rendiconti Online Società Geologica Italiana 2013; 24 p. 55-57.

[10] Cherubini C, Giasi CI, Pastore N. Un modello fisico di laboratorio per analizzare dinamiche di flusso e trasporto in un campione di roccia fratturata a scala di banco [A laboratory physical model to analyse flow and transport processes in fractured rock sample at bench scale level]. Italian Journal Engineering Geology and Environment 2013; (1) p. 19-32.

[11] Cherubini C, Giasi CI, Pastore N. On the reliability of analytical models to predict solute transport in a fracture network. Hydrology and Earth System Sciences 2014; 18 p. 2359-2374.

[12] Kocabas I. Geothermal reservoir characterization via thermal injection backflow and interwork tracer testing. Geothermics 2005; 34 p. 27-46.

Geophysical Research Abstracts
Vol. 18, EGU2016-11145, 2016
EGU General Assembly 2016


# Experimental investigations of heat transport dynamics in a 1D porous medium column

Nicola Pastore (1), Claudia Cherubini (2), Concetta I Giasi (1), and Nicoletta Maria Allegretti (1)

(1) Polytechnic of Bari, DICATECh, Bari, Italy (nicola.pastore@poliba.it), (2) The University of Quensland, Australia (c.cherubini@uq.edu.au)

A laboratory physical model has been set up to analyse the forced convective flow and the related heat transport dynamics through a 1d porous medium column. In particular, the experiments regard the observation of thermal breakthrough curves obtained through a continuous flow injection in correspondence of eight thermocouple positioned uniformly along a thermally isolated column of porous medium.
The experiment has been conducted for different flow rates in order to investigate the critical issues regarding heat transport phenomena such as the influence of non-linear flow regime, the relationship between the thermal dispersion with the flow velocity and the validity of the local thermal equilibrium assumption between the fluid and solid phase. The results emphasize the magnitude of the errors of the commonly used assumptions in the numerical modelling of heat transport.

Geophysical Research Abstracts
Vol. 18, EGU2016-10145, 2016
EGU General Assembly 2016


# Groundwater recharge dynamics in unsaturated fractured chalk: a case study

Claudia Cherubini (1), Nicola Pastore (2), Concetta I Giasi (2), and Nicolaetta M Allegretti (2)
(1) The University of Queensland, School of Civil Engineering , (2) DICATECh Politecnico di Bari

The heterogeneity of the unsaturated zone controls its hydraulic response to rainfall and the extent to which pollutants are delayed or attenuated before reaching groundwater. It plays therefore a very important role in the recharge of aquifers and the transfer of pollutants because of the presence of temporary storage zones and preferential flows. A better knowledge of the physical processes in the unsaturated zone would allow an improved assessment of the natural recharge in a heterogeneous aquifer and of its vulnerability to surface-applied pollution.
The case study regards the role of the thick unsaturated zone of the Cretaceous chalk aquifer in Picardy (North of France) that controls the hydraulic response to rainfall. In the North Paris Basin, much of the recharge must pass through a regional chalk bed that is composed of a porous matrix with embedded fractures.
Different types of conceptual models have been formulated to explain infiltration and recharge processes in the unsaturated fractured rock.
The present study analyses the episodic recharge in fractured Chalk aquifer using the kinematic diffusion theory to predict water table fluctuation in response to rainfall.
From an analysis of the data, there is the evidence of 1) a seasonal behavior characterized by a constant increase in the water level during the winter/spring period and a recession period, 2) a series of episodic behaviors during the summer/autumn.
Kinematic diffusion models are useful for predict preferential fluxes and dynamic conditions. The presented approach conceptualizes the unsaturated flow as a combination of 1) diffusive flow refers to the idealized portion of the pore space of the medium within the flow rate is driven essentially by local gradient of potential; 2) preferential flow by which water moves across macroscopic distances through conduits of macropore length.

Available online at www.sciencedirect.com

ScienceDirect

Energy Procedia 97 (2016) 233 – 239

Energy Procedia

European Geosciences Union General Assembly 2016, EGU
Division Energy, Resources & Environment, ERE

# Experimental investigations of heat transport dynamics in a 1d porous medium column

N. Pastore[a]*, C. Cherubini[b], C. I. Giasi[a], N. M. Allegretti[a]

[a]*DICATECh - Politecnico di Bari, via E. Orabona, 70125 Bari, ITALY*
[b] *Department of Mechanical, Aerospace & Civil Engineering - Brunel University London, Uxbridge, UB8 3PH, UNITED KINGDOM*

**Abstract**

The present study involves the experimental investigation of heat transport due to the forced convective flow through a thermally isolated porous medium column.
The experiments regard the observation of thermal breakthrough curves obtained through a hot flow injection in correspondence of two thermocouples positioned along a thermally isolated column of porous medium. The experiment has been carried out for three flow rates in order to investigate the critical issues regarding heat transport phenomena such as the relationship between the thermal dispersion with the flow velocity and the validity of the local thermal equilibrium assumption between the fluid and solid phase.


Peer-review under responsibility of the organizing committee of the General Assembly of the European Geosciences Union (EGU)

*Keywords:* heat, thermal equilibirum, porous medium, Damköhler number

## 1. Introduction

In recent years, considerable interest has been given to the study of heat transfer through porous media because of its wide applications in many fields like crude oil extractions, petroleum reservoirs, agricultural engineering, coal

* Corresponding author. Tel.: +39-080-596-3371; fax: +39-080-596-3414.
*E-mail address:* nicola.pastore@poliba.it


Peer-review under responsibility of the organizing committee of the General Assembly of the European Geosciences Union (EGU)
doi:10.1016/j.egypro.2016.10.063

combustors, solar collectors, electronic cooling, energy storage units and nuclear waste repositories [1]. The study of heat transfer phenomena in the subsurface is also relevant for geothermal energy extraction.

**Nomenclature**

| | |
|---|---|
| $\alpha_L$ | Longitudinal dispersion coefficient (L) |
| $c_f$ | Specific heat capacity of the fluid phase ($L^2T^2K^{-1}$) |
| $c_s$ | Specific heat capacity of the solid phase ($L^2T^2K^{-1}$) |
| $d_p$ | Average particle diameter (L) |
| $Da$ | Damköhler number (-) |
| $D_0$ | Thermal diffusion ($L^2T^{-1}$) |
| $D_{eff}$ | Effective thermal dispersion ($L^2T^{-1}$) |
| $k_{eff}$ | Effective thermal conductivity of the fluid phase ($MLT^{-3}K^{-1}$) |
| $k_s$ | Thermal conductivity of the solid phase ($MLT^{-3}K^{-1}$) |
| $h^*$ | Convective heat transfer coefficient ($MT^{-3}K^{-1}$) |
| $n$ | Porosity (-) |
| $Nu$ | Nusselt number (-) |
| $\mu$ | Viscosity ($MT^{-1}L^{-1}$) |
| $L$ | Characteristic length (L) |
| $q$ | Specific discharge ($LT^{-1}$) |
| $q_{fs}$ | Heat flux between fluid to solid phase ($MT^{-3}$) |
| $Pr$ | Prandtl number (-) |
| $Re$ | Reynolds number (-) |
| $R$ | Retardation factor (-) |
| $\rho_f$ | Density of the fluid phase ($ML^{-3}$) |
| $\rho_s$ | Density of the solid phase ($ML^{-3}$) |
| $s_f$ | specific surface of the grain ($L^{-1}$) |
| $t$ | time (T) |
| $T_f$ | Temperature of the fluid phase (K) |
| $T_s$ | Temperature of the solid phase (K) |
| $v$ | Fluid velocity ($LT^{-1}$) |
| $x$ | coordinate along the direction of the flow (L) |

Heat transfer dynamics in porous media are substantially different from solutes transport in that conduction is through both the matrix and the fluid and therefore conductive heat transport is more rapid than diffusive solute transport. On the contrary, the advective transport of heat (convection) is slower than advective solute transport since the heat capacity of the solid grains will retard the advance of the thermal front [2], [3].

Thermal dispersion is analogous to hydrodynamic dispersion and results from local velocity variations due to the mechanical interaction of the fluid with the porous medium structure [4]. But the hydrodynamic component of thermal dispersion is often neglected because thermal diffusion is more efficient than molecular diffusion by several orders of magnitude [4]. However, the literature contains conflicting descriptions of the thermal dispersivity coefficient [5]. An issue that has not been properly addressed experimentally is the quantification of thermal dispersivity as far as heat transport and its relationship with velocity.

Another issue to take into account is that the structure and porosity of the porous medium may affect the flow patterns and thermal transport phenomena in the porous channels [6].

Few authors have carried out laboratory experiments on heat transfer in porous media. Among those, the principal investigated issues have been the influence of non-linear flow regime, the relationship between the thermal dispersion with the flow velocity and the validity of the local thermal equilibrium assumption between the fluid and solid phase.

[6] investigated experimentally and theoretically the flow and heat transfer characteristics inside packed and fluidized beds. The purpose of their study was to investigate the heat transfer performance of the porous channels by using a modified version of the local thermal nonequilibrium model (LTNE) which neglected the effects of thermal dispersion in both fluid and solid. The results showed a highly non-Fourier behaviour which combined rapid thermal breakthrough with extremely long-tailing, that was attributed to disequilibrium between the fluid and the porous matrix. However, the adopted model was unable to fully capture the thermal breakthrough observed in some experimental runs.

[7] applied the continuous time random walk (CTRW) to three of the experiments carried out by Wu and Hwang (1998) over a range of different flow rates. CTRW is capable of quantifying both local equilibrium and nonequilibrium heat transfer in heterogeneous domains, and showed to successfully capture the observed nonequilibrium thermal breakthrough curves.

[5] carried out laboratory experiments on heat transfer in a specifically designed hydraulic tank containing well-sorted saturated sand. The experiments were aimed at analysing heat and solute transport behaviour separately, but under the same conditions, representative of naturally occurring groundwater flow systems.

They found that the thermal dispersion behavior for Darcy-related velocities in natural porous media did not exceed beyond a transition regime. The thermal dispersion can be approximated by a thermal dispersivity coefficient and a square dependency on the thermal front velocity. This result deviates from the linear description of thermal dispersion, which is assumed in analogy to solute transport. The difference can be explained with the different characteristics of heat and solute transport in porous media as expressed by the respective transport Peclet numbers. The results indicated that for relatively uniform coarse sand the thermal dispersivity term in the thermal dispersion equation can be neglected for $Pe < 0.5$.

This study is aimed at investigating the critical issues regarding heat transport phenomena in porous media by means of laboratory experiments. A physical model has been realised to analyse the forced convective flow and the related heat transport dynamics through a 1d porous medium column.

## 2. Theoretical background

### *2.1. Heat transport in one dimensional porous medium column*

The behavior of heat transport in porous media is strongly dependent from the fluid velocity.

For high velocity flow, the interaction between the solid and fluid phase is rapid and then the solid and fluid phase cannot exchange sufficient amount of energy to establish local thermal equilibrium. At a given location the solid and fluid phases have different temperatures. In this situation each phase needs an energy equation for the description of heat transport. Assuming that porosity, densities and heat capacities are constant in time, energy equations can be written for the fluid and solid phase:

$$\frac{\partial T_f}{\partial t} = -v\frac{\partial T_f}{\partial x} + \frac{\partial}{\partial x}\cdot\left(\frac{k_{eff}}{\rho_f c_f}\frac{\partial T_f}{\partial x}\right) + \frac{q_{fs}}{\rho_f c_f} \tag{1}$$

$$\frac{\rho_s c_s}{\rho_f c_f}\frac{\partial T_s}{\partial t} = \frac{\partial}{\partial x}\cdot\left(\frac{k_s}{\rho_f c_f}\frac{\partial T_s}{\partial x}\right) - \frac{q_{fs}}{\rho_f c_f} \tag{2}$$

The interaction between the two phases is represented by the sink/source terms $q_{fs}$ given by following equation:

$$q_{fs} = h^* s_f \left(T_s - T_f\right) \tag{3}$$

The convective heat transfer coefficient can be expressed as:

$$h^* = \left( \frac{d_p}{10k_s} + \frac{d_p}{\mathrm{Nu}\left(\mathrm{Pr},\mathrm{Re}\right)k_f} \right)^{-1} \tag{4}$$

[8] redefined the Reynolds number to describe non-Darcy flow in porous media as:

$$\mathrm{Re} = \frac{\rho_f d_p v}{\mu} \frac{1}{1-n} \tag{5}$$

[9] suggest Re = 10 as a critical value for non-Darcy flow.

In low velocity flow regimes the solid and fluid phase are in contact for a sufficient period of time, and there exists the possibility for energy exchange locally and to establish a local thermal equilibrium. In such a case, only one energy equation is sufficient for the description of heat transport. The energy equation for the fluid and solid phase are combined into a single equation as:

$$\left( 1 + \frac{1-n}{n} \frac{\rho_s c_s}{\rho_f c_f} \right) \frac{\partial T_f}{\partial t} = \frac{\partial}{\partial x} \left( \frac{k_{eff}}{\rho_f c_f} \frac{\partial T_f}{\partial x} \right) - v \frac{\partial T_f}{\partial x} \tag{6}$$

Damköhler number *Da* can be used in order to evaluate the presence of local thermal equilibrium. *Da* relates the convection time scale to the exchange time scale between the two phases:

$$Da = \frac{h^* s_f L}{\rho_f c_f v} \tag{7}$$

When $Da \gg 1$ the heat exchange between the two phases is rapid and there is instantaneous equilibrium between the two phases. On the contrary for $Da \ll 1$ the heat exchange velocity between the two phases is very low and it does not influence the heat propagation. When the convection time scale approaches the exchange time scale $Da \cong 1$, the impact of local thermal non equilibrium behavior of heat transport is stronger and the temperature distribution is characterized by a long tail.

## 3. Materials and methods

### *3.1. Experimental setup*

The experiments have been performed on a laboratory physical model constituted by a thermal insulated plastic circular pipe with diameter of 0.11 m and height of 1.66 m filled with a porous medium with hydraulic and thermal parameters described in the Table 1.

Water inside the column flows from the bottom to the top according to the hydraulic head difference between the upstream tank connected to the inlet port positioned at the bottom and the outlet port positioned at the top. Water that enters into the column is heated by an electric water boiler with a volume of $10^{-2}$ $m^3$. The instantaneous flow rate that flows across the block is measured by an ultrasonic velocimeter (DOP3000 by Signal Processing). Two thermocouples have been positioned at the center of the circular section of the pipe at the height of 0.25 m and 1.55 m respect to the inlet port. They have been connected to a TC – 08 Thermocouple Data Logger (pico Technology) and a sampling rate of 1 second has been used.

Table 1. Properties of porous medium.

| Property | Value |
|---|---|
| Porosity (-) | 0.47 |
| Average grain size (mm) | 9.21 |
| Average specific surface ($m^{-1}$) | 337.90 |
| Soil density ($Kg \cdot m^{-3}$) | 2210 |
| Soil heat capacity ($J \cdot Kg^{-1} \cdot K^{-1}$) | 840 |
| Soil thermal conductivity ($W \cdot m^{-1} K^{-1}$) | 2.15 |

### *3.2. Heat transport tests*

Temperature tracer tests have been conducted through the following steps.

First a hydraulic head difference between the upstream tank and the outlet port has been imposed. At time t = 0 s the cold water valve has been opened. At time t = 60 s the cold water valve has been closed and at the same time the hot water valve has been opened. In this manner the thermal breakthrough curves (BTCs) are measured by the thermocouples. The BTC measured by the first thermocouple located at the height of 0.25 from the inlet port is used as the injection temperature function $T_{inj}(t)$ whereas the BTC measured by the second thermocouple located at the height of 1.55 m from the inlet port is used as the observed temperature function $T_{obs}(t)$.

## 4. Results

### *4.1. Fitting thermal breakthrough curves and interpretation of estimated parameter models*

Three tests have been conducted at different flow rates. As shown in the Table 2 for the investigated range of velocity the Damköhler number is much higher than the unit and then local thermal equilibrium model can be used to describe the behavior of heat transport.

Table 2. Specific discharge, fluid velocity, Reynolds number, heat transfer rate coefficient and Damköhler number at different flow rates.

| $Q$ ($m^3 s^{-1}$)×$10^{-6}$ | $q$ (m/s)×$10^{-3}$ | $v$ (m/s)×$10^{-3}$ | Re (-) | $hs_f/\rho_f c_f$ ($s^{-1}$) | $Da$ (-) |
|---|---|---|---|---|---|
| 2.32 | 2.45 | 5.69 | 42.2 | 0.1847 | 23.56 |
| 1.60 | 1.68 | 3.61 | 29.0 | 0.1824 | 33.93 |
| 0.99 | 1.04 | 2.23 | 17.9 | 0.1774 | 53.30 |

Using the analogy with solute transport the Equation 6 can be rewritten as:

$$R\frac{\partial T_f}{\partial t} = \frac{\partial}{\partial x}\left( D_{eff}\frac{\partial T_f}{\partial x}\right) - v\frac{\partial T_f}{\partial x} \tag{8}$$

Where:

$$R = 1 + \frac{1-n}{n}\frac{\rho_s c_s}{\rho_f c_f} \tag{9}$$

$$D_{eff} = D_0 + \alpha_L v \tag{10}$$

On the basis of the analytical solution for the instantaneous temperature injection of the Equation 8 the probability density function of the residence time (*PDF*) for the temperature in the one dimensional column of porous medium can be written as:

$$PDF(x,t) = \frac{1}{\sqrt{\pi D_{eff} R^{-1} t}} \exp\left(\frac{x - vR^{-1}t}{4D_{eff} R^{-1} t}\right) \tag{11}$$

Using the convolution theorem the $T_{obs}$(t) can be related to $T_{inj}$(t) as:

$$T_{obs}(t) = T_{inj}(t) * PDF(t) \tag{12}$$

The observed BTCs for different flow rates have been individually fitted using the Equation 10. Figure 1 shows the fitting results.

Fig. 1. Fitting BTCs at different specific discharge.

Figure 2a shows the relationship between the transport parameter *v/R* and the convective velocity evaluated as *v=q/n*. The estimated value of the retardation factor is $R = 1.3772$ and it is close to the theoretical value that is equal to $R = 1.5084$. Figure 2b shows the relationship between $v$ and $D_{eff}$. A linear relationship is evident between the thermal convective velocity and the effective thermal dispersion for the investigated range of velocity with a longitudinal dispersion coefficient equal to $\alpha_L = 0.0121$ m. The estimated value of thermal diffusion is equal to $D_0 = 9.74\times10^{-5}$ m$^2$/s and it is much higher than the theoretical value equal to $D_0 = 2.82\times10^{-7}$ m$^2$/s.

## 5. Conclusions

Experimental investigations have been carried out to analyze the behavior of heat transport through a one dimensional porous medium column. For the investigated range of velocity the fluid and solid phases are in thermal equilibrium. *Da* is much higher than the unit, varying in the range between 23.5 – 53.3.

In a previous study that analyzed heat transfer dynamics in a fractured limestone block [10] the heat transfer velocity between the fluid in the fracture and the matrix was comparable with transport velocity and a non-local thermal equilibrium has been detected.

This puts into evidence that $s_f$ plays an important role on heat transport behavior. When $s_f$ reduces $h$ reduces consequently and then the heat transfer velocity between the fluid and solid phases could be comparable with the convective velocity giving rise to a strong local thermal non equilibrium effect.

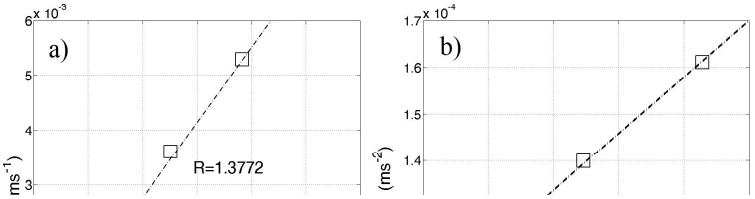


Fig. 2. a) Relationship between the transport parameter $v/R$ and the fluid velocity $v=q/n$. b) relationship between fluid convective velocity $v$ and the effective thermal dispersion $D_{eff}$.

Assuming valid the local thermal equilibrium model, the thermal BTCs have been fitted using the analytical solution of the 1d advection dispersion model. The estimated thermal convective velocity approaches the fluid convective velocity with an error in the range of 0.58% - 6.38% whereas regarding the effective thermal dispersion the results put into evidence a discrepancy between the estimated and theoretical values of the thermal diffusion coefficient.

The obtained results encourage further experimental work to increase the knowledge of the key parameters that govern heat propagation in porous media.

## References

[1] Singh. Experimental study on heat transfer in porous media Partridge India, 2015 ISBN 10: 1482852446 ISBN 13: 9781482852448.
[2] Bodvarsson G. Thermal problems in the siting of reinjection wells, Geothermics 1972; 1(2), 63–66.
[3] Oldenburg CM, Pruess K. Layered thermohaline convection in hypersaline geothermal systems, Transp. Porous Med 1998; 33(1–2) p. 29–63.
[4] Bear J. Dynamics of Fluids in Porous Media 1972 764 pp., Elsevier, N.Y.
[5] Rau GC, Andersen MS, Acworth. Experimental investigation of the thermal dispersivity term and its significance in the heat transport equation for flow in sediments Water Resources Research 2012; 48 (3), W03511
[6] Wu CC, Hwang GJ. Flow and heat transfer characteristics inside packed and fluidized beds. J. Heat Trans 1998; 120 p. 667–673.
[7] Emmanuel S, Berkowitz B. Continuous time random walks and heat transfer in porous media. Transport in Porous Media 2007; 67 p. 413-430.
[8] Ergun S. Fluid flow through packed columns, Chem. Eng. Prog. 1952; 48(2) p. 89–94.
[9] Hassanizadeh SM, Gray WG. High velocity flow in porous media, Transport Porous Media 1987; 2 p. 521–531.
[10] Pastore N, Cherubini C, Giasi CI, Allegretti NM, Redondo JM, Tarquis AM. Experimental study of heat transport in fracture network. Energy Procedia 2015; 76 p. 273 – 281.

Nonlin. Processes Geophys., 24, 23–42, 2017
www.nonlin-processes-geophys.net/24/23/2017/
doi:10.5194/npg-24-23-2017


Nonlinear Processes in Geophysics
Open Access
EGU

# Laboratory experimental investigation of heat transport in fractured media

**Claudia Cherubini**[1,2], **Nicola Pastore**[3], **Concetta I. Giasi**[3], **and Nicoletta Maria Allegretti**[3]

[1]Department of Mechanical, Aerospace & Civil Engineering, Brunel University London, Uxbridge, UB8 3PH, UK
[2]School of Civil Engineering, The University of Queensland, Queensland, Australia
[3]DICATECh, Department of Civil, Environmental, Building Engineering, and Chemistry, Politecnico di Bari, Bari, Italy

*Correspondence to:* Claudia Cherubini (claudia.cherubini@brunel.ac.uk) and Nicola Pastore (nicola.pastore@poliba.it)

Received: 14 September 2016 – Published in Nonlin. Processes Geophys. Discuss.: 10 October 2016
Revised: 6 December 2016 – Accepted: 22 December 2016 – Published: 26 January 2017

**Abstract.** Low enthalpy geothermal energy is a renewable resource that is still underexploited nowadays in relation to its potential for development in society worldwide. Most of its applications have already been investigated, such as heating and cooling of private and public buildings, road defrosting, cooling of industrial processes, food drying systems or desalination.

Geothermal power development is a long, risky and expensive process. It basically consists of successive development stages aimed at locating the resources (exploration), confirming the power generating capacity of the reservoir (confirmation) and building the power plant and associated structures (site development). Different factors intervene in influencing the length, difficulty and materials required for these phases, thereby affecting their cost.

One of the major limitations related to the installation of low enthalpy geothermal power plants regards the initial development steps that are risky and the upfront capital costs that are huge.

Most of the total cost of geothermal power is related to the reimbursement of invested capital and associated returns.

In order to increase the optimal efficiency of installations which use groundwater as a geothermal resource, flow and heat transport dynamics in aquifers need to be well characterized. Especially in fractured rock aquifers these processes represent critical elements that are not well known. Therefore there is a tendency to oversize geothermal plants.

In the literature there are very few studies on heat transport, especially on fractured media.

This study is aimed at deepening the understanding of this topic through heat transport experiments in fractured networks and their interpretation.

Heat transfer tests have been carried out on the experimental apparatus previously employed to perform flow and tracer transport experiments, which has been modified in order to analyze heat transport dynamics in a network of fractures. In order to model the obtained thermal breakthrough curves, the Explicit Network Model (ENM) has been used, which is based on an adaptation of Tang's solution for the transport of the solutes in a semi-infinite single fracture embedded in a porous matrix.

Parameter estimation, time moment analysis, tailing character and other dimensionless parameters have permitted a better understanding of the dynamics of heat transport and the efficiency of heat exchange between the fractures and the matrix. The results have been compared with the previous experimental studies on solute transport.

## 1 Introduction

An important role in transport of natural resources or contaminant transport through subsurface systems is given by fractured rocks. Interest in the study of dynamics of heat transport in fractured media has grown in recent years because of the development of a wide range of applications, including geothermal energy harvesting (Gisladottir et al., 2016).

Quantitative geothermal reservoir characterization using tracers is based on different approaches to predicting thermal

breakthrough curves in fractured reservoirs (Shook, 2001; Kocabas, 2005; Read et al., 2013).

The characterization and modeling of heat transfer in fractured media are particularly challenging as open and well-connected fractures can induce highly localized pathways which are orders of magnitude more permeable than the rock matrix (Klepikova et al., 2016; Cherubini and Pastore, 2011).

The study of solute transport in fractured media has recently become a widespread research topic in hydrogeology (Cherubini, 2008; Cherubini et al., 2008, 2009, 2013d; Masciopinto et al., 2010), whereas the literature about heat transfer in fractured media is somewhat limited.

Hao et al. (2013) developed a dual continuum model for the representation of discrete fractures and the interaction with the surrounding rock matrix in order to give a reliable prediction of the impacts of fracture–matrix interaction on heat transfer in fractured geothermal formations.

Moonen et al. (2011) introduced the concept of a cohesive zone which represents a transition zone between the fracture and undamaged material. They proposed a model to adequately represent the influences of fractures or partially damaged material interfaces on heat transfer phenomena.

Geiger and Emmanuel (2010) found that matrix permeability plays an important role in thermal retardations and attenuation of thermal signals. At high matrix permeability, poorly connected fractures can contribute to the heat transport, resulting in heterogeneous heat distributions in the whole matrix block. For lower matrix permeability heat transport occurs mainly through fractures that form a fully connected pathway between the inflow and outflow boundaries, which results in highly non-Fourier behavior characterized by early breakthrough and long tailing.

Numerous field observations (Tsang and Neretnieks, 1998) show that flow in fractures is being organized in channels due to the small-scale variations in the fracture aperture. Flow channeling causes dispersion in fractures. Such channels will have a strong influence on the transport characteristics of a fracture, such as, for instance, its thermal exchange area, crucial for geothermal applications (Auradou et al., 2006). Highly channelized flow in fractured geologic systems has been credited with early thermal breakthrough and poor performance of geothermal circulation systems (Hawkins et al., 2012).

Lu et al. (2012) conducted experiments of saturated water flow and heat transfer in a regularly fractured granite at meter scale. The experiments indicated that the heat advection due to water flow in vertical fractures nearest to the heat sources played a major role in influencing the spatial distributions and temporal variations of the temperature, impeding heat conduction in the transverse direction; such an effect increased with larger water fluxes in the fractures and decreased with a higher heat source and/or a larger distance of the fracture from the heat source.

Neuville et al. (2010) showed that fracture–matrix thermal exchange is highly affected by the fracture wall roughness. Natarajan et al. (2010) conducted numerical simulation of thermal transport in a sinusoidal fracture–matrix coupled system. They affirmed that this model presents a different behavior with respect to the classical parallel plate fracture–matrix coupled system. The sinusoidal curvature of the fracture provides high thermal diffusion into the rock matrix.

Ouyang (2014) developed a three-equation local thermal non-equilibrium model to predict the effective solid-to-fluid heat transfer coefficient in geothermal system reservoirs. They affirmed that due to the high rock-to-fracture size ratio, the solid thermal resistance effect in the internal rocks cannot be neglected in the effective solid-to-fluid heat transfer coefficient. Furthermore the results of this study show that it is not efficient to extract the thermal energy from the rocks if fracture density is not large enough.

Analytical and semi-analytical approaches have been developed to describe the dynamics of heat transfer in fractured rocks. Such approaches are amenable to the same mathematical treatment as their counterparts developed for mass transport (Martinez et al., 2014). One of these is the analytical solution derived by Tang et al. (1981).

While the equations of solute and thermal transport have the same basic form, the fundamental difference between mass and heat transport is that (1) solutes are transported through the fractures only, whereas heat is transported through both fractures and matrix, and (2) the fracture–matrix exchange is large compared with molecular diffusion. This means that the fracture–matrix exchange is more relevant for heat transport than for mass transport. Thus, matrix thermal diffusivity strongly influences the thermal breakthrough curves (BTCs) (Becker and Shapiro, 2003).

Contrarily, since the heat capacity of the solids will retard the advance of the thermal front, the advective transport for heat is slower than for solute transport (Rau et al., 2012).

The quantification of thermal dispersivity in terms of heat transport and its relationship with velocity has not been properly addressed experimentally and has conflicting descriptions in the literature (Ma et al., 2012).

Most studies neglect the hydrodynamic component of thermal dispersion because of thermal diffusion being more efficient than molecular diffusion by several orders of magnitude (Bear, 1972). Analysis of heat transport under natural gradients has commonly neglected hydrodynamic dispersion (e.g., Bredehoeft and Papadopulos, 1965; Domenico and Palciauskas, 1973; Taniguchi et al., 1999; Reiter, 2001; Ferguson et al., 2006). Dispersive heat transport is often assumed to be represented by thermal conductivity and/or to have little influence in models of relatively large systems and modest fluid flow rates (Bear, 1972; Woodbury and Smith, 1985).

Some authors suggest that thermal dispersivity enhances the spreading of thermal energy and should therefore be part of the mathematical description of heat transfer in analogy to solute dispersivity (de Marsily, 1986), and have incorporated this term into their models (e.g., Smith and Chapman, 1983; Hopmans et al., 2002; Niswonger and Prudic, 2003). In

the same way, other researchers (e.g., Smith and Chapman, 1983; Ronan et al., 1998; Constanz et al., 2002; Su et al., 2004) have included the thermomechanical dispersion tensor representing mechanical mixing caused by unspecified heterogeneities within the porous medium.

By contrast, some other researchers argue that the enhanced thermal spreading is either negligible or can be described simply by increasing the effective diffusivity; thus, the hydrodynamic dispersivity mechanism is inappropriate (Bear, 1972; Bravo et al., 2002; Ingebritsen and Sanford, 1998; Keery et al., 2007). Constantz et al. (2003) and Vandenbohede et al. (2009) found that thermal dispersivity was significantly smaller than the solute dispersivity. Others (de Marsily, 1986; Molina-Giraldo et al., 2011) found that thermal and solute dispersivity was on the same order of magnitude.

Tracer tests of both solute and heat were carried out at Bonnaud, Jura, France (de Marsily, 1986), and the thermal dispersivity and solute dispersivity were found to be of the same order of magnitude.

Bear (1972), Ingebritsen and Sanford (1998), and Hopmans et al. (2002), among others, concluded that the effects of thermal dispersion are negligible compared to conduction and set the former to zero.

However, Hopmans et al. (2002) showed that dispersivity is increasingly important at higher flow water velocities, since it is only then that the thermal dispersion term is of the same order of magnitude or larger than the conductive term.

Sauty et al. (1982) suggested that there was a correlation between the apparent thermal conductivity and Darcy velocity; thus, they included the hydrodynamic dispersion term in the advective–conductive modeling.

Other similar formulations of this concept are present in the literature (e.g., Papadopulos and Larson, 1978; Smith and Chapman, 1983; Molson et al., 1992). Such treatments have not explicitly distinguished between macrodispersion, which occurs due to variations in permeability over larger scales, and the components of hydrodynamic dispersion that occur due to variations in velocity at the pore scale.

One group of authors have utilized a linear relationship to describe the thermal dispersivity and the relationship between thermal dispersivity and fluid velocity (e.g., de Marsily, 1986; Anderson, 2005; Hatch et al., 2006; Keery et al., 2007; Vandenbohede et al., 2009; Vandenbohede and Lebbe, 2010; Rau et al., 2012), while others have identified the possibility of a nonlinear relationship (Green et al., 1964).

The present study is aimed at providing a better understanding of heat transfer mechanisms in fractured rocks. Laboratory experiments on mass and heat transport in a fractured rock sample have been carried out in order to analyze the contribution of thermal dispersion in heat propagation processes, the influence of nonlinear flow dynamics on the enhancement of thermal matrix diffusion and finally the optimal conditions for thermal exchange in a fractured network.

Section 1 shows a short review of mass and heat transport in fractured media highlighting what is still unresolved or contrasting in the literature.

In Sect. 2 the theoretical background related to nonlinear flow and solute and heat transport behavior in fractured media has been reported.

A better development of the Explicit Network Model (ENM), based on Tang's solution developed for solute transport in a single semi-infinite fracture inside a porous matrix, has been used for the fitting of the thermal BTCs. The ENM model explicitly takes the fracture network geometry into account and therefore permits one to understand the physical meaning of mass and heat transfer phenomena and to obtain a more accurate estimation of the related parameters. In an analogous way, the ENM has been used in order to fit the observed BTCs obtained from previous experiments on mass transport.

Section 3 shows the thermal tracer tests carried out on an artificially created fractured rock sample that has been used in previous studies to analyze nonlinear flow and non-Fickian transport dynamics in fractured formations (Cherubini et al., 2012, 2013a, b, c, 2014).

In Sect. 4 have been reported the interpretation of flow and transport experiments together with the fitting of BTCs and interpretation of estimated model parameters. In particular, the obtained thermal BTCs show more enhanced early arrival and long tailing than solute BTCs.

The travel time for solute transport is an order of magnitude lower than for heat transport experiments. Thermal convective velocity is thus more delayed with respect to solute transport. The thermal dispersion mechanism dominates heat propagation in the fractured medium in the carried out experiments and thus cannot be neglected.

For mass transport the presence of the secondary path and the nonlinear flow regime are the main factors affecting non-Fickian behavior observed in experimental BTCs, whereas for heat transport the non-Fickian nature of the experimental BTCs is governed mainly by the heat exchange mechanism between the fracture network and the surrounding matrix. The presence of a nonlinear flow regime gives rise to a weak growth on heat transfer phenomena.

Section 5 reports some practical applications of the knowledge acquired from this study on the convective heat transport in fractured media for exploiting heat recovery and heat dissipation. Furthermore the estimation of the average effective thermal conductivity suggests that there is a solid thermal resistance in the fluid-to-solid heat transfer processes due to the rock–fracture size ratio. This result matches previous analyses (Pastore et al., 2015) in which a lower heat dissipation with respect to Tang's solution in correspondence to the single fracture surrounded by a matrix with more limited heat capacity has been found.

## 2 Theoretical background

### 2.1 Nonlinear flow

With few exceptions, any fracture can be envisioned as two rough surfaces in contact. In cross section the solid areas representing asperities might be considered the grains of porous media.

Therefore, in most studies examining hydrodynamic processes in fractured media, the general equations describing flow and transport in porous media are applied, such as Darcy's law, which depicts a linear relationship between the pressure gradient and fluid velocity (Whitaker, 1986; Cherubini and Pastore, 2010).

However, this linearity has been demonstrated to be valid in low flow regimes ($Re < 1$). For $Re > 1$ a nonlinear flow behavior is likely to occur (Cherubini et al., 2013d).

When $Re \gg 1$, a strong inertial regime develops that can be described by the Forchheimer equation (Forchheimer, 1901):

$$-\frac{\mathrm{d}p}{\mathrm{d}x} = \frac{\mu}{k} \cdot u_f + \rho\beta \cdot u_f^2, \tag{1}$$

where $x$ (m) is the coordinate parallel to the axis of the single fracture (SF), $p$ ($\mathrm{ML^{-1}T^{-2}}$) is the flow pressure, $\mu$ ($\mathrm{ML^{-1}T^{-1}}$) is the dynamic viscosity, $k$ ($\mathrm{L^2}$) is the permeability, $u_f$ ($\mathrm{LT^{-1}}$) is the convective velocity, $\rho$ ($\mathrm{ML^{-3}}$) is the density and $\beta$ ($\mathrm{L^{-1}}$) is called the inertial resistance coefficient, or non-Darcy coefficient.

It is possible to express the Forchheimer law in terms of hydraulic head $h$ (L):

$$-\frac{\mathrm{d}h}{\mathrm{d}x} = a' \cdot u_f + b' \cdot u_f^2. \tag{2}$$

The coefficients $a'$ ($\mathrm{TL^{-1}}$) and $b'$ ($\mathrm{TL^{-2}}$) represent the linear and inertial coefficient, respectively, equal to

$$a' = \frac{\mu}{\rho g k}; b' = \frac{\beta}{g}. \tag{3}$$

The relationship between hydraulic head gradient and flow rate $Q$ ($\mathrm{L^3\,T^{-1}}$) can be written as

$$-\frac{\mathrm{d}h}{\mathrm{d}x} = a \cdot Q + b \cdot Q^2. \tag{4}$$

The coefficients $a$ ($\mathrm{TL^{-3}}$) and $b$ ($\mathrm{T^2L^{-6}}$) can be related to $a'$ and $b'$:

$$a = \frac{a'}{\omega_{\mathrm{eq}}}; b = \frac{b'}{\omega_{\mathrm{eq}}^2}, \tag{5}$$

where $\omega_{\mathrm{eq}}$ ($\mathrm{L^2}$) is the equivalent cross-sectional area of SF.

### 2.2 Heat transfer by water flow in single fractures

Fluid flow and heat transfer in a single fracture (SF) undergo advective, diffusive and dispersive phenomena. Dispersion is caused by small-scale fracture aperture variations. Flow channeling is one example of macrodispersion caused by preferred flow paths, in that mass and heat tend to migrate through the portions of a fracture with the largest apertures.

In fractured media another process is represented by diffusion into the surrounding rock matrix. Matrix diffusion attenuates the mass and heat propagation in the fractures.

According to the boundary layer theory (Fahien, 1983), solute mass transfer $q_{\mathrm{M}}$ ($\mathrm{ML^{-2}}$) per unit area at the fracture–matrix interface (Wu et al., 2010) is given by

$$q_{\mathrm{M}} = \frac{D_{\mathrm{m}}}{\delta}\left(c_{\mathrm{f}} - c_{\mathrm{m}}\right), \tag{6}$$

where $c_{\mathrm{f}}$ ($\mathrm{ML^{-3}}$) is the concentration across fractures, $c_{\mathrm{m}}$ ($\mathrm{ML^{-3}}$) is the concentration of the matrix block surfaces, $D_{\mathrm{m}}$ ($\mathrm{LT^{-2}}$) is the molecular diffusion coefficient, and $\delta$ (m) is the thickness of the boundary layer (Wu et al., 2010). For small fractures, $\delta$ may become the aperture $w_{\mathrm{f}}$ (m) of the SF.

In an analogous manner, the specific heat transfer flux $q_{\mathrm{H}}$ ($\mathrm{MT^{-3}}$) at the fracture–matrix interface is given by

$$q_{\mathrm{H}} = \frac{k_m}{\delta}\left(T_{\mathrm{f}} - T_{\mathrm{m}}\right), \tag{7}$$

where $T_{\mathrm{f}}$ (K) is the temperature across fractures, $T_{\mathrm{m}}$ (K) is the temperature of the matrix block surfaces, and $k_m$ ($\mathrm{MLT^{-3}K^{-1}}$) is the thermal conductivity.

The continuity conditions at the fracture–matrix interface require a balance between mass transfer rate and mass diffused into the matrix described as

$$q_M = -D_{\mathrm{e}}\left.\frac{\partial c_{\mathrm{m}}}{\partial z}\right|_{z = w_{\mathrm{f}}/2}, \tag{8}$$

where $z$ (m) is the coordinate perpendicular to the fracture axis and $w_{\mathrm{f}}$ is the aperture of the fracture.

In the same way, the specific heat flux must be balanced by heat diffused into the matrix described as

$$q_{\mathrm{H}} = -k_{\mathrm{e}}\left.\frac{\partial T_{\mathrm{m}}}{\partial z}\right|_{z = w_{\mathrm{f}}/2}. \tag{9}$$

The effective diffusion coefficient takes into account the fact that diffusion can only take place through pore and fracture openings because mineral grains block many of the possible pathways. The effective thermal conductivity of a formation consisting of multiple components depends on the geometrical configuration of the components as well as on the thermal conductivity of each.

The effective terms ($D_{\mathrm{e}}$ instead of $D_{\mathrm{m}}$ and $k_{\mathrm{e}}$ instead of $k_m$) have been introduced in order to include the effect of various system parameters such as fluid velocity, porosity, surface area, and roughness that may enhance the mass and heat transfer effect. For instance, when large flow velocity occurs, convective transport is stronger along the center of the fracture, enhancing the concentration or temperature gradient at the fracture–matrix interface. As is known, roughness plays

an important role in increasing mass or heat transfer because of increasing turbulent flow conditions.

According to Bodin (2007) the governing equation for the 1-D advective–dispersive transport along the axis of a semi-infinite fracture with 1-D diffusion in the rock matrix, in perpendicular direction to the axis of the fracture, is

$$\frac{\partial c_\mathrm{f}}{\partial t} + u_f \frac{\partial c_\mathrm{f}}{\partial x} = \frac{\partial}{\partial x}\left(D_f \frac{\partial c_\mathrm{f}}{\partial x}\right) - \frac{D_\mathrm{e}}{\delta}\frac{\partial c_m}{\partial z}\bigg|_{z=w_\mathrm{f}/2}, \quad (10)$$

where $D_\mathrm{f}$ ($\mathrm{L^2T^{-1}}$) is the dispersion in the fracture. The latter mainly depends on two processes: Aris–Taylor dispersion and geometrical dispersion. Previous experiments (Cherubini et al., 2012a, b, c, 2014) show that, due to the complex geometrical and topological characteristics of the fracture network that create tortuous flow paths, Aris–Taylor dispersion may not develop. A linear relationship has been found between velocity and dispersion, so geometrical dispersion is mostly responsible for the mixing process along the fracture:

$$D_f = \alpha_\mathrm{LM} u_f, \quad (11)$$

where $\alpha_\mathrm{LM}$ (L) is the dispersivity coefficient for mass transport.

Assuming that fluid flow velocity in the surrounding rock matrix is equal to zero, the equation for the conservation of heat in the matrix is given by

$$\frac{\partial c_\mathrm{m}}{\partial t} = D_\mathrm{a}\frac{\partial^2 c_\mathrm{m}}{\partial z^2}, \quad (12)$$

where $D_\mathrm{a}$ is the apparent diffusion coefficient of the solute in the matrix expressed as a function of the matrix porosity $\theta_\mathrm{m}$, $D_\mathrm{a} = D_\mathrm{e}/\theta_\mathrm{m}$ (Bodin et al., 2007).

Tang et al. (1981) presented an analytical solution for solute transport in a semi-infinite single fracture embedded in a porous rock matrix with a constant concentration at the fracture inlet ($x = 0$) equal to $c_0$ ($\mathrm{ML^{-3}}$) and with an initial concentration equal to zero. The solute concentration in the fracture $\overline{c}_\mathrm{f}$ and in the matrix $\overline{\mathbf{c}}_\mathrm{m}$ are as follows:

$$\overline{\mathbf{c}}_f = \frac{c_0}{s}\exp(vL)\exp\left[-vL\left\{1+\beta^2\left(\frac{s^{1/2}}{A}+s\right)\right\}^{1/2}\right], \quad (13)$$

$$\overline{\mathbf{c}}_\mathrm{m} = \overline{\mathbf{c}}_f \exp\left[-Bs^{1/2}(z - w_\mathrm{f}/2)\right], \quad (14)$$

where $s$ is the integral variable of the Laplace transform and $L$ (L) is the length of SF; the $v$, $A$, $\beta^2$ and $B$ coefficients are expressed as follows:

$$v = \frac{u_f}{2D_f}, \quad (15)$$

$$A = \frac{\delta}{\sqrt{\theta_\mathrm{m} D_\mathrm{e}}}, \quad (16)$$

$$\beta^2 = \frac{4D_f}{u_f^2}, \quad (17)$$

$$B = \frac{1}{\sqrt{D_\mathrm{e}}}, \quad (18)$$

whereas the gradient of $\overline{\mathbf{c}}_\mathrm{m}$ at the interface $z = w_f/2$ is

$$\frac{\mathrm{d}\overline{\mathbf{c}}_\mathrm{m}}{\mathrm{d}x}\bigg|_{x=w_\mathrm{f}/2} = -\overline{\mathbf{c}}_f B s^{1/2}. \quad (19)$$

Defining the residence time as the average amount of time that the solute spends in the system, on the basis of these analytical solutions the probability density function (PDF) of the solute residence time in the single fracture in the Laplace space can be expressed as

$$\overline{\Gamma}(s) = \exp(vL)\exp\left[-vL\left\{1+\beta^2\left(\frac{s^{1/2}}{A}+s\right)\right\}^{1/2}\right]. \quad (20)$$

Assuming that density and heat capacity are constant in time, the heat transport conservation equation in SF can be expressed as follows:

$$\frac{\partial T_\mathrm{f}}{\partial t} + u_f \frac{\partial T_\mathrm{f}}{\partial x} = \frac{\partial}{\partial x}\left(D_\mathrm{fH}\frac{\partial T_\mathrm{f}}{\partial x}\right) - \frac{k_\mathrm{e}}{\rho_w C_w \delta}\frac{\partial T_\mathrm{m}}{\partial z}\bigg|_{z=w_\mathrm{f}/2}, \quad (21)$$

where $\rho_w$ ($\mathrm{ML^{-3}}$) and $C_w$ ($\mathrm{L^2T^2K^{-1}}$) represent the density and the specific heat capacity of the fluid within SF, respectively. $D_\mathrm{f}$ for heat transport assumes the following expression:

$$D_\mathrm{fH} = \frac{\lambda_L}{\rho_w C_w}, \quad (22)$$

where $\lambda_L$ is the thermodynamic dispersion coefficient ($\mathrm{MLT^{-3}K^{-1}}$). Sauty et al. (1982) and de Marsily (1986) proposed an expression for the thermal dispersion coefficient where the thermal dispersion term varies linearly with velocity and depends on the heterogeneity of the medium, as for solute transport:

$$\lambda_L = k_0 + \alpha_\mathrm{LH}\rho_w C_w u_f, \quad (23)$$

where $k_0$ is the bulk thermal conductivity ($\mathrm{MLT^{-3}K^{-1}}$) and $\alpha_\mathrm{LH}$ (L) is the longitudinal thermal dispersivity.

The heat transport conservation equation in the matrix is expressed as follows:

$$\rho_m C_m \frac{\partial T_\mathrm{m}}{\partial t} = k_\mathrm{e}\frac{\partial^2 T_\mathrm{m}}{\partial z^2}. \quad (24)$$

Note that the governing equations of heat and mass transport highlight similarities between the two processes; thus, Tang's solution can also be used for heat transport.

In terms of heat transport, the coefficients $v$, $A$, $\beta^2$ and $B$ are expressed as follows:

$$v = \frac{u_f}{2D_\mathrm{fH}}, \quad (25)$$

$$A = \frac{\delta}{\sqrt{\theta D_\mathrm{e}}}, \quad (26)$$

where $\theta = \rho_m C_m / \rho_w C_w$ and $D_e = k_e / \rho_w C_w$.

$$\beta^2 = \frac{4 D_f}{u_f^2} \tag{27}$$

$$B = \frac{1}{\sqrt{D_e}} \tag{28}$$

Three characteristic timescales can be defined:

$$t_u = \frac{L}{u_f}; t_d = \frac{L^2}{D_f}; t_e = \frac{\delta^2}{D_e}, \tag{29}$$

where $L$ (L) is the characteristic length; $t_u$ (T), $t_d$ (T) and $t_e$ (T) represent the characteristics timescales of convective transport, dispersive transport and loss of the mass or heat into the surrounding matrix.

The relative effect of dispersion, convection and matrix diffusion on mass or heat propagation in the fracture can be evaluated by comparing the corresponding timescale.

Peclet number $P_e$ is defined as the ratio between dispersive ($t_d$) and convective ($t_u$) transport times:

$$Pe = \frac{t_d}{t_u} = \frac{u_f L}{D_f}. \tag{30}$$

At high Peclet numbers transport processes are mainly governed by convection, whereas at low Peclet numbers it is mainly dispersion that dominates.

Another useful dimensionless number, generally applied in chemical engineering, is the Damköhler number that can be used in order to evaluate the influence of matrix diffusion on convection phenomena. $Da$ relates the convection timescale to the exchange timescale:

$$Da = \frac{t_u}{t_e} = \frac{\alpha L}{u_f}, \tag{31}$$

where $\alpha$ ($T^{-1}$) is the exchange rate coefficient corresponding to

$$\alpha = \frac{D_e}{\delta^2}. \tag{32}$$

Note that the inverse of $t_e$ has the same meaning as the exchange rate coefficient $\alpha$ ($T^{-1}$).

When $t_e$ values are of the same order of magnitude as the transport time $t_u$ ($Da \cong 1$), diffusive processes in the matrix are more relevant. In this case concentration or temperature distribution profiles are characterized by a long tail.

When $t_e \gg t_u$ ($Da \ll 1$), the fracture–matrix exchange is very slow and it does not influence mass or heat propagation. By contrast, when $t_e \ll t_u$ ($Da \gg 1$), the fracture–matrix exchange is rapid, there is instantaneous equilibrium between the fracture and the matrix, and they have the same concentration or temperature. These two circumstances close the standard advective–dispersive transport equation.

The product between $Pe$ and $Da$ represents another dimensionless group which is a measure of transport processes:

$$Pe \times Da = \frac{t_d}{t_e} = \frac{\alpha L^2}{D_f}. \tag{33}$$

When $Pe \times Da$ increases, $t_e$ decreases more rapidly than $t_d$, and subsequently the mass or heat diffusion into the matrix may be dominant on the longitudinal dispersion.

### 2.3 Explicit Network Model (ENM)

The 2-D Explicit Network Model (ENM) depicts the fractures as 1-D pipe elements forming a 2-D pipe network, and therefore expressly takes the fracture network geometry into account. The ENM permits one to understand the physical meaning of flow and transport phenomena and therefore to obtain a more accurate estimation of flow and transport parameters.

With the assumption that a $j$th SF can be schematized by a 1-D pipe element, the Forchheimer model can be used to write the relationship between head loss $\Delta h_j$ (L) and flow rate $Q_j$ ($L^3T^{-1}$) in finite terms:

$$\frac{\Delta h_j}{L_j} = a Q_j + b Q_j^2 \Rightarrow \Delta h_j = \left[ L_j \left( a + b Q_j \right) \right] Q_j, \tag{34}$$

where $L_j$ (L) is the length of $j$th SF, and $a$ ($TL^{-3}$) and $b$ ($T^2L^{-6}$) represent the Forchheimer parameters written in finite terms. The term in the square brackets constitutes the resistance to flow $R_j\left(Q_j\right)$ ($TL^{-2}$) of $j$th SF.

In case of steady-state conditions and for a simple 2-D fracture network geometry, a straightforward manner can be applied to obtain the solution of a flow field by applying the first and second Kirchhoff laws.

In a 2-D fracture network, fractures can be arranged in series and/or in parallel. Specifically, in a network in which fractures are set in a chain, the total resistance to flow is calculated by simply adding up the resistance values of each single fracture. The flow in a parallel fracture network breaks up, with some flowing along each parallel branch and recombining when the branches meet again. In order to estimate the total resistance to flow, the reciprocals of the resistance values have to be added up, and then the reciprocal of the total has to be calculated. The flow rate $Q_j$ across the generic fracture $j$ of the parallel network can be calculated as (Cherubini et al., 2014)

$$Q_j = \sum_{i=1}^{n} Q_i \left[ \frac{1}{R_j \left( \sum_{i=1}^{n} \frac{1}{R_i} \right)^{-1}} \right], \tag{35}$$

where $\sum_{i=1}^{n} Q_i$ ($LT^{-3}$) is the sum of the mass flow rates at fracture intersections in correspondence to the inlet bond of $j$ fracture, whereas the term in square brackets represents the probability of water distribution of $j$ fracture $P_{Q,j}$.

Once the flow field in the fracture network is known, to obtain the PDF at a generic node, the PDFs of each elementary path that reaches the node have to be summed up. They can be calculated as the convolution product of the PDFs of each single fracture composing the elementary path.

Definitely, the BTC describing the concentration in the fracture as a function of time at the generic node, using the convolution theorem, can be obtained as follows:

$$c_{\mathrm{f}}(t) = c_0 + c_{\mathrm{inj}}(t) \cdot \mathcal{L}^{-1}\left[\sum_{i=1}^{N_{\mathrm{p}}} \prod_{j=1}^{n_{f,i}} P_{\mathrm{M},j}\,\overline{\Gamma}_j(s)\right], \tag{36}$$

where $c_0$ ($\mathrm{ML}^{-3}$) is the initial concentration and $c_{\mathrm{inj}}$ ($\mathrm{ML}^{-3}$) is the concentration injection function, $*$ is the convolution operator, $\mathcal{L}^{-1}$ represents the inverse Laplace transform operator, $N_{\mathrm{p}}$ is the number of the paths reaching the node, $n_{f,i}$ is the number of the SF belonging to the elementary path $i$th, and $P_{\mathrm{M},j}$ and $\overline{\Gamma}(s)$ are the mass distribution probability and the PDF in the Laplace space of the generic $j$th SF, respectively. The inverse Laplace transform $\mathcal{L}^{-1}$ can be solved numerically using the Abate and Ward (2006) algorithm.

In the same way the BTC $T_{\mathrm{f}}$ which describes the temperature in the fracture as a function of time at the generic node can be written as

$$T_{\mathrm{f}}(t) = T_0 + T_{\mathrm{inj}}(t) \cdot \mathcal{L}^{-1}\left[\sum_{i=1}^{N_{\mathrm{p}}} \prod_{j=1}^{n_{f,i}} P_{\mathrm{H},j}\,\overline{\Gamma}_j(s)\right], \tag{37}$$

where $T_0$ (K) is the initial temperature, $T_{\mathrm{inj}}$ (K) is the temperature injection function and $P_{\mathrm{H},j}$ is the heat distribution probability.

$P_{\mathrm{M},j}$ and $P_{\mathrm{H},j}$ can be estimated as the probabilities of the mass and heat distribution at the inlet bond of each individual SF, respectively. The mass and heat distribution is proportional to the correspondent flow rates:

$$P_{\mathrm{M},j} = P_{\mathrm{H},j} = \frac{Q_j}{\sum_{i=1}^{n} Q_i}. \tag{38}$$

Note that if Eq. (38) is valid, the probability of water distribution is equal to the probabilities of mass and heat distribution (term in square brackets in Eq. 34). Therefore, the ENM model regarding each SF can be described by four parameters ($u_{f,j}$, $D_{f,j}$, $\alpha_j$, $P_{Q,j}$).

## 3 Material and methods

### 3.1 Description of the experimental apparatus

The heat transfer tests have been carried out on the experimental apparatus previously employed to perform flow and tracer transport experiments at bench scale (Cherubini et al. 2012, 2013a, b, c, 2014). However, the apparatus has been modified in order to analyze heat transport dynamics. Two thermocouples have been placed at the inlet and the outlet of a selected fracture path of the limestone block with parallelepiped shape ($0.6 \times 0.4 \times 0.08\,\mathrm{m}^3$) described in previous studies. A TC-08 Thermocouple Data Logger (pico Technology) with a sampling rate of 1 s has been connected to the thermocouples. An extruded polystyrene panel with thermal conductivity equal to $0.034\,\mathrm{Wm}^{-1}\,\mathrm{K}^{-1}$ and thickness 0.05 m has been used to thermally insulate the limestone block which has then been connected to a hydraulic circuit. The head loss between the upstream tank connected to the inlet port and the downstream tank connected to the outlet port drives flow of water through the fractured block. An ultrasonic velocimeter (DOP3000 by Signal Processing) has been adopted to measure the instantaneous flow rate that flows across the block. An electric boiler with a volume of $10^{-2}\,\mathrm{m}^3$ has been used to heat the water. In a flow cell located in correspondence to the outlet port, a multiparametric probe is positioned for the instantaneous measurement of pressure (dbar), temperature (°C) and electric conductivity ($\mu\mathrm{S\,cm}^{-1}$). Figure 1a shows the fractured block sealed with epoxy resin and Figure 1b shows the thermal insulated fractured block connected to the hydraulic circuit, whereas the schematic diagram of the experimental apparatus is shown in Fig. 2.

### 3.2 Flow experiments

The average flow rate through the selected path can be evaluated as

$$\overline{Q} = \frac{S_1}{t_1 - t_0}(h_1 - h_0), \tag{39}$$

where $S_1$ ($\mathrm{L}^2$) is the cross-sectional area of the flow cell, and $\Delta t = t_1 - t_0$ is the time for the flow cell to be filled from $h_0$ (L) and $h_1$ (L). To calculate the head loss between the upstream tank and the flow cell, the following expression is adopted:

$$\Delta h = h_c - \frac{h_0 + h_1}{2}, \tag{40}$$

where $h_c$ is the hydraulic head measured in the upstream tank. Several tests have been carried out varying the control head, and in correspondence to each value of the average flow rate and head loss, the average resistance to flow has been determined as

$$\overline{R}(\overline{Q}) = \left[\frac{S_1}{t_1 - t_0} \ln\left(\frac{h_0 - h_c}{h_1 - h_c}\right)\right]^{-1}. \tag{41}$$

### 3.3 Solute and temperature tracer tests

Solute and temperature tracer tests have been conducted through the following steps.

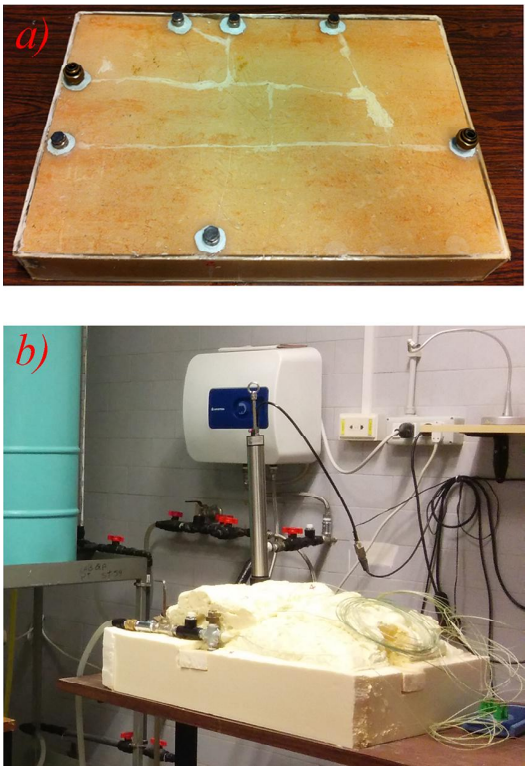


**Figure 1. (a)** Fractured block sealed with epoxy resin. **(b)** Thermal insulated fracture block connected to the hydraulic circuit.

As an initial condition, a specific value of the hydraulic head difference between the upstream tank and the downstream tank has been assigned. At $t = 0$, valve $a$ is closed so that the hydrostatic head inside the block assumes the same value as the one in the downstream tank. At $t = 10$ s, valve $a$ is opened.

For the solute tracer test at time $t = 60$ s by means of a syringe, a mass of $5 \times 10^{-4}$ kg sodium chloride is injected into the inlet port. Due to the very short source release time, the instantaneous source assumption can be adopted which assumes the source of a solute as an instantaneous injection (pulse). The multiparametric probe located within the flow cell measures the solute BTC.

As concerns thermal tracer tests at the time $t = 60$ s, the valve $d$ is opened, while the valve $c$ is closed. In such a way a step temperature function in correspondence to the inlet port $T_{\mathrm{inj}}(t)$ is imposed and measured by the first thermocouple. The other thermocouple located inside the outlet port is used to measure the thermal BTC.

The ultrasonic velocimeter is used in order to measure the instantaneous flow rate, whereas a multiparametric probe located at the outlet port measures the pressure and the electric conductivity.

## 4 Results and discussion

### 4.1 Flow characteristics

The Kirchhoff laws have been used in order to estimate the flow rates flowing in each single fracture. In Fig. 3 a sketch of the 2-D pipe conceptualization of the fracture network is reported.

The resistance to flow of each SF can be evaluated as the square bracket in Eq. (34). For simplicity the linear and nonlinear terms have been considered constant and equal for each SF.

The resistance to flow for the whole fracture network $\overline{R}(\overline{Q})$ can be evaluated as the sum of the resistance to flow of each SF arranged in a chain and the total resistance of the parallel branches equal to the reciprocal of the sum of the reciprocal of the resistance to flow of each parallel branch:

$$\overline{R}(\overline{Q}) = R_1(Q_0) + R_2(Q_0) + \left(\frac{1}{R_6(Q_1)} + \frac{1}{R_3(Q_2) + R_4(Q_2) + R_5(Q_2)}\right)^{-1} + R_7(Q_0) + R_8(Q_0) + R_9(Q_0), \quad (42)$$

where $R_j$ with $j = 1$–$9$ represents the resistance to flow of each SF, $Q_0$ is the injection flow rate, and $Q_1$ and $Q_2$ are the flow rates flowing in parallel branches 6 and 3–5, respectively.

The flow rate $Q_1$ is determined in an iterative manner using the following iterative equation derived by Eq. (35) at node 3:

$$Q_1^{k+1} = Q_0 \cdot \left[\frac{1}{R_6(Q_1^k)}\left(\frac{1}{R_3(Q_0 - Q_1^k) + R_4(Q_0 - Q_1^k) + R_5(Q_0 - Q_1^k)} + \frac{1}{R_6(Q_1^k)}\right)^{-1}\right], \quad (43)$$

whereas the flow rate $Q_2$ is determined merely as

$$Q_2 = Q_0 - Q_1. \quad (44)$$

The linear and nonlinear terms representative of the whole fracture network have been estimated by matching the average experimental resistance to flow resulting from Eq. (41) with resistance to flow estimated from Eq. (42).

The linear and nonlinear terms are equal, respectively, to $a = 7.345 \times 10^4$ sm$^{-3}$ and $b = 11.65 \times 10^9$ s$^2$ m$^{-6}$. Inertial forces dominate viscous ones when the Forchheimer number ($Fo$) is higher than one. $Fo$ can be evaluated as the ratio between the nonlinear loss $(bQ^2)$ and the linear loss $(aQ)$. The critical flow rate $Q_{\mathrm{crit}}$ which represents the value of the

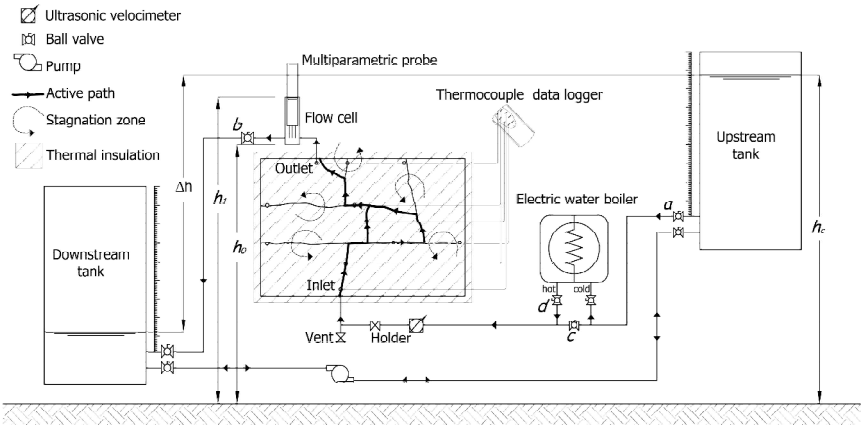


**Figure 2.** Schematic diagram of the experimental setup.

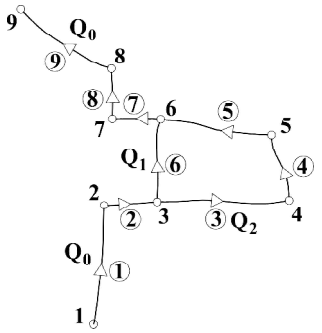


**Figure 3.** Two-dimensional pipe network conceptualization of the fracture network of the fractured rock block in Fig. 1. $Q_0$ is the injection flow rate; $Q_1$ and $Q_2$ are the flow rates that flow in parallel branches 6 and 3–5, respectively.

flow rate for which $Fo = 1$ is derived as the ratio between $a$ and $b$ resulting in $Q_{\text{crit}} = 6.30 \times 10^{-6}\ \text{m}^3\ \text{s}^{-1}$.

Because of the nonlinearity of flow, varying the inlet flow rate $Q_0$, the ratio between the flow rates $Q_1$ and $Q_2$ flowing, respectively, in branches 6 and 3–5 is not constant. When $Q_0$ increases, $Q_2$ increases faster than $Q_1$. The probability of the water distribution of the branch 6 $P_{Q,6}$ is evaluated as the ratio between $Q_0$ and $Q_1$, whereas the probability of the water distribution of branches 3–5 is equal to $P_{Q,3\text{–}5} = 1 - P_{Q,6}$.

### 4.2 Fitting of breakthrough curves and interpretation of estimated model parameters

The behavior of mass and heat transport has been compared by varying the injection flow rates. In particular, 21 tests in the range $1.83 \times 10^{-6}$–$1.26 \times 10^{-5}\ \text{m}^3\ \text{s}^{-1}$ ($Re$ in the range 17.5–78.71) for heat transport have been performed and compared with the 55 tests in the range 1.32–$8.34 \times 10^{-6}\ \text{m}^3\ \text{s}^{-1}$ ($Re$ in the range 8.2–52.1) for solute transport presented in previous studies.

The observed heat and mass BTCs for different flow rates have been individually fitted using the ENM approach presented in Sect. 2.3. For simplicity, the transport parameters $u_f$, $D_f$ and $\alpha$ are assumed equal for all branches of the fracture network. The probability of mass and heat distribution is assumed equal to the probability of water distribution.

The experimental BTCs are fitted using Eqs. (36) and (37) for mass and heat transport, respectively. Note that, for mass transport, $c_{\text{inj}}(t)$ supposing the instantaneous injection condition becomes a Dirac delta function.

The determination coefficient ($r^2$) and the root mean square error (RMSE) have been used in order to evaluate the goodness of fit.

Tables 1 and 2 show the values of transport parameters, the RMSE and $r^2$ for mass and heat transport, respectively. Furthermore Figs. 4 and 5 show the fitting results of BTCs for some values of $Q_0$.

The results presented in Tables 1 and 2 highlight that the estimated convective velocities $u_f$ for heat transport are lower than for mass transport, whereas the estimated dispersion $D_f$ for heat transport is higher than for mass transport. Regarding the transfer rate coefficient $\alpha$, it assumes very low values for mass transport relative to the convective velocity. Instead, for heat transport the exchange rate coefficient is on the same order of magnitude of the convective velocity and, considering a characteristic length equal to $L = 0.601$ m corresponding to the length of the main path of the fracture network, the effect of dual porosity is very strong and cannot be neglected relative to the investigated injection flow range.

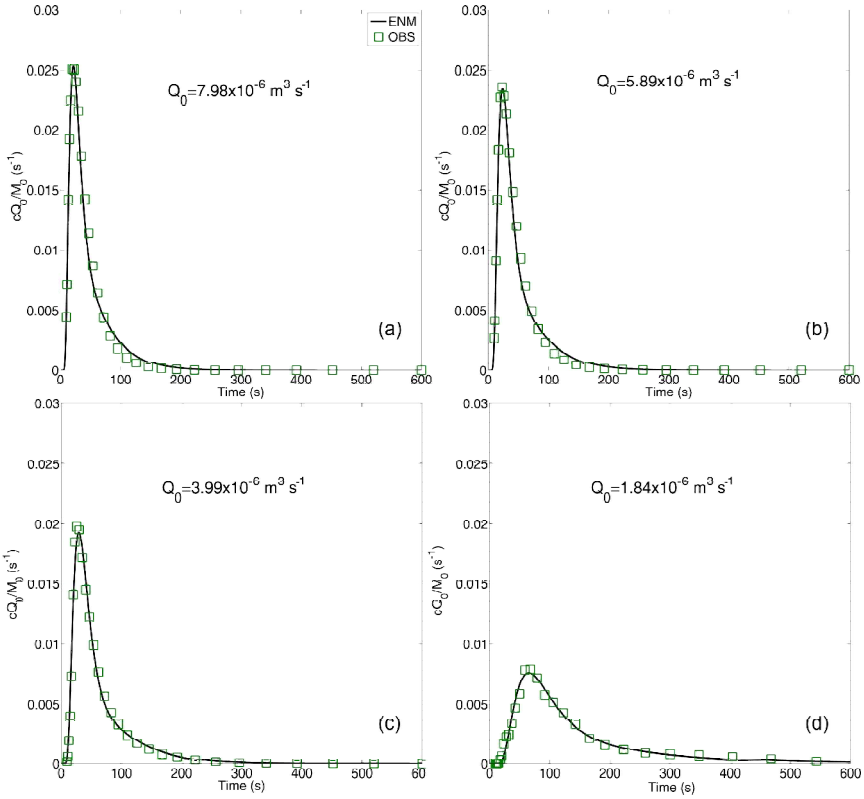


**Figure 4.** Fitting of BTCs at different injection flow rates using the ENM with Tang's solution for mass transport. The green square curve is the observed specific mass flux at the outlet port; the continuous black line is the simulated specific mass flux.

Both mass and heat transport show a satisfactory fitting. In a particular manner, *RMSE* varies in the range 0.0015–0.0180 for mass transport and in the range 0.0030–0.236 for heat transport, whereas $r^2$ varies in the range 0.9863–0.9987 for mass transport and in the range 0.0963–0.9998 for heat transport.

In order to investigate the different behavior between mass and heat transport, the relationships between injection flow rate and the transport parameters have been analyzed. In Fig. 6 the relationship between $u_f$ and $Q_0$ is reported, whereas in Figs. 7 and 8 the dispersion coefficient $D_f$ and the exchange term $\alpha$ as a function of $u_f$, respectively, are reported. The figures show a very different behavior between mass and heat transport.

Regarding mass transport experiments according to previous studies (Cherubini at al., 2013a, b, c, 2014), Fig. 5 shows that for values of $Q_0$ higher than $4 \times 10^{-6}\,\mathrm{m^3\,s^{-1}}$ $u_f$ increases less rapidly. This behavior was due to the presence of inertial forces that gave rise to a retardation effect on solute transport.

Instead, Fig. 7 shows a linear relationship between $u_f$ and $D_f$, suggesting that inertial forces did not exert any effect on dispersion and that geometrical dispersion dominates the Aris–Taylor dispersion.

In the same way as for mass transport, for heat transfer a linear relationship is evident between dispersion and convective velocity. Even if heat convective velocity is lower than solute advective velocity, the longitudinal thermal dispersivity assumes higher values than the longitudinal solute dispersivity. Also, for heat transport experiments, a linear relationship between $u_f$ and $D_f$ has been found.

Figure 8 shows the exchange rate coefficient $\alpha$ as a function of the convective velocity $u_f$ for both mass and heat transport.

Regarding the mass transport, the estimated exchange rate coefficient $\alpha$ is much lower than the convective velocity. These results suggest that in the case study fracture–matrix

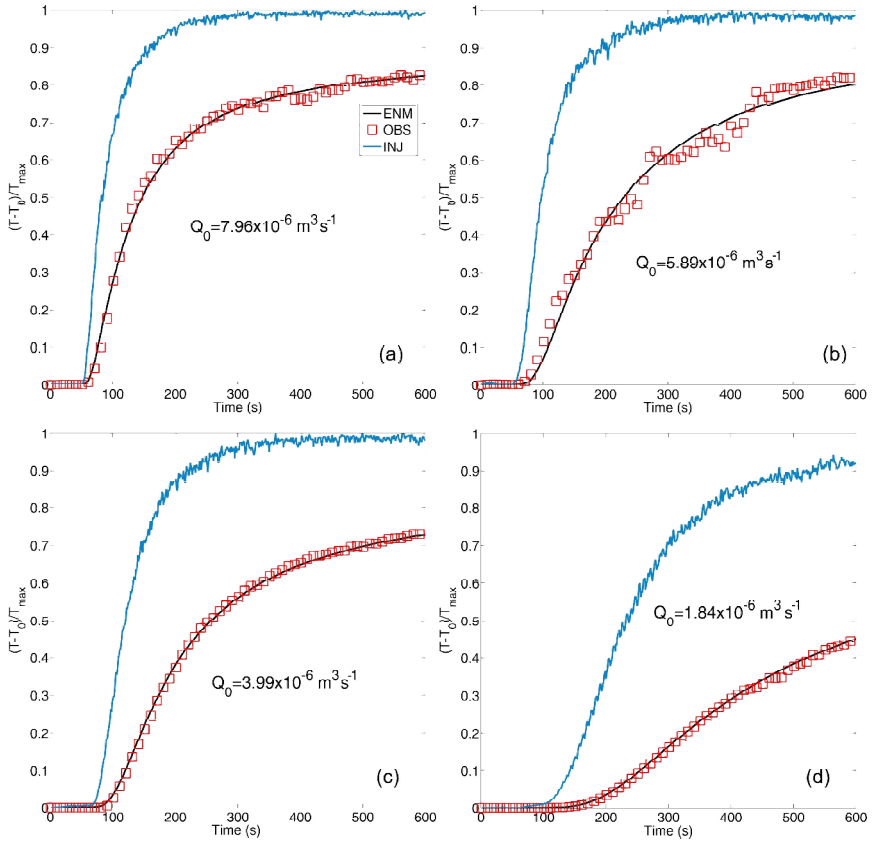


**Figure 5.** Fitting of BTCs at different injection flow rates using the ENM with Tang's solution for heat transport. The blue curve is the temperature observed at the inlet port used as the temperature injection function, the red square curve is the observed temperature at the outlet port, and the black continuous curve is the simulated temperature at the outlet port.

exchange is very slow and that it may not influence mass transport. Non-Fickian behavior observed in the experimental BTCs is therefore dominated mainly by the presence of inertial forces and the parallel branches.

A very different behavior is observed for heat transport. Heat convective velocity does not seem to be influenced by the presence of the inertial force, whereas $u_f$ is influenced by fracture–matrix exchange phenomena resulting in a significant retardation effect. Once the model parameters for each flow rate have been determined, the unit response function ($f_{\mathrm{URF}}$), corresponding to the PDF obtained from impulsive injection of both solute and temperature tracers, is obtained. The unit response function can be characterized using the time moments and tail character analysis.

The mean residence time $t_{\mathrm{m}}$ assumes the following expression:

$$t_{\mathrm{m}} = \frac{\int_0^\infty t\, f_{\mathrm{URF}}(t)\,\mathrm{d}t}{\int_0^\infty f_{\mathrm{URF}}(t)\,\mathrm{d}t}, \tag{45}$$

whereas the $n$th normalized central moment of distribution of $f_{\mathrm{URF}}$ versus time can be written as

$$\mu_n = \frac{\int_0^\infty (t - t_{\mathrm{m}})^n\, f_{\mathrm{URF}}(t)\,\mathrm{d}t}{\int_0^\infty f_{\mathrm{URF}}(t)\,\mathrm{d}t}. \tag{46}$$

The second moment $\mu_2$ can be used in order to evaluate the dispersion relative to $t_{\mathrm{m}}$, whereas the skewness is a measure

**Table 1.** Estimated values of parameters, RMSE, and determination coefficient $r^2$ for the ENM with Tang's solution at different injection flow rates for mass transport.

| Injection flow rate $Q_0$ ($m^3\ s^{-1}$) $\times 10^{-6}$ | Convective velocity $u_f$ ($ms^{-1}$) $\times 10^{-3}$ | Dispersion $D_f$ ($ms^{-2}$) $\times 10^{-3}$ | Exchange rate coefficient ($s^{-1}$) $\times 10^{-6}$ | RMSE | $r^2$ |
|---|---|---|---|---|---|
| 1.319 | 4.38 ÷ 4.47 | 0.68 ÷ 0.70 | 4.80 ÷ 5.06 | 0.0053 | 0.9863 |
| 1.843 | 6.21 ÷ 6.28 | 0.57 ÷ 0.58 | 2.86 ÷ 3.01 | 0.0026 | 0.9954 |
| 2.234 | 6.54 ÷ 6.59 | 0.66 ÷ 0.67 | 3.09 ÷ 3.13 | 0.0017 | 0.9976 |
| 2.402 | 7.64 ÷ 7.68 | 0.67 ÷ 0.67 | 2.65 ÷ 2.68 | 0.0015 | 0.9983 |
| 2.598 | 9.88 ÷ 9.94 | 0.80 ÷ 0.82 | 2.76 ÷ 2.84 | 0.0015 | 0.9987 |
| 2.731 | 8.27 ÷ 8.35 | 0.75 ÷ 0.76 | 2.80 ÷ 2.91 | 0.0018 | 0.9977 |
| 2.766 | 8.35 ÷ 8.41 | 0.84 ÷ 0.85 | 2.65 ÷ 2.69 | 0.0021 | 0.9978 |
| 3.076 | 11.33 ÷ 11.43 | 0.89 ÷ 0.91 | 2.53 ÷ 2.59 | 0.0029 | 0.9982 |
| 3.084 | 10.86 ÷ 10.95 | 0.87 ÷ 0.89 | 3.11 ÷ 3.18 | 0.0022 | 0.9982 |
| 4.074 | 15.88 ÷ 16.02 | 1.19 ÷ 1.21 | 2.89 ÷ 2.94 | 0.0048 | 0.9979 |
| 4.087 | 15.07 ÷ 15.20 | 1.11 ÷ 1.13 | 3.75 ÷ 3.83 | 0.0045 | 0.9976 |
| 4.132 | 14.71 ÷ 14.82 | 1.08 ÷ 1.09 | 2.93 ÷ 2.98 | 0.0028 | 0.9985 |
| 4.354 | 15.63 ÷ 15.77 | 1.14 ÷ 1.16 | 3.24 ÷ 3.30 | 0.0052 | 0.9979 |
| 4.529 | 17.05 ÷ 17.21 | 1.30 ÷ 1.32 | 2.88 ÷ 2.94 | 0.0055 | 0.9978 |
| 5.852 | 19.26 ÷ 19.38 | 1.44 ÷ 1.46 | 4.21 ÷ 4.25 | 0.0042 | 0.9983 |
| 5.895 | 19.38 ÷ 19.54 | 1.37 ÷ 1.39 | 3.77 ÷ 3.82 | 0.0058 | 0.9981 |
| 6.168 | 18.98 ÷ 19.17 | 1.36 ÷ 1.39 | 2.87 ÷ 2.92 | 0.0091 | 0.9973 |
| 7.076 | 20.64 ÷ 20.86 | 1.36 ÷ 1.39 | 3.33 ÷ 3.39 | 0.0123 | 0.9963 |
| 7.620 | 20.47 ÷ 20.75 | 1.52 ÷ 1.55 | 2.33 ÷ 2.39 | 0.0180 | 0.9951 |
| 7.983 | 21.33 ÷ 21.58 | 1.61 ÷ 1.64 | 2.92 ÷ 2.98 | 0.0137 | 0.9965 |
| 8.345 | 21.71 ÷ 21.97 | 1.65 ÷ 1.68 | 2.81 ÷ 2.86 | 0.0136 | 0.9964 |

**Table 2.** Estimated values of parameters, RMSE, and determination coefficient $r^2$ for the ENM with Tang's solution at different injection flow rates for heat transport.

| Injection flow rate $Q_0$ ($m^3\ s^{-1}$) $\times 10^{-6}$ | Convective velocity $u_f$ ($ms^{-1}$) $\times 10^{-3}$ | Dispersion $D_f$ ($ms^{-2}$) $\times 10^{-3}$ | Exchange rate coefficient ($s^{-1}$) $\times 10^{-3}$ | RMSE | $r^2$ |
|---|---|---|---|---|---|
| 1.835 | 2.20 ÷ 2.91 | 1.91 ÷ 1.95 | 6.27 ÷ 6.59 | 0.0065 | 0.9997 |
| 2.325 | 1.74 ÷ 2.73 | 1.82 ÷ 1.91 | 5.39 ÷ 9.26 | 0.0098 | 0.9992 |
| 2.462 | 0.35 ÷ 0.52 | 2.42 ÷ 2.57 | 2.25 ÷ 2.33 | 0.0138 | 0.9984 |
| 2.605 | 0.44 ÷ 0.54 | 2.33 ÷ 2.40 | 0.74 ÷ 0.77 | 0.0073 | 0.9995 |
| 2.680 | 2.18 ÷ 2.95 | 1.77 ÷ 1.83 | 5.68 ÷ 8.31 | 0.0030 | 0.9998 |
| 2.800 | 0.36 ÷ 0.79 | 2.53 ÷ 2.68 | 3.54 ÷ 3.72 | 0.0213 | 0.9982 |
| 2.847 | 1.73 ÷ 3.16 | 1.98 ÷ 2.06 | 4.95 ÷ 13.45 | 0.0283 | 0.9978 |
| 3.003 | 2.34 ÷ 2.87 | 2.24 ÷ 2.32 | 5.33 ÷ 6.55 | 0.0033 | 0.9998 |
| 3.998 | 2.56 ÷ 2.75 | 6.63 ÷ 6.80 | 2.05 ÷ 2.11 | 0.0150 | 0.9993 |
| 4.030 | 2.60 ÷ 2.83 | 7.18 ÷ 7.36 | 1.42 ÷ 1.52 | 0.0147 | 0.9993 |
| 4.217 | 3.85 ÷ 4.56 | 8.92 ÷ 9.29 | 4.86 ÷ 5.77 | 0.0228 | 0.9945 |
| 4.225 | 2.43 ÷ 2.64 | 7.53 ÷ 7.84 | 1.64 ÷ 1.80 | 0.0251 | 0.9987 |
| 4.471 | 2.30 ÷ 3.13 | 9.18 ÷ 9.50 | 1.06 ÷ 1.33 | 0.1115 | 0.9957 |
| 5.837 | 3.51 ÷ 4.13 | 4.95 ÷ 5.36 | 0.61 ÷ 0.79 | 0.2360 | 0.9872 |
| 5.880 | 2.71 ÷ 3.10 | 4.23 ÷ 4.60 | 0.04 ÷ 0.05 | 0.1997 | 0.9926 |
| 6.445 | 4.71 ÷ 5.12 | 6.18 ÷ 6.81 | 1.49 ÷ 1.54 | 0.2156 | 0.9863 |
| 7.056 | 8.15 ÷ 8.46 | 10.05 ÷ 10.74 | 5.63 ÷ 6.00 | 0.0694 | 0.9951 |
| 7.959 | 9.64 ÷ 10.11 | 18.40 ÷ 19.47 | 10.92 ÷ 11.55 | 0.0662 | 0.9971 |
| 8.971 | 13.40 ÷ 13.79 | 24.57 ÷ 25.82 | 15.35 ÷ 15.85 | 0.0303 | 0.9985 |
| 12.364 | 11.01 ÷ 11.67 | 21.97 ÷ 22.63 | 5.23 ÷ 5.25 | 0.0631 | 0.9939 |
| 12.595 | 13.71 ÷ 14.26 | 26.65 ÷ 27.61 | 9.26 ÷ 9.41 | 0.0426 | 0.9955 |

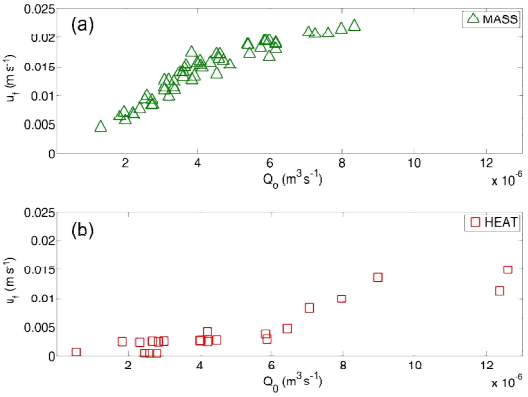


**Figure 6.** Velocity $u_f$ (m s$^{-1}$) as a function of the injection flow rate $Q_0$ (m$^3$ s$^{-1}$) for the ENM with Tang's solution for both mass and heat transport.

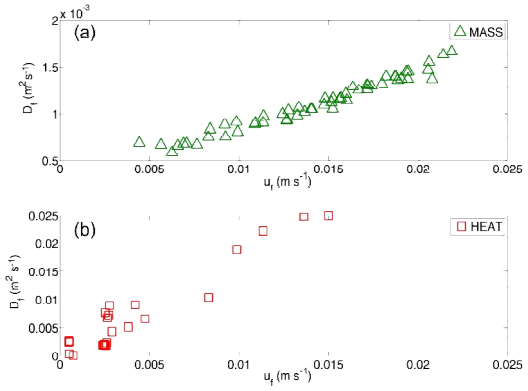


**Figure 7.** Dispersion $D_f$ (m s$^{-2}$) as a function of velocity $u_f$ (m s$^{-1}$) for the ENM with Tang's solution for both mass and heat transport.

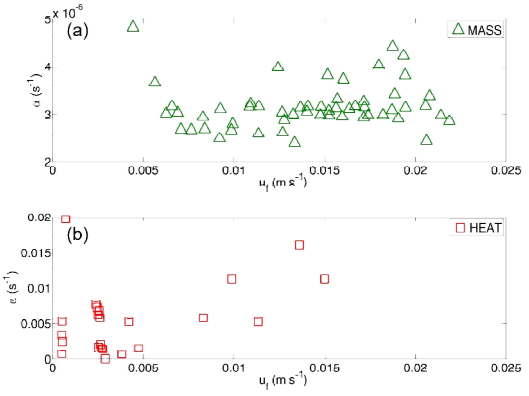


**Figure 8.** Transfer coefficient $\alpha$ (s$^{-1}$) as a function of velocity $u_f$ (m s$^{-1}$) for both mass and heat transport.

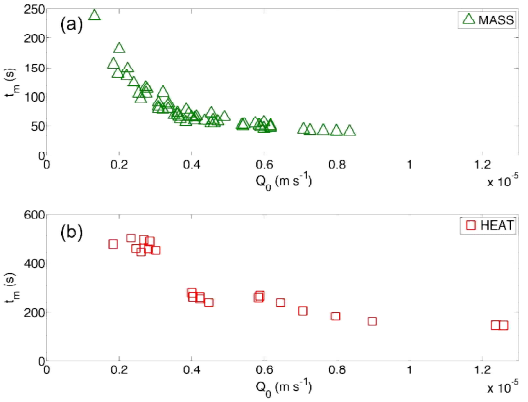


**Figure 9.** Mean travel time $t_m$ (s) as a function of the injection flow rate for both mass and heat transport.

of the degree of asymmetry and is defined as follows:

$$S = \mu_3/\mu_2^{3/2}. \tag{47}$$

The tailing character $t_c$ can be described as

$$t_c = \frac{\Delta t_{fall}}{\Delta t_{rise}}, \tag{48}$$

where $\Delta t_{fall}$ denotes the duration of the falling limb defined as the time interval from the peak to the tail cutoff, which is the time when the falling limb first reaches a value that is 0.05 times the peak value. $\Delta t_{rise}$ is defined as the time interval from the first arrival to the peak. This quantity provides a measure of the asymmetry between the rising and falling limbs. A value of $t_c$ significantly higher than 1 indicates an elongated tail compared to the rising limb (Cherubini et al., 2010).

In Fig. 9 is reported the residence time versus the injection flow rates. The figure highlights that $t_m$ for heat transport is about 3 times higher than for mass transport. In a particular way, $t_m$ varies in the range 40.3–237.1 s for mass transport and in the range 147.8–506.9 s for heat transport. This result still highlights that heat transport is more delayed than mass transport.

In the same way the skewness $S$ (Fig. 10) and the tailing character $t_c$ (Fig. 11) are reported as a function of $Q_0$.

A different behavior for heat and mass transport is observed for the skewness coefficient. For heat transfer the skewness shows a growth trend which seems to decrease af-

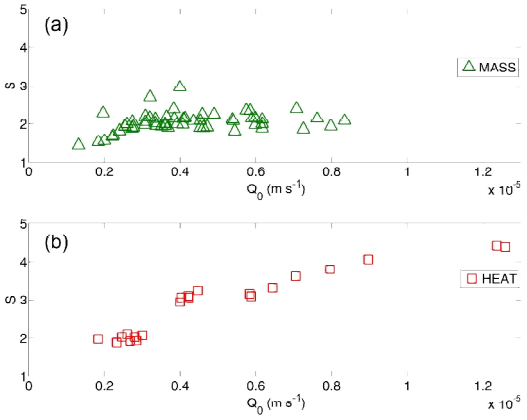


**Figure 10.** Skewness as a function of the injection flow rate for both mass and heat transport.

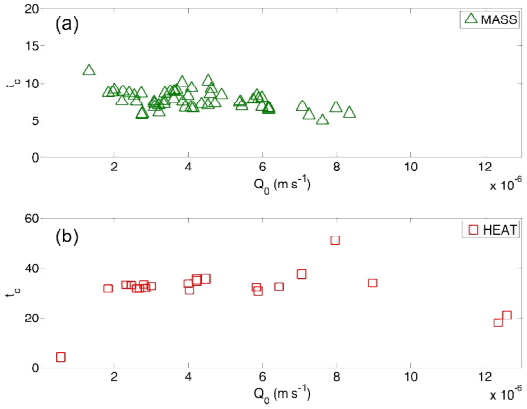


**Figure 11.** Tailing character $t_c$ as a function of the injection flow rate for both mass and heat transport.

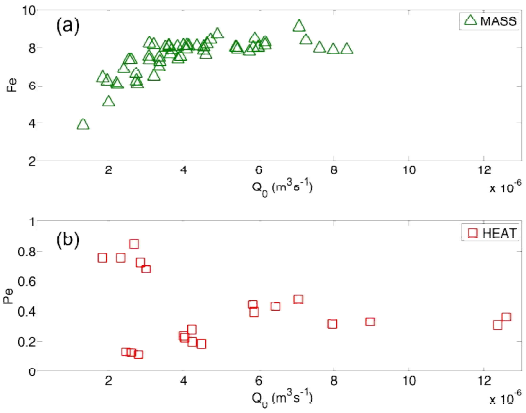


**Figure 12.** Peclet number as a function of the injection flow rate $Q_0$ (m$^3$ s$^{-1}$) for both mass and heat transport.

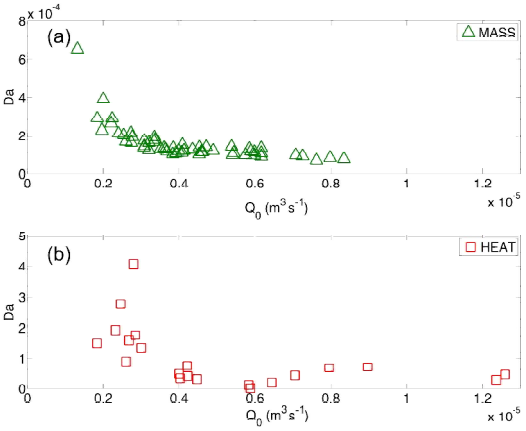


**Figure 13.** *Da* number as a function of the injection flow rate $Q_0$ (m$^3$ s$^{-1}$) for both mass and heat transport.

ter $Q_0 = 3 \times 10^{-6}$ m$^3$ s$^{-1}$. Its mean value is equal to 2.714. For solute transport the $S$ does not show a trend, and assumes a mean value equal to 2.018.

The tailing character does not exhibit a trend for either mass and heat transport. In either cases $t_c$ is significantly higher than 1, specifically 7.70 and 30.99 for mass and heat transport, respectively.

In order to explain the transport dynamics, the trends of dimensionless numbers *Pe* and *Da* varying the injection flow rate have been investigated. Figure 12 shows the *Pe* as a function of $Q_0$ for both mass and heat experiments. As concerns mass experiments, *Pe* increases as $Q_0$ increases, assuming a constant value for high values ($Pe = 7.5$) of $Q_0$. For heat transport a different behavior is observed, $P_e$ showing a constant trend and being always lower than one. Even if the injection flow rate is relatively high, thermal dispersion is the dominating mechanism in heat transfer.

Figure 12 reports *Da* as a function of $Q_0$. For mass transport *Da* assumes very low values, on the order of magnitude of $10^{-4}$.

The convective transport scale is very low with respect to the exchange transport scale; thus, the mass transport in each single fracture can be represented with the classical advection dispersion model.

As regards heat transport, *Da* assumes values around the unit showing a downward trend as injection flow rate increases, switching from higher to lower values than the unit.

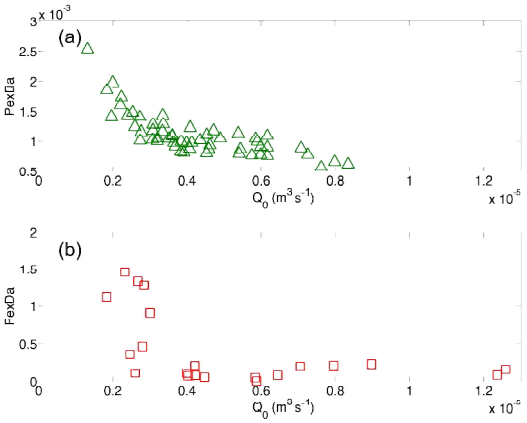


**Figure 14.** $Pe \times Da$ number as a function of the injection flow rate $Q_0$ (m$^3$ s$^{-1}$) for both mass and heat transport.

As injection flow rate increases, the convective transport timescale reduces more rapidly than the exchange timescale.

These arguments can be explained because the relationships between $Q_0$ and $u_f$ show a change in slope when $Da$ becomes lower than the unit. In other words, when $Da$ is higher than the unit, the exchange between fracture and matrix dominates on the convective transport, giving rise to a more enhanced delay on heat transport; conversely, when $Da$ is lower than one, convective transport dominates on fracture–matrix interactions and the delay effect is reduced.

Furthermore this effect is evident also in the trend observed in the graph $S - Q_0$ (Fig. 10). For values of $Da$ lower than the unit, a change in slope is evident; the skewness coefficient increases more slowly. Thus for $Da > 1$ the early arrival and the tail effect of BTC increase more rapidly than for $Da < 1$.

Note that even if $Da$ presents a downward trend as $Q_0$ increases, when the latter exceeds $Q_{\text{crit}}$ a weak growth trend for $Da$ is detected, which however assumes values lower than the unit.

Figure 14 shows the dimensionless group $Pe \times Da$ varying the injection flow rate. Regarding mass transport, $Pe \times Da$ is on the order of magnitude of $10^{-3}$, confirming the fact that the fracture–matrix interaction can be neglected relative to the investigated range of injection flow rates. For heat transport, $Pe \times Da$ assumes values just below the unit, with a downward trend as $Q_0$ increases. $t_d$ and $t_e$ have the same order of magnitude.

In order to find the optimal conditions for heat transfer in the analyzed fractured medium, the thermal power exchanged per unit temperature difference $\dot{Q}$ (ML$^2$ T$^{-1}$ K$^{-1}$) for each injection flow rate in quasi-steady-state conditions can be estimated. The thermal power exchanged can be written as

$$\dot{Q} = \rho C_w Q_0 \left(T_{\text{inj}} - T_{\text{out}}\right). \tag{49}$$

The outlet temperature $T_{\text{out}}$ can be evaluated as a function of the $f_{\text{URF}}$ using the following expression:

$$T_{\text{out}} = T_0 + \left(T_{\text{inj}} - T_0\right) \int_0^\infty f_{\text{URF}}(t)\,\mathrm{d}t. \tag{50}$$

Substituting Eq. (50) into Eq. (49), the thermal power exchanged per unit temperature difference is

$$\frac{\dot{Q}}{\left(T_{\text{inj}} - T_0\right)} = \left(1 - \int_0^\infty f_{\text{URF}}(t)\,\mathrm{d}t\right) \rho C_W Q_0. \tag{51}$$

Figure 15 shows the similarities between the relationship $\dot{Q}/\left(T_{\text{inj}} - T_0\right) - Q_0$ (Fig. 15a) and $Da - Q_0$ (Fig. 14b). Higher $Da$ values correspond to higher values of $\dot{Q}/\left(T_{\text{inj}} - T_0\right)$. The thermal power exchanged increases as the Damköhler number increases, as shown in Fig. 15c. These results highlight that for the observed case study the optimal condition for thermal exchange in the fractured medium is obtained when the exchange timescale is lower than the convective transport scale, or rather when the dynamics of fracture–matrix exchange are dominant on the convective ones.

Moreover, in a similar way to $Da$, $\dot{Q}/\left(T_{\text{inj}} - T_0\right)$ shows a weak growth trend when $Q_0$ exceeds $Q_{\text{crit}}$. This means that the nonlinear flow regime improves the fracture–matrix thermal exchange; however, at high values of injection flow rates, convective and dispersion timescales are less than the exchange timescale. Nevertheless, these results have been observed in a small range of $Da$ numbers close to the unit. In order to generalize these results, a larger range of $Da$ numbers should be investigated.

In order to estimate the effective thermal conductivity coefficient $k_e$, the principle of conservation of heat energy can be applied to the whole fractured medium. Neglecting the heat stored in the fractures, the difference between the heat measured at the inlet and at the outlet must be equal to the heat diffused into the matrix:

$$\rho C_W Q_0 \left(T_{\text{inj}} - T_{\text{out}}\right) = \int_{A_f} k_e \left.\frac{\mathrm{d}T_m}{\mathrm{d}z}\right|_{z=wf/2} \mathrm{d}A_f, \tag{52}$$

where $A_f$ is the whole surface area of the whole active fracture network and the gradient of $T_m$ can be evaluated according to Eq. (19) using temperature instead of concentration as a variable. Then the average effective thermal conductivity $\overline{k}_e$ can be obtained as

$$\overline{k}_e = \frac{\rho_w C_w Q_0 \left(T_{\text{inj}} - T_{\text{out}}\right)}{\int_{A_f} \left.\frac{\mathrm{d}T}{\mathrm{d}z}\right|_{z=wf/2} \mathrm{d}A_f}. \tag{53}$$

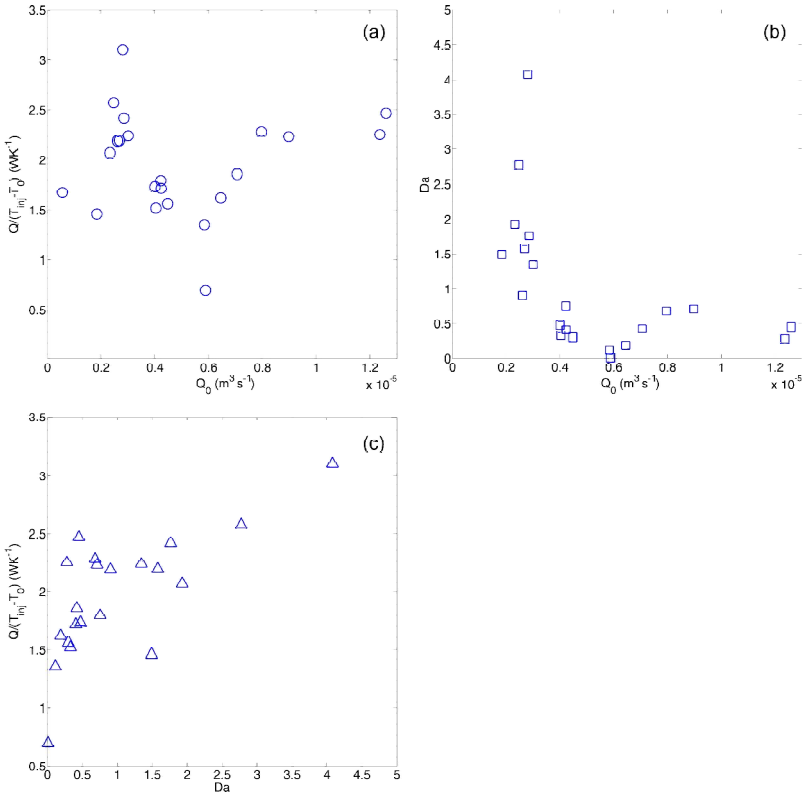


**Figure 15.** Heat power exchanged per difference temperature unit $\dot{Q}/(T_{\mathrm{inj}} - T_0)$ as a function of the injection flow rate $Q_0$ ($\mathrm{m}^3\,\mathrm{s}^{-1}$) **(a)**, Damköhler number *Da* as a function of the injection flow rate **(b)**, and power exchanged per difference temperature unit as a function of the Damköhler number **(c)**.

The average effective thermal conductivity has been estimated for each injection flow rate (Fig. 16) and assumes a mean value equal to $\overline{k}_{\mathrm{e}} = 0.1183\,\mathrm{Wm}^{-1}\,\mathrm{K}^{-1}$. The estimated $\overline{k}_{\mathrm{e}}$ is 1 order of magnitude lower than the thermal conductivity coefficient reported in the literature (Robertson, 1988). Fractured media have a lower capacity for diffusion, as opposed to Tang's model, which has unlimited capacity. There is a solid thermal resistance in the fluid to solid heat transfer processes which depends on the rock–fracture size ratio.

This result is coherent with previous analyses on heat transfer carried out on the same rock sample (Pastore et al., 2015). In this study Pastore et al. (2015) found that the ENM model failed to model the behavior of heat transport, in correspondence to parallel branches where the hypothesis of Tang's solution of a single fracture embedded in a porous medium having unlimited capacity cannot be considered valid. In parallel branches the observed BTCs are characterized by less retardation of heat propagation as opposed to the simulated BTCs.

## 5 Conclusions

Aquifers offer a possibility of exploiting geothermal energy by withdrawing the heat from groundwater by means of a heat pump and subsequently supplying the water back into the aquifer through an injection well. In order to optimize the efficiency of the heat transfer system and minimize the environmental impacts, it is necessary to study the behavior of convective heat transport especially in fractured media, where flow and heat transport processes are not well known.

Laboratory experiments on the observation of mass and heat transport in a fractured rock sample have been carried out in order to analyze the contribution of thermal dispersion in heat propagation processes, the contribution of nonlinear flow dynamics to the enhancement of thermal matrix diffu-

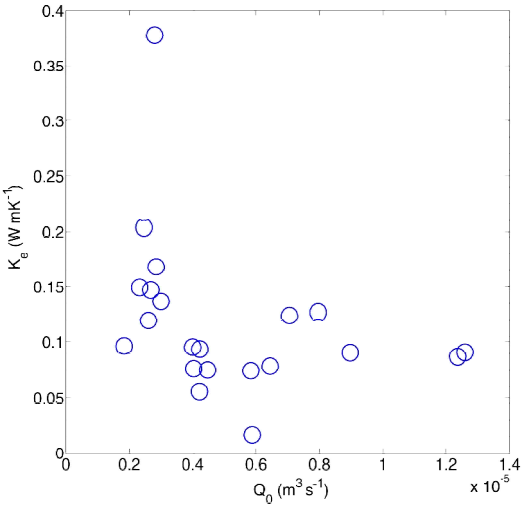


**Figure 16.** Effective thermal conductivity $k_e$ ($Wm^{-1}K^{-1}$) as a function of the injection flow rate $Q_0$ ($m^3 s^{-1}$).

sion, and finally the optimal heat recovery and heat dissipation strategies.

The parameters that control mass and heat transport have been estimated using the ENM model based on Tang's solution.

Heat transport shows a very different behavior compared to mass transport. The estimated transport parameters show differences of several orders of magnitude. Convective thermal velocity is lower than solute velocity, whereas thermal dispersion is higher than solute dispersion, mass transfer rate assumes a very low value, suggesting that fracture–matrix mass exchange can be neglected. Non-Fickian behavior of observed solute BTCs is mainly due to the presence of the secondary path and the nonlinear flow regime. Contrarily, heat transfer rate is comparable with convective thermal velocity giving rise to a retardation effect on heat propagation in the fracture network.

The discrepancies detected in transport parameters are moreover observable through the time moment and tail character analysis which demonstrate that the dual porosity behavior is more evident in the thermal BTCs than in the solute BTCs.

The dimensionless analysis carried out on the transport parameters proves that, as the injection flow rate increases, thermal convection timescale decreases more rapidly than the thermal exchange timescale, explaining the reason why the relationship $Q_0 - u_f$ shows a change in slope for *Da* lower than the unit.

Thermal dispersion dominates heat transport dynamics and the Peclet number, and the product between the Peclet number and the Damköhler number is almost always less than the unit.

The optimal conditions for thermal exchange in a fracture network have been investigated. The power exchanged increases in a potential way as *Da* increases in the observed range.

The Explicit Network Model is an efficient computation methodology to represent flow, mass and heat transport in fractured media, as 2-D and/or 3-D problems are reduced to resolving a network of 1-D pipe elements. Unfortunately, in field case studies, it is difficult to obtain full knowledge of the geometry and parameters such as the orientations and aperture distributions of the fractures needed by the ENM, even by means of field investigation methods. However, in real case studies the ENM can be coupled with continuum models in order to represent greater discontinuities with respect to the scale of study, which generally gives rise to preferential pathways for flow, mass and heat transport.

A method to represent the topology of the fracture network is represented by multifractal analysis as discussed in Tijera at al. (2009) and Tarquis at al. (2014).

This study has permitted one to detect the key parameters to design devices for heat recovery and heat dissipation that exploit the convective heat transport in fractured media.

Heat storage and transfer in fractured geological systems is affected by the spatial layout of the discontinuities.

Specifically, the rock–fracture size ratio which determines the matrix block size is a crucial element in determining matrix diffusion on the fracture–matrix surface.

The estimation of the average effective thermal conductivity coefficient shows that it is not efficient to store thermal energy in rocks with high fracture density because the fractures are surrounded by a matrix with more limited capacity for diffusion giving rise to an increase in solid thermal resistance. In fact, if the fractures in the reservoir have a high density and are well connected, such that the matrix blocks are small, the optimal conditions for thermal exchange are not reached, as the matrix blocks have a limited capability to store heat.

On the other hand, isolated permeable fractures will tend to lead to more distribution of heat throughout the matrix.

Therefore, subsurface reservoir formations with large porous matrix blocks will be the optimal geological formations to be exploited for geothermal power development.

The study could help to improve the efficiency and optimization of industrial and environmental systems, and may provide a better understanding of geological processes involving transient heat transfer in the subsurface.

Future developments of the current study will be carrying out investigations and experiments aimed at further deepening of the quantitative understanding of how fracture arrangement and matrix interactions affect the efficiency of storing and dissipating thermal energy in aquifers. This could be achieved by means of using different formations with different fracture density and matrix porosity.

*Competing interests.* The authors declare that they have no conflict of interest.

*Acknowledgements.* Research founded with the regional program in support of the smart specialization and social and environmental sustainability – FutureInResearch.

Edited by: J. M. Redondo
Reviewed by: three anonymous referees

## References

Abate, J. and Ward, W.: A unified Framework for numerically inverting laplace transforms, INFORMS J. Comp., 18, 408–421, 2006.

Anderson, M. P.: Heat as a ground water tracer, Ground Water, 43, 951–968, doi:10.1111/j.1745-6584.2005.00052.x, 2005.

Auradou, H., Deazerm, G., Boschan, A., Hulin, J., and Koplik, J.: Flow channeling in a single fracture induced by shear displacement, Geothermics, 35, 575–588, 2006.

Bear, J.: Dynamics of Fluids in Porous Media, Environmental Science Series, Elsevier, Amsterdam, 764, SD-008, 1972.

Becker, M. W. and Shapiro, A. M.: Interpreting tracer breakthrough tailing from different forced gradient tracer experiment configurations in fractured bedrock, Water Resour. Res., 39, 1024, doi:10.1029/2001WR001190, 2003.

Bodin, J., Porel, G., Delay, F., Ubertosi, F., Bernard, S., and de Dreuzy, J. R.: Simulation and analysis of solute transport in 2D fracture/pipe networks, The SOLFRAC program, J. Contam. Hydrol., 89, 1–28, 2007.

Bravo, H. R., Jiang, F., and Hunt, R. J.: Using groundwater temperature data to constrain parameter estimation in a groundwater flow model of a wetland system, Water Resour. Res., 38, 1153, doi:10.1029/2000WR000172, 2002.

Bredehoeft, J. and Papadopulos, I. S.: Rates of vertical groundwater movement estimated from the Earth's thermal profile, Water Resour. Res., 1, 325–328, 1965.

Cherubini, C.: A modeling approach for the study of contamination in a fractured aquifer, Geotech. Geol. Eng., 26, 519–533, doi:10.1007/s10706-008-9186-3, 2008.

Cherubini, C. and Pastore, N.: Modeling contaminant propagation in a fractured and karstic aquifer, Fresen. Environ. Bull., 19, 1788–1794, 2010.

Cherubini, C. and Pastore, N.: Critical stress scenarios for a coastal aquifer in southeastern Italy, Nat. Hazards Earth Syst. Sci., 11, 1381–1393, doi:10.5194/nhess-11-1381-2011, 2011.

Cherubini, C., Pastore, N., and Francani, V.: Different approaches for the characterization of a fractured karst aquifer, WSEAS Trans. Fluid Mech., 1, 29–35, 2008.

Cherubini, C., Giasi, C. I., and Pastore, N.: Application of Modelling for Optimal Localisation of Environmental Monitoring Sensors, Proceedings of the Advances in sensor and Interfaces, Trani, Italy, 222–227, 2009.

Cherubini, C., Hsieh, P. A., and Tiedeman, C. R.: Modeling the effect of heterogeneity on forced-gradient flow tracer tests in heterogeneous aquifers, I Congreso Internacional de Hidrologia de Lianuras Azul, Buenos Aires, Argentina, 21–24 September, 809–816, 2010.

Cherubini, C., Giasi, C. I., and Pastore, N.: Bench scale laboratory tests to analyze non-linear flow in fractured media, Hydrol. Earth Syst. Sci., 16, 2511–2522, doi:10.5194/hess-16-2511-2012, 2012.

Cherubini, C., Giasi, C. I., and Pastore, N.: Evidence of non-Darcy flow and non-Fickian transport in fractured media at laboratory scale, Hydrol. Earth Syst. Sci., 17, 2599–2611, doi:10.5194/hess-17-2599-2013, 2013a.

Cherubini, C., Giasi, C. I., and Pastore, N.: Laboratory tests to analyze solute transport behavior in fractured media, Rendiconti Online Società Geologica Italiana, 24, 55–57, 2013b.

Cherubini, C., Giasi, C. I., and Pastore, N.: A laboratory physical model to analyse flow and transport processes in fractured rock sample at bench scale level, J. Eng. Geol. Environ., 1, 19–32, 2013c.

Cherubini, C., Giasi, C. I., and Pastore, N.: Fluid flow modeling of a coastal fractured karstic aquifer by means of a lumped parameter approach, Environ. Earth Sci., 70, 2055–2060, 2013d.

Cherubini, C., Giasi, C. I., and Pastore, N.: On the reliability of analytical models to predict solute transport in a fracture network, Hydrol. Earth Syst. Sci., 18, 2359–2374, doi:10.5194/hess-18-2359-2014, 2014.

Constantz, J., Cox, M. H., and Su, G. W.: Comparison of Heat and Bromide as Ground Water Tracers Near Streams, Ground Water, 41, 647–656, 2003.

de Marsily, G.: Quantitative Hydrogeology: Groundwater Hydrology for Engineers, Academic Press, Orlando, Florida, 440 pp., 1986.

Domenico, P. A. and Palciauskas, V. V.: Theoretical analysis of forced convective heat transfer in regional ground-water flow, Geol. Soc. Am. Bull., 84, 3803–3814, 1973.

Fahien, R. W.: Fundamental of Transport Phenomena, McGraw-Hill, New York, 614 pp., 1983.

Ferguson, G., Beltrami, H., and Woodbury, A. D.: Perturbation of ground surface temperature reconstruction by groundwater flow, Geophys. Res. Lett., 33, L13708, doi:10.1029/2006GL026634, 2006.

Forchheimer, P.: Wasserbewegung durch Boden, Z. Ver. Dtsch. Ing., 45, 1781–1788, 1901.

Geiger, S. and Emmanuel, S.: Non-fourier thermal transport in fractured geological media, Water Resour. Res., 46, W07504, doi:10.1029/2009WR008671, 2010.

Gisladottir, V. R., Roubinet, D., and Tartakovsky, D. M.: Particle Methods for Heat Transfer in Fractured Media, Transport Porous. Med., 115, 311–326, doi:10.1007/s11242-016-0755-2, 2016.

Green, D., Perry, R., and Babcock, R.: Longitudinal dispersion of thermal energy through porous media with a flowing fluid, Aiche J., 10, 645–651, 1964.

Hao, Y., Fu, P., and Carrigan, C. R.: Application of a dual-continuum model for simulation of fluid flow and heat transfer in fractured geothermal reservoir, Proceedings, 38th Workshop on Geothermal Reservoir Engineering Stanford University, Stanford, California, 11–13 February 2013, SGP-TR-198, 2013.

Hatch, C. E., Fisher, A. T., Revenaugh, J. S., Constantz, J., and Ruehl, C.: Quantifying surface water-groundwater interactions using time series analysis of streambed thermal

records: Method development, Water Resour. Res., 42, W10410, doi:10.1029/2005WR004787, 2006.

Hawkins, A. J. and Becker, M. W.: Measurement of the Spatial Distribution of Heat Exchange in a Geothermal Analog Bedrock Site Using Fiber Optic Distributed Temperature Sensing, PROCEEDINGS, 37th Workshop on Geothermal Reservoir Engineering Stanford University, Stanford, California, 30 January–1 February 2012 SGP-TR-194, 2012.

Hopmans, J. W., Simunek, J., and Bristow, K. L.: Indirect estimation of soil thermal properties and water flux using heat pulse probe measurements: Geometry and dispersion effects, Water Resour. Res., 38, 1006, doi:10.1029/2000WR000071, 2002.

Ingebritsen, S. E. and Sanford, W. E.: Groundwater in Geologic Processes, 341 pp., Cambridge Univ. Press, Cambridge, UK, 1998.

Keery, J., Binley, A., Crook, N., and Smith, J. W. N.: Temporal and spatial variability of groundwater-surface water fluxes: Development and application of an analytical method using temperature time series, J. Hydrol., 336, 1–16, 2007.

Klepikova, M. V., Le Borgne, T., Bour, O., Dentz, M., and Hochreutener, R.: Heat as a tracer for understanding transport processes in fractured media: Theory and field assessment from multiscale thermal push-pull tracer tests, Water Resour. Res., 52, 5442–5457, 2016.

Kocabas, I.: Geothermal reservoir characterization via thermal injection backflow and interwell tracer testing, Geothermics, 34, 27–46, 2005.

Lu, W. and Xiang, Y.: Experiments and sensitivity analyses for heat transfer in a meter-scale regularity fracture granite model with water flow, Appl. Phys. Eng. 13, 958–968, 2012.

Ma, R., Zheng, C., Zachara, J. M., and Tonkin, M.: Utility of bromide and heat tracers for aquifer characterization affected by highly transient flow conditions, Water Resour. Res., 48, W08523, doi:10.1029/2011WR011281, 2012.

Martinez, A. R., Roubinet, D., and Tartakovsky, D. M.: Analytical models of heat conduction in fractured rocks, J. Geophys. Res. Sol.-Ea., 119, 83–98, doi:10.1002/2012JB010016, 2014.

Masciopinto, C., Volpe, A., Palmiotta, D., and Cherubini, C.: A combined PHREEQC-2/parallel fracture model for the simulation of laminar/non-laminar flow and contaminant transport with reactions, J. Contam. Hydrol., 117, 94–108, 2010.

Molina-Giraldo, N., Bayer, P., and Blum, P.: Evaluating the influence of thermal dispersion on temperature plumes from geothermal systems using analytical solutions, Int. J. Therm. Sci., 50, 1223–1231, doi:10.1016/j.ijthermalsci.2011.02.004, 2011.

Molson, J. W., Frind, E. O., and Palmer, C. D.: Thermal energy storage in an unconfined aquifer 2. Model development, validation and application, Water Resour. Res., 28, 2857–2867, 1992.

Moonen, P., Sluys, L. J., and Carmeliet, J.: A continous – Discontinous Approach to simulate heat transfer in fractured media, Transport Porous Med., 89, 399–419, 2011.

Natarajan, N. and Kumar, G. S.: Thermal transport in a coupled sinusoidal fracture-matrix system, Int. J. Eng. Sci. Technol., 2, 2645–2650, 2010.

Neuville, A., Toussaint, R., and Schmittbuhl, J.: Fracture roughness and thermal exchange: a case study at Soultz-sous-Forêts, C. R. Geosci., 342, 616–625, 2010.

Niswonger, R. G. and Prudic, D. E.: Modeling heat as a tracer to estimate streambed seepage and hydraulic conductivity, in: Heat as a Tool for Studying the Movement of Ground Water Near Streams, edited by: Stonestrom, D. A. and Constantz, J., 81–89, USGS Circular 1260, Reston, Virginia, USGS, 2003.

Ouyang, X. L., Xu, R. N., and Jiang, P. X.: Effective solid-to-fluid heat transfer coefficient in egs reservoirs, Proceedings of the 5th International Conference on porous Media and its Applications in Science and Engineering ICPM5, 22–27 June 2014, Kona, Hawaii, 2014.

Papadopulos, S. S. and Larson, S. P.: Aquifer storage of heated water: Part II – Numerical simulation of field results, Ground Water, 16, 242–248, 1978.

Pastore, N., Cherubini, C., Giasi, C. I., Allegretti, N. M., Redondo, J. M., and Tarquis, A. M.: Experimental study of heat transport in fractured network, Energy Proc., 76, 273–281, 2015.

Rau, G. C., Andersen, M. S., and Acworth, R. I.: Experimental investigation of the thermal dispersivity term and its significance in the heat transport equation for flow in sediments, Water Resour. Res., 48, W03511, doi:10.1029/2011WR011038, 2012.

Read, T., Bour, O., Bense, V., Le Borgne, T., Goderniaux, P., Klepikova, M. V., Hochreutener, R., Lavenant, N., and Boshero, V.: Characterizing groundwater flow and heat transport in fractured rock using fiber-optic distributed temperature sensing, Geophys. Res. Lett., 40 1–5, 2013.

Reiter, M.: Using precision temperature logs to estimate horizontal and vertical groundwater flow components, Water Resour. Res., 37, 663–674, 2001.

Robertson, E. C.: Thermal Properties of Rocks, United States Department of the Interior Geological Survey Open-File Report 88-441, Reston, Virginia, 1988.

Ronan, A. D., Prudic, D. E., Thodal, C. E., and Constantz, J.: Field study and simulation of diurnal temperature effects on infiltration and variably saturated flow beneath an ephemeral stream, Water Resour. Res., 34, 2137–2153, 1998.

Sauty, J. P., Gringarten, A. C., Fabris, H., Thiery, D., Menjoz, A., and Landel, P. A.: Sensible energy storage in aquifers 2. Field experiments and comparison with theoretical results, Water Resour. Res., 18, 253–265, 1982.

Shook, G. M.: Predicting thermal breakthrough in heterogeneous media from tracer tests, Geothermics, 30, 573–580, 2001.

Smith, L. and Chapman, D. S.: On the thermal effects of groundwater flow. 1. Regional scale systems, J. Geophys. Res., 88, 593–608, 1983.

Su, G. W., Jasperse, J., Seymour, D., and Constantz, J.: Estimation of hydraulic conductivity in an alluvial system using temperatures, Ground Water, 42, 890–901, 2004.

Tang, D. H., Frind, E. O., and Sudicky, E. A.: Contaminant transport in fractured porous media: analytical solutions for a single fractures, Water Resour. Res., 17, 555–564, 1981.

Taniguchi, M., Williamson, D. R., and Peck, A. J.: Disturbances of temperature-depth profiles due to surface climate change and subsurface water flow: 2, an effect of step increase in surface temperature caused by forest clearing in southwest-western Australia, Water Resour. Res., 35, 1519–1529, 1999.

Tarquis, A. M., Platonov, A., Matulka, A., Grau, J., Sekula, E., Diez, M., and Redondo, J. M.: Application of multifractal analysis to the study of SAR features and oil spills on the ocean surface, Nonlin. Processes Geophys., 21, 439–450, doi:10.5194/npg-21-439-2014, 2014.

Tijera, M., Cano, J., Cano, D., Bolster, D., and Redondo, J. M.: Filtered Deterministic waves and analysis of the Fractal dimension

of the components of the wind velocity, Il Nuovo Cimento C, 5–6, 653–667, 2009.

Tsang, C. F. and Neretnieks, I.: Flow channeling in heterogeneous fractured rocks, Rev. Geophys., 36 257–298, 1998.

Vandenbohede, A., Louwyck, A., and Lebbe L.: Conservative solute versus Heat transport porous media during push-pull tests, Transport Porous Med., 76, 265–287, doi:10.1007/s11242-008-9246-4, 2009.

Vandenbohede, A. and Lebbe, L.: Parameter estimation based on vertical heat transport in the surficial zone, Hydrogeol. J., 18, 931–943, doi:10.1007/s10040-009-0557-5, 2010.

Whitaker, S.: Flow in porous media. I: A theoretical derivation of Darcy's law, Transport Porous Med., 1, 3–25, 1986.

Woodbury, A. D. and Smith, J. L.: On the thermal effects of three dimensional groundwater flow, J. Geophys. Res., 90, 759–767, 1985.

Wu, Y. S., Ye, M., and Sudicky, E. A.: Fracture-Flow-Enhanced Matrix Diffusion in Solute Transport Through Fractured Porous Media, Transport Porous Med., 81, 21–34, doi:10.1007/s11242-009-9383-4, 2010.